Università degli Studi di Milano

Facoltà di Scienze e Tecnologie

Dipartimento di Chimica

Doctorate Course in Chemistry – XXXI Cycle

Insertion (co)polymerization of olefins catalyzed by first row transition metal complexes

Giorgia Zanchin

R11305

Supervisor:
prof. Emma Gallo (UniMi)

Co-supervisor:
dr. Giuseppe Leone (CNR – ISMAC)

Coordinator:
prof. Emanuela Licandro (UniMi)

2015 ~ 2018

This PhD was funded by the ISMAC Institute of the Italian National Research Council. I'm deeply grateful to dr. Giuseppe Leone and dr. Giovanni Ricci for this opportunity.

«Mi basterebbe essere padre
di una buona idea»
Niccolò Fabi

A tutti coloro che hanno creduto in me
e in questo dottorato,
e a chi, oltre tutto, continua a crederci.
Grazie!

Abstract

Since polyolefins are an integral part of everyday life and given the ever-growing global demand for these polymers, the insertion polymerization of olefins is one of the most industrially relevant synthetic reaction, widely investigated also in academia. It is in this context that this PhD project is located. The developed research activity was aimed at synthesizing new catalytic systems capable of stereochemically drive the polymerization of various (di)olefins, in particular cyclic olefins such as norbornene and its derivatives. The investigated catalysts are made up of two components: the organometallic complex (pre-catalyst) and an aluminum alkyl compound (co-catalyst or activator). Among the series of the organometallic complexes, during my PhD, complexes of the first row transition metals, *i.e.*, titanium, vanadium, and chromium, bearing nitrogen and phosphorous based ligands were investigated. They were later applied as catalysts for the homopolymerization of ethylene, cyclic olefins (norbornene, dicyclopentadiene and norbornene derivatives) and 1,3-butadiene, and the copolymerization of ethylene with various cyclic olefins. Depending on the employed catalyst and the polymerization conditions, we obtained oligomers or high-polymers. All the products were carefully characterized with different techniques, in order to get more information on the properties of the obtained (co)polymers as well as on the polymerization mechanism.

Norbornene and dicyclopentadiene oligomers were mainly obtained from titanium and chromium catalysts, activated by Et_2AlCl and methylalumoxane (MAO), respectively, while cyclic olefin copolymers were obtained from the copolymerization of ethylene with cyclic olefins promoted by vanadium based catalysts. In addition, we demonstrated that some vanadium and chromium complexes, in combination with MAO, were active in the polymerization of 1,3-butadiene, affording poly(1,3-butadiene) with different microstructure (*cis*-1,4, *trans*-1,4 or 1,2) and stereospecificity (*i.e.*, iso- or syndiotactic polymers), depending on the type of ligand.

This study allowed to understand the correlations between the catalyst's features and the polymerization outcome in terms of activity, regio- and stereoselectivity. Moreover, particular emphasis has been devoted to the study of the catalyst stability over the polymerization time and temperature.

At the same time, particular interest has been developed toward the post–polymerization functionalization, as a strategy to modify some polymer properties (*e.g.*, solubility and processability) and thus to obtain polymers hardly obtainable by direct (co)polymerization with polar (co)monomers.

This PhD dissertation reports the results achieved during the three-year research activity, together with the main difficulties encountered and the actions put in place trying to overcome them.

Table of contents

1. Introduction 1
   - 1.1 The transition metals in the periodic table 2
   - 1.2 The polymer revolution: from 1950s to modern days 3
   - 1.3 Polymer properties 7
   - 1.4 Polymerization mechanism 8
   - 1.5 Different classes of polymers 9
   - 1.6 Post–polymerization modification 14
   - *References* 14

2. Motivation 17

3. Materials & Methods 21
   - 3.1 Materials and chemicals 21
   - 3.2 General polymerization procedures 22
   - 3.3 General post–polymerization modification procedures 24
   - 3.4 Complexes characterization 24
   - 3.5 Polymers characterization 25
   - 3.6 Microstructure determination via NMR spectroscopy 26
     - 3.6.1 Cyclic olefin polymers [poly(norbornene) and poly(dicyclopentadiene)] 27
     - 3.6.2 Cyclic olefin copolymers (COCs) 27
     - 3.6.3 Poly(1,3-butadiene) 29
   - *References* 29

4. Titanium 31
   - 4.1 $TiCl_4$: the state-of-the-art 32
   - 4.2 Ti–mediated dicyclopentadiene polymerization 34
     - 4.2.1 The starting point 34
     - 4.2.2 Polymerization of *endo*/*exo* DCPD mixture 35
     - 4.2.3 Polymerization of *endo*-DCPD, *exo*-DCPD, and H-DCPD 38
     - 4.2.4 Post–polymerization modification 41
   - 4.3 Other cyclic olefins: the case of norbornadiene 43
   - *References* 45

5. Vanadium 47
   - 5.1 Vanadium: the state-of-the-art 48
   - 5.2 The kick-off: the case of $VCl_3(PMePh_2)_2$ 53
     - 5.2.1 Synthesis and characterization of $VCl_3(PMePh_2)_2$ 53
     - 5.2.2 Catalytic behavior 54
   - 5.3 How does the ligand make the difference? 63
     - 5.3.1 Synthesis and characterization of V(III) monodentate phosphine complexes 63
     - 5.3.2 Catalytic behavior 64
   - 5.4 Enhancing catalyst stability: bidentate chelating ligands 68
     - 5.4.1 Synthesis and characterization of V(III) bidentate phosphine complexes 68
     - 5.4.2 Catalytic behavior 70

5.5 Enhancing catalyst stability: imido–phosphine ligands 75
5.5.1 Synthesis and characterization of (imido)V(IV) phosphine complexes 76
5.5.2 Catalytic behavior 79
5.5.3 Copolymerization of ethylene with norbornene derivatives 85
5.6 Functionalization of COCs 88
5.7 Beyond COCs: vanadium for the polymerization of 1,3-butadiene 89
5.7.1 Catalytic behavior 90
5.8 Experimental section 92
5.8.1 Synthesis of vanadium(III) complexes 92
5.8.2 Synthesis of (imido)vanadium(IV) complexes 96
References 98

6. Chromium 103
6.1 Chromium: the state-of-the-art 104
6.1.1 The Phillips catalyst 104
6.1.2 Homogeneous chromium catalysts 104
6.1.3 The versatility of chromium catalysts 105
6.2 Iminopyridine chromium complexes 107
6.2.1 Synthesis and characterization of the complexes 107
6.2.2 Catalytic behavior 112
6.3 Porphyrin chromium complexes 122
6.3.1 Synthesis of porphyrin chromium complexes 123
6.3.2 Copolymerization of cyclohexene oxide and succinic anhydride 123
6.4 Experimental section 126
6.4.1 Synthesis of chromium iminopyridine complexes 126
6.4.2 Synthesis of chromium porphyrin complexes 127
6.4.3 General epoxide – anhydride copolymerization procedure 127
References 128

7. Conclusions 133

8. Other projects 135

9. What's next? 137

Appendix 141

Acknowledgments 147

Chapter 1
Introduction

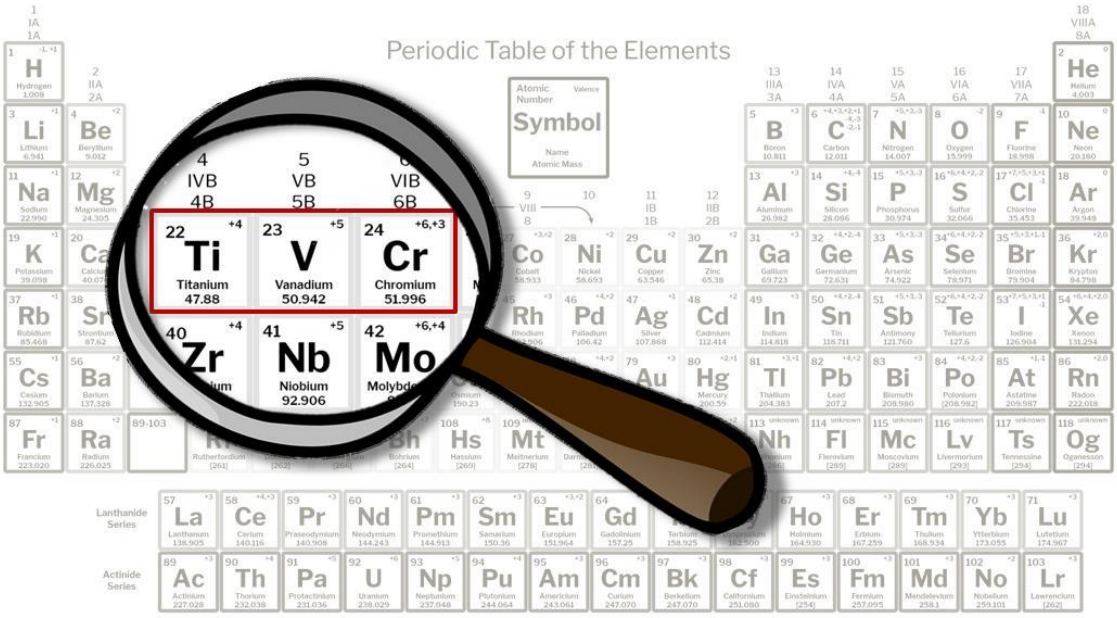

«Sandro was surprised when I tried to explain to him some of the ideas that at the time I was confusedly cultivating. That the nobility of man, acquired in a hundred centuries of trial and error, lay in making himself the conqueror of matter, and that I had enrolled in chemistry because I wanted to remain faithful to this nobility. That conquering matter is to understand it, and understanding matter is necessary to understanding the universe and ourselves: and that therefore Mendeleev's Periodic Table, which just during those weeks we were laboriously learning to unravel, was poetry, loftier and more solemn than all the poetry we had swallowed down in liceo; and come to think of it, it even rhymed!»

Primo Levi, *The Periodic Table*

1.1 The transition metals in the periodic table

When walking along the rows in the periodic table, gradual changes in properties across the periods from left to right are expected, due to the increase in the atomic number and collateral variations. However, once reached the fourth row, just after calcium, an abrupt break of this trend takes place: this is the point of the first transition series. These elements are remarkably similar in their physical and chemical properties. The general similarity in properties has been explained in terms of their relatively small difference in effective nuclear charge over the series. This occurs because each additional electron enters the penultimate 3*d* shell providing an effective shield between the nucleus and the outer 4*s* shell: indeed, they all feature the electron configuration of [Ar]$3d^p4s^q$.

Ionization energies and electronegativities increase slowly across a row as a consequence of the fact that the effective nuclear charge experienced by valence electrons in the *d*-block elements does not change greatly as the nuclear charge increases across a row. Consistent with this trend, transition metals become steadily less reactive and more "noble" in character from left to right across a row.

The relatively small increase in successive ionization energies causes most of the transition metal to exhibit multiple oxidation states separated by a single electron. This feature of varying greatly the oxidation state is what makes them hold a relevant role in the world of catalysis.

Transition metals can be ligated by different ligands, allowing for a wide variety of organometallic complexes. Transition metal complexes often have spectacular colors caused by electronic transitions by the absorption of light; for this reason, they are often applied as pigments. Most transitions related to colored metal complexes are either *d*–*d* transitions or charge transfer bands. In a *d*–*d* transition, an electron in a *d* orbital on the metal is excited by a photon to another *d* orbital of higher energy. A charge transfer band entails promotion of an electron from a metal-based orbital into an empty ligand-based orbital (Metal–to–Ligand Charge Transfer or MLCT). The converse also occurs: excitation of an electron in a ligand-based orbital into an empty metal-based orbital (Ligand–to–Metal Charge Transfer or LMCT). These phenomena can be observed with the aid of the UV-vis spectroscopy.

Transition metal complexes are commonly used in catalysis, both in homogeneous and heterogeneous conditions. Major industrial processes include hydrogenation, hydrosilylation, hydrocyanation, hydrocarboxylation, methanol carbonylation, hydroformylation, and olefin metathesis, oligomerization and polymerization. The last two processes are those that are more related to this thesis, and will be presented into details hereafter.

Among all the possible transition metal–mediated organometallic reactions mentioned, metal–catalyzed olefin polymerization is rather different from the other applications: Ziegler–Natta catalysis, instead, «*means much more than just making plastics out of the light fraction of oil.*

With its precision syntheses, it is an endless source of exactly defined chain architectures on which new concepts in polymer and materials science can be formulated and validated».[1]

1.2 The polymer revolution: from 1950s to modern days

When in the mid of last century, in the wake of Staudinger's discoveries and hypotheses on the chemical structure of several macromolecular substances, Karl Ziegler and Giulio Natta reported for the first time that titanium, in combination with an aluminum compound, was an active catalyst for the polymerization of ethylene and α-olefins, they were probably not completely aware of the great relevance and consequences of their groundbreaking discoveries and the subsequent huge impact on worldwide industry and society. Today, every aspect of life can be correlated to a product of the plastic industry: from cosmetic and sanitary applications to the synthesis of plastics.

Generally, the so-called Ziegler–Natta type catalysis (or coordination–insertion polymerization) involves the combination of a transition metal compound (pre-catalyst) and an alkyl/aryl/hydride derivative of a metal, generally from Group 3 (co-catalyst) as activator. The nature and the combination of the two species give rise to catalytic systems with different characteristics and behavior, concerning activity, stereospecificity and regioselectivity. The presence of the co-catalyst is required for the alkylation of the metal center, that is the formation of the active specie, the first step of the polymerization. The following steps are coordination of the olefin to the metal center and insertion of the olefin in the transition metal–carbon bond. The mechanism of the polymerization will be discussed in detail further on (paragraph 1.4).

Despite the years and efforts of research in this field (and well documented in various reviews on this topic (see for example the issue "*Frontiers in Metal-Catalyzed Polymerization*"[2]), still nowadays the synthesis of polyolefins at industrial level is based on heterogeneous systems, both Ziegler–Natta (catalytic system $MgCl_2$/ID/$TiCl_4$/ED/Al–activator ID = internal donor, ED = external donor) and Phillips (Cr grafted on a porous support such as SiO_2) catalysts, as reported in Figure 1.

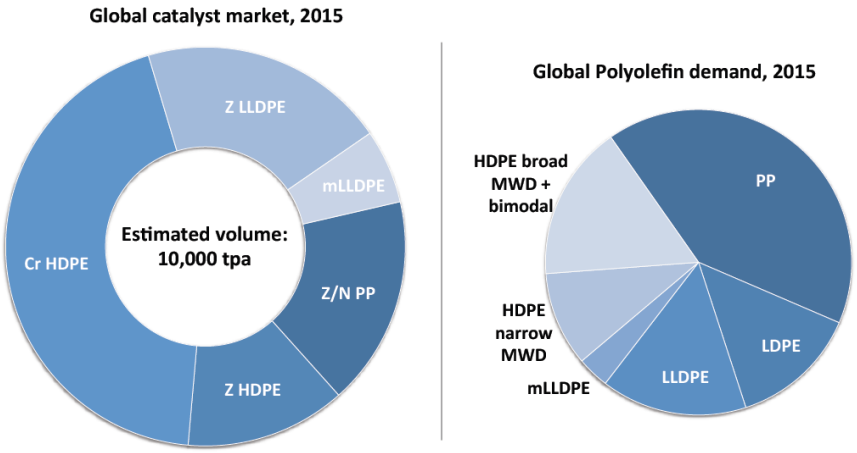

Figure 1 *2015 annual report on global catalyst market and polyolefin demand (Source CMR 2013 and IHS 2016, EBB analysis).*

One of the main reasons for the long–term golden age of these heterogeneous catalysts is correlated to the cheapness and easy handling of them, together with the possibility to control the shape of the produced particles of polymer as replication of the catalyst particles.[3]

However, the 50 and more years of research in the field brought about improvements in the polymerization process, and also many other innovations, such as the "living" Zielger–Natta polymerization,[4] chain–walking polymerization,[5] olefin block copolymerization via chain shuttling,[6] controlled radical polymerization,[7] and the helpful tool of the High Throughput Experimentation (HTE)[8] for catalyst discovery and screening.

Beyond heterogeneous catalysis, **homogeneous catalytic systems** for olefin polymerization have been extensively studied and, to some little extent, implemented on industrial scale for the production of some specialties, like the new olefin block copolymers, UHMWPE (Ultra-High-Molecular-Weight PolyEthylene),[9] COCs (Cyclic Olefin Copolymers),[10] and the synthetic rubber EPDM (Ethylene-Propylene-Diene Material).[11] Homogeneous pre-catalysts are generally made up of a transition metal halide and an organic ligand, that can be coordinated or covalently bonded to the metal.

In comparison to heterogeneous catalysts, homogeneous ones have some nice advantages: the presence of only one type of active site allows the formation of polymers with narrow molecular weight distribution (Fig. 2), and the possibility of easily tuning their activity by either changing the metal ions or modifying their ligands.

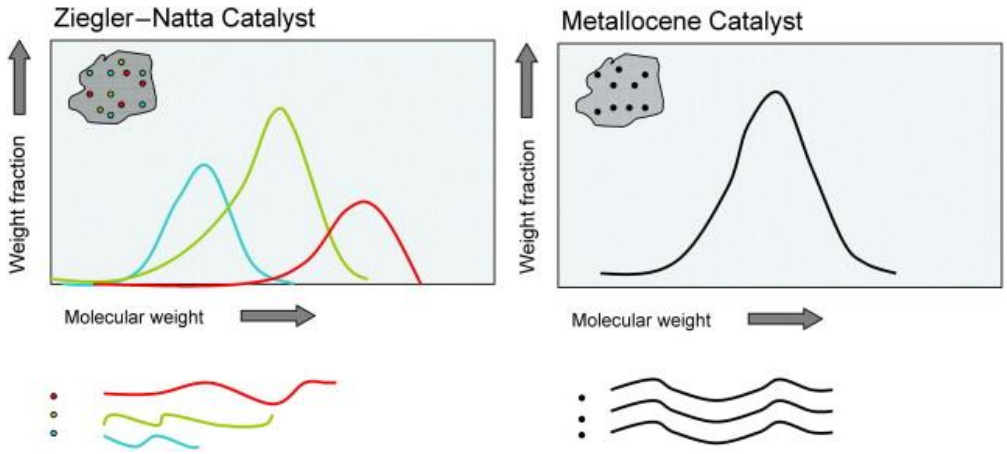

Figure 2 *Traditional Ziegler–Natta vs Metallocene catalyst: differences in the molecular weight of the polymers.*

The history of homogeneous molecular catalysis is dated back to 1951 with the serendipitous synthesis of metallocenes,[12] especially with Group 4 metals (Ti, Zr, Hf) (Fig. 3). Nevertheless the field remained inactive for decades until 1977, when Kaminsky demonstrated that metallocenes, with the help of methylaluminoxane (MAO) as co-catalyst, can be useful in polymerizing olefins.

The active site, sandwiched between the constrained geometries of the cyclopentadienyl structures, has the potential to knit together olefin monomers with great accuracy.[13]

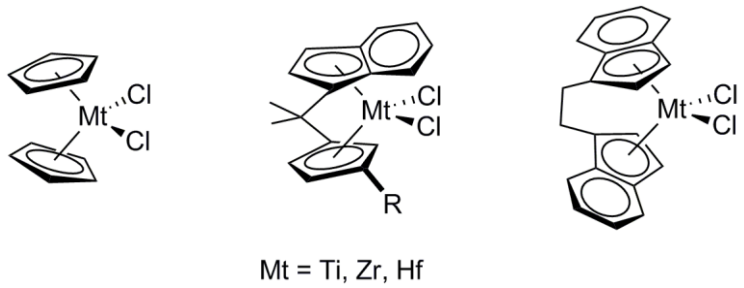

Figure 3 *Some exemplary metallocenes.*

Metallocenes allow a great control over the stereochemistry, molecular weight, molecular weight distribution, and comonomer incorporation, thus providing a wide range of high performance materials.[14] Some metallocene catalysts have been also implemented on industrial scale for the production of certain grades of poly(ethylene) (LLDPE, Linear-Low-Density PE) by many industries (*e.g.*, Exxon Mobil Corporation, DOW Chemical Company, Lyondellbasell Industries Holdings B.V., Sabic, Borealis AG).

However, metallocenes have some drawbacks: their synthesis is not straightforward and quite expensive, they do not show great stability over temperature (>80 °C), and they have some limitations correlated to polymer molecular weight and comonomer incorporation; moreover, they require the use of expensive Lewis acids (MAO or perfluoroarylboron derivatives) as activators.

In the 1990s, the interest in single–site catalysts expanded to another class of metal complexes with other ligand motifs, known with the name of 'post–metallocenes', extending the commercially useful metals across the transition series but also broadening the range of polyolefins accessible by coordination/insertion polymerization technology.[15,16]

With the term post–metallocenes are intended a family of complexes of transition metals with ligands containing donor heteroatoms (mainly N, O, P, S). Important events in the development of post–metallocene systems were the discovery by Brookhart *et al.* of nickel(II) bis(imine) complexes capable of catalyzing ethylene polymerization,[17] and the discovery of iron bis(imino)pyridyl complexes as highly active catalysts for the polymerization of ethylene.[18] Moreover, it was found that, unlike metallocenes, this type of complexes can be activated by Lewis acids other than MAO, such as trialkylaluminum derivatives. This decreased the cost of the catalytic system.

During the last two decades, an increasing number of polymerization processes employing post– or non–metallocene catalysts have been developed and employed at different extent. The results obtained so far are a myriad, and various reviews and book chapters have been published

concerning post–metallocene complexes for olefin polymerization.[15] Just to cite some examples of classes of post–metallocenes (Fig. 4), we can consider:

- Monocyclopentadienyl complexes (**1**), especially with Group 4 metals. Generally, they are less active in olefin polymerization than their bis(cyclopentadienyl)analogues.
- Bis(imino) complexes (**2**), especially of Ni and Pd. They are widely used thanks to the specific properties of the ligands, namely their ability to effectively stabilize the metal, the great steric hindrance, and the possibility of fine tuning the steric and electronic properties by introducing substituents on the aryl ring.
- Bis(imino)pyridyl complexes (**3**), with Fe, Co, V, and Cr. They showed extremely high activity in the polymerization of ethylene. The activity of the catalyst and the molecular weight of the polymers obtained are greatly influenced by the steric hindrance of the ligand and the presence of nitrogen donor atom.
- Phenoxyimine complexes (**4**), with Ti, Zr, and Hf. The activity of these complexes is modulated by the substituents on the phenoxy group, as well as the type of imine moiety.
- Phosphinimide complexes (**5**), with Group 4 metals. They have been studied for the possibility of mimicking a cyclopentadienyl ligand, but with synthetically readily accessible compounds, bringing to an efficient shielding of the metal centre, but at the same time a sterically more open geometry. The activity of these complexes is somewhat low and significant higher activities were obtained by methylation.

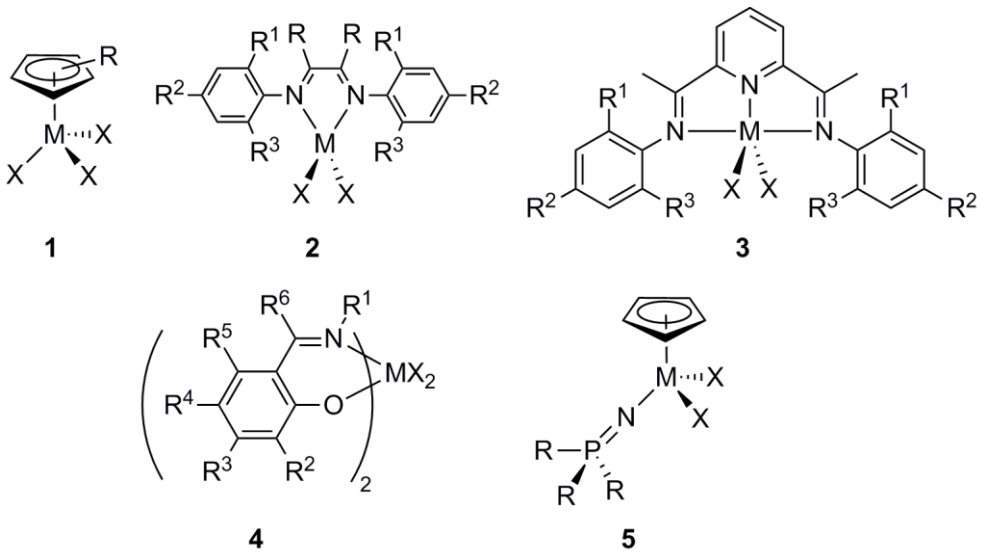

Figure 4 *Some exemplary classes of post–metallocene complexes (R = H, alkyl or aryl groups; generally X = halogen atom or Me group).*

The development of methods for the polymerization of olefins are mainly focused on achieving fine control over macromolecular architectures, especially chain composition, molecular weight,

and stereochemistry, already in the polymerization process; this allows for the synthesis of "high performance polyolefins", with virtually new properties or unusual combinations of them. Today, the use of well-characterized molecular structures allows to synthesize extremely uniform copolymers with the desired properties by varying catalyst's composition and geometry.

Precise control over product structure is the goal of all chemical synthesis. In particular, in the field of polymer synthesis, the structure of the resultant macromolecules is intimately linked to its properties, which ultimately determine the potential applications of it.

1.3 Polymer Properties

The properties of polyolefins at a molecular scale (such as the molecular weight distribution and the microstructure) influence the macroscopic properties of the whole material, in terms of mechanical, rheological and thermal behavior. Hence, it is important to perform a detailed characterization of the synthesized polymers, also to determine their possible application and at which extent can be employed.

The molecular weight

A polymer is usually a mixture of numerous individual chains characterized by different chain lengths. As a consequence, the molecular weight of polymers is not univocally determined, but it is characterized by a distribution around an average value.

In this thesis the technique applied for the determination of the molecular weight is the Size Exclusion Chromatography (SEC) (also known as Gel Permeation Chromatography, GPC), that is a method of separation in which the macromolecules are fractionated according to their size.

Different average values can be defined, depending on the statistical method applied.

The main are:

- Number average molar weight (M_n)
- Mass average molar weight (M_w)

It is useful also to define the molecular weight distribution (M_w/M_n) that describes the relationship between the number of moles of each polymer species and the molar mass of that species. The minimum value is 1, but generally the value is always above. It is an instructive parameter because a broad molecular weight distribution is characteristic of a system in which there are different active sites, producing polymers with rather different molecular weights.

Molecular structure

One of the main feature that determines polymer properties is the molecular structure: the monomer of which the polymer is formed by, the repeating units (homopolymer, copolymer, terpolymer), the microstructure, that essentially describes the arrangement of these monomers within the polymer at the scale of a single chain. These basic structural properties play a major role

in determining bulk physical properties of the polymer, which describe how the polymer behaves as a continuous macroscopic material.

In consideration of the fact that polymers are organic molecules with higher molecular weights, it is possible to use the same analytical techniques applied to determine the molecular structure of unknown organic compounds. Spectroscopic techniques (infrared spectroscopy and nuclear magnetic resonance) are used to identify common functional groups.

In particular, the following techniques have been applied:

- Fourier Transformed Infrared Spectroscopy (FTIR) for qualitative analysis of the polymer obtained;
- Nuclear Magnetic Resonance (NMR) for a more detailed determination of the molecular structure, determination of the microstructure and branching degree, monomer enchainment, tacticity, and comonomer content in case of copolymers;
- X-ray Diffraction (XRD) for determining the (co)polymers crystallinity, and, in some cases, the molecular structure.

Thermal properties

The glass transition temperature (T_g) and the melting temperature (T_m) of a polymer (determined through the Differential Scanning Calorimetry, DSC) are two relevant parameters because they determine the applicability of a polymer for certain applications in a given range of temperatures. T_g and T_m are influenced by changes in the compositional and structural parameters of the material, in particular by the tacticity, crystallinity, molecular weight, and comonomer content.

Thermogravimetric analysis (TGA) can also give an indication of the polymer thermal stability and degradation temperature.

1.4 Polymerization Mechanism

In the Ziegler–Natta catalysis the formation of the polymer is the result of multiple monomer insertions into a metal–carbon (Mt–C) bond. Up to now, the so called "Cossee–Arlman mechanism" is one of the main mechanisms proposed for the polymerization of ethylene and α-olefins catalyzed by transition metal complexes (Fig. 5).[19]

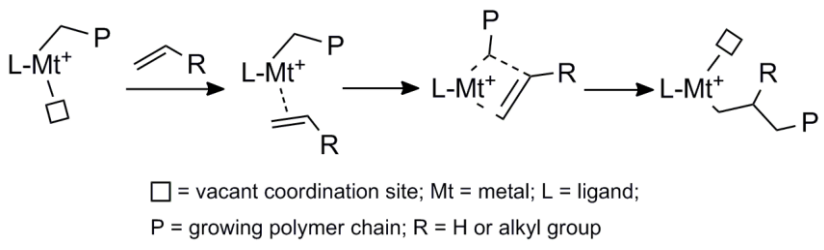

Figure 5 *Coordination/insertion olefin polymerization: the Cossee–Arlman mechanism.*

It occurs in two steps: (*i*) the olefin coordination to a vacant site, and (*ii*) the alkyl migration of the growing chain to the σ–coordinated olefin. At the end of the reaction, a migration of the Mt–P (P = growing polymer chain) σ–bond to the coordination position, previously occupied by the olefin, occurs.

Common features of olefins polymerization catalysts are chain-transfer reactions that terminate the growth of the polymer chain and result in the initiation of a new polymer chain. The most common chain transfer reactions are: (*i*) β–hydrogen elimination, (*ii*) β–alkyl elimination and (*iii*) transalkylation to the aluminium cocatalyst. A detailed description of these reactions is beyond the purpose of this thesis; elegant reviews are published on the topic.[20]

Concerning cyclic olefins, there are different mechanistic paths for the polymerization by transition metal catalysts, that will be discussed more in detail in the following paragraph. It is only worth mentioning here that in the case of ethylene–cyclic olefin copolymerization, the vinyl–addition polymerization leaves the bicyclic structural unit intact, opening only the double bond of the π-component, giving a 2,3-enchainment (see for example Figure 8 in paragraph 1.5). The reactivity of cyclic olefins in the vinyl–addition (co)polymerization is affected by the ring strain of the monomer (which may be quantified calculating the difference in energy of the olefin and the corresponding alkane by force field methods) and by the non-planarity of the reacting double bond (it depends on their possibility to give symmetric or antisymmetric deformation). For these reasons, cyclic olefins with symmetric out-of-plane bending of the double bond protons, such as norbornene and cyclopentene, can be polymerized.

1.5 Different classes of polymers

The classes of polymers are very vast, and potentially as infinite as scientists' creativity.

Within this thesis, the classes investigated are:

- Cyclic olefin homopolymers [(poly(norbornene) and poly(dicyclopentadiene)]
- Cyclic olefins copolymers (COCs)
- Poly(1,3-butadiene)

Cyclic olefin homopolymers [poly(norbornene) and poly(dicyclopentadiene)]

Cyclic olefin homopolymers are a family of specialty and engineering polymers derived from ring shaped molecules that express characteristics different from those of linear co-monomer macromolecules. There are several cyclic monomers that can be used; in this thesis the focus was put on the "norbornene family" (Fig. 6).

Norbornene (NB) (IUPAC name bicyclo[2.2.1]hept-2-ene) is a bridged cyclic hydrocarbon. The molecule consists of a cyclohexene ring with a methylene bridge between C1 and C4. The molecule carries a double bond which induces significant ring strain and significant reactivity. NB is made by Diels–Alder reaction of cyclopentadiene and ethylene; many NB derivatives with substituents in

the 5 and 6 positions [*i.e.*, dicyclopentadiene (DCPD), 5-vinyl-2-norbornene (VyNB), and 5-ethylidene-2-norbornene (ENB), norbornadiene (NBD), Fig. 6] can be prepared similarly.

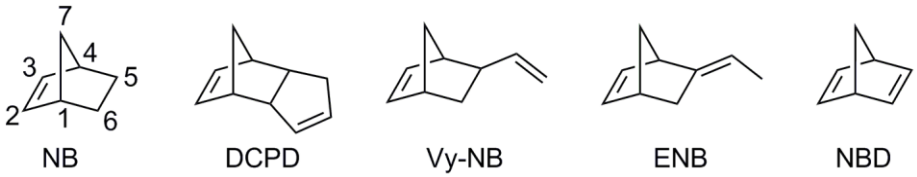

Figure 6 *Norbornene and some 5,6-substituted derivatives.*

NB can be homopolymerized by three different catalytic routes (Fig. 7): (*i*) ring-opening metathesis polymerization (ROMP), which gives polymers containing double bonds within the main chain, (*ii*) vinyl addition polymerization, which gives completely saturated polymer, and (*iii*) cationic polymerization, which gives low–molecular weight products containing rearranged monomer units.[21]

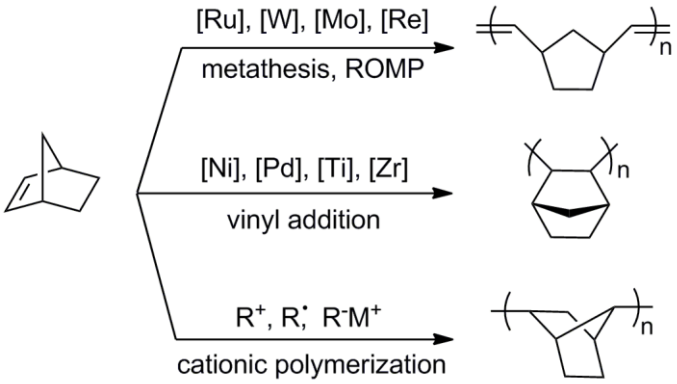

Figure 7 *Schematic representation of the two most common types of NB polymerization.*

Vinyl–type poly(norbornene) (PNB) exhibits properties (high glass transition and decomposition temperature, and excellent transparency as main ones) that make it suitable for optical and electronic applications, for example as cover layer for liquid-crystal displays and as electro-optical material. Due to the industrial relevance of this polymer, much work has been done to identify catalysts for its preparation; a review on the vinyl–addition polymerization of NB has recently appeared.[22]

Most of the catalysts known so far give atactic or low–tactic PNBs, which are amorphous by X-ray examination;[23] however, crystalline PNBs have been obtained as well.[24]

Information on the microstructure of crystalline PNBs is rather scarce, because these polymers are insoluble in chlorinated solvents and NMR data are limited to solid state spectra.

From this the idea of using cyclic non-conjugated diolefins bearing a reactive group that can be subsequently modified, in order to improve some properties such as solubility. Examples of NB derivatives of this type are DCPD, ENB, and Vy-NB and NBD (see Fig. 6).

Cyclic olefins copolymers (COCs)

In the last two decades, considerable attention has been paid to fabricate new polyolefins with specific functions.[15,25] A promising class is the cyclic olefin homopolymers class, as already discussed in the previous paragraph. However, polycycloalkenes from an addition vinyl–type polymerization showed extremely high melting points, even above their decomposition temperatures (in air), and also under vacuum the temperatures were above 600 °C for PNB.[26] Also due to their insolubility in common organic solvents, such polymers are generally difficult to process and are of little commercial interest.

Copolymers based on cyclic olefins and α-olefins (COCs) overcame all these issues for their good processability, good thermal, optical and mechanical properties that made COCs a new class of engineering plastics with several applications.[27] COCs are thermoplastics, ranging from highly crystalline solids to thermoplastic elastomers, whose properties depend on the comonomer content and copolymers microstructure. They are usually obtained through the copolymerization of ethylene with cyclic olefins [*i.e.*, NB, DCPD, and ENB, Fig. 6] promoted by transition metal-based catalysts.

The most versatile and interesting COCs are the copolymers of ethylene with NB [poly(E-*co*-NB)], in which a NB unit is connected to the ethylene inserted unit through the C2–C3 double bond (Fig. 8). These copolymers have gained much attention as high-tech engineering plastics. Indeed, their high transparency in visible and near ultraviolet region, high refraction index, glass transition temperatures up to 220 °C, heat-resistance and good processability make such copolymers useful coatings for high-capacity CDs and DVDs, optical lenses, medical equipments, blisters, toner binder and packaging.[28] Moreover, they are highly resistant to chemicals, including polar solvents, and exhibit a low water absorption and for this reason they are also used as substrate for microfluidic devices.[29]

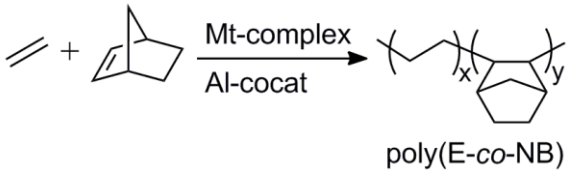

Figure 8 *Schematic synthesis of poly(E-co-NB).*

Nowadays, poly(E-*co*-NB)s have been developed to commercial products under the trade names of APEL®, by Mitsui Chemicals Inc.,[30] and TOPAS® by Ticona Polymers Inc.,[10] now Celanese. The industrially produced copolymers have NB contents in the range from 30 to 60 mol% and T_gs from 120 to 180 °C. It is worth mentioning that copolymers with a higher NB content are often rigid, brittle, and hence with poor mechanical properties. To overcome this limitation, without losing high T_gs, bulky DCPD is employed.[31]

As with all types of copolymers, poly(E-*co*-NB)s can be classified as a function of the monomeric units arrangements along the polymer chain. These include (Fig. 9): (*i*) random (or statistical) copolymers, where the two monomers are present without order in the polymer backbone, (*ii*) alternating copolymers, with regular alternating ethylene and NB units,[32] (*iii*) block copolymers, where to a sequence of ethylene succeeds one of NB or vice versa,[33] (*iv*) graft copolymers, where from a main chain, formed by only one of the two monomers, lateral chains of the second monomer start and (*v*) gradient copolymers, where the monomers composition changes gradually along the chain.[34] All these copolymers exhibit different chemical and physical properties, which in turn are also strongly affected by the (co)monomers ratio.[35]

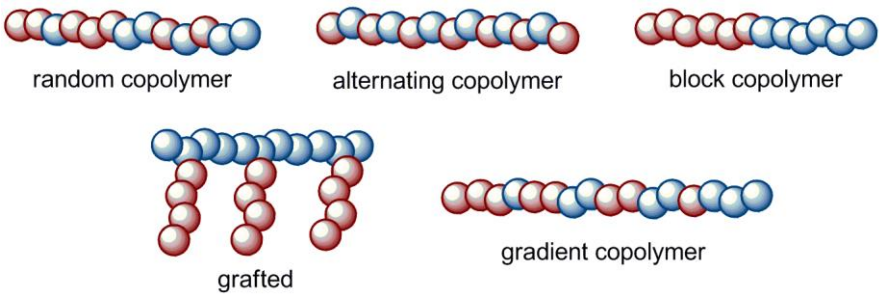

Figure 9 *Different types of copolymer architectures.*

Beyond poly(E-*co*-NB), co- and ter-polymers of ethylene with different cyclic olefins, and in particular with cyclic olefin dienes, is also of great industrial interest in itself. For example, ethylene–propylene–diene terpolymer (EPDM) is a synthetic rubber of great commercial importance,[36] commonly used in seals. Moreover, the presence in the final (co)polymer of unreacted functionalities represents an advantage, since it allows further chemical modification.

Poly(1,3-butadiene)

Poly(1,3-butadiene) (PB) is a synthetic rubber, obtained from the polymerization of 1,3-butadiene, the main and most distinctive member of conjugated dienes. 1,3-butadiene can produce polymers containing different types of monomeric units: *cis*-1,4, *trans*-1,4, and 1,2 (Fig. 10).

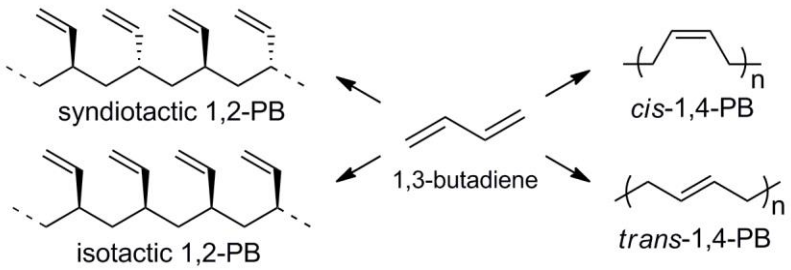

Figure 10 *Different microstructure of stereoregular polymers from 1,3-butadiene.*

1,3-Butadiene can be polymerized with different polymerization methods: radical polymerization, anionic polymerization and stereospecific polymerization. However, the stereoregular PBs (*i.e.*, with a high molar content of one of the monomeric unit *cis*- 1,4, *trans*-1,4, syndiotactic 1,2, or isotactic 1,2) can be obtained only through the stereospecific polymerization using Ziegler–Natta catalysis based on a combination of transition metal and lanthanide compounds with different aluminum alkyls.[37]

Only c*is*-1,4 and syndiotactic 1,2-PB are polymers industrially produced and commercialized. High *cis*-1,4-PB is a polymer with a melting point (T_m) of about –2°C, a crystallization temperature (T_c) around –25°C, and a glass transition temperature (T_g) below –100°C. It is produced with various catalysts based on Ti, Co, Ni and Nd, and its main use is in the manufacture of passenger car and truck tires. Syndiotactic 1,2-PB is a crystalline polymer, with a T_m in the range 200–220°C, depending on its degree of syndiotacticity, with poor solubility characteristics. This stereoregular polymer is obtained with Co–based catalysts, and it is used to make transparent stretch films, tubes, hoses, shoe soles, and various sponges without plasticization and vulcanization.

Trans-1,4-PB instead is a polymer with a T_m at about 80 °C. It was formerly used for the outer layer of golf balls. Today it is little employed industrially, but some companies are investigating other possible applications.

The annual production of PB was 2.1 million tons in 2003. This makes it the second most produced synthetic rubber by volume, behind the styrene–butadiene rubber (SBR).[38]

Following a coordination–insertion polymerization pathway, the Mt–C bond is of allyl-type (η^3–allyl bond), and this particular feature is responsible for the great variety of polymeric structures obtainable in the polymerization of 1,3-dienes. The allylic unit can exist in two forms (*anti* and *syn*), both exhibiting two reactive positions: C1 and C3. Depending on weather the new incoming monomer reacts at C1 or C3, it is possible to obtain respectively a *cis*-1,4 unit (*trans*-1,4 in the case of *syn* coordination) or a 1,2-unit (Fig. 11).[37]

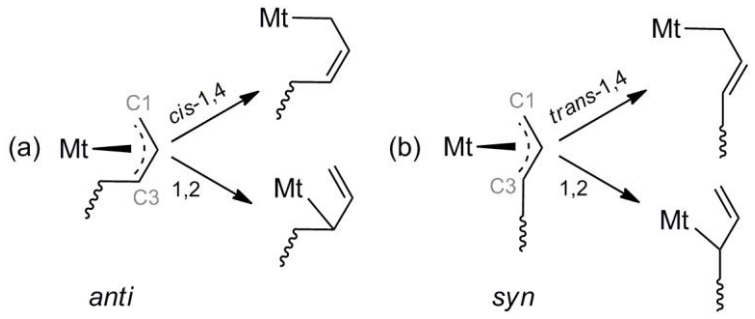

Figure 11 *Formation of 1,4 vs 1,2 monomeric units from (a) anti and (b) syn Mt–η^3–butenyl group.*

1.6 Post–polymerization modification

Synthesis of polyolefins bearing polar functionalities is a long-term challenge: indeed, the introduction of some polar groups in polyolefins is of importance for improving the polymer properties such as adhesion, dyeability, and compatibility with other polymers. In coordination–insertion polymerization, the use of monomers with polar functionalities is limited and applicable only to late transition metal catalysts, which have lower sensitivity to polar monomers. However, the amount of incorporated polar monomer remains low in comparison to other monomers such as α-olefins and cyclic monomers.

Hence, to bypass this problem, a possible solution is the post–polymerization modification, either through solution chemistry or reactive extrusion. The first of these two approaches is feasible when the catalytic system is able to copolymerize monomers bearing reactive groups that have unfavorable interaction with the metal center and that, therefore, are not involved in the polymerization process. Examples are non–conjugated (cyclic) dienes. As already mentioned, this is the approach of choice for increasing the solubility of the family of NB and for inserting some polar functionalities in COCs.

In particular, in this thesis two reactions have been mainly explored to modify the obtained polymeric materials: epoxidation and hydrogenation.

Considering epoxidation, it can be performed either generating *in situ* the peroxidic species[39] or with the aid of organic peroxides, such as *m*-chloroperbenzoic acid.[40] Epoxidation brings to the formation of an oxirane on the (co)monomer moiety, that can be further converted into polar groups by ring opening.

Otherwise, it is possible to hydrogenate the remaining double bond to fully saturated (co)polymers. Hydrogenation of unsaturated cyclic olefin polymers has been largely employed as a means of eliminating the long–term instability of the polymers exposed to air.[41]

Generally, the hydrogenation reaction can be performed following either a catalytic (*e.g.* Pd/C, Rh-Wilkinson catalyst) or non–catalytic (*e.g.* via the *in situ* formation of diimide by thermolysis of *p*-toluensulphonyl hydrazide, *p*TsNH) route. Despite the lower atom economy, this second approach is cheaper, and it allows for easier product purification, since reaction byproducts can be removed by simple polymer extraction with boiling acetone.

References

[1] V. Busico *Dalton Trans.* **2009**, 8794-8802.

[2] Vv. Aa. *Chem. Rev.* **2000**, *100*, 1167-1682.

[3] M.P. McDaniel *Adv. Catal.* **2010**, *53*, 123-606.

[4] (a) M.J. Szwarc *Polym. Sci. Part A: Polym. Chem.* **1998**, *36*, 9-15; (b) G.J. Domski, J.M. Rose, G.W. Coates, A.D. Bolig, M. Brookhart *Prog. Pol. Sci.* **2007**, *32*, 30-92.

[5] (a) L. Guo, S. Dai, X. Sui, C. Chen *ACS Catalysis* **2016**, *6*, 428-441; (b) L.K. Johnson, S. Mecking, M. Brookhart *J. Am. Chem. Soc.* **1996**, *118*, 267-268; (c) L.K. Johnson, C.M. Killian, M. Brookhart *J. Am. Chem. Soc.* **1995**, *117*, 6414-6415.

[6] P. Zinck *Polym. Int.* **2016**, *65*, 11-15. D.J. Arriola *Science* **2006**, *312*, 714–719.

[7] K. Matyajeszewski "*Handbook of Radical Polymerization*" **2002** T.P. Davis, Eds., Wiley–VCH, Hoboken.

[8] "*High Throughput Screening in Catalysis*" **2004**, eds. A. Hagemeyer, P. Strasser and A. F. Volpe, Jr., Wiley–VCH, Weinheim.

[9] (a) S. Honma, K. Tominari, M. Kurisu US Patent **1991**, 5, 019, 627; (b) J.C. Liu US Patent **2004**, 6, 767, 975.

[10] M.J. Brekner, F. Osan, J. Rohrmann, M. Antberg US Patent **1994**, 5, 324, 801.

[11] http://keltan.com/

[12] T.J. Kealy, P. Pauson *Nature* **1951**, *168*, 1039-1040.

[13] H. Sinn, W. Kaminsky, H.-J. Vollmer, R. Woldt *Angew. Chem., Int. Ed.* **1980**, *19*, 390-392.

[14] (a) H.H. Brintzinger, D. Fischer, R. Mülhaupt, B. Rieger, R.M. Waymouth *Angew. Chem., Int. Ed.* **1995**, *34*, 1143-1170; (b) W. Kaminsky *Macromol. Chem. Phys.* **1996**, *197*, 3907–3945. (c) H. Sinn, W. Kaminsky *Adv. Organomet. Chem.* **1980**, *18*, 99–149.

[15] M.C. Baier, M.A. Zuideveld, S. Mecking *Angew. Chem., Int. Ed.* **2014**, *53*, 9722–9744.

[16] (a) L. Guo, W. Liu, C. Chen *Mater. Chem. Front.* **2017**, *1*, 2487-2494; (b) J.M. Eagan, J. Xu, R. Di Girolamo, C.M. Thurber, C.W. Macosko, A.M. LaPointe, F.S. Bates, G.W. Coates *Science* **2017**, *355*, 814-816; (c) D. Peng, X. Yan, C. Yu, S. Zhang, X. Li *Polym. Chem.* **2016**, *7*, 2601-2634. (d) J.P. McInnis, M. Delferro, T.J. Marks *Acc. Chem. Res.* **2014**, *47*, 2545-2557.

[17] L.K. Johnson, C.M. Killian, M. Brookhart *J. Am. Chem. Soc.* **1995**, *117*, 6414-6415.

[18] (a) T.R. Younkin, E.F. Conner, J.I. Henderson, S.K. Friedrich, R.H. Grubbs, D.A. Bansleben *Science* **2000**, *287*, 460-462; (b) B.L. Small, M. Brookhart, A.M.A. Bennet *J. Am. Chem. Soc.* **1998**, *120*, 4049-4050.

[19] (a) P. Cossee, *Tetrahedron Lett.* **1960**, *17*, 12-16; (b) P. Cossee, in "*The Stereochemistry of Macromolecules*", A. D. Ketley, Ed.; Marcel Dekker: New York, **1967**; Vol. 1.

[20] L. Cavallo, G. Guerra, P. Corradini *J. Am. Chem. Soc.* **1998**, *120* , 2429–2436.

[21] C. Janiak, P.G. Lassahn, *J. Mol. Catal. A* **2001**, *166*, 193-209.

[22] F. Blank, C. Janiak *Coord. Chem. Rev.* **2009**, *253*, 827-61.

[23] (a) D. A. Barnes, G.M. Benedikt, B.L. Goodall, S.S. Huang, H.A. Kalamarides, S. Lenhard, L.H. McIntosh III, K.T. Selvy, R.A. Shick, L.F. Rhodes *Macromolecules* **2003**, *36*, 2623-2632; (b) Q. Wu, Y. Lu, *J. Polym. Sci., Part A: Polym. Chem.* **2002**, *40*, 1421-1425; (c) X. Mi, Z. Ma, N. Cui, L. Wang, Y. Ke, Y. Hu, *J. Appl. Polym. Sci.* **2003**, *88*, 3273-3278; (d) S. Borkar, P.K. Saxena, *Polym. Bull.* **2000**, *44*, 167-172; (e) B.L. Goodall, L.H. McIntosh III, L.F. Rhodes *Macromol. Symp.*

1995, *89*, 421-432; (f) F. Pelascini, F. Peruch, P.J. Lutz, M. Wesolek, J. Kress *Macromol. Rapid Commun.* **2003**, *24*, 768-771.

[24] (a) G. Sartori, F. Ciampelli, N. Cameli *Chim. Ind. (Milan)* **1963**, *45*, 1478-1482; (b) W. Kaminsky, A. Bark, M. Arndt *Macromol. Symp.* **1991**, *47*, 83-93; (c) W. Kaminsky, A. Bark, R. Steiger *J. Mol. Catal*. **1992**, *74*, 109-119; (d) W. Kaminsky, A. Noll *Polym. Bull.* **1993**, *31*, 175-182; (e) M. Arndt, W. Kaminsky *Macromol. Symp.* **1995**, *97*, 225-246; (f) M. Arndt, R. Engehausen, W. Kaminsky, K. Zoumis *J. Mol. Catal. A* **1995**, *101*, 171-178; (g) M. Arndt, M. Gosmann *Polym. Bull.* **1998**, *41*, 433-440.

[25] R. Mülhaupt, M. Stürze, S. Mihan *Chem. Rev.* **2016**, *116*, 1398–1433.

[26] W. Kaminsky, A. Bark, I. Dake, in "*Catalytic Olefin Polymerization*" **1990**, T. Keii, K. Soga (Eds.), Kodansha–Elsevier, Tokyo–Amsterdam, p. 425.

[27] (a) X. Li, Z. Hou, *Coord. Chem. Rev.* **2008**, *252*, 1842–1869. (b) I. Tritto, L. Boggioni, D.R. Ferro *Coord. Chem. Rev.* **2006**, *250*, 212–241.

[28] R.R. Lamonte, D. Mc Nally *Adv. Mater. Processes* **2001**, *3*, 33–36.

[29] S.P. Nunes, P.D. Ohlsson, O. Ordeig, P.J. Kutter *Microfluid. Nanofluid.* **2010**, *9*, 145–161.

[30] *Modern Plastics* **1995**, *72*, 137.

[31] M. Hong, L. Cui, S. Liu, Y.S. Li *Macromolecules* **2012**, *45*, 5397–5402.

[32] C. De Rosa, A. Buono, F. Auriemma, A. Grassi *Macromolecules* **2004**, *37*, 9489–9502.

[33] Z. Hou *Angew. Chem. Int. Ed.* **2005**, *6*, 962–965.

[34] P.J. Xiang *Polym. Sci., Part A: Polym. Chem.* **2013**, *51*, 672–686.

[35] M. Kryszewski *Adv. Polym. Tech.* **1998**, *9*, 244–259.

[36] G. Van der Velden *Macromolecules* **1983**, *16*, 85-89.

[37] G. Ricci, G. Leone *Polyolefins Journal* **2014**, *1*, 43-60.

[38] L. Friebe, O. Nuyken, W. Obrecht *Adv. Polym. Sci.* **2006**, *204*, 1-154.

[39] B.C. Peoples, V.N. Dougnac, G.B. Galland, F.M. Rabagliati, R. Quijada *Poly. Bull.* **2012**, 69, 925-935.

[40] J. Suzuki, Y. Kino, T. Uozumi, T. Sano, T. Teranishi, J. Jin, K. Soga, T. Shiono *J. Appl. Polym. Sci.* **1999**, *72*, 103-108.

[41] J.G. Hamilton, K.J. Ivin, J.J. Rooney *J. Mol. Catal. A: Chem.* **1986**, *36*, 115-125; (b) S. Hayano, Y. Takeyama, Y. Tsunogae, I. Igarashi *Macromolecules* **2006**, *39*, 4663-4670; (c) M. Yamazaki *J. Mol. Catal. A: Chem.* **2004**, *213*, 81-87; (d) B. Al-Samak, V. Amir-Ebrahimi, A.G. Carvill, J.G. Hamilton, J. Rooney *Polym. Int.* **1996**, *41*, 85-92; (e) L.W. Lee, R.A. Register *Macromolecules* **2005**, *38*, 1216-1222.

Chapter 2
Motivation

Research on catalysis for polymers: is it still worth it?

The global production of plastics has been a sector in continuous growth for more than 50 years, and still nowadays. In 2016 the global production of plastic materials (thermoplastics and polyurethanes) and other plastics (thermosets, adhesives, coatings and sealants) was of 335 millions of tons (Fig. 1).[1] More than a half of these plastic materials are polyolefins intended mainly for packaging, buildings and automotive sectors. These polyolefins are produced with "traditional" heterogeneous catalysts (Ziegler–Natta and Phillips catalysts); a small portions is constituted by high performance polymers for high-engineering and technical applications.

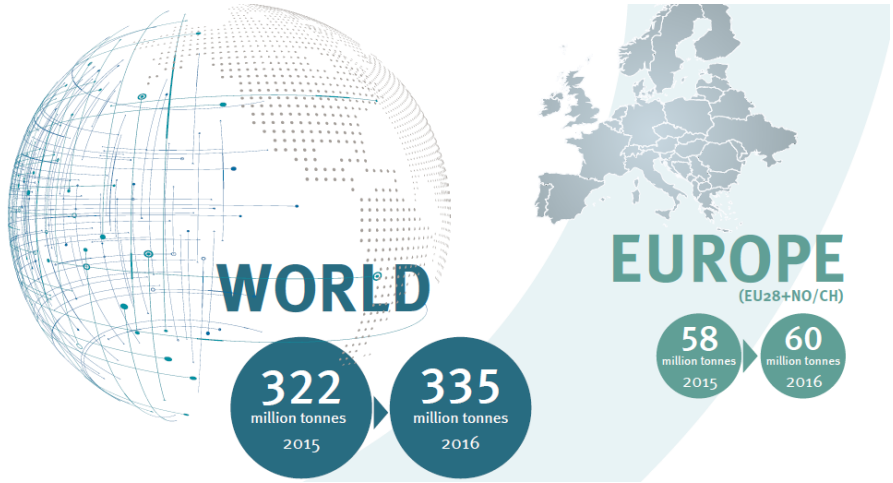

Figure 1 *World and EU plastics production data (Source PlasticsEurope (PEMRG) / Conversio Market & Strategy GmbH).*

In parallel to the industrial production, the research activity on polymeric materials keeps on growing as well: the research for new catalytic systems for polymer synthesis is still of great interest, as demonstrated also by the considerable number of research groups involved, and articles and reviews published, as reported in the table below (number of publications in given topics and year ranges according to the *Web of Science*).

		Number of pubblications	
Entry	***Topic searched***	***2013–2017***	***2018***
1	Olefin polymerization	2892	527
2	Ethylene polymerization	7927	1369
3	Traditional Ziegler–Natta catalyst	753	156
4	Metallocene catalyst	812	132
5	Functionalized polymers	12850	2807

As many researchers and scientists pointed out in interesting perspective articles,[2] there is still room for research on this topic, and there are at least three good reasons to further invest in research: (*i*) the endeavor towards the development of cost–effective processes involving molecular catalysts, that are now too high for application in the market and not competitive with the traditional Ziegler–Natta catalysts, (*ii*) the synthesis of specialties like the new olefin block copolymers or technopolymers for advanced and unpredictable applications, and (*iii*) an intensive understanding of structure–property relations of the existing precision polymers and polymers that came from nature, from which we can get an idea of what can be possible in the future.

Then the answer is yes, it is still worth it.

The PhD research activity: the initial aim and the project development

At the beginning of this three–year research project, the aim was to synthetize and characterize polymeric materials based on cyclic olefins, in particular within the field of materials for gas storage, that up to some years ago were constituted mainly of inorganic compounds, like zeolites and silicates. Substituting them with organic materials has some nice advantages, for instance lightness, low costs and easier processability. Some interesting materials for this purpose have been obtained in the last decades (*e.g.* syndiotactic poly(styrene) (sPS),[3] poly(2,6-dimethyl-1,4-phenyleneoxide) (PPO),[4] and aerogels of sPS and PPO[5]), proving the applicability of these polymeric materials.

Another promising class of polymers for this type of application is norbornene–derived polymers. Preliminary data on poly(norbornene) were obtained by professor Porri *et al.*, who first synthesized and characterized the disyndiotactic poly(norbornene) (sPBN).[6]

The synthesis of new catalytic systems able to stereochemically drive the reaction, and as a consequence fine tuning the polymer properties, and the synthesis of new polymers from cyclic olefins were the strategies that were set out to follow to achieve the initial aim. As the research activity went on, good and encouraging developments came out, together with some unexpected but still defying ones.

In this thesis, the main results obtained are presented, together with the challenges encountered and tackled, especially concerning the oxidation state of the metals and complexes stability.

Various and new organometallic complexes were synthesized and characterized, with a special focus on first row transition metals, namely titanium, vanadium, chromium, and ligands with nitrogen and phosphorous donor atoms, to examine the effects of the structure of the investigated complexes on the catalytic activity. Indeed, the resultant complexes were applied, in combination with an aluminum alkyl as activator, as catalysts for the synthesis of ethylene, cyclic olefins, and 1,3-butadiene (co)polymers.

All the synthesized polymers were carefully characterized with different techniques, in order to get more information about the polymerization mechanism, and their chemical, thermal and mechanical properties.

At the same time, the post–polymerization modification was attempted and applied to some unsaturated polymers to introduce polar functionalities in the main polymer chain backbone. The final goal was to increase the solubility and the processability of the obtained polyolefins as well as to enhance the miscibility with other plastics. This is a very important goal since nowadays the plastics on the market are blends of several polymers, even of different nature.

The work carried out within this PhD project is hereafter presented as follows:

- Chapter 3 contains the main and general experimental procedures;
- Chapter 4 describes the Ti–catalyzed polymerization of cyclic olefins (dicyclopentadiene and norbornadiene), and a study on the influence of the conformation of dicyclopentadiene isomers on the reaction outcome;
- Chapter 5 reports on the synthesis of a series of vanadium(III) and vanadium(IV) complexes ligated by phosphine and imido ligands and their use in the (co)polymerization of ethylene with cyclic olefins (norbornene, dicyclopentadiene and 5-ethylidene-2-norbornene);
- Chapter 6 is devoted to chromium, and in particular to the synthesis of chromium(II) and chromium(III) complexes with iminopyridine ligands and their use in the polymerization of various (di)olefins;
- Chapter 7 presents some general conclusions;
- Chapter 8 briefly describes the other research projects in which I was involved;
- Chapter 9 suggests some perspectives for future research activity from both a scientific and personal point of view.

Each chapter is introduced by the "Chapter highlights", illustrating the main results achieved, and a brief overview of the state-of-the-art on the specific topic.

References

[1] "*Plastics – the Facts 2017*" PlasticsEurope, www.plasticseurope.org

[2] (a) W. Kaminsky *Macromol. Chem. Phys.* **2008**, *209*, 459-466; (b) V. Busico *Dalton Trans.* **2009**, 8794-8802; (c) B. Voit *Angew. Chem. Int. Ed.* **2017**, *56*, 2810-2812; (d) K. Matyjaszewski *Chemistry International*, **2017**, *39*, 7-11.

[3] (a) O. Tarallo, A. Buono, V. Califano, V. Petraccone *Macromol. Symp.* **2003**, *203*, 123-130; (b) C. De Rosa, A. Buono, A. Ricci, F. De Luca, L. Caporaso *Macromolecules* **2003**, *36*, 6389-6400; (c) G. Guerra, G. Mensitieri, V. Venditto, E. Reverchon, C. Daniel US Patent **2004** 10, 565, 433.

[4] C. Daniel, S. Logno, G. Fasano, J. Vitillo, G. Guerra *Chem. Mater.* **2011**, *23*, 3195-3200.

[5] (a) C. Daniel, D. Alfano, V. Venditto, S. Cardea, E. Reverchon, D. Larobina, G. Mensitieri, G. Guerra *Adv. Mater.* **2005**, *17*, 1515-1518; (b) C. Daniel, D. Sannino, G. Guerra *Chem. Mater.* **2008**, *20*, 577-582; (c) C. Daniel, S. Giudice, G. Guerra *Chem. Mater.* **2009**, *21*, 1028-1034.

[6] (a) L. Porri, S.V. Meille, A. Famulari, A. Buono, G. Ricci Italian Patent **2008**, MI2008A001944; (b) A. Buono, A. Famulari, S.V. Meille, G. Ricci, L. Porri *Macromolecules* **2011**, *44*, 3681-3684.

Chapter 3
Materials & Methods

The organometallic complexes and the Lewis acids employed are sensible to the presence of polar impurities like oxygen and humidity; the collateral reactions with these impurities produce deactivation of the catalyst. Because of this high affinity to polar substances, all the experiments were conducted with a dual vacuum/nitrogen line and standard Schlenk–line techniques, consisting in using Schlenk–type glassware and high vacuum lines (10^{-6} Torr) with atmospheric pressure nitrogen, and dry and distilled solvents, monomers and reagents.

3.1 Materials and chemicals

Gasses

Ethylene and nitrogen were purified by passage over columns of $CaCl_2$ and molecular sieves. Oxygen was removed by fluxing the gases through BTS catalysts.

Solvents

THF (Sigma-Aldrich, ≥99.9%) was refluxed over Na/benzophenone alloy for 8 h, and then distilled and stored over molecular sieves. Toluene (Sigma-Aldrich, 99.5%) was refluxed over Na for 8 h, and then distilled and stored over molecular sieves. Heptane (Sigma-Aldrich, 99%) was dried by refluxing for about 10 h over K-diphenylketyl and then distilled and stored over molecular sieves under nitrogen. Pentane (Sigma-Aldrich, 99%) was refluxed over Na/K alloy for 5 h, and then distilled and stored over molecular sieves. Diethyl ether (Sigma-Aldrich, >99.8%) was refluxed over Na/K alloy, distilled and collected when needed. Dichloromethane (Sigma-Aldrich ≥99.9%) was degassed under vacuum then by bubbling nitrogen, kept over molecular sieves and used without any further purification. Deuterated solvent for NMR measurements ($C_2D_2Cl_4$) (Sigma-Aldrich, >99.5% atom D), was used as received.

Monomers

Norbornene (NB) (Sigma-Aldrich, 99%) was stirred over molten potassium at 80 °C under nitrogen for 4h, and then distilled. A stock solution was prepared by dissolving 50 g of freshly distilled norbornene in 86.2 mL of toluene (0.58 g mL^{-1}). 5-Vinyl-2-norbornene (VyNB) (Sigma-Aldrich, 95%), 5-ethylidene-2-norbornene (ENB) (Sigma-Aldrich, 99%) and dicyclopentadiene (DCPD) (Sigma-Aldrich, 95%) were dried over CaH_2 at 60 °C under nitrogen for 4h and distilled under reduced pressure. VyNB, ENB and DCPD were of commercial grade (mixtures of *endo* and *exo* isomers). *endo*-, *exo*-DCPD, and H-DCPD (ChemSapCo) were dried over CaH_2 at 60 °C under nitrogen for 4 h and then distilled under reduced pressure. 1,3-Butadiene (Sigma-Aldrich ≥99%)

was evaporated from the container prior to each run and condensed into the reactor which had been precooled to –20 °C. Cyclohexene oxide (CHO) (Sigma-Aldrich, 98% pure) was dried over CaH_2, distilled under reduced pressure and stored under nitrogen. Succinic anhydride (SA) (Sigma-Aldrich, ≥99% pure) was used as received without further purification.

Organic ligands

Phosphinic ligands (dimethylphenylphosphine (PMe_2Ph) (Strem, 99%), methyldiphenylphosphine ($PMePh_2$) (Strem, 99%), triphenylphosphine (PPh_3) (Sigma-Aldrich, ≥95%), tricyclohexylphosphine (PCy_3) (Strem, 97%), tri-tert-butylphosphine ($PtBu_3$) (Sigma-Aldrich, 95%), 1,2-bis(dimethylphosphino)ethane (dmpe) (Sigma-Aldrich, 97%), 1,2-bis(diethylphosphino)ethane (depe) (Sigma-Aldrich, 97%), 1,2-bis(diphenylphosphine)ethane (dppe) (Sigma-Aldrich, 99%),) were used as received without further purification.

Iminopyridine ligands were synthesized following the methodology previously reported.[1]

Other chemicals

Ethyltrichloro acetate (ETA, Sigma-Aldrich, 97%) was stirred over CaH_2 for about 4 hours, and then distilled under reduced pressure. Diethylaluminum chloride (Et_2AlCl, Sigma-Aldrich, 97%), methylaluminoxane (MAO, Sigma-Aldrich, 7 wt% aluminum in toluene), *p*-toluensulphonyl hydrazide (*p*-TsNH, Sigma-Aldrich, 97%), 4-(*N*,*N*-dimethylamino)pyridine (DMAP) (Sigma Aldrich, ≥99% pure) were used as received without further purification. *m*-Chloroperbenzoic acid (*m*-CPBA, Sigma-Aldrich, ≤77%) was purified according to literature.[2]

Complexes precursors $TiCl_4$ (Sigma-Aldrich, 99.95% pure), $CrCl_2$ (Sigma-Aldrich, 99.99%), $VCl_3(THF)_3$ (Sigma-Aldrich, 97%) were used as received without further purification. $CrCl_3(THF)_3$ was prepared as reported in the literature,[3] through Soxhlet extraction of anhydrous $CrCl_3$ with boiling THF through the aid of Zn dust.

3.2 General polymerization procedures

General cyclic olefin polymerization procedure

Polymerizations were carried out in a 25 mL Schlenk flask. Prior to starting polymerization, the reactor was heated to 110 °C under vacuum for 1 h and backfilled with nitrogen. The reactor vessel was charged at room temperature with the solvent (heptane or toluene), the appropriate amount of monomer, and then brought to the desired temperature. The reaction was started by adding the Al–activator and the pre-catalyst (as toluene solution, 2 mg mL^{-1}) in that order, and stopped with methanol containing a small amount of hydrochloridric acid. The precipitated products were collected by filtration, repeatedly washed with fresh methanol and finally dried in vacuum at room temperature to constant weight. When required, the materials were fractionated by extraction with boiling solvents with a Kumagawa extractor.

General ethylene – cyclic olefin (co)polymerization procedure

Polymerizations were carried out in a 50 mL round-bottom Schlenk flask. Prior to starting polymerization, the reactor was heated to 110 °C under vacuum for 1 h and backfilled with nitrogen. The reactor was charged at room temperature with toluene, the selected cyclic olefin comonomer, ETA and Et_2AlCl in that order. After thermal equilibration at the desired temperature, the solution was degassed, and ethylene was added until saturation. Polymerization was started by adding a toluene solution (2 mg mL^{-1}) of organometallic complex via syringe under continuous flow of ethylene. Polymerizations were stopped with methanol containing a small amount of hydrochloric acid; the precipitated polymers were collected by filtration, repeatedly washed with fresh methanol and finally dried in vacuum at room temperature to constant weight.

Ethylene concentration in toluene was calculated according to Henry's law:

$$C_E = P_E \times H_0 e^{\frac{\Delta H_L}{RT}}$$

where C_E = ethylene concentration (mol L^{-1}); P_E = ethylene pressure (atm); H_0 = Henry coefficient = 0.00175 mol L^{-1} atm^{-1}; ΔH_L = enthalpy of solvatation of ethylene in toluene = 2569 cal mol^{-1}; R = 1.989 cal mol^{-1} K^{-1}.

Concerning the concentration of comonomer in the feed, knowing the ethylene concentration for each experimental condition, it is possible to calculate the required amount of comonomer according to the proper comonomer/ethylene ratio for the specific experiment. As an example, in the case of ethylene-norbornene copolymers, it is possible to determine the NB feedstock percentage from the following equation:

$$\frac{[\mathrm{NB}]}{[\mathrm{E}]} = a \qquad [\mathrm{E}] = 1/a\,[\mathrm{NB}]$$

$$\mathrm{NB}(\%) = \frac{[\mathrm{NB}]}{[\mathrm{NB}]+[\mathrm{E}]} \times 100 = \frac{[\mathrm{NB}]}{[\mathrm{NB}](1+1/a)} \times 100 = \frac{1}{1+1/a} \times 100$$

Polymerization of 1,3-Butadiene

Polymerizations were carried out in a 25 mL Schlenk flask. Prior to starting polymerization, the reactor was heated to 110 °C under vacuum for 1 h and backfilled with nitrogen. 1,3-Butadiene was condensed into the Schlenk flask kept at −20 °C, then toluene was added and the solution was brought to the desired polymerization temperature. The aluminum alkyl and a toluene solution (2 mg mL^{-1}) of the organometallic complex were then added in that order. Polymerization was stopped with methanol containing a small amount of hydrochloric acid. The polymer obtained was then coagulated by adding 60 mL of a methanol solution, repeatedly washed with fresh methanol and finally dried in vacuum at room temperature to constant weight.

Polymer fractionation

Since a polymer sample is given by a mixture of numerous individual chains characterized by different chain lengths, microstructure and tacticity, sometimes it becomes necessary to have more information about the mixture composition. This can be made through polymer fractionation. In this procedure, the polymers were fractionated by boiling solvent extraction with a Kumagawa extractor. The polymerization products were first extracted for about 16 h with different solvents, generally following the order: acetone, diethyl ether, heptane, toluene. From each extraction step it is possible to recover the soluble and insoluble fraction.

3.3 General post–polymerization modification procedures

Hydrogenation

The hydrogenation was performed by diimine generated *in situ* via thermal decomposition of *p*-TsNH, according to the procedure reported in literature.[4] The starting material was dissolved in hot *o*-xylene (20 mg mL^{-1}) in a round-bottom flask equipped with a stirring bar under nitrogen atmosphere; then *p*-TsNH (4 equivalents per monomeric unit bearing a double bond) was added to the reaction vessel and refluxed at 130 °C for 7 h. The reaction mixture was poured in methanol; the precipitated polymer was washed with fresh methanol and dried at room temperature to constant weight. The hydrogenated product was subsequently purified by extraction with boiling acetone for 8 h to remove reaction byproducts and give the acetone residue polymer.

Epoxidation

The epoxidation was performed according to the literature.[5] The starting product was dissolved in toluene (10 mg mL^{-1}) in a round-bottom flask equipped with a stirring bar under nitrogen atmosphere. The reaction mixture was heated at 55 °C until the polymer was completely dissolved. The corresponding amount of *m*-CPBA (2 equivalents per monomeric unit bearing a double bond) was dissolved in toluene (8 g mL^{-1}) and the acid solution was added dropwise in the reaction mixture, and left stirring at 55 °C for 5 h. The reaction mixture was poured in methanol; the precipitated product was washed with fresh methanol and dried at room temperature to constant weight. The epoxidized product was subsequently purified by extraction with boiling acetone for 8 h to remove reaction byproducts and give the acetone residue polymer.

3.4 Complexes characterization

The synthesized complexes were characterized via elemental analysis, attenuated total reflectance Fourier transform infrared spectroscopy (ATR–FTIR), and, when possible, single crystal X-ray diffraction.

Elemental analysis were performed by using a Perkin–Elmer CHN Analyzer 2400 Series II.

ATR–FTIR spectra were recorded at room temperature in the 4000–600 cm^{-1} range with a resolution of 4 cm^{-1} using a Perkin-Elmer Spectrum Two spectrometer. The diffraction data for chromium and vanadium(III) bidentate-phosphine complexes were recorded at 100 K and at room temperature, respectively, using a Bruker X8 Prospector APEX-II/CCD diffractometer equipped with a focusing mirror (Cu-Kα radiation, λ = 1.54056 Å). The structures were determined using direct methods and refined (based on F^2 using all independent data) by full-matrix least-square methods (SHELXTL-97).[6] All non-hydrogen atoms were located from different Fourier maps and refined with anisotropic displacement parameters. Hydrogen atoms were added in riding positions.

The diffraction data for vanadium(III) monodentate-phosphine complexes were collected on a Bruker Smart Apex CCD area detector using graphite-monochromated Mo Kα radiation (λ = 0.71073 Å). Data reduction was made using SAINT programs; absorption corrections based on multiscan were obtained by SADABS.[7] The structures were solved by SHELXS-97,[6] and refined on F^2 by full-matrix least-squares using SHELXL-14.[8] All the non-hydrogen atoms were refined anisotropically, hydrogen atoms were included as 'riding' and not refined. The isotropic thermal parameters of H atoms were fixed at 1.2 (1.5 for methyl groups) times the equivalent thermal parameter of the atoms to which they are bonded.

The diffraction data for vanadium(IV) imido complexes were recorded at 180 K on a Bruker Kappa APEX II using molybdenum (λ = 0.71073 Å) and equipped with an Oxford Cryosystems cooler device or an Oxford Cryosystems Cryostream Cooler Device. The unit cell determination and data integration were carried out using CrysAlis RED package or APEX II.[9] The structures have been solved by Direct Methods using SIR92,[10] and refined by least-squares procedures with SHELXS-2016.[11]

3.5 Polymers characterization

In order to give insight into the catalytic process and properties, all the (co)polymers obtained were fully characterized with the aid of different techniques, to determine polymer properties, such as the molecular weight, microstructure and branching degree, morphology, thermal properties, and mechanical properties.

The analytical techniques used in this thesis work are:

- Infrared spectroscopy, for preliminary and qualitative analysis;
- Size Exclusion Chromatography (SEC) to evaluate the molecular weight (M_w) and the molecular weight distribution (M_w/M_n);
- ^1H and ^{13}C NMR spectroscopy to evaluate the microstructure, and eventually to calculate the content of co-monomer in the polymeric chain;

- Differential Scanning Calorimetry (DSC) and Thermo Gravimetric Analysis (TGA) to observe the thermal properties (glass transition temperature (T_g), melting temperature (T_m), and crystallization enthalpy (ΔH_c));
- Wide-angle X-ray diffraction (XRD) spectroscopy to determine the crystallinity degree and crystal structure when possible.

ATR–FTIR spectra were recorder at room temperature using a Perkin-Elmer Spectrum Two in the spectral range of 4000–450 cm^{-1}.

NMR spectra were recorded on a Bruker NMR advance 400 Spectrometer equipped with a SEX 10 mm probe with automatic matching and tuning, operating at 400 MHz (^1H) and 100.58 MHz (^{13}C) working in the PFT mode at 103°C. Experiments were performed dissolving 70 mg of polymer in $C_2D_2Cl_4$ in a 10 mm tube and referred to HMDS as internal standard.

Molecular weights and molecular weight distributions were obtained by a high temperature Waters GPCV2000 size exclusion chromatography (SEC) system using an online refractometer detector. The experimental conditions consisted of three PL Gel Olexis columns, *ortho*-dichlorobenzene as the mobile phase, 0.8 mL min^{-1} flow rate, and 145 °C temperature. The calibration of the SEC system was constructed using eighteen poly(styrene) standards with molar weights ranging from 162 to 5.6×10^6 g mol^{-1}. For SEC analysis, about 12 mg of polymer was dissolved in 5 mL of *ortho*-dichlorobenzene with 0.05% of BHT as antioxidant.

Differential scanning calorimetry (DSC) measurements were performed on a Perkin–Elmer DSC 8000 instrument equipped with a liquid nitrogen device. The scans were carried out from –100 to 200 °C under nitrogen atmosphere using heating and cooling rates of 20 °C min^{-1}. Thermogravimetric analysis (TGA) was performed on a Perkin–Elmer TGA-7 instrument under a nitrogen atmosphere. Before performing the TGA run, the sample (2–3 mg) was held at 50 °C for 30 min; the scan was carried out from 50 to 700 °C at a heating rate of 10 °C min^{-1}. Wide-angle X-ray diffraction (XRD) experiments were performed at 25°C under nitrogen flux, using Siemens D-500 diffractometer equipped with Soller slits (2°) placed before sample, 0.3° aperture and divergence windows, and VORTEX detector with extreme energy resolution specific for thinner films. Cu-Kα radiation at 40 KV x 40 mA power was adopted; each spectrum was carried out with steps of 0.05° (2θ) and 6s measure time.

3.6 Microstructure determination via NMR spectroscopy

The comonomer content and copolymer microstructure were established by both ^1H and ^{13}C NMR spectroscopy. Many helpful papers appeared in the literature concerning peaks assignment and detailed microstructure analysis.

This section has been divided according to the classes of (co)polymers, and a careful description of the microstructure determination is reported.

3.6.1 Cyclic olefin polymers [poly(norbornene) and poly(dicyclopentadiene)]

In this thesis, only vinyl–type cyclic olefin homopolymers (NB and DCPD) have been investigated. As already mentioned in paragraph 1.5, information on the microstructure of the PNBs from NMR spectroscopy is rather scarce, because these polymers show low solubility in chlorinated solvents. Hence, when possible, other techniques that do not require the dissolution of the sample in solvents, such as FTIR or XRD, were used to resolve the structure.

Some papers appeared in the literature in recent years by Porri *et al.*, who studied and determined the microstructure of crystalline oligomers and polymers of NB,[12] and oligomers of DCPD[13] using a combination of different analytical and computational techniques.

The NMR spectra of both NB and DCPD polymers present many and broad peaks, due to the low solubility in deuterated solvents; however peak assignment was possible on the basis of ^{13}C DEPT experiments and by comparison with ^{13}C NMR chemical shifts of PNBs already reported in the literature,[14] and it is reported in the Table, distinguished for tacticity. An example of ^{13}C NMR spectrum of PNB is also reported in Figure 1.

C atom	chemical shift (ppm)	
	mr	***rr***
C5	28.2	30.3–28.7
C6	29.0	30.3–28.7
C7	33.3	34.9–35.5
C4	37.8	36.5–37.2
C1	38.6–41.0	36.5–37.2
C3	45.7	44.1–49.7
C2	49.8	44.1–49.7

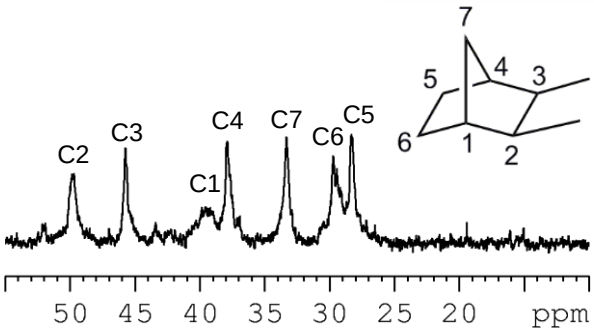

Figure 1 *^{13}C NMR spectrum of PNB and carbon assignment as reported in the table.*

Since DCPD can be considered as a NB derivative, by structural analogy with NB it is possible to resolve the NMR spectrum of the corresponding polymer. There are however, some differences in the resonance of some carbon atoms (*e.g.*, C5 and C6 undergo a downfield shift), in the presence of another carbon atom in the aliphatic region (C10), and in the olefinic region for the presence of the two residual sp^2 carbon atoms of the cyclopentenyl moiety (128–131 ppm).

3.6.2 Cyclic olefins copolymers (COCs)

Poly(E-*co*-NB)

^{13}C NMR spectroscopy is the most useful tool for microstructural investigation of cyclic olefin copolymers: a detailed analysis of the spectrum permits to determine the microstructure of the copolymer and, as a consequence, kinetic copolymerization parameters (*i.e.*, the reactivity ratios)

and polymerization mechanisms. However, in the case of E/NB copolymers, the spectra are quite complex for the presence of two stereogenic centers per NB unit (the C5 and C6 atoms). Luckily, in the past years a number of groups accepted the challenge of carefully assign the numerous peaks in the spectrum.

In general, the ^{13}C NMR resonances of poly(E-*co*-NB) fall into four areas that can be assigned as follow: 42.0–54.0 ppm, C2/C3; 34.5–42.0 ppm, C1/C4; 31.0–34.5 ppm, C7; 26.0–31.0 ppm, C5/C6 and ethylene CH_2. The region of the ethylene resonances (27.7 ppm CH_2 for the homopolymer) overlaps with the region of C5/C6 carbon atoms of NB (from 26.2 to 30.6 ppm). Hence, generally, the NB content in the copolymers is calculated from ^{13}C NMR as the ratio between the average intensities for carbons C1, C2, and C7 and the total intensity for the CH_2 carbons (carbons C5/C6 and E) with the equation:[16]

$$\text{NB}\ (mol\%) = \frac{[\text{NB}]}{[\text{NB}] + [\text{E}]} = \frac{{}^{1}/_{3}\,(I_{C1} + I_{C2} + 2I_{C7})}{I_{CH_2}} \times 100$$

Early studies demonstrated that in the case of coordination/insertion copolymerization of ethylene, NB is enchained by *cis*-2,3-*exo* addition (Fig. 2).[17]

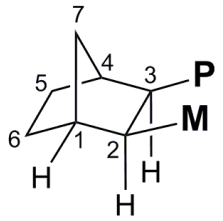

Figure 2 *Schematic representation of a cis-2,3-exo NB enchained unit (M = metal, P = growing polymer chain).*

Poly(E-*co*-DCPD)

With the exception of the olefinic region (120–140 ppm), the ^{13}C NMR spectrum of poly(E-*co*-DCPD) is somewhat similar to that of poly(E-*co*-NB). The peaks at 130.62 and 128.87 ppm in ^{13}C NMR spectrum as well as those at 5.56 and 5.44 ppm in the ^{1}H NMR spectra were assigned to sp^2 C and H atoms, respectively, revealing that the copolymers contained unreacted cyclopentene units.[18] This suggests that the reaction took place selectively at the C2–C3 double bond, and that no crosslinking occurred. The microstructure of the E/DCPD copolymers was determined via the ^{13}C NMR spectrum, according to the literature.[19,20] The dominant signals are those at 51.69 (C9), 44.46 (C6), 42.83 (C7), 40.86 (C4), 38.97 (C8), 35.98 (C5), 34.27 (C10), and 30.54 (C3) ppm assigned to isolated DCPD units, while a number of weak signals at 45.03 (C6), 43.32 (C7), 39.64 (C8) and 36.61 (C5) ppm are characteristic of alternating sequences.

The comonomer content is calculated from the ^{1}H NMR spectrum as reported in the literature[20] with the following equation:

$$\text{DCPD}\ (mol\%) = \frac{[\text{DCPD}]}{[\text{DCPD}] + [\text{E}]} = \frac{4I_B}{I_A} \times 100$$

where I_A is the integral of the region between 0.5 and 1.7 ppm and I_B is the integral of the region at 3 ppm.

Poly(E-*co*-ENB)

The same considerations reported for poly(E-*co*-DCPD) can be referred also to E/ENB copolymers. In this case, in the olefinic region it is possible to identify the carbon atoms of the two isomers of ENB, in a E/Z molar ratio similar to that of the monomer, thus meaning that both isomers copolymerize with ethylene equally.

The dominant signals are those in the regions at 144–145 and 108–109 ppm (the sp^2 C5 and C8 carbon atoms respectively), 48.0–50.0 ppm (C4), 42.0–46.0 ppm (C1/C3, with the signals ascribed to C3 located at the higher field), 34.0–38.0 ppm (C6), 31.0–33.0 ppm (C7), 27.0–30.0 ppm (C10/C11 and ethylene CH_2) and 11.5–12.5 ppm (C9).[21]

The comonomer content is calculated from the ^{1}H NMR spectrum as reported in the literature[22] with the following equation:

$$\text{ENB}(mol\%) = \frac{[\text{ENB}]}{[\text{ENB}] + [\text{E}]} = \frac{I_B}{{}^1\!/_4\,(I_A - 11I_B) + I_B} \times 100$$

where I_A is the integral of the region between 4.8 and 5.3 ppm and I_B is the integral of the region between 0.5 and 3.5 ppm.

3.6.3 Poly(1,3-butadiene)

As already discussed in paragraph 1.5, 1,3-butadiene can polymerize following different pathways, bringing to the formation of a polymer containing different types of monomer units: *cis*-1,4, *trans*-1,4, and 1,2; moreover, in the case of 1,2 unit, as a consequence of the formation of a stereocenter for each unit, isotactic and syndiotactic units can be formed. NMR analysis of poly(1,3-butadiene) is very relevant to understand the type of polymer obtained and the possible applications, and also to shed light on the region- and stereoselectivity of each catalyst.

Important information on the microstructure can be obtained from the analysis of both the ^{1}H and ^{13}C NMR spectrum. Peak assignment was made according to the literature.[23]

References

[1] A. Köppl, H.G. Alt *J. Mol. Catal. A: Chem.* **2000**, *154*, 45-53.

[2] C. W. Bielawski, R.H. Grubbs *Prog. Polym. Sci.* **2007**, *32*, 1-29.

[3] J.Y. Jeon, J.H. Park, D.S. Park, S.Y. Park, C.S. Lee, M.J. Go, J. Lee, B.Y. Lee *Inorg. Chem. Commun.* **2014**, *44*, 148-150.

[4] B. Autenrieth, R.R. Schrock *Macromolecules* **2015**, *48*, 2493-2503.

[5] J. Suzuki, Y. Kino, T. Uozumi, T. Sano, T. Teranishi, J. Jin, K. Soga, T. Shiono *J. Appl. Polym. Sci.* **1999**, *72*, 103-108.

[6] (a) G.M. Sheldrick *SHELXTL Reference Manual* **1996**, Siemens Analytical X-ray Systems, Inc., Madison, Wisconsin, USA; (b) G.M. Sheldrick *Acta Cryst.* **2008**, *A64*, 112-122.

[7] Bruker, SMART, SAINT and SADABS **1997**, Bruker AXS Inc., Madison, WI, USA.

[8] G.M. Sheldrick *Acta Cryst.* **2015**, *C71*, 3–8.

[9] (a) Agilent Technologies **2011**, Agilent Technologies UK Ltd., O., UK, Xcalibur CCD system, CrysAlisPro Software system, Version 1.171.35.19; (b) CrysAlis CCD, CrysAlis RED and associated programs: Oxford Diffraction **2006**, Program name(s). Oxford Diffraction Ltd, Abingdon, England; (c) SAINT Bruker **2007**, Bruker AXS Inc., Madison, Wisconsin, USA.

[10] A. Altomare, G. Cascarano, C. Giacovazzo, A. Guagliardi *J. Appl. Crystallogr.* **1993**, *26*, 343–350.

[11] G.M. Sheldrick **1998** *SHELX97: Programs for Crystal Structure Analysis (Release 97-2)*, Institüt für Anorganische Chemie der Universität, Tammanstrasse 4, D-3400 Göttingen, Germany.

[12] (a) L. Porri, V.N. Scalera, M. Bagatti, A. Famulari, S.V. Meille *Macromol. Rapid Commun.* **2006**, *27*, 1937-1941; (b) G. Ricci, A. Boglia, A.C. Boccia, L. Zetta *Macromol. Symp.* **2007**, *260*, 172–178; (c) G. Ricci, A. Boglia, A.C. Boccia, L. Zetta, A. Famulari, S.V. Meille *Macromolecules* **2008**, *41*, 3109-3113; (d) G. Leone, A. Boglia, A.C. Boccia, S. Taglialatela Scafati, F. Bertini, G. Ricci *Macromolecules* **2009**, *42*, 9231-9237; (e) G. Ricci, G. Leone, A. Rapallo, P. Biagini, G. Guglielmetti, L. Porri *Polymer* **2011**, *52*, 5708-5715; (f) A. Buono, A. Famulari, S.V. Meille, G. Ricci, L. Porri *Macromolecules* **2011**, *44*, 3681-3684.

[13] A. Rapallo, G. Ricci, W. Porzio, G. Arrighetti, G. Leone *Cryst. Growth Des.* **2014**, *14*, 5767-5772.

[14] M. Arndt, R. Engehausen, W. Kaminsky, K. Zpumis *J. Mol. Catal. A: Chem.***1995**, *101*, 171-178.

[15] I. Tritto, C. Marestin, L. Boggioni, L. Zetta, A. Provasoli, D.R. Ferro *Macromolecules* **2000**, *33*, 8931-8944.

[16] I. Tritto, L. Boggioni, D.R. Ferro *Coord. Chem. Rev.* **2006**, *250*, 212–241.

[17] W. Kaminsky, A. Bark, M. Arndt *Makromol. Chem. Macromol. Symp.* **1991**, *47*, 83-93.

[18] G. Zanchin, G. Leone, I. Pierro, A. Rapallo, W. Porzio, F. Bertini, G. Ricci *Macromol. Chem. Phys.* **2017**, *218*, 1600602.

[19] G. Leone, M. Mauri, S. Losio, F. Bertini, G. Ricci, L. Porri *Polym. Chem.* **2014**, *5*, 3412–3423.

[20] X. Li, Z. Hou *Macromolecules* **2005**, *38*, 6767-6769.

[21] (a) J.Y. Liu, S.R. Liu, L. Pan, Y.S. Li *Adv. Synth. Catal.* **2009**, *351*, 1505–1511; (b) H. Li, J. Li, Y. Zhang, Y. Mu *Polymer* **2008**, *49*, 2839–2844.

[22] T. Hasan, T. Ikeda, T. Shiono *J. Polym. Sci., Part A: Polym. Chem.* **2007**, *45*, 4581–4587.

[23] G. Velden, C. Didden, T. Veermans, J. Beulen *Macromolecules* **1987**, *20*, 1252-1256.

Chapter 4
Titanium

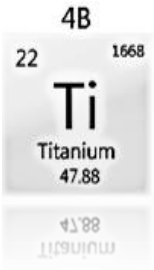

Chapter highlights

→ The catalytic system $TiCl_4$–Et_2AlCl promotes the polymerization of cyclic olefins (*e.g.* norbornene, dicyclopentadiene and norbornadiene)

→ The conformation of dicyclopentadiene isomers has a great effect on the polymerization activity and polymers crystallinity

→ Hydrogenation and epoxidation reactions of the unsaturated polymers give rise to functional al thermostable materials

→ The polymerization of norbornadiene catalyzed by $TiCl_4/Et_2AlCl$ involves the formation of cationic species, bringing to a peculiar 3,5-enchainment between monomeric units

Parts of this chapter have been published and are reproduced here from:

G. Zanchin, G. Leone, I. Pierro, A. Rapallo, W. Porzio, F. Bertini, G. Ricci *Macromol. Chem. Phys.* **2017**, 1600602

Titanium is the element of the periodic table with atomic number 22 belonging to the Group 4 of the transition series. The most common compound is titanium dioxide (TiO_2); other common compounds include titanium tetrachloride ($TiCl_4$) and titanium trichloride ($TiCl_3$), which are used as catalysts in different fields.

4.1 $TiCl_4$: the state-of-the-art

$TiCl_4$, also referred as "tickle" or "tickle 4", is a volatile liquid, very reactive to air humidity, producing a white smoke of titanium dioxide (TiO_2) and hydrogen chloride; its reactivity is connected to the Lewis acid character. Many organometallic compounds used in the olefin polymerization are produced starting from $TiCl_4$, for example titanocene dichloride, $(\eta^5\text{–}C_5H_5)_2TiCl_2$,[1] obtained by reaction with sodium cyclopentadienyl.

As anticipated, titanium has a relevant role in the world of catalysis for olefin polymerization, in particular in the heterogeneous Mg–supported catalyst for the production of PE and PP.[2] Much research has been done on this topic, and yet many research groups remain involved in these issues because not all doubts have already been dispelled, due to the great complexity of this system.

However, over the years, this metal has been studied also for the polymerization of different olefins. Concerning the field of interest of this thesis, basing also on the initial purpose of the research project, in the plethora of the olefins available, cyclic olefins were chosen as monomers, and among them the family of norbornene (NB) and its derivatives.

As already discussed in paragraph 1.5, the polymerization of NB can occur via three different catalytic routes: (*i*) ring-opening metathesis polymerization (ROMP), which gives polymers containing double bonds within the main chain, (*ii*) vinyl addition polymerization, which gives completely saturated polymer, and (*iii*) cationic polymerization, which gives low–molecular weight products containing rearranged monomer units (Fig. 7 in Chapter 1 – Introduction).[3]

Other than titanium,[4] stereoregular poly(norbornene)s were obtained also with chiral zirconocene–MAO catalytic system.[5] However in this case, the higher molecular weight polymers showed the presence of a C7–linkage, deriving from σ-bond methatesis reaction between the Zr–C bond of the growing chain and the C7–H bond. Instead, it is known that σ–bond methatesis reactions are less frequent with titanium than with zirconium catalysts.[6]

This is what prompted prof. Lido Porri (Politecnico di Milano) and co-workers, and later in collaboration with dr. Giovanni Ricci (CNR – ISMAC) to investigate the polymerization of NB catalyzed by titanium, and in particular the microstructure of NB oligomers obtained with $TiCl_4$–Et_2AlCl. Basing on the article published by some co-workers of Natta,[3] they discovered that *naked* $TiCl_4$ (naked because the metal is only sourrounded by the growing polymer chain, the new incoming monomer, the chlorine atom, and the weakly coordinating anion, with no ancillary

ligands) in combination with an aluminum alkyl of the type R_2AlCl (R = H, Me, Et, *i*Bu) gave crystalline oligomers[7] and polymers,[8,9] depending on the monomer/Ti molar ratio (Fig. 1).

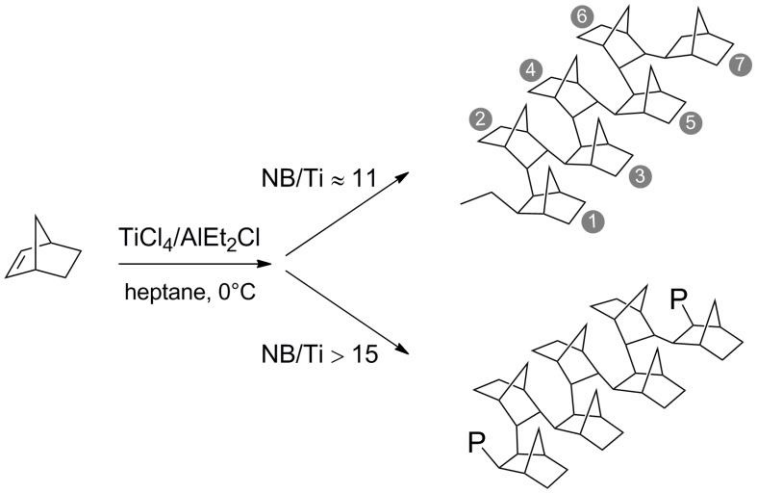

Figure 1 *Ti–catalyzed polymerization of NB at different NB/Ti molar ratios, to give an heptamer (NB/Ti ≈ 11, top) and a higher-M_w polymer (NB/Ti > 15, bottom).*

The resulting oligomers and polymers showed high stereoregularity. At low NB/Ti ratio (~11), a crystalline heptamer was obtained, whose structure, determined via X-ray diffraction, showed for the first time for such polymers a disyndiotactic stereochemistry, that is rather unusual for vinyl–type polymers. At higher NB/Ti ratio instead, a crystalline polymer having a 2,3-*exo*-disyndiotactic structure with an unique helical conformation was obtained (Fig. 2); the structural rearrangement allowed the formation of an empty accessible tubular channel at the core. This structural feature made the polymer also of particular interest for porous materials in sensing and recognition/separation technologies.

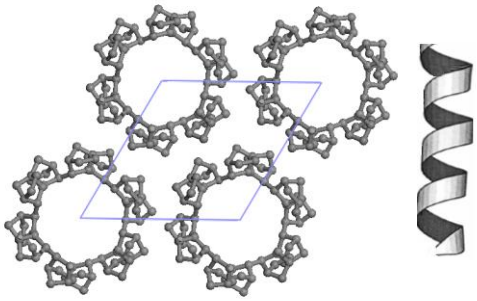

Figure 2 *sPNB projection views, as it results from X-ray and computational studies.*

However, these possible applications are offset by the poor solubility and hard processability of the polymeric material. Aiming at overcome this drawback, the use of functional NBs (Fig. 6 in Chapter 1 – Introduction) was conceived. In addition to the ready availability of these monomers, the resulting polymers are expected to have double bonds which can be useful for further chemical modification and functionalization. Following the idea that the presence of substituents at the NB

unit could improve the processability of the obtainable polymers, and that the polymers from substituted NBs and their functionalized derivatives (*e.g.*, epoxidized derivatives) could adopt helical structures similar to that found for disyndiotactic PNB, thus yielding interesting polar tubular molecules with apolar cavities, the polymerization of DCPD with the catalytic system $TiCl_4$–Et_2AlCl was investigated.

4.2 Ti–mediated dicyclopentadiene polymerization

4.2.1 The starting point

The first steps of this research brought to the synthesis of low–molecular weight, but highly crystalline products, by using the same $TiCl_4$–Et_2AlCl catalyst (Fig. 3). By combining X-ray diffraction techniques and the VARICELLA computational method,[10] it was possible to establish that the crystallizing species is a tetramer (species made up of 4 monomeric units) having a 2,3-*exo*-disyndiotactic structure (Fig. 3).[11] As expected, the crystals have the same configuration of those obtained from NB.

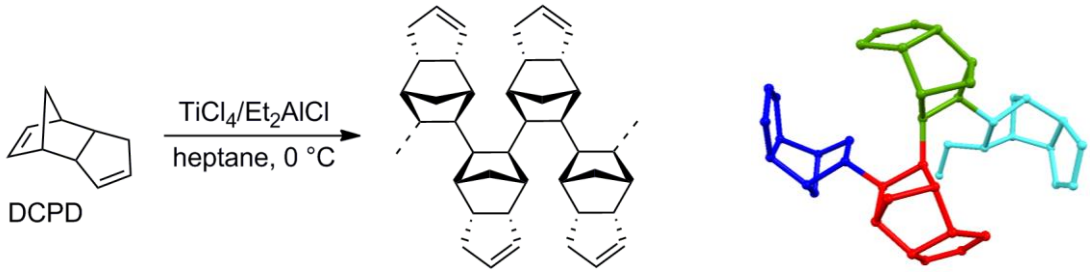

Figure 3 *Scheme of DCPD vinyl-type polymerization (left) and a view of the molecular structure of the crystalline DCPD tetramer (right).*

Starting from these preliminary and encouraging results, the investigation on DCPD went on more into detail during this PhD research activity; in particular, questions concerning the polymerization mechanism and conditions, and polymers microstructure were still open. Indeed, from the first investigations came out that, among the oligomers formed in solution, only the tetramer can adopt such conformation that allows for crystal packing. The other terms remain in the semicrystalline powder and contribute to the amorphous part of it, which is the major component, amounting to 71% as evaluated by XRD background profiles.

Before getting in the details of the results obtained, it is worth mentioning some information about the monomer. DCPD (IUPAC name tricyclo[5.2.1.$0^{2,6}$]deca-3,8-diene) is a chemical compound that can be obtained from the dimerization of cyclopentene via Diels-Alder reaction; it is coproduced in large quantities in the steam cracking of naphta and gas oil to ethylene. DCPD has two stereoisomers, namely the *endo* and the *exo* isomer,[12] depending on the position of the cyclopentene ring with respect to the carbon bridge (Fig. 4).

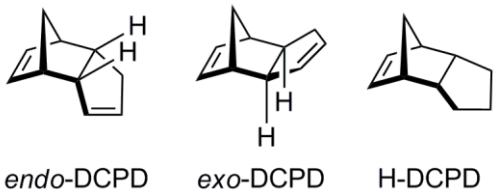

Figure 4 *DCPD isomers (endo and exo), and the 8,9-dihydrogenated monomer (H-DCPD).*

It has been demonstrated that the spatial disposition of the cyclopentene ring may have some influence on the polymerization mechanism, as reported by Sen *et al*. Indeed, in a study on the polymerization of functionally substituted NBs, they found that the *endo* isomer was polymerized more slowly compared to the *exo* isomer because of the coordination of the donor atom to the transition metal and steric reasons.[13]

The results obtained are discussed hereafter; specifically, the influence of the monomer conformation, the monomer/Ti molar ratio, and the relevance of the presence of the double bond on the cyclopentene ring were evaluated.

4.2.2 Polymerization of *endo*/*exo* DCPD mixture

Polymerization of *endo*/*exo* DCPD mixture was carried out at two different DCPD/Ti ratios in heptane at 0 °C (Table 1, entries 1 and 2) and in toluene at 22 °C for DCPD/ Ti = 15 (Table 1, entry 3). All the obtained products were characterized by FTIR, NMR, and XRD and then fractionated with boiling solvents. The recovered fractions were thoroughly characterized as well.

Table 1 *Polymerization of DCPD (endo/exo, 90/10).*[a]

entry	solvent	T (°C)	[DCPD]/[Ti]	yield		M_w[b] (g/mol)	M_w/M_n[b]
				(g)	(%)		
1	heptane	0	15	1.0	58	2123	2.7
2	heptane	0	25	1.5	52	2186	2.5
3[c]	toluene	22	15	1.6	90	1322	1.4

[a] polymerization conditions: total volume, 16 mL; Et_2AlCl 1.73 mmol; $TiCl_4$ 0.867 mmol; temperature, 0°C; time, 8 days; [b] determined by SEC; [c] polymerization time, 6 days.

In heptane at 0 °C and DCPD/Ti ratio of 15 (Table 1, entry 1) we obtained a creamy colored powder product mainly consisting of oligomers. The fractionation of sample 1 in boiling solvents gave a fraction soluble in diethyl ether (24% of the total), a fraction soluble in heptane (50% of the total), and an insoluble residue (26% of the total). The diethyl ether soluble fraction and the heptane residue are amorphous, while the fraction soluble in boiling heptane is highly crystalline (Fig. 5a). The diffraction profile of the crystalline fraction resembles the one of the above reported tetramer. This data, in addition to the results from the molecular weight analysis of the boiling heptane soluble fraction (M_w = 620, M_w/M_n = 1.6, not reported in Table 1) confirmed the results previously obtained: the crystallizing species were unambiguously found to be tetramers with a

2,3-*exo*-disyndiotactic enchainment in the conformation sketched in Figure 3.[11] It appears highly plausible, from the way of polymerization of the corresponding monocyclic NB,[7-9] and the fact that DCPD tetramer has the same stereoregular 2,3-*exo*-disyndiotactic enchainment of the NB heptamer,[7,9] that the formation of the tetramer occurs through a vinyl-type addition oligomerization.

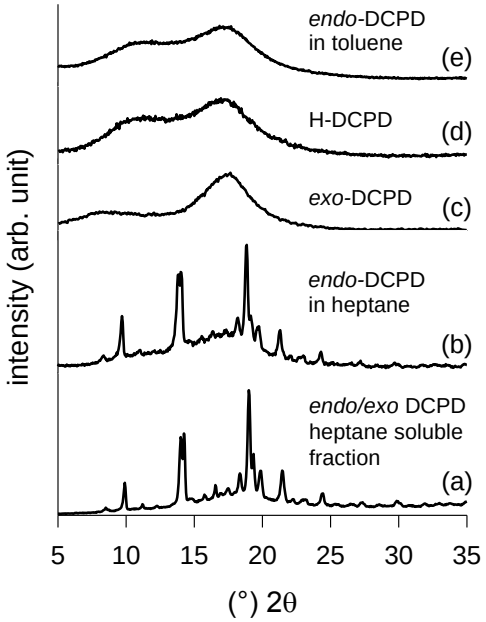

Figure 5 *X-ray powder diffraction pattern of the crystalline tetramer, heptane fraction of the DCPD oligomers from the polymerization of the endo/exo mixture [entry 1, (a), entry 6 (b), entry 9 (c), entry 4 (d), and entry 7 (e)].*

The product obtained at DCPD/Ti molar ratio of 25 (Table 1, entry 2) consists of a cream colored powder. The fractionation of sample 2 in boiling solvents gave a fraction soluble in diethyl ether (16% of the total), a fraction soluble in heptane (38% of the total), a fraction soluble in toluene (42% of the total), and an insoluble residue (4% of the total). The raw product and all the fractions are amorphous. In contrast, the oligomerization of DCPD in toluene at 22 °C gave a waxy product (Table 1, entry 3, M_n = 940) completely soluble in boiling diethyl ether and amorphous by X-ray examination. An increase of the reaction temperature from 0 to 22 °C has a beneficial effect on the monomer conversion (entries 1 *vs* 3), likely due to an enhancement in the rate of the reaction paths. However, this enhancement is not beneficial to the polymer properties: indeed, the molecular weight decreases, probably as a consequence of the enhancement also of those paths that cause chain termination. In addition, the higher reaction temperature may inhibit the crystal packing among the polymer chains, causing the formation of amorphous polymers. From this result, it can be evidenced that the solvent, and especially the low temperature, are fundamental for obtaining crystalline materials.

For this reason, and in analogy with the reaction conditions of previous studies,[7-9; 11] the reactions were performed in heptane at 0 °C.

The NMR and FTIR investigations reveal the extreme complexity of these materials especially in terms of molecular microstructure. In general, fine microstructural analysis, either by ^{1}H or ^{13}C NMR is difficult because of the broadness of the signals likely due to the presence of several diastereoisomers.

In Figure 6 the ^{1}H NMR spectra of samples 1 and 3, respectively, are shown. The intense resonance at 2.98 ppm corresponds to the allylic proton in the equatorial position (when the cyclopentene ring is *endo* fused),[14] while the resonance of the allylic proton in the axial position (when the cyclopentene ring is *exo* fused), which should be at about 2.5 ppm, is overlapped; therefore, a precise peak integration and estimation of the percentage of the two isomers in the final product is not possible.

FTIR spectra (Fig. 7) show characteristic absorption bands at 3038 (s), 1610 (w), 945 (m), 737 (s), and 695 (s) cm^{-1} (marked with an asterisk).

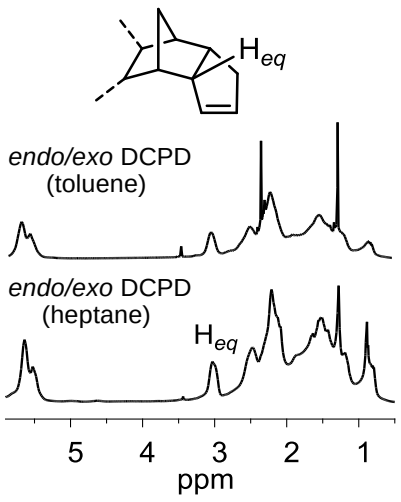

Figure 6 *^{1}H NMR spectra in $C_2D_2Cl_4$ of sample obtained from the endo/exo DCPD in heptane (Table 1, entry 1)and in toluene (Table 1, entry 3).*

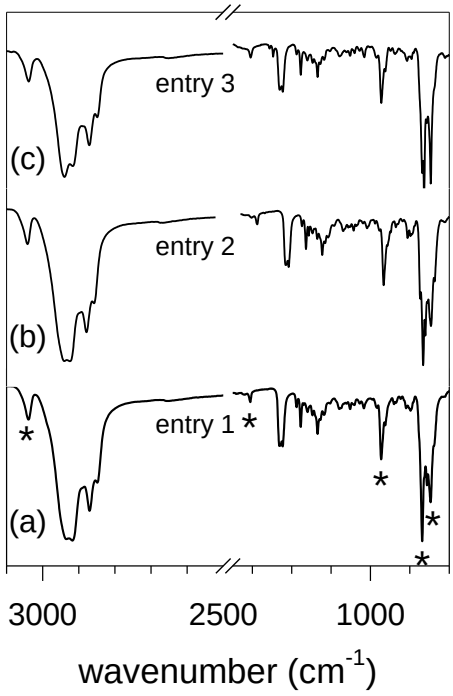

Figure 7 *FTIR spectra of the sample obtained from the endo/exo DCPD mixture.*

The presence of bands at 3038 and 1610 cm^{-1} and the absence of any band at about 1580 cm^{-1} means that all the bicycloheptene double bonds were consumed during the reaction. The remaining unsaturations are entirely due to the cyclopentene double bond. The bands at 3038 and 1610 cm^{-1} are characteristic the olefinic C–H stretching vibration and C=C stretching vibration, respectively. The absorption peak at 945 cm^{-1} is assigned to the bending of the C–H bonds in the ring system of NB,[15] thus confirming that the oligomerization occurs through a 2,3-addition rather than via ROMP. The two bands at 740 and 695 cm^{-1} can be assigned to the out-of-plane bending vibrations of =C–H bond of the cyclopentene ring.[16,17]

4.2.3 Polymerization of *endo*-DCPD, *exo*-DCPD, and H-DCPD

In order to evaluate the influence of the conformation of the monomer on the reaction outcome (mechanism, activity, polymer stereoregularity), the polymerizations of the two conformationally pure isomers, and the corresponding hydrogenated analogous were performed (Fig. 4).

Polymerizations were carried out at different DCPD/Ti ratio (*i.e.*, 15 and 25) in heptane at 0 °C; in the case of *endo* isomer the reaction was carried out also in toluene at 22 °C (entry 7).

Polymerization of H-DCPD gave moderate yield (Table 2, entries 4 and 5). The resulting products are oligomers (around 4 monomeric units), soluble in boiling diethyl ether (100% of the total); the ^{13}C NMR spectrum (not reported here) showed the great complexity that makes the microstructural investigation tough, likely due to the presence of several diastereoisomers.

Table 2 *Polymerization of endo-/exo-/H-DCPD monomers.*[a]

entry	monomer	[DCPD]/[Ti]	yield		M_w[b]	M_w/M_n[b]
			(g)	(%)	(g/mol)	
4	H-DCPD	15	0.7	42	713	1.3
5	H-DCPD	25	1.1	40	846	1.4
6	*endo*-DCPD	15	0.5	30	620	1.6
7[c]	*endo*-DCPD	15	1.4	88	560	1.6
8	*endo*-DCPD	25	1.1	43	885	1.8
9	*exo*-DCPD	15	1.3	76	1138	1.6
10	*exo*-DCPD	25	1.5	68	2288	1.6

[a] polymerization conditions: total volume, 16 mL; solvent, heptane; Et_2AlCl 1.73 mmol; $TiCl_4$ 0.867 mmol; temperature, 0°C; time, 8 days; [b] determined by SEC; [c] solvent, toluene; temperature, 22 °C.

Interestingly, while tetramers of the *endo*-DCPD are able to crystallize, tetramers of the saturated species give amorphous phases (Fig. 5d). Inspection of the unsaturated DCPD tetramers crystalline structure shows that the planarity of cyclopentenes favourably concurs to the packing of the molecules (Fig. 3). If the planar unsaturated rings are turned into saturated cyclopentanes, the planarity is lost and the typical envelope conformation is assumed by the five carbon rings. This causes an increase of the steric hindrance of each monomer unit, which may hamper the organization of the molecules into a crystal structure similar to that observed for the tetramer.

We found that the *exo* isomer is more reactive, the *endo* isomer being polymerized more slowly. For DCPD/Ti = 15, 76 and 30% of the initial amount of the *exo* and *endo* isomer was consumed, respectively (Table 2, entries 9 *vs* 6). Likewise, at DCPD/Ti = 25, 68 and 43% of the initial amount of *exo* and *endo* DCPD was consumed, respectively (Table 2, entries 10 *vs* 8). This result parallels the case of ROMP for the *endo* and *exo* DCPD,[18] and substituted NBs.[19] The lower reactivity of the *endo* isomer can be likely due to steric repulsion between the cyclopentene adjacent groups of *endo*-substituted bicyclic structures disfavouring, or at least slowing down, the successive insertion of the monomer. At the moment, we are unable to further substantiate this hypothesis,

but we have indications toward excluding the possibility that the rate depression of *endo*-DCPD could be due to the formation of a chelated structure between the last-coordinated *endo*-DCPD unit and the metal, since the saturated H-DCPD shows almost the same reactivity of *endo*-DCPD (Table 2, entries 4 and 5 *vs* 6 and 8).

The crude samples were first characterized by XRD. Sample 6, obtained from the polymerization of the *endo* isomer, exhibits considerable crystallinity (Fig. 5b). Granting the slightly larger width of the diffraction maxima and increased noise, likely attributed to crude sample examination, the XRD pattern of sample 6 shows a very close correspondence to the diffraction profile of the heptane soluble fraction of sample 1 (Fig. 5a) obtained from the polymerization of the *exo*/*endo* mixture, *i.e.*, the crystalline tetramer (Fig. 3).[11] This evidence strongly suggests that a single phase of the same stereoregular DCPD tetramer has been formed in the oligomerization of the *endo* isomer.

In contrast, the crude sample obtained from the *exo* isomer (Table 2, entry 9) as well as the fraction soluble in boiling diethyl ether (80% of the total, M_n = 1010 g mol^{-1}) and that soluble in heptane (15% of the total, M_n = 1140 g mol^{-1}) were found to be amorphous by XRD, namely only two broad bumps evidenced at about 9 and 17 °2θ, respectively (Fig. 5c). In the case of the *endo* isomer, yield and monomer conversion increased only when the reaction was carried out in toluene at 22 °C (88% yield, Table 2, entry 7). However, a waxy product, amorphous (Fig. 5e) and completely soluble in boiling diethyl ether was obtained.

FTIR spectra of samples obtained at monomer/Ti ratio of 15, in heptane at 0 °C (Table 2, entry 6 and 9) and in toluene at 22 °C (Table 2, entry 7) are shown in Figure 8.

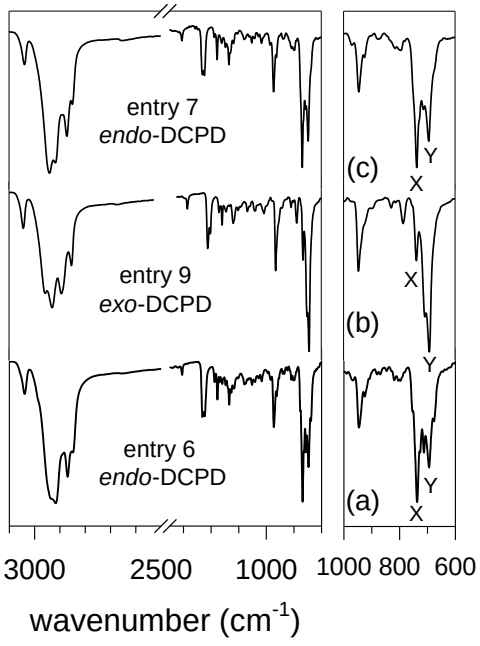

Figure 8 *FTIR spectra of sample obtained from endo-DCPD in heptane (a), exo-DCPD (b), and from endo-DCPD in toluene (c).*

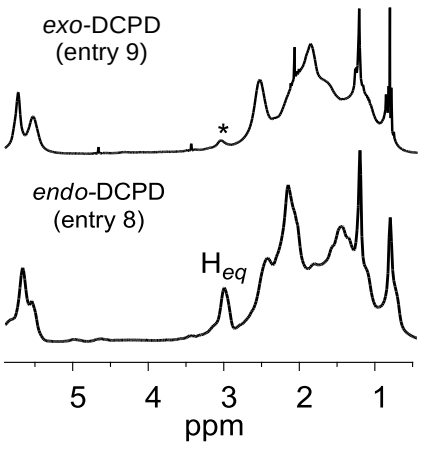

Figure 9 *^{1}H NMR spectra in $C_2D_2Cl_4$ of sample obtained from endo-DCPD (entry 8), and exo-DCPD (entry 9).*

In 1966 De Kock and Veermans,[16] investigated the FTIR spectra of different derivatives of *endo* and *exo* DCPDs and showed that products in the *exo* series have a weak band at about 740 cm^{-1} and a stronger one at about 695 cm^{-1}, while those in the *endo* series have the same bands but with their relative intensities reversed. According to this study, the FTIR spectra of sample 6 and 9, from the *endo* and *exo* isomer, respectively, show that bands at 740 and 695 cm^{-1} (marked with X and Y, respectively, Fig. 8) for sample 9 have the shape of typical *exo* units, namely it has their relative intensities reversed with respect to sample 6. In the same manner, the FTIR spectra of sample 8, obtained from the *endo* isomer in toluene at 22 °C, is close to that of the same isomer prepared in heptane at 0 °C.

^1H NMR spectra of sample 6 and 9 are shown in Figure 9. As already stated above, the intense resonance at 2.98 ppm corresponds to the allylic proton in the equatorial position (when the cyclopentene ring is *endo* fused);[14] the intensity ratio between this signal and the signal corresponding to the two olefin protons (in the range from 5.3 to 6.0 ppm) is 1:2 for the product from the *endo* isomer. The fact that the same peak (marked with an asterisk in Figure 9) is still evident in the spectrum of the sample from the *exo* isomer means that a small amount of the *endo* impurities was present in the *exo* isomer.

Yet, we found that the residue to the boiling toluene fractionation of sample 8, obtained in heptane from the *endo*-DCPD isomer at high DCPD/Ti ratio, exhibits a considerable crystallinity. Specifically, the boiling solvents fractionation of sample 8 gave a fraction soluble in boiling diethyl ether (58% of the total, mainly trimers), a fraction soluble in heptane (26% of the total) and a fraction soluble in toluene (10% of the total). In Figure 10 the XRD pattern of sample 8 (Fig. 10a), the diethyl ether soluble fraction (Fig. 10b) and the residue (Fig. 10c) are shown. All the soluble fractions are amorphous, while the fraction residue to the boiling toluene exhibits, as anticipated, a good crystallinity.

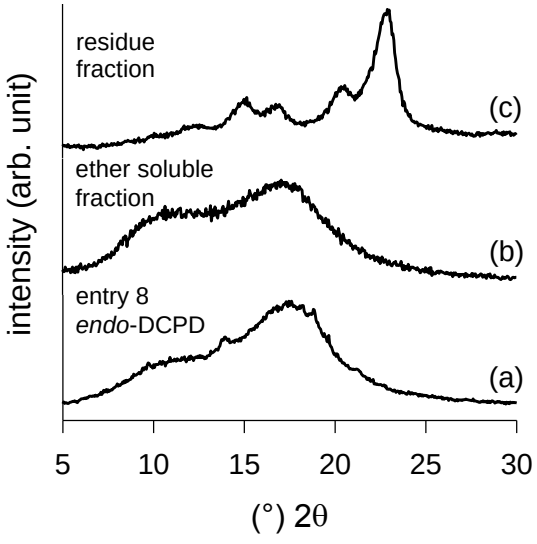

Figure 10 *X-ray powder diffraction pattern of entry 8 (a), the diethyl ether soluble fraction (b) and the residue fraction (c).*

The diffraction patterns are very different from that of the DCPD tetramer (Fig. 5a and 5b), indicating the formation of a new crystalline phase. Possibly, the molecular weight of the residue fraction is higher than that of the tetramer, but the molar mass determination is unfeasible because of the residue insolubility. In addition, it is not possible to rule out the possibility that some crosslinking may occur during the boiling toluene extraction. These facts together with the high level of uncertainty in the molecular masses and the small number of broad peaks in the XRD pattern (Figure 10c), leave opened many hypothesis concerning the identity of the crystallizing species, and, in turn, their crystal structure.

The thermal stability of the obtained products was investigated by TGA under inert atmosphere. In general, TGA curves evidence a complex multi–stage decomposition. In Figure 11a the thermograms for sample 8 (from *endo*-DCPD) and 10 (from *exo*-DCPD) are reported as an example. Sample 10 was found to be more thermally stable, being the initial degradation temperature corresponding to 5% weight loss (T_o) of sample 10 markedly higher than that of sample 8, 290 and 220 °C, respectively. Anyway, at higher temperatures both the materials show a fast weight loss with a maximum rate at 470–480 °C. The main degradation stage ends at about 550 °C and the residue yield at 700 °C is *ca*. 20 wt. % for both samples. However, the carboneous residue disappears when exposed to air.

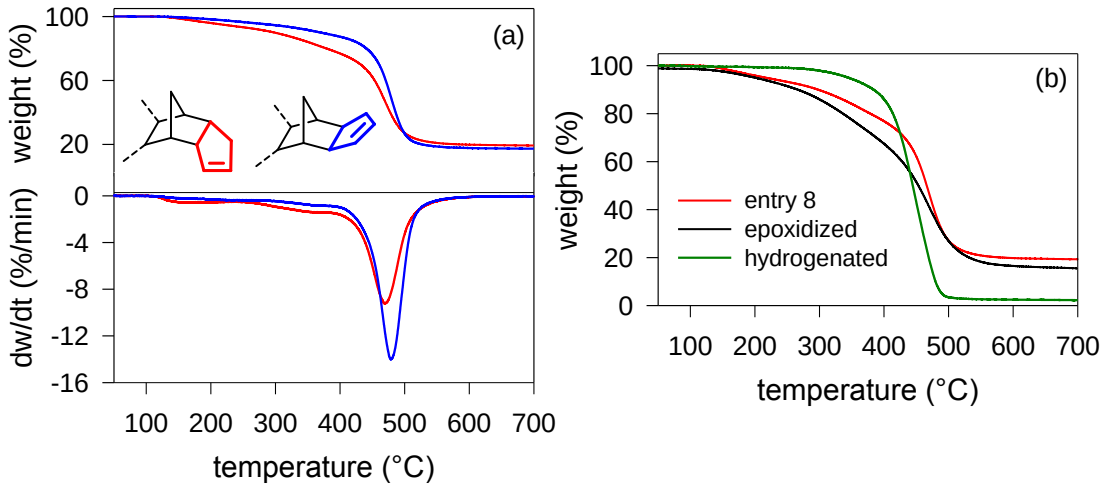

Figure 11 *(a) TGA (upper) and DTG (bottom) curves under nitrogen flow of entry 8 (from endo-DCPD; red line) and entry 10 (from exo-DCPD; blue line); (b) TGA of entry 8 and its epoxidized and hydrogenated products.*

4.2.4 Post–polymerization modification

As mentioned in paragraph 1.6, the possibility of modifications of the final polymer is a feasible and useful strategy to improve the polymer properties. In particular, in the case of homopolymers of the family of NB, it was important to find a way to increase the polymer solubility, in order to make materials characterization easier. The use of DCPD allows to pursue this strategy, since the double bond of the cyclopentene ring is not involved in the polymerization reaction.

Hydrogenation and epoxidation of polyDCPD (Fig. 12) have been attempted with interesting results, which will be discussed hereafter. The general hydrogenation and epoxidation procedures are reported in Chapter 3 – Materials & Methods (paragraph 3.3).

Epoxidation

The intracyclic double bonds of DCPD polymers can be functionalized and completely converted into epoxy groups. Epoxidation is generally performed with organic peroxides, either added directly,[20] or generated in situ.[21] In this work, epoxidation was performed with *m*-chloroperbenzoic acid (*m*-CPBA) (2 eq of the insaturations) in toluene at 55 °C for 7 h (Fig. 12). The complete conversion of the double bonds in the epoxide functionality was confirmed by FTIR and NMR spectroscopy.

The characteristic peaks of the aliphatic protons in the range from 5.3 to 6.3 ppm disappeared in the ^{1}H NMR spectra, as well as the signal of the allylic ones in the region from 2.5 to 3.0 ppm.

In addition, the FTIR spectrum is analogous to that of a typical epoxidized compound, exhibiting a new absorption peak at 833 cm^{-1} associated with the formation of oxirane,[20] while the peaks corresponding to sp^2 carbons (bending of =C–H bond at 700 cm^{-1} and stretching above 3000 cm^{-1}) disappeared, thus indicating that the epoxidation reaction has been achieved and gone to completeness. The epoxidized products are amorphous, and exhibit a thermal degradation behavior close to that of the unsaturated precursors up to 250 °C, while at higher temperature the decomposition proceeds more quickly (Fig. 11b), likely due to the great reactivity of the oxirane moiety.

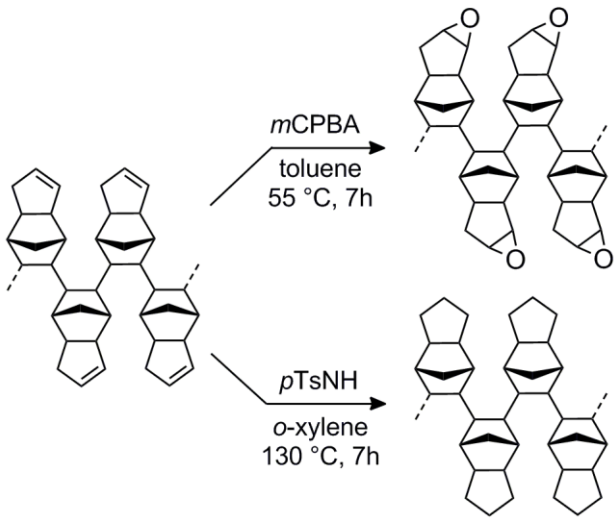

Figure 12 *Schematic representation of the epoxidation and hydrogenation of DCPD polymers, with the reaction conditions employed.*

Hydrogenation

Hydrogenation was performed with diimine generated *in situ* via thermal decomposition of *p*-toluensulphonyl hydrazide (*p*-TsNH) (Fig. 12), according to the procedure reported in the literature.[22] A high degree of saturation is proven by the absence of the allylic proton of the cyclopentene ring in the ^{1}H-NMR spectra in the region spanning from 2.5 to 3.0 ppm. Moreover, no signals can be detected in the spectral regions of unsatured carbons (peaks at ~700 cm^{-1} and above 3000 cm^{-1} in FTIR spectra). All the hydrogenated products are amorphous, while TGA (Fig. 11b) reveals that the hydrogenated products exhibit an increased thermostability relative to the corresponding unsaturated precursors (for example, T_o values for entry 8 and its hydrogenated derivate are 220 and 345°C, respectively).

Interesting enough, the hydrogenation of the crystalline tetramer (Table 2, entry 6) brought to the formation of an amorphous product, showing once more how fundamental is the presence of the cyclopentene ring for crystal packing.

4.3 Other cyclic olefins: the case of norbornadiene

Keeping in mind the initial aim of exploring the catalytic activity of some NB derivatives, beyond DCPD, other monomers have been studied with the catalytic system $TiCl_4$–Et_2AlCl under optimized conditions (*i.e.*, heptane, 0 °C). Specifically, the polymerization of norbornadiene (NBD) was investigated (Fig. 14), and results are reported in Table 3.

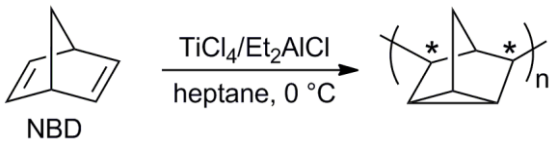

Figure 13 *Schematic representation of the polymerization of norbornadiene. The asterisks mark the formation of sterocenters.*

Table 3 *Polymerization of NBD catalyzed by $TiCl_4/Et_2AlCl$.*[a]

entry	[NBD]/[Ti]	yield		M_w[b]	M_w/M_n[b]
		(g)	(%)	(g/mol)	
1	5	0.38	95	1820	3.1
2	15	1.2	100	1440	2.8
3	30	2.2	94	1610	2.3

[a] polymerization conditions: total volume, 16 mL; solvent, heptane; Et_2AlCl 1.73 mmol; $TiCl_4$ 0.867 mmol; temperature, 0°C; time, 8 days; [b] determined by SEC.

The catalytic system was very active, giving almost complete conversion of the monomer.

The characterization of the compound obtained gave interesting and surprising results. Indeed, the analysis of the FTIR spectrum (Fig. 14a) demonstrated the formation of a cyclopropylic ring

(signal at 800 cm^{-1}) and a 3,5-enchainment among the monomers, different from the expected vinyl-type 2,3-enchainment, as norbornene does.[23]

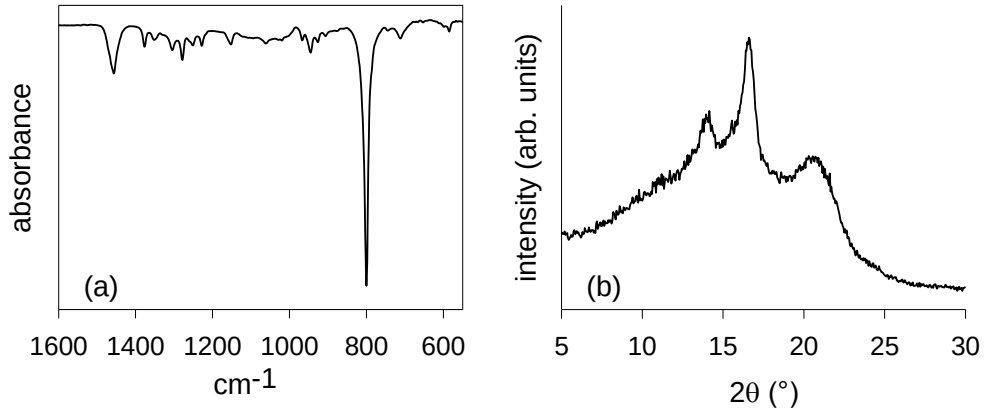

Figure 14 *X-ray powder diffraction pattern (left) and FTIR spectrum (right) of polyNBD (entry 2).*

The hypothesis is that during the reaction a cationic species (R^+) is formed and a carbocation rearrangement takes place (Fig. 15): the proposed cationic reaction mechanism involves a transannular rearrangement of the initially formed intermediate, prior to the addition of another NBD monomer, bringing to an enchainment that involves the formation of a cyclopropylic ring.[24]

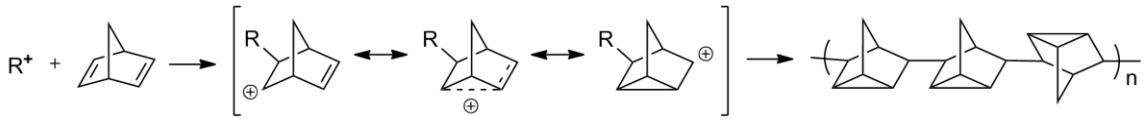

Figure 15 *Schematic rapresentation of a possible NBD cationic polymerization mechanism.*

This cationic behavior was already observed by Kennedy *et al.*[23,24b]. No direct *in* situ experimental detection of the carbocationic species was performed so far, even if the formation of the cyclipropylic structure suggest that the proposed mechanism is highly plausible.

Interesting enough, the obtained products are semicrystalline by X-ray examination (Fig. 14b).

The great complexity of these polymers makes them particularly fascinating concerning the structural study, but at the same time also particularly intrigued. Indeed, as pointed out in the schematic representation above (Fig. 13), the 3,5-enchainment brings to the formation of two stereocenters per each momonomeric unit, meaning that many different stereosequences along the backbone are possible.

As in the case of NB and DCPD, through a synergistic approach involving experimental data from X-ray spectroscopy and computational methods, it is possible to attempt to solve the structure of these compounds. Studies are underway, in collaboration with dr. Arnaldo Rapallo (CNR – ISMAC), and prof. Claudio De Rosa (Università Federico II – Naples) to shed light on the structure of this interesting and novel material.

References

[1] G. Wilkinson, J.G. Birmingham, *J. Am. Chem. Soc.* **1954**, *76*, 4281–4284.

[2] *Market Report: Global Catalyst Market*, 3rd Ed. Acmite Market Intelligence **2015**, Ratingen, Germany.

[3] C. Janiak, P.G. Lassahn *J. Mol. Catal. A* **2001**, *166*, 193-209.

[4] G. Sartori, F. Ciampelli, N. Cameli *Chim. Ind. (Milan)* **1963**, *45*, 1478-1482.

[5] W. Kaminski, A. Bark, M. Arndt *Macomol. Symp.***1991**, *47*, 83-93.

[6] T.K. Woo, P.M. Margl, T. Ziegler, P.E. Blochl *Organometallics* **1997**, *16*, 3454-3468.

[7] L. Porri, V. Scalera, M. Bagatti, A. Famulari, S.V. Meille *Macromol. Rapid Commun.* **2006**, *27*, 1937-1941.

[8] A. Buono, A. Famulari, S.V. Meille, G. Ricci, L. Porri *Macromolecules* **2011**, *44*, 3681-3684.

[9] G. Ricci, G. Leone, A. Rapallo, P. Biagini, G. Guglielmetti, L. Porri *Polymer* **2011**, *52*, 5708-5715.

[10] A. Rapallo *J. Chem. Phys.* **2009**, *131*, 044113.

[11] A. Rapallo, G. Ricci, W. Porzio, G. Arrighetti, G. Leone *Crys. Growth Des.* **2014**, *14*, 5767-5772.

[12] J.J. Zou, Y. Xu, X. Zhang, L. Wang *Appl. Catal., A* **2012**, *421–422*, 79-85.

[13] (a) M. Kang, A. Sen *Organometallics* **2004**, *23*, 5396-5398; (b) J.K. Funk, C.E. Andes, A. Sen, *Organometallics* **2004**, *23*, 1680-1683.

[14] T. Corner, R.G. Foster, P. Hepworth *Polymer* **1969**, *10*, 393-397.

[15] X. Mi, Z. Ma, N. Cui, L. Wang, Y. Ke, Y. Hu *J. Appl. Polym. Sci.* **2003**, *88*, 3273-3278.

[16] R.J. De Kock, A. Veermans *Macromol. Chem. Phys.* **1996**, *95*, 179.

[17] A.S. Abu-Surrah, K. Lappalainen, M. Kettunen, T. Repo, M. Leskelä, H.A. Hodali, B. Rieger *Macromol. Chem. Phys.* **2001**, *202*, 599.

[18] J.S. Moore, J.D. Rule *Macromolecules* **2002**, *35*, 7878-7882.

[19] (a) B. Commarieu, J. P. Claverie *Chem. Sci.* **2015**, *6*, 2172-2181; (b) J.P. Mathew, A. Reinmuth, J. Melia, N. Swords, W. Risse *Macromolecules* **1996**, *29*, 2755-2763; (c) N. Seehof, S. Grutke, W. Risse *Macromolecules* **1993**, *26*, 695-700.

[20] J. Suzuki, Y. Kino, T. Uozomi, T. Sano, T. Teranishi, J. Jin, K. Saga, T. Shiono *J. Appl. Polym. Sci.* **1999**, *72*, 103-108.

[21] (a) X. Wang, H. Zhang, Z. Wang, B. Jiang *Polymer* **1997**, *38*, 5407-5410; (b) B.C. Peoples, V.N. Dougnac, G.B. Galland, F.M. Rabagliati, R. Quijada *Polym. Bull.* **2013**, *70*, 117-129.

[22] B. Autenrieth, R.R. Schrock *Macromolecules* **2015**, *48*, 2493-2503.

[23] J.K. Gillham, M.B. Roller, J.P. Kennedy *J. Appl. Polym. Sci.* **1973**, *17*, 2223-2233.

[24] (a) A. Mizuno, M. Onda, T. Sagane *Polymer* **1991**, *32*, 2953-2957; (b) R.M. Peetz, A.F. Moustafa, J.P. Kennedy *J. Polym. Sci.* **2003**, *41*, 732-739.

Chapter 5
Vanadium

Chapter highlights

- → New vanadium complexes, in the oxidation state (III) and (IV), bearing different ligands (*i.e.*, monodentate phosphines, bidentate phosphines and imido functionalities) have been synthesized and characterized
- → It is possible to counteract vanadium reduction to inactive V(II) by using a reoxidant and employing multidentate ligands
- → All the complexes, activated with a suitable aluminum alkyl, proved to be from moderately to highly active catalysts for the synthesis of cyclic olefin copolymers
- → Some of the complexes proved to be active also in the polymerization of conjugated dienes

Parts of this chapter have been published and are reproduced here from:

G. Leone, I. Pierro, **G. Zanchin**, A. Forni, F. Bertini, A. Rapallo, G. Ricci *J. Mol. Catal. A: Chem.* **2016**, *424*, 220–231.

G. Leone, **G. Zanchin**, I. Pierro, A. Sommazzi, A. Forni, G. Ricci *Catalysts* **2017**, *7*, 369–381.

G. Zanchin, I. Pierro, E. Parisini, J. Martì-Rujas, G. Ricci, G. Leone *J. Organomet. Chem.* **2018**, *861*, 142–150.

G. Zanchin, L. Vendier, I. Pierro, F. Bertini, G. Ricci, C. Lorber, G. Leone *Organometallics* **2018**, *37*, 3181–3195.

Vanadium is the element of the periodic table with atomic number 23 belonging to the Group 5 of the transition series. The chemistry of vanadium is noteworthy for the accessibility of the four adjacent oxidation states (II)–(V). Vanadium is an important element for many catalytic applications.[1] The most commercially important compound is vanadium pentoxide (V_2O_5), used as catalyst for the production of sulfuric acid.

In the world of catalysis for olefins polymerization, the combination of VCl_4 or $V(acac)_3$ with aluminum alkyl compounds are among the first catalysts reported for the copolymerization of cyclic olefins.[2]

5.1 Vanadium: the state-of-the-art

Since the early stages of his studies, Natta established the ability of simple tri- and tetravalent vanadium salts to promote olefin copolymerization.[3] Despite the lower catalytic activity, vanadium catalysts proved to be able to bring to the formation of polymers (particularly synthetic rubber and elastomers) with unique properties. For example, the VCl_4–$AlBr_3$–$AlPh_3$ system afforded linear PEs with high catalytic activity,[4] VCl_4 in combination with Et_2AlCl and anisole afforded high molecular weight amorphous ethylene/propylene copolymers,[5] and ethylene/cyclic olefin copolymers.

Notwithstanding the fact that vanadium–based Ziegler–Natta technology is well established and widely used in the industrialized world [*e.g.* the commercially used trivalent $V(acac)_3$ (acac = acetylacetone) for the production of ethylene/propylene/diene elastomers (EPDM)],[6] Group 5 metals remained relatively ignored, and their knowledge was limited to patent literature until late '90s. A reason for this can be encountered in the intrinsic instability of the V–C bond, and the poor activity of vanadium catalysts correlated to the tendency to undergone reductive elimination towards inactive divalent species.[7] To prevent the reduction to inactive V(II) species, the employment of mild oxidizing agents (chlorinated esters or halocarbons) able to restore the trivalent state is generally applied,[8] even if the actual role and the way these molecules act is still unclear and debated in the most recent literature.

Aiming at controlling the oxidation state (stabilization of the oxidation state, catalytically active species) and hence prolonging the catalyst's lifetime, many ancillary ligands with different denticity, and containing different combinations of donor atoms such as N, O, P, and S, have been synthesized and employed in the synthesis of vanadium complexes in different oxidation states, from (III) to (V). Most of these complexes are based on V(V) complexes with arylimido–aryloxo,[9] amine pyridine(s) phenolate,[10] and tetradentate amine trihydroxy ligands,[11] and V(III) complexes supported by multidentate ligands having, in different combinations, N and O hard donor atoms.[7,8,12,13]

The combination of these complexes with aluminum alkyl compounds are among the first catalysts reported for the copolymerization of cyclic olefins.[2] In particular, $VCl_4/Al(C_6H_{13})_3$ and

$V(acac)_3$/ Et_2AlCl systems copolymerized ethylene with several cyclic olefins such as cyclopentene, cycloheptene, cyclooctene and cyclohexene.[14] Hence, various systems based on vanadium were synthesized and used as pre-catalysts for the copolymerization of cyclic olefins, and exhaustive reviews on this topic appeared recently in the literature.[7,8,12,13]

In the next section some of them are reported, according to their oxidation states.

Vanadium(V) complexes

The most active catalysts based on V(V) complexes are those containing arylimido–aryloxo,[9] amine pyridine(s) phenolate,[10] and tetradentate amine trihydroxy ligands.[11] The (arylimido)(aryloxo)V(V) complexes VCl_2(2,6-$Me_2C_6H_3N$)(2,6-$R_2C_6H_3O$) (R= Me, *i*Pr, Ph) (**V-1**, Fig. 1) were largely investigated for the E/NB copolymerization.

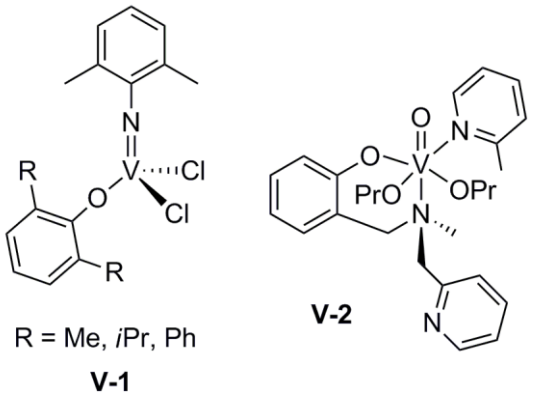

Figure 1 *(arylimido)(aryloxo) (**V-1**) and amine pyridine phenolate (**V-2**) V(V) complexes.*

These complexes, in combination with MAO or Et_2AlCl, show high catalytic activity, giving atactic, alternating copolymers. The substituents on the aryloxide ligand show a significant influence on the catalytic activity and molecular weight of the resulting copolymers, but do not strongly affect the NB incorporation and copolymers microstructure.[9] The bis(benzimidazole)amino V(V) complexes were also effective for the E/NB copolymerization even at 50 °C: in combination with Me_2AlCl, they showed very high activity [11250 kg_{pol} mol_V^{-1} h^{-1}] and high NB incorporation (up to 33 mol%).[15]

V(V) complexes bearing amine pyridine phenolate ligands were firstly reported by Li *et al*. (**V-2**, Fig. 1).[10] These novel complexes exhibited very high catalytic activities for the E/NB copolymerization in the presence of Et_2AlCl as cocatalyst and ETA (ethyltrichloro acetate, $Cl_3CCOOEt$) as reactivating agent even at high temperatures, affording high molecular weight copolymers with unimodal molecular weight distribution. The substituents both in the aryloxo group and N–bridge fragment significantly affected the copolymerization behavior as well as the polymers properties. In fact, reducing the steric congestion around the metal center, the NB

incorporation in the copolymer increased, although the observed catalytic activity was lower with respect to the more hindered complexes.

Vanadium(IV) complexes

Complexes of vanadium in the (IV) oxidation state are quite uncommon compared to V(V). Ligands that have been employed with V(IV) are aryl(imido) ligands (**V-3**, Fig. 2),[16,17,18,19,20] bis(amide) ligands (**V-4**, Fig. 2),[21] O,N-chelating aminophenolate ligands (**V-5**, Fig. 2),[22] and among them also salen-type tetradentate ligands (**V-6**, Fig. 2).[23]

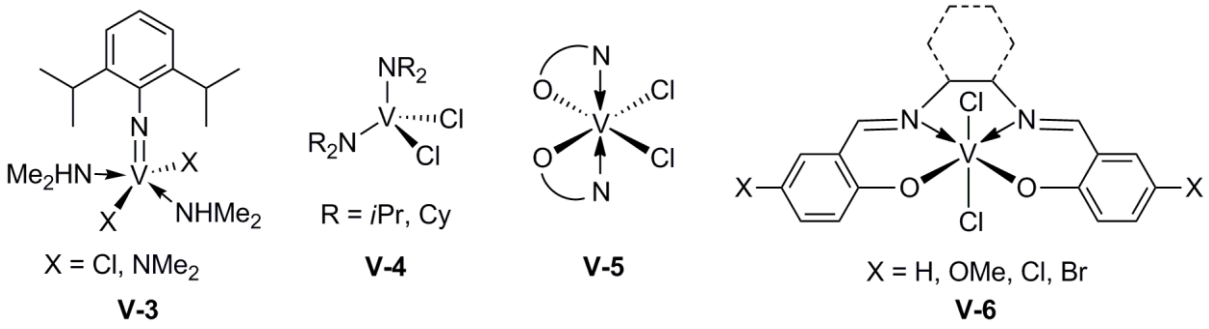

Figure 2 *V(IV) complexes bearing different N and O donor atom ligands.*

In particular, Lorber *et al.* reported many examples of (arylimido)vanadium(IV) dichloride complexes (**V-3**, Fig. 2) that showed high catalytic activities for ethylene polymerization in the presence of Et_2AlCl cocatalyst.[20] The activity by **V-3** in the presence of MAO (59 kg_{PE} mol_V^{-1} h^{-1}; Al/V = 500) was lower than that in the presence of Et_2AlCl (120 kg_{PE} mol_V^{-1} h^{-1}; Al/V = 10; ethylene 1 atm, 20 °C in toluene, 2 or 10 min). The resultant polymers possessed uniform molecular weight distributions. In this respect, they found that the introduction of a 2,6-disubstituted arylimido moiety seems to be effective in terms of stabilization of the catalytically active species. This type of complexes will be discussed in detail in paragraph 5.5.

Vanadium(III) complexes

In 2005, Lorber *et al.*[24] reported some new amine bis(phenolate) complexes of V(III) (Fig. 3) and showed that complex **V-7** exhibited from low to modest activities (66–347 kg_{pol} mol_V^{-1} h^{-1}) for E/NB copolymerization and gave a NB incorporation from 14 to 29 mol%, strongly depending on the polymerization conditions.

Catalysts exhibiting excellent activities and high NB incorporation were successively obtained with multidentate ligands having, in different combination, N and O hard donor atoms.[25] Indeed, the use of mono(β-enaminoketonato) N^AO ligands improved the overall productivity, and mainly alternating copolymers were obtained. A series of complexes analogous to **V-8** (Fig. 3) were found to be efficient catalysts for olefins (co)polymerization. In combination with Et_2AlCl and in the

presence of ETA, they exhibited activities in the range from 1500 to 6800 $kg_{pol}\ mol_V^{-1}\ h^{-1}$ and NB incorporation from 32.6 to 42.7 mol%.[25]

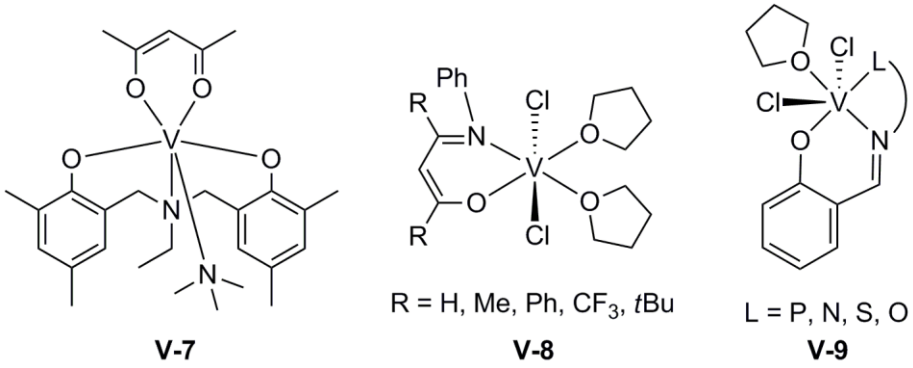

V-7 **V-8** **V-9**

Figure 3 *V(III) complexes bearing different N^O and N^O^L ligands.*

Later, the introduction of a pendant L heteroatom in the bidentate N^O Schiff base ligand gave V(III) complexes (**V-9**, Fig. 3) which exhibited the highest activity for the E/NB copolymerization (17300 $kg_{pol}\ mol_V^{-1}\ h^{-1}$ with L = phosphorus donor). Indeed, N^O ligands with pendant phosphine group, in which the phosphorous atom is bound to the nitrogen through a rigid phenylene bridge, help to strengthen the phospine coordination, stabilizing the V(III) species.[26]

Phosphine ligands

Phosphines can be considered as one of the most important ancillary ligands for transition metal (*d*-block) coordination and organometallic chemistry.[27] Phosphine ligands are typically constructed with combinations of alkyl and aryl groups, and both steric and electronic properties of the ligand can be adjusted for specific applications by simply tuning the organic substituents. In addition, the relatively low cost and large variety of phosphines are incentives for the development of metal phosphine complexes. The synthesis, structure, bonding and reactivity of transition metal phosphine complexes continue to attract considerable interest driven by their capacity to promote a variety of transformations in which the phosphine ligand is directly involved in the reactivity or may act as spectator ligand.[28] Moreover, phosphine–containing complexes were recently found to promote various reactions, and, among them, the copolymerization of cyclic olefin.[29]

Vanadium–phosphine complexes have been known since the mid '80s by the pioneer work of Caulton and Larkworthy,[30,31] but currently they are less investigated in the context of olefin (co)polymerization with respect to vanadium complexes bearing multidentate chelating and anionic ligands having, in different combination, N and O hard donor atoms.[8]

The main reason for this may be likely due to the fact that, in the oxidation states (III), the V–P bond tends to be relatively long, weak and labile. In addition, it has been reported that the synthesis of vanadium complexes with many aliphatic phosphines was unsuccessful likely due to a reduction-hydrolysis process that occurs during the reaction and subsequent workup.

In this context, during the PhD research activity, a library of vanadium complexes has been synthesized, and it is reported below, subdivided in three classes according to the complexes characteristics (Fig. 4); all the complexes have been fully characterized, and, in some cases, the solid state structure was determined by X-ray diffraction. Successively, in order to study their catalytic behavior, and the influence of the polymerization conditions (time, temperature, co-catalyst, reactivator, feed composition) and of the type of ligand, a series of ethylene homopolymerization and copolymerization with NB were performed. E/NB copolymer (poly(E-*co*-NB)) was chosen as the target polymer for the interesting properties that exhibits, as already discussed in paragraph 1.5. Moreover, as in case of Ti–catalyzed polymerization, some NB derivatives were also tested to fabricate COCs with pendant reactive moiety. Finally, for some selected complexes, the polymerization of 1,3-butadiene was also investigated.

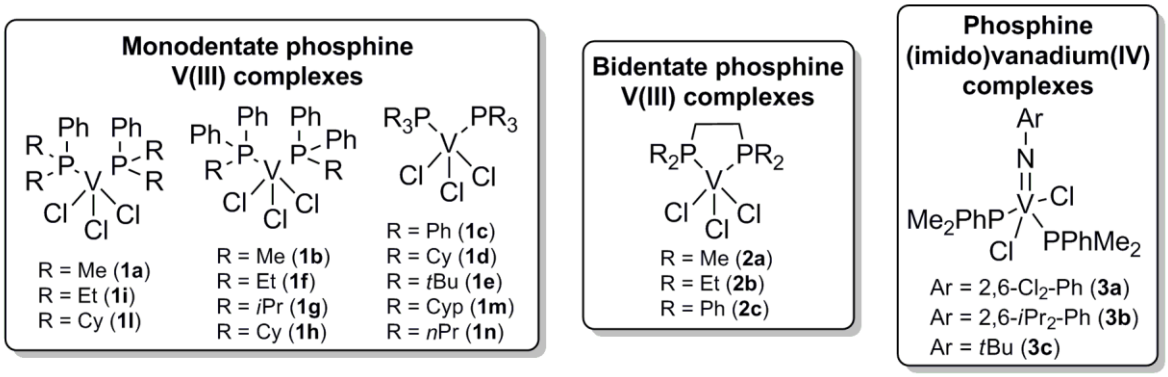

Figure 4 *Library of vanadium–phosphine complexes synthesized in this thesis, divided according to the vanadium oxidation state and ligand denticity.*

The **main difficulties** tackled in this part of the research activity were connected to (*i*) the easiness with which vanadium reduces to inactive V(II) species, (*ii*) the low molecular weight of the resulting (co)polymers, and (*iii*) the unavoidable compositional drift (*i.e.*, a variation of the composition of the feed as the mass of the macromolecular chain grows) which is the consequence of differences in monomer reactivity and can lead to compositionally non-uniform polymers that may hamper establishing structure–property relationships, and negatively influences the thermal properties of the copolymers.

Before getting into the results of the research on vanadium phosphine catalyzed polymerizations, it is worth mention some parameters useful for the description of phosphine ligands.

In order to describe electronic and steric properties of phosphines, Tolman identified two parameters: the electronic parameter ν_{CO} and the steric parameter θ. The electronic parameter, named also Tolman electronic parameter (TEP) is a measure of the electron donating or withdrawing ability of a ligand. It is determined by measuring the variation of the frequency of the C–O vibrational mode of $LNi(CO)_3$ (L = ligand) by IR spectroscopy with respect to its frequency in

$Ni(CO)_4$. It is expressed as a frequency (ν, cm^{-1}) and the values for many phosphine ligands were measured and tabulated in reference 32.

Furthermore, to describe the steric properties, the ligand cone angle θ, also known as Tolman cone angle, is employed as a measure of the size of a ligand. It is defined as the solid angle formed with the metal at the vertex and the hydrogen atoms at the perimeter of the cone. The concept of cone angle is most easily visualized with symmetrical ligands, *e.g.* PR_3, but the approach has been refined to include less symmetrical ligands of the type PRR′R″. In such asymmetric cases, the substituent angles' half angles, $\theta/2$, are averaged and then doubled to find the total cone angle.

For bidentate phosphines, the cone angle is defined as the average of the cone angle for the two substituents attached to the phosphorus atoms, the bisector of the P–Mt–P angle, and the angle between each Mt–P bond.[33] Moreover, dealing with bidentate ligands, it is important to define also another parameter, the natural bite angle (β_n), introduced by Casey and Whiteker;[34] β_n is defined as the selective chelation angle (P–Mt–P bond angle) that is determined by the diphosphine ligand backbone.

5.2 The kick-off: the case of $VCl_3(PMePh_2)_2$

5.2.1 Synthesis and characterization of $VCl_3(PMePh_2)_2$

The reaction of $VCl_3(THF)_3$ with $PMePh_2$ in toluene gave a red-purple solid of stoichiometry $VCl_3(PMePh_2)_2$ (**1b**, Fig. 4). Single crystals, suitable for X-ray structure determination, were obtained by recrystallization from a pentane solution at low temperature. The structure of the complex was first published in the mid-80s,[30] and it was determined again, in collaboration with dr. Alessandra Forni (CNR – ISTM), under different conditions (130 K instead of 113 K, and room temperature), owing to the significantly improved accuracy of the data. The structure of the two molecules (*a* and *b*) present in the asymmetric unit of $VCl_3(PMePh_2)_2$ is shown in Figure 5.

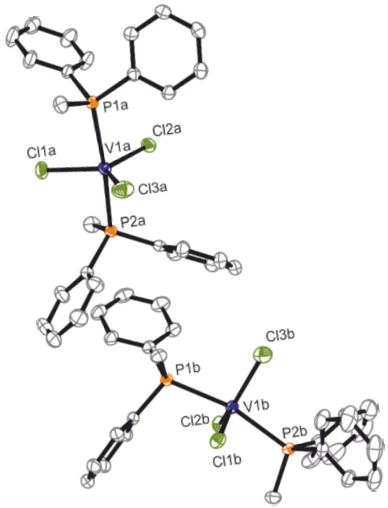

Figure 5 *Molecular structure of $VCl_3(PMePh_2)_2$ (**1b**) [molecule A (top), molecule B (bottom)] with thermal ellipsoids drawn at 50% probability level. Hydrogen atoms are omitted for clarity.*

The structure has been determined as having a distorted trigonal-bipyramidal geometry on account of intermolecular interactions.

5.2.2 Catalytic behavior

Polymerization of ethylene

Series of ethylene polymerizations were performed with $VCl_3(PMePh_2)_2$ (**1b**) and, for comparison, with the precursors $VCl_3(THF)_3$ and VCl_3. Two different aluminum alkyls, *i.e.*, Et_2AlCl and MAO, were used, both in the presence and absence of the reoxidant ETA. The results are summarized in Table 1.

Table 1 *Polymerization of ethylene catalyzed by $VCl_3(PMePh_2)_2$, $VCl_3(THF)_3$, and VCl_3.*[a]

entry	catalyst system	yield (g)	act[b]	M_w[c] (kg mol^{-1})	M_w/M_n[c]
1	$VCl_3(PMePh_2)_2/Et_2AlCl$	0.13	156	308.1	4.2
2	$VCl_3(PMePh_2)_2/Et_2AlCl/ETA$	0.50	1200	22.4	4.3
3	$VCl_3(PMePh_2)_2/MAO$	*traces*			
4	$VCl_3(PMePh_2)_2/MAO/ETA$	0.16	384	900.0	25
5	$VCl_3(THF)_3/Et_2AlCl$	0.13	156	178.4	2.2
6	$VCl_3(THF)_3/Et_2AlCl/ETA$	0.57	1368	19.4	5.6
7	$VCl_3(THF)_3/MAO$	*traces*			
8	$VCl_3(THF)_3/MAO/ETA$	0.31	744	367.0	12.5
9	VCl_3/Et_2AlCl	*not active*			
10	$VCl_3/Et_2AlCl/ETA$	*traces*			

[a] polymerization conditions: ethylene pressure, 1.01 bar; total volume, 25 mL (toluene); V-complex, 5 μmol; Al/V = 2000; ETA/V = 300; temperature, 22 °C; time, 5 min; [b] activity in kg_{pol} mol_V^{-1} h^{-1}; [c] determined by SEC.

VCl_3 proved to be almost inactive to produce PE (Table 1, entry 9 and 10). $VCl_3(PMePh_2)_2$ and $VCl_3(THF)_3$, in combination with Et_2AlCl, gave from low to good activities. Low activities were registered in the absence of ETA likely due to the rapid formation of inactive V(II),[35] while good activities were obtained in the presence of ETA (Table 1, entry 1 *vs* 2, and entry 5 *vs* 6), confirming that it plays a fundamental role in restoring the active specie.[36]

By using MAO in place of Et_2AlCl, only traces of PE were recovered without ETA (Table 1, entries 1 *vs* 3, and 5 *vs* 7) while a modest activity was observed in the co-presence of reoxidant (Table 1, entry 8). This result can be likely due to the different nature of the ion pairing species formed by the two aluminum alkyls. Indeed, the V–alkyl species formed by vanadium complexes and Et_2AlCl was observed to be in an equilibrium between chloro–bridged ($L_nRV\cdots Cl\cdots AlRCl_2$) and cationic alkyl species (L_nRV^+ $AlRCl_3^-$), due to the smaller bulkiness and stronger nucleophilic nature of Et_2AlCl, while an isolated cationic species would be formed in the presence of MAO (L_nMeV^+ X–

MAO-).[8] The equilibrium between the two species by Et_2AlCl would stabilize the active site, leading to higher polymerization activities.

PEs obtained from $VCl_3(PMePh_2)_2$ were semicrystalline materials with a melting temperature of 127 °C, a crystallinity of about 74% (ΔH_m = 220 J/g), and molecular weight higher than those from $VCl_3(THF)_3$.

Keeping these preliminary results in mind, we demonstrated that (*i*) the presence of a ligand coordinated to vanadium (either THF or the phosphine) is fundamental and it is a *necessary conditions* to "activate" the complex, and (*ii*) the reoxidant ETA plays a key role. Moreover, among the possible Al–activators, Et_2AlCl proved to be the *right partner* for this type of complexes.

Copolymerization of ethylene with norbornene

Preliminary studies on E/NB copolymerization catalyzed by $VCl_3(PMePh_2)_2$, $VCl_3(THF)_3$ and VCl_3, in combination with Et_2AlCl, were performed in toluene at atmospheric pressure and room temperature. A series of experiments were carried out at different comonomers feedstock compositions (NB/E from 0.5 to 6). The results are summarized in Table 2.

None of the V(III) complexes was practically active in the homopolymerization of NB. On the contrary, when both E and NB were available for the vanadium active species, an extremely rapid copolymerization took place: $VCl_3(PMePh_2)_2$ and $VCl_3(THF)_3$ were instantaneously activated and the reaction was accompanied by a color shift to orange. The enhanced copolymerization activity may be likely due to the coordination of the highly nucleophilic and sterically encumbered NB cyclic olefin which is expected to stabilize the active species, and to reduce the electrophilicity of vanadium center.[37] As in the case of ethylene homopolymerization, moderate activities were registered in the absence of ETA, while excellent activities were attained with the reoxidant. It should be pointed out that $VCl_3(PMePh_2)_2$ gave activities comparable to those of $VCl_3(THF)_3$ despite a considerable difference in the ligand steric and electronic properties. Possibly, as generally accepted for phosphine-containing catalysts,[38] $VCl_3(PMePh_2)_2$ may be activated through a dissociative mechanism and the structure of vanadium active site is different from that in which we assume two phosphines around the metal. Indeed, both the labile $PMePh_2$ and THF ligands could be easily abstracted by the aluminum alkyl.[39] Nonetheless, what we can state with confidence, is that the ligand abstraction should be only partial and governed by equilibrium. This is because no activity was observed with VCl_3 (Table 2, entry 25), meaning that the presence of THF and $PMePh_2$ ligand in the coordination sphere of vanadium is necessary to the catalytic cycle.

Moreover, with the aim of validating the dissociative mechanism, we carried out the same copolymerization by VCl_3/Et_2AlCl/ETA but with the addition of free $PMePh_2$ (10 equiv to V). In this case, the polymerization productivity remained very low (Table 2, entry 26), confirming that $VCl_3(PMePh_2)_2$ should be activated through a dissociative mechanism where the dissociation of the phosphine is the first and possibly the rate-determining step.

It is worth noting that, as depicted in Figure 6, the polymerization activity of $VCl_3(THF)_3/Et_2AlCl/ETA$ was always slightly higher than that of $VCl_3(PMePh_2)_2/Et_2AlCl/ETA$. This difference can be ascribed to the different ratio of the rate of re-insertion of the dissociated ligand and the rate of the (co)monomers insertion/coordination between the two cases (*i.e.*, $PMePh_2$ *vs* THF).

Table 2 *Copolymerization of ethylene with NB catalyzed by $VCl_3(PMePh_2)_2$, $VCl_3(THF)_3$, and VCl_3 in combination with Et_2AlCl and in the presence or absence of ETA and free $PMePh_2$.*[a]

entry	NB (mol L^{-1})	[NB]/[E][b]	yield (g)	act[c]	NB[d] (mol%)	M_w[e] (kg mol^{-1})	M_w/M_n[e]	T_g (T_m)[f] (°C)
$VCl_3(PMePh_2)_2/Et_2AlCl$								
11	0.57	4	0.17	408	38.4	145.0	1.7	93
$VCl_3(PMePh_2)_2/Et_2AlCl/ETA$								
12	0.08	0.5	0.84	2016	7.1	17.1	3.5	0 (127)
13	0.15	1	0.94	2256	11.6			23 (126)
14	0.29	2	1.20	2880	23.8			42 (126)
15	0.43	3	1.32	3168	35.6	19.5	1.9	33
16	0.57	4	1.38	3312	39.9	19.2	2.1	60
17	0.71	5	1.29	3096	42.5	17.8	2.0	83
18	0.86	6	1.24	2976	43.7	17.6	2.2	86
$VCl_3(THF)_3/Et_2AlCl$								
19	0.57	4	0.33	792	37.8	103.5	1.8	77
$VCl_3(THF)_3/Et_2AlCl/ETA$								
20	0.08	0.5	0.83	1992	8.7	13.7	5.2	1 (122)
21	0.29	2	1.40	3360	19.6			41 (122)
22	0.57	4	1.60	3840	38.9	11.9	1.9	45
23	0.86	6	1.60	3840	45.7	9.0	2.1	42
$VCl_3(THF)_3/Et_2AlCl/ETA + PMePh_2$								
24	0.57	4	1.35	3250	39.2	20.2	1.9	46
$VCl_3/Et_2AlCl/ETA$								
25	0.57	4	inactive					
$VCl_3/Et_2AlCl/ETA + PMePh_2$								
26	0.57	4	traces					
$VCl_3(PMePh_2)_2/Et_2AlCl/ETA$								
27[g]	0.57	4		17950	42.1			
$VCl_3(THF)_3/Et_2AlCl/ETA$								
28[g]	0.57	4		19340	43.2			

[a] polymerization conditions: ethylene pressure, 1.01 bar; total volume, 25 mL (toluene); V-complex, 5 μmol; Al/V = 2000; ETA/V = 300 temperature, 22 °C; time, 5 min; [b] [NB]/[E] feed ratio (mol/mol) in liquid phase; [c] activity in kg_{pol} $mol_V^{-1}h^{-1}$; [d] determined by ^{13}C NMR; [e] determined by SEC; [f] determined by DSC (determination of M_w of sample 13, 14 and 21 with a NB content from 11.6 to 23.8 mol% was complicated and the refractive index detection did not show a significant response; [g] polymerization time = 15 s.

Indeed, the V(III) species is not a particularly hard Lewis acid, and the replacement of the electronegative chlorides in $VCl_3(L)_n$ (L = generic ligand) by an ethyl group and the polymer growing chain increases the covalent character of the bonding in the complex. In this situation, re-addition of the dissociated THF (hard Lewis base) should be slower than successive insertions of the (co)monomers (weak Lewis base), while re-addition of phosphine (weaker Lewis base) should compete with coordination and insertion of (co)monomers.[40] This competition could play a key role in giving lower activities in the case of $VCl_3(PMePh_2)_2$. To support this thesis, we repeated the copolymerization experiment catalyzed by $VCl_3(THF)_3/Et_2AlCl$/ETA (Table 2, entry 22) **but with the addition of free $PMePh_2$** (10 equiv. to V, Table 2 entry 24). By adding the phosphine, the activity decreased from 3840 to 3250 $kg_{pol}\ mol_V^{-1}\ h^{-1}$, thus confirming our claim and data reported with a V(III) complex containing a cyclopentadienyl–amine ligand in the presence of PMe_3.[41]

Regarding the influence of NB feedstock concentration on the activities, it is shown in Figure 7 that the activity increased with increasing the NB/E ratio up to a plateau. There is a marked increasing dependence of the activity on NB concentration up to 0.43 mol L^{-1} likely due to a facile comonomer coordination,[42] and to the fact that the copolymerization was preferred to the homopolymerization of each of the two monomers.

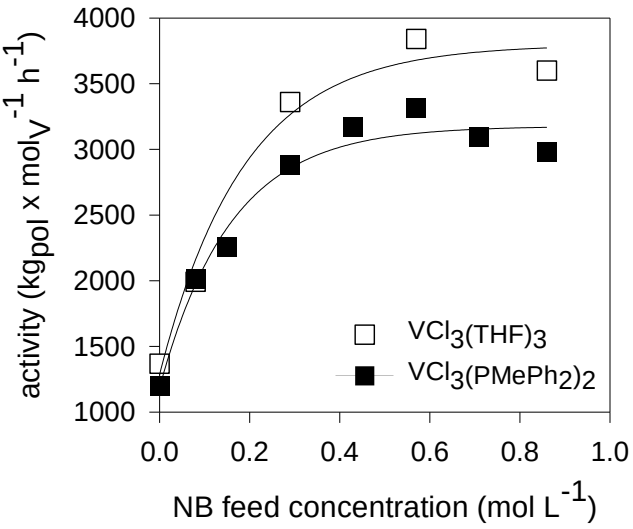

Figure 6 *Plot of catalytic activity vs NB feedstock concentration.The solid lines are guides to the eye and illustrate the overall trend.*

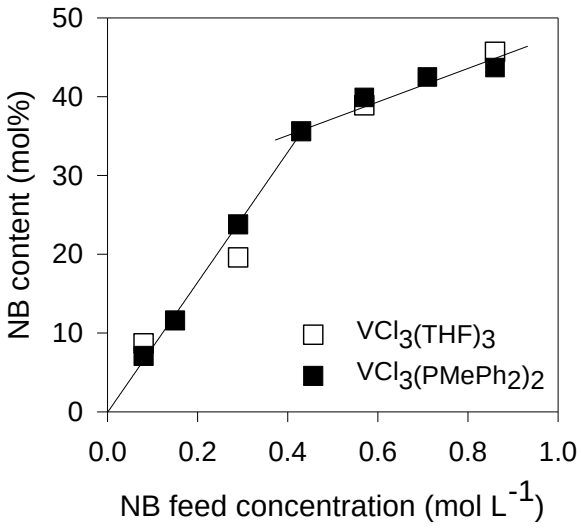

Figure 7 *NB content in the copolymer vs NB feedstock concentration. The solid lines are guides to the eye and illustrate the overall trend.*

It seems that the incorporation of NB is somehow independent of the catalyst structure (Fig. 7). The comonomer content in the copolymers increased linearly with the NB feedstock concentration from 0.08 to 0.43 mol L^{-1} after which increased slightly up to 43.7 and 45.7 mol% for $VCl_3(PMePh_2)_2$ and $VCl_3(THF)_3$, respectively.

All the copolymers had unimodal and relatively narrow molecular weight distribution (M_w/M_n = 1.6–3.5) consistent with the predominance of a single homogenous catalytic active species.

Copolymers with high molecular weight were obtained in the absence of ETA, while in the presence of the reoxidant both the V(III) complexes gave low molecular weight polymers (Table 2, entries 11 *vs* 16, and entries 19 *vs* 22). Specifically, copolymers from $VCl_3(PMePh_2)_2$ had higher molecular weights than those obtained with $VCl_3(THF)_3$, and in some cases even double (Table 2). This result may be ascribed to the lower tendency of $VCl_3(PMePh_2)_2$ to give β–H elimination at a last enchained ethylene unit as revealed by the low amount of vinyl-end chain groups observed in the ^1H NMR spectrum of copolymers (not reported here, see ref. 47).

The thermal properties of the copolymers were investigated by DSC. The heating profiles of all the copolymers obtained at very low NB feedstock concentration (Table 2, entries 12–14, and 20–21) showed both a glass transition event and a melting endotherm. To ascertain that the obtained materials were not a mixture of PE and the copolymer, fractionation with boiling solvents were carried out, and only a single fraction was collected, hence showing that the homopolymerization of one of the two monomers did not take place. This means that the copolymerization is always preferred to the homopolymerization of each of the two monomers.

On the other hand, by increasing the NB/E ratio (Table 2, entries 15–19 and 22–24), the copolymers showed only a single T_g, consistent with a completely amorphous structure. T_gs of the copolymers from $VCl_3(THF)_3$ (Table 2, entries 22–24) did not increase with increasing NB content, while T_gs of those from $VCl_3(PMePh_2)_2$ increased accordingly (Table 2, entries 15–19), as in general observed for poly(E-*co*-NB)s.[43] Moreover, T_gs for $VCl_3(THF)_3$ are always lower than those for $VCl_3(PMePh_2)_2$ at comparable NB incorporation. These facts indicate that copolymers from $VCl_3(THF)_3$ are less homogenous in terms of composition distribution. This may be likely due to a more pronounced compositional drift in the semi-batch copolymerization process catalyzed by $VCl_3(THF)_3$, leading to NB–rich copolymer chains at the beginning of the copolymerization, and E–rich at the end of the reaction (Fig. 8).

Figure 8 *Schematic representation of the compositional drift in an E/NB copolymer.*

The microstructure of E/NB copolymers was investigated by ^{13}C NMR. The signals of each chemical shift region were assigned according to the literature, as already reported in paragraph 3.6.2.

^{13}C NMR spectra of two copolymers obtained with $VCl_3(PMePh_2)_2$ (entry 16, NB = 39.9 mol%) and $VCl_3(THF)_3$ (entry 22, NB = 38.9 mol%) are shown in Fig. 9a and 9b, respectively. The spectra showed the typical pattern of alternating copolymers from an addition–type NB copolymerization

with *cis exo-exo* enchainment. The dominant signals are those of alternating and isolated NB units, with traces of diads. The relative intensities of peak at 45.7 and 45.2 ppm, assigned to C2/C3 of NB in the alternating isotactic and syndiotactic NB–E–NB–E–NB sequences, respectively, also revealed that the copolymers have a random tacticity.

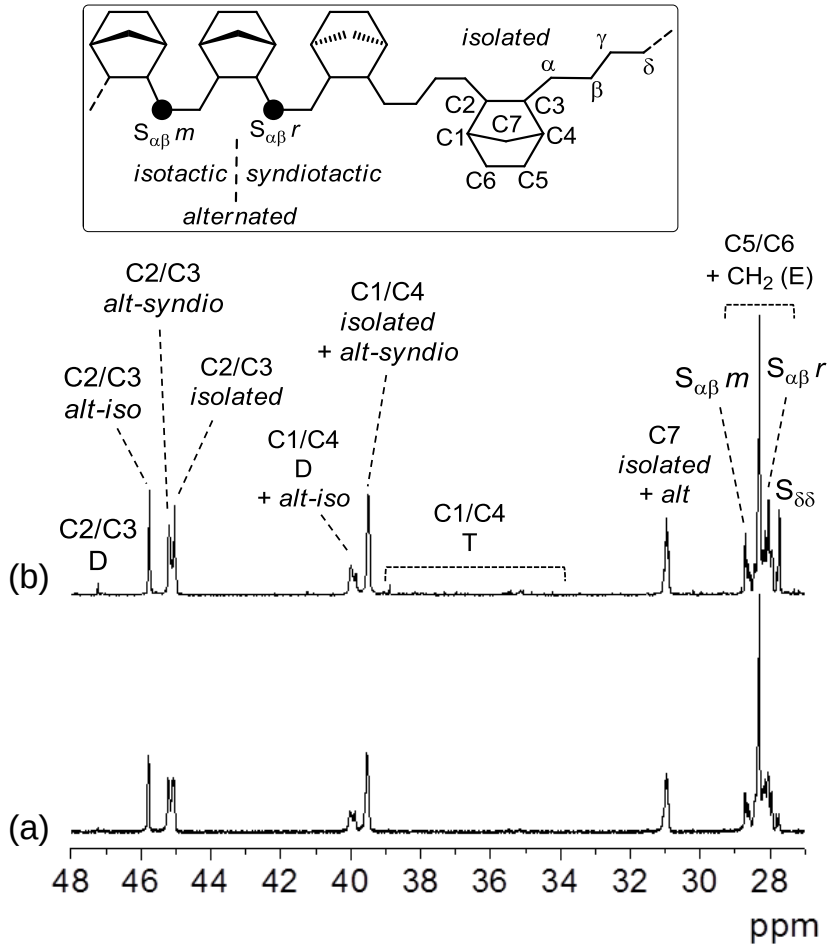

Figure 9 *^{13}C NMR spectra of the E/NB copolymers obtained with (a) $VCl_3(PMePh_2)_2$ (entry 16, NB = 39.9 mol%) and (b) $VCl_3(THF)_3$ (entry 22, NB = 38.9 mol%). D and T refer respectively to NB dyads and triads*

Much work has been done to develop general procedures for the investigation of E/NB copolymers microstructure by ^{13}C NMR, and hence to calculate the reactivity ratios and elucidate the copolymerization mechanism.

However, the previously reported equations assume a homogeneous Markov process for the copolymerization, where the conditional probabilities of insertion of the comonomers into the growing chain are constants. For this reason, they must be used under low conversion regimes (≤ 5%), where the compositional drift that takes place during the polymer formation, and consequent change in the insertion probabilities, can be neglected.

Unfortunately, V(III) based catalysts studied herein displayed an impressive activity, and NB conversions beyond 50% were reached already in experiments less than one minute long, thus

breaking the applicability of the standard theoretical tools to study the catalytic mechanisms. Hence, ad-hoc experiments (polymerization times in the order of seconds, at NB/E = 4, Table 2, entries 27 and 28) were designed to ensure the uniformity of the catalytic copolymerization process.

At this point, the fruitful collaboration with dr. Arnaldo Rapallo (CNR–ISMAC) was fundamental. He developed an appropriate procedure for ^{13}C NMR spectrum deconvolution and a Monte Carlo based computational original approach to model the copolymerization process, which fully takes into account the non-homogeneity conditions proper to the high conversion regimes. With these new tools in hand, both the order of the catalytic mechanism and the reactivity ratios can be evaluated at high conversions. It was found that $VCl_3(THF)_3$ was more sensitive to penultimate effects from the growing polymer chain (second–order Markov statistics, MK2), while copolymerizations with $VCl_3(PMePh_2)_2$ were well described by first–order Markov statistics (MK1). Anyway, the two catalysts produced copolymers with essentially the same microstructure, the differences between the two cases being quite small, as can be seen in Figure 10. The more complex MK2 mechanism invoked for $VCl_3(THF)_3$ is required to fine tune the details of the microstructure, though the MK1 model already captured the main features of microstructure. The biggest microstructural differences between the copolymers generated by the two catalytic systems are about 2% for ENEE and NENE tetrads, and 1.5% for ENNN (N = a norbornene enchained unit). The analysis presented above shows that the two copolymers are alternated (r_1r_2 « 1). The most abundant tetrad is ENEN, followed by EENE with slightly more than one half of its frequency. The microstructures at tetrad level are essentially the same, even if $VCl_3(THF)_3$ complex seems to be more sensitive to penultimate effects than $VCl_3(PMePh_2)_2$.

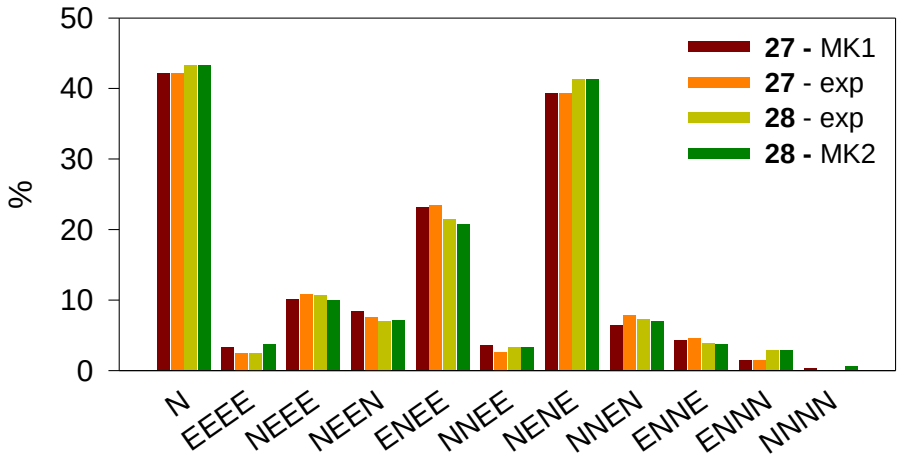

Figure 10 *Experimental and calculated tetrad distributions. Also the norbornene content (N) is shown in the first column.*

Finally, the response of the complex to reaction conditions variations was examined by modifying three parameters, namely ETA/V ratio, Et_2AlCl dosage, and copolymerization temperature.

Copolymerization of ethylene with norbornene at different ETA/V ratio

A series of copolymerizations were performed with $VCl_3(PMePh_2)_2/Et_2AlCl$/ETA at different ETA/V ratio from 10 to 900, and NB feedstock concentration of 0.57 mol L^{-1} (NB/E = 4). Relevant data are summarized in Table 3.

As shown in Figure 11, there was an approximate linear dependence of the activity on ETA/V ratio up to 150. It is worth noting that an excellent activity was observed also in the presence of a low excess of ETA (10 equiv to V, entry 29), while at higher amount of ETA the productivity dropped off rapidly, implying that excess of chloro reagent suppresses the copolymerization and potentially competes with (co)monomer coordination/insertion, likely through a chelation of the carbonyl oxygen to the vanadium center.[44]

Table 3 *Copolymerization of ethylene with NB catalyzed by $VCl_3(PMePh_2)_2/Et_2AlCl$/ETA at different ETA/V ratio.*[a]

entry	ETA/V	yield (g)	act[b]	NB[c] (mol%)	M_w[d] (kg mol^{-1})	M_w/M_n[d]	T_g[e] (°C)
11[f]	–	0.17	408	38.4	145.0	1.7	93
29	10	1.30	3120	38.0	49.5	1.9	74
30	50	1.36	3264	36.8	38.3	1.9	65
31	150	1.50	3600	38.9	31.0	1.8	60
16[f]	300	1.38	3312	39.9	19.2	2.1	60
32	900	1.12	2688	40.9	10.1	1.8	24

[a] polymerization conditions: ethylene pressure, 1.01 bar; total volume, 25 mL (toluene); $VCl_3(PMePh_2)_2$, 5 μmol; Al/V = 2000; [NB]/[E] = 4; temperature, 22 °C; time, 5 min; [b] activity in kg_{pol} mol_V^{-1} h^{-1}; [c] determined by ^{13}C NMR; [d] determined by SEC; [e] determined by DSC; [f] first reported in Table 2.

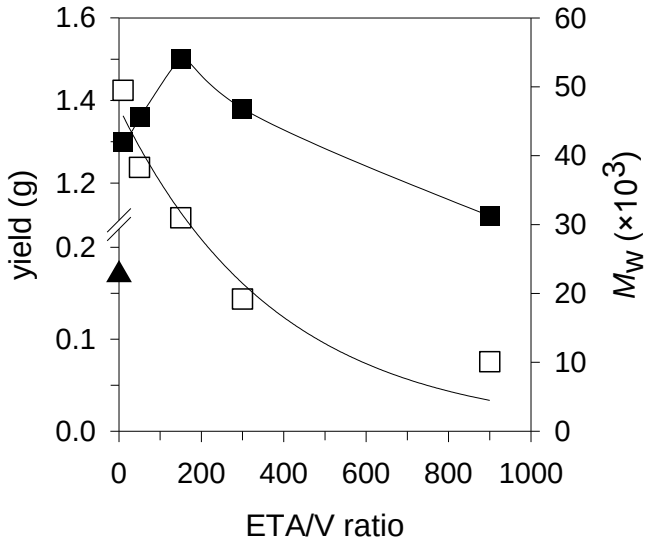

Figure 11 *Plot of copolymerization yield (■) and copolymers molecular weight (□) vs ETA/V mole ratio in the copolymerization by $VCl_3(PMePh_2)_2/Et_2AlCl$/ETA at NB/E = 4 and 20°C. Polymerization yield (▲) vs ETA/V ratio for the copolymer obtained with $VCl_3(PMePh_2)_2/Et_2AlCl$ at NB/E = 4 but without ETA is also shown (entry 11, M_w = 145000 g mol^{-1}).*

The molecular weight of the copolymers lowered increasing ETA concentration, meaning that the reoxidant behaved also as chain termination/transfer agent. Addition of 4.53 mmol of ETA (ETA/V = 900) gave a copolymer with a molecular weight lowered to 10100 g mol^{-1} (Fig. 11). The copolymers obtained at different ETA/V ratio have comparable NB content (37–41 mol%), while T_gs increased from 24 to 74 °C with increasing the copolymer molecular weight.

Copolymerization of ethylene with norbornene at different Al/V ratio

The effect of Et_2AlCl dosage was also examined at NB feedstock concentration of 0.57 mol L^{-1} (NB/E = 4) and ETA/V = 300 (Table 4).

The copolymerizations were performed over the range of Al/V from 250 to 4000. A relatively low excess of Et_2AlCl (Al/V = 250) was sufficient for exhibiting activity as high as 1848 kg_{pol} mol_V^{-1} h^{-1} (entry 33). Then the activity increased gradually reaching a maximum value of 3360 kg_{pol} mol_V^{-1} h^{-1} when Al/V = 4000 (entry 36). By contrast, the copolymer's composition and microstructure as well as the molecular weight were almost unchanged over the increasing of the Al/V ratio, confirming that the chain transfer to the aluminum was not the dominant chain transfer. This result is quite different from that observed for the polymerization of ethylene by *N*,*N*-chelating iminopyrrolide V(III) complex,[45] but it is comparable to that for the copolymerization of ethylene with 1-hexene with mono(β-enaminoketonato)V(III) complexes.[46]

Table 4 *Copolymerization of ethylene with NB catalyzed by $VCl_3(PMePh_2)_2$/Et_2AlCl/ETA at different Al/V ratio.*[a]

entry	Al/V	yield (g)	act[b]	NB[c] (mol%)	M_w[d] (kg mol^{-1})	M_w/M_n[d]
33	250	0.77	1848	37.7	18.4	2.0
34	500	0.98	2352	39.9	17.5	1.9
35	1000	1.35	3240	40.4	18.5	2.0
16[e]	2000	1.38	3312	39.9	19.2	2.1
36	4000	1.40	3360	42.0	16.7	1.8

[a] polymerization conditions: ethylene pressure, 1.01 bar; total volume, 25 mL (toluene); $VCl_3(PMePh_2)_2$, 5 μmol; ETA/V = 300; [NB]/[E] = 4; temperature, 22 °C; time, 5 min; [b] activity in kg_{pol} mol_V^{-1} h^{-1}; [c] determined by ^{13}C NMR; [d] determined by SEC; [e] first reported in Table 2.

Copolymerization of ethylene with norbornene at different temperatures

With the feed of 2000 equivalents of Et_2AlCl, a series of copolymerizations were carried out at different temperature from 0 to 70 °C (Table 5).

The activity decreased at higher temperature likely due to the rapid deactivation even for a short polymerization time (5 min) and in the presence of an excess of the reoxidant (300 equiv to V). The NB content in the copolymers increased from 37.0 mol% at 0 °C to 44.9 mol% at 70 °C. The copolymer molecular weight decreased with temperature likely due to an increase of chain-transfer side reactions. In contrast, the molecular weight distribution remained relatively narrow,

meaning that the copolymerization took place with uniform catalytically active species even at 70 °C. By increasing the polymerization temperature, the copolymer molecular weight decreased from 98.0 to 7.0×10^3 g mol^{-1} and, in the same manner, the T_g decreased from 80 to 51 °C.

Table 5 *Copolymerization of ethylene with NB catalyzed by $VCl_3(PMePh_2)_2$/Et_2AlCl/ETA at different temperature.*[a]

entry	*T* (°C)	yield (g)	act[b]	NB[c] (mol%)	M_w[d] (kg mol^{-1})	M_w/M_n[d]	T_g[e] (°C)
37	0	1.40	3360	37.0	98.3	2.4	80
16[f]	22	1.38	3312	39.9	19.2	2.1	60
38	50	0.65	1548	42.7	10.8	2.0	56
39	70	0.31	732	44.9	7.0	2.1	51

[a] polymerization conditions: ethylene pressure, 1.01 bar; total volume, 25 mL (toluene); $VCl_3(PMePh_2)_2$, 5 μmol; Al/V = 2000; ETA/V = 300; [NB]/[E] = 4; time, 5 min; [b] activity in kg_{pol} mol_V^{-1} h^{-1}; [c] NB determined by ^{13}C NMR; [d] determined by SEC;
[e] determined by DSC; [f] first reported in Table 2.

5.3 How does the ligand make the difference?

5.3.1 Synthesis and characterization of V(III) monodentate phosphine complexes

In order to better understand the role of the phosphine ligand, and its effects on the activity by varying the electronic and steric properties, vanadium(III) complexes with different tertiary phosphines were synthesized.

The synthetic procedure was analogous to that reported for complex **1b**, and it was accomplished by addition of the phosphine to a suspension of $VCl_3(THF)_3$ (P/V = 4:1 mole ratio). The solvent was chosen as a function of the type of ligand (toluene in the case of the more aryl complexes **1c**, **1d**, **1f**, **1g**, **1h**, **1m**, while THF in the case of the more alkyl complexes **1a**, **1e**, **1i**, **1l**, **1n**). The complexes were generally obtained in good yields as microcrystalline solids.

Beyond **1b**, whose structure was already described at the beginning of this chapter (paragraph 5.2), single crystals suitable for X-ray structure determination were obtained for $VCl_3(PEtPh_2)_2$ (**1f**), $VCl_3(PEt_2Ph)_2$ (**1i**), and $VCl_3(PCyp_3)_2$ (**1m**) from cold pentane, and the exact structure was solved in collaboration with dr. Alessandra Forni (CNR – ISTM). A view of the molecular structure of the complexes is reported in Figure 12. The complexes adopt slightly distorted trigonal–bipyramidal geometry, where the main distortion comes from the deviation (by up to 13°) of the P–V–P angles from 180°. The solid state structure of these complexes confirms our first formulation of five-coordinate mononuclear VCl_3 complexes with two phosphine ligands, analogous to the one found for complex **1b**.

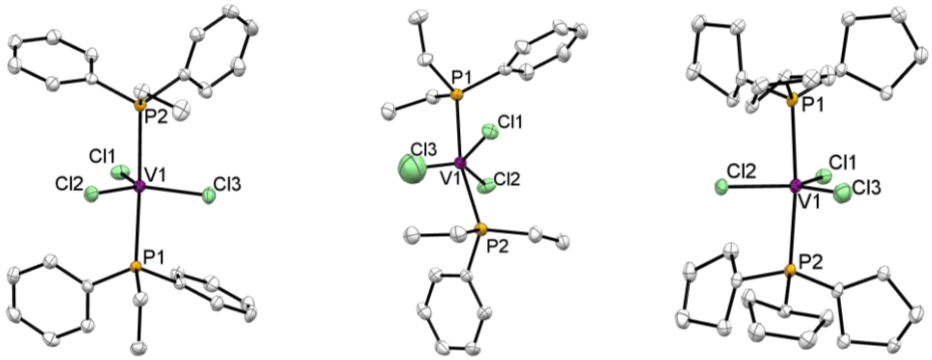

Figure 12 *Molecular structure of $VCl_3(PEtPh_2)_2$ (**1f**), $VCl_3(PEt_2Ph)_2$ (**1i**) and $VCl_3(PCyp_3)_2$ (**1m**) with thermal ellipsoids drawn at 50% probability level. Hydrogen atoms are omitted for clarity.*

5.3.2 Catalytic behavior

Some complexes were tested as pre-catalysts in the (co)polymerization of ethylene with NB. The three-term series of complexes **1a** (PMe_2Ph), **1b** ($PMePh_2$) and **1c** (PPh_3) was chose for the increasing "aryl character" corresponding to a decrease in the σ–donor character (or, in other terms, a decreased donor strength), while the second series **1c** (PPh_3), **1d** (PCy_3), **1e** ($PtBu_3$) was mainly selected to compare the steric variations, since the cone angle increases along the series.

Polymerization of ethylene

All the vanadium(III) phosphine complexes were firstly screened for the homopolymerization of ethylene. The polymerization conditions were chosen accordingly to the optimized ones previously identified by using $VCl_3(PMePh_2)_2$ (**1b**). The results are summarized in Table 6 and are presented as a function of the phosphine donor ability (measured with the Tolman electronic parameter, ν_{CO}) and steric properties (measured by cone angle, θ). A comparison with $VCl_3(PMePh_2)_2$ (**1b**) is also reported.

Table 6 *Polymerization of ethylene catalyzed by monodentate phosphine V(III) complexes in combination with Et_2AlCl and in the presence of ETA.* [a]

entry	cat	phosphine			yield	act[d]	M_w[e]	M_w/M_n[e]
		(type)	ν_{CO}[b] (cm^{-1})	θ[c] (°)	(g)		(kg mol^{-1})	
1	**1a**	PMe_2Ph	2065.3	122	0.19	1170	65.5	6.8
2	**1b**	$PMePh_2$	2067.0	136	0.28	1686	44.6	3.9
3	**1c**	PPh_3	2068.9	145	0.30	1812	35.3	4.2
4	**1d**	PCy_3	2056.4	170	0.22	1326	56.9	6.3
5	**1e**	$PtBu_3$	2056.1	182	0.29	1770	84.3	7.9

[a]polymerization conditions: ethylene pressure, 1.01 bar; total volume, 25 mL (toluene); V-complex, 5 μmol; Al/V = 500; ETA/V = 50; time, 2 min; temperature, 22 °C; [b] measure of the electron-donating properties of phosphine ligands, as reported by Tolman;[32] [c] phosphine cone angle, as reported by Tolman;[32] [d] activity in kg_{pol} $molv^{-1}$ h^{-1}; [e] determined by SEC.

All the investigated vanadium complexes exhibited good activities for the polymerization of ethylene. Specifically, the activity increased in the order **1a** (1170 kg_{pol} mol_V^{-1} h^{-1}) < **1d** (1326) < **1f** (1560) < **1b** (1686) < **1e** (1770) < **1c** (1812), suggesting that the productivity is strongly affected by the ligand substituents on the phosphorus atom. All the obtained PEs were linear, semicrystalline materials with a T_m of about 130 °C.

We found that also the polymer molecular weight was strongly affected by the substituents on the phosphorus atom. However, the relationship between the catalytic activity, the (co)polymer molecular weight and the type of ligand is not straightforward. This is because the phosphine ligands are involved in dynamic "*on*/*off*" events, which include dissociative and associative pathways, multiple mechanistic steps, and competitive reactions,[47] and electronic and steric effects are intimately related and difficult to separate in any pure way. Changing the substituents on the phosphorus atoms can cause large changes in the ligand donor properties, aryl phosphines (weaker σ-donor character) being weakly coordinated to the metal than alkyl phosphines (stronger σ-donor character).[48]

Nonetheless, according to the parameters defined by Tolman,[32] a general trend seems to emerge clearly. Indeed, for complexes having at least one phenyl group at the phosphorus atoms, *i.e.*, $VCl_3(PMe_nPh_{3-n})_2$ and $VCl_3(PPh_3)_2$, the activity increased in the order **1a** (PMe_2Ph, 1170 kg_{pol} mol_V^{-1} h^{-1}) < **1b** ($PMePh_2$, 1690) < **1c** (PPh_3, 1810) according to the phosphine ligand donor strength (Table 6 and Figure 13).

Steric effects also play a role.[48] In fact, **1e** (P*t*Bu_3, the strongest σ-donor, θ = 182°) gave an activity close to that of **1b** ($PMePh_2$, θ = 136°): in this case the bigger size of **1e** relative to **1b** more than compensates for its higher donor strength (Figure 13). In addition, the effect of steric perturbations is better illustrated by the differences in the activity between complexes **1d** (PCy_3) and **1e** (P*t*Bu_3). These two complexes have similar electronics (**1d**: ν_{CO} = 2056.1 cm^{-1}; **1e**: ν_{CO} = 2056.4 cm^{-1}), but **1e** exhibited the highest activity likely due to the larger cone angle of P*t*Bu_3 (θ = 182°) compared to that of PCy_3 (θ = 170°) (Table 6 and Fig. 13).

The differences in ligand properties influence the polymer molecular weights as well. Complexes bearing phosphines with an increased σ-donor character gave PEs with higher molecular weight: **1e** (P*t*Bu_3, the strongest σ-donor in the series) gave the polymer with the highest molecular weight (Table 6, entry 5 M_w = 84300 g mol^{-1}), while PPh_3 (the weakest σ-donor in the series) gave the polymer with the lowest molecular weight (Table 6, entry 3 M_w = 35300 g mol^{-1}). Also of note, the molecular weight of PEs obtained from complexes having aryl phosphines increased in the reverse order with respect to the activity, that is **1c** (PPh_3, M_w = 35300 g mol^{-1}) < **1b** ($PMePh_2$, 44600) < **1a** (PMe_2Ph, 65500).

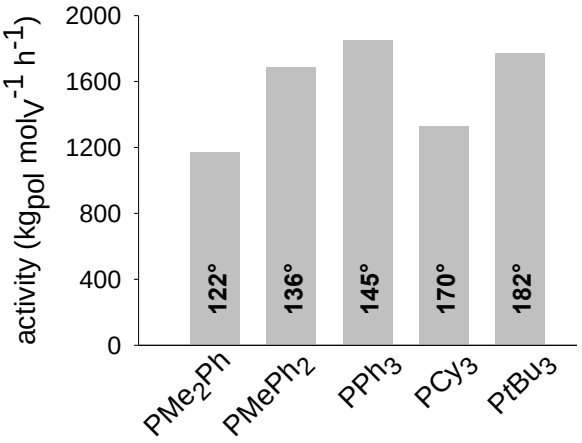

Figure 13 *Ethylene polymerization. Plot of the catalytic activity vs the vanadium complexes employed [PMe_2Ph (**1c**), $PMePh_2$ (**1b**), PPh_3 (**1c**), PCy_3 (**1d**) and $PtBu_3$ (**1e**)]. In each bar the phosphine cone angle is reported.*

Copolymerization of ethylene with norbornene

The phosphine V(III) complexes were successively employed for the E/NB copolymerization under the same set of conditions of 1 atm of ethylene, at 20 °C, in toluene, with Et_2AlCl (500 equiv. to V), ETA (50 equiv. to V) and for a NB/E ratio of 4. To ensure the uniformity of the catalytic copolymerization process even in the presence of a relevant compositional drift, the copolymerization time was fixed at 10 sec. All these conditions were found optimal for balancing the displacement of the labile phosphine ligand, for generating the active species, preventing reduction to inactive V(II), and limiting the unavoidable compositional drift. All the results are summarized in Table 7. A comparison with $VCl_3(PMePh_2)_2$ (**1b**) under the same experimental conditions is also reported.

Table 7 *Copolymerization of ethylene with NB catalyzed by monodentate phosphine V(III) complexes in combination with Et_2AlCl and in the presence of ETA.* [a]

entry	cat	phosphine			yield	act[d]	NB[e]	M_w[f]	M_w/M_n[f]	T_g[g]
		(type)	ν_{CO}[b] (cm^{-1})	θ[c] (°)	(g)		(mol%)	(kg mol^{-1})		(°C)
6	**1a**	PMe_2Ph	2065.3	122	0.16	11520	38.0	90.3	4.2	90
7	**1b**	$PMePh_2$	2067.0	135	0.24	17352	37.8	61.4	3.8	90
8	**1c**	PPh_3	2068.9	145	0.37	26424	38.7	42.6	4.2	81
9	**1d**	PCy_3	2056.4	170	0.23	16272	39.3	86.4	5.9	93
10	**1e**	$PtBu_3$	2056.1	182	0.25	17784	38.8	353.2	11.5	85

[a] polymerization conditions: ethylene pressure, 1.01 bar; total volume, 25 mL (toluene); V-complex, 5 μmol; Al/V = 500; ETA/V = 50 temperature, 22 °C; time, 10 sec; [NB]/[E] feed ratio, 4 mol/mol; NB feedstock concentration, 0.57 mol L^{-1}; [b] measure of the electron-donating properties of phosphine ligands, as reported by Tolman;[32] [c] phosphine cone angle, as reported by Tolman;[32] [d] activity in kg_{pol} mol_V^{-1} h^{-1}; [e] determined by ^{13}C NMR; [f] determined by SEC; [g] determined by DSC.

None of the investigated complexes was active in the homopolymerization of NB under the conditions employed, while excellent activities, in the range from 10080 to 26420 kg_{pol} mol_V^{-1} h^{-1},

were obtained for the E/NB copolymerization. When both the comonomers were available for the vanadium active species, all the complexes were instantaneously activated and an extremely rapid copolymerization took place. Excellent yields were obtained, the activities being in the range from 10080 to 26424 $kg_{pol}\ mol_V^{-1}\ h^{-1}$. In general, as observed for the homopolymerization of ethylene, complexes with aryl phosphines were more active than those with alkyl phosphines, complex **1c** with PPh_3 being the most active one (Table 7, entry 8), according to the lower donor strength of PPh_3 (Fig. 14). Yet, in the case of complex **1e**, the significant high activity can be likely ascribed to the bigger P*t*Bu$_3$ size (θ = 182°) despite the fact that P*t*Bu$_3$ is the strongest σ-donor in the series.

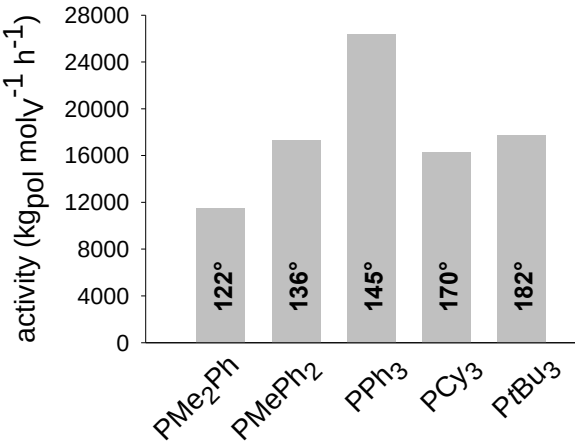

Figure 14 *Copolymerization of ethylene with NB. Plot of the catalytic activity vs the vanadium complexes employed [PMe_2Ph (**1c**), $PMePh_2$ (**1b**), PPh_3 (**1c**), PCy_3 (**1d**) and $PtBu_3$ (**1e**)]. In each bar the phosphine cone angle is reported.*

The resulting poly(E-*co*-NB)s have from rather low to very high molecular weights, and molecular weight distribution ranging from 2.8 to 11.5. As observed for the ethylene homopolymerization, the nature of the phosphine ligand considerably influences the copolymer molecular weight. Overall, an increase of the ligand σ-donor ability has a positive effect on the molecular weight: complex **1e** with P*t*Bu$_3$ (the strongest σ-donor) yielded the copolymer with the highest molecular weight (Table 7, entry 10, M_w = 353200 g mol^{-1}), while **1c** with PPh_3 (the weakest σ-donor) gave the copolymer with the lowest molecular weight (Table 7, entry 8, M_w = 42600 g mol^{-1}). A more strongly electron-donating ligand may stabilize the electron-deficient intermediate and reduce the rate of β–hydride elimination and subsquent chain transfer.[49] Conversely, electron-withdrawing groups on the phosphine ligand reduce electron density at the metal center, resulting in higher rates of β–hydride elimination, but significantly enhancing the catalytic performance. This could be explained assuming that the β–hydride elimination is the rate-determining step.

In constrast, the type of phosphine ligand had no significant effect on the NB incorporation and microstructure of the copolymers. All the obtained copolymers had a NB content ranging from 37.8 to 39.3 mol%, regardless of steric and electronic properties of the phosphine ligand. The same

result was found by Yue-Sheng Li *et al*. by using vanadium(III) complexes bearing β-enaminoketonato ligands,[25] and different tridentate salicyladiminato ligands.[26]

The copolymers microstructure was investigated by ^{13}C NMR. The spectra show the typical pattern of alternating copolymers from an addition–type NB copolymerization with *cis exo-exo* enchainment. The dominant signals are those of alternating and isolated NB units, with tiny traces of diads.

Analysis of the copolymers thermal properties revealed no melting events, but only a unique glass transition temperature (T_g) in the range from 81 to 93 °C, thus suggesting that the copolymers are amorphous with an homogeneous composition.[50] It is expected that for random copolymers the T_g should increase with increasing the comonomer content in the copolymers.[51] However, a different behavior was identified in this case: copolymers from V(III)–phosphine complexes have higher T_g with respect to the copolymer from $VCl_3(THF)_3$ despite the higher comonomer content (NB content = 41.2 mol%, T_g = 73 °C, results not reported in Table 7). This can be attributed to a lower homogeneity of the copolymer in terms of composition distribution, likely due to a faster initiation catalyst efficiency of $VCl_3(THF)_3$, and hence to a pronounced compositional drift (Fig. 8). This result confirms the relevant role of phosphine ligands.

5.4 Enhancing catalyst stability: bidentate chelating ligands

As abovementioned, one of the major disadvantage of working with V(III) complexes is the high instability of the metal in the oxidation state (III) and its facile reduction to inactive V(II) species. Up to now, this drawback has been overcome by the use of ETA. However, as discussed above for monodentate phosphine vanadium complex **1b** at different ETA/V ratio (see Table 3), ETA acts also as chain-transfer agent, lowering the molecular weight of the resulting copolymers.[47] In this respect, the use of multidentate ligands might represent an alternative solution to stabilize V(III) species and hence to improve the overall catalytic activity.[26] For example, it is expected that diphosphines can impart greater stability in their complexes due to the chelate effect, and a specific geometry to the resulting complex, since the P–V–P bite angle should be strongly dependent on the bridge between the two phosphorous atoms.[52] As a consequence, it is supposed that the structure of the vanadium–diphosphine complex would retard chain transfer.

5.4.1 Synthesis and characterization of V(III) bidentate phosphine complexes

In the light of the abovementioned considerations, three new V(III) complexes with bidentate phosphine ligands of type $R_2P(CH_2)_2PR_2$ [R = Me (**2a**), Et (**2b**), Ph (**2c**)] (Fig. 15) were synthesized by reacting $VCl_3(THF)_3$ with the phosphine in toluene at room temperature. The ligands have the same backbone, but they differ in the substituents on the phosphorous donor atom.

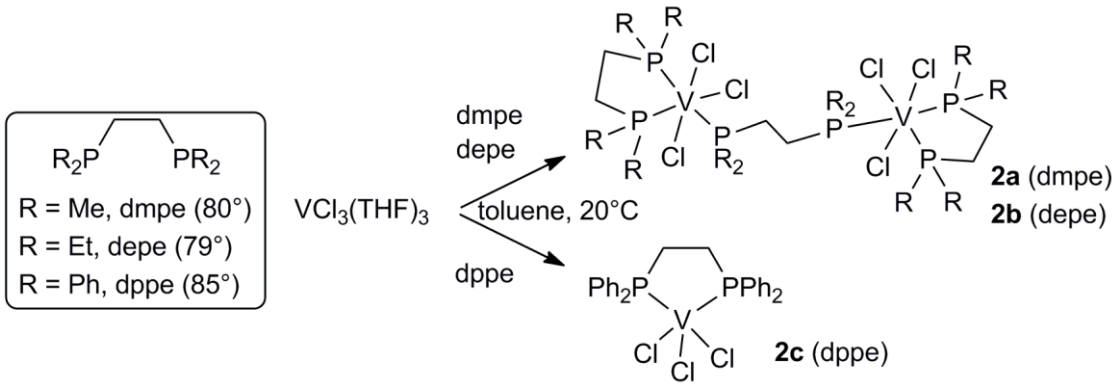

Figure 15 *Diphosphine ligands used in this work (with abbreviations and natural bite angles) and synthesis of the corresponding vanadium(III) complexes (dmpe = 1,2-bis(dimethylphosphino)ethane, depe = 1,2-bis(diethylphosphino)ethane, dppe =1,2-bis(diphenylphosphino)ethane).*

All the complexes were characterized by ATR–FTIR, elemental analysis, and the molecular structure of **2a** and **2b** were determined by X-ray diffraction, in collaboration with dr. Emilio Parisini (IIT Milan). Single crystals of **2a**, suitable for X-ray diffraction analysis, were grown from a cold pentane solution. The crystal structure is shown in Fig. 16. As revealed by the X-ray structure determination, **2a** is a dimer of formula $[VCl_3(dmpe)]_2(\mu\text{-}P,P'\text{-}dmpe)$, containing one chelating dmpe ligand on each of the vanadium atom plus an additional dmpe ligand bridging the two metals. Three chlorides complete the octahedral coordination around each metallic center. The two chelating phosphines form five-membered rings with their coordinated metal, one having a 2.02° and the other a 5.40° out-of-plane distortion.

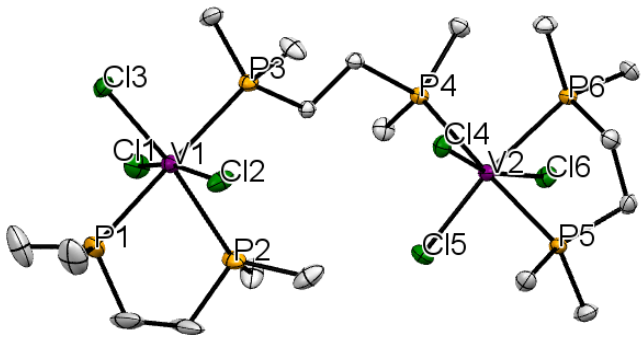

Figure 16 *ORTEP drawing of **2a**.*
Thermal ellipsoids are drawn at the 30% probability level. Hydrogen atoms are omitted for clarity.

Single crystals of **2b**, suitable for X-ray diffraction analysis, were grown from a cold diethyl ether solution. The crystal structure is shown in Fig. 17. Complex **2b** is a dimer of formula $[VCl_3(depe)]_2(\mu\text{-}P,P'\text{-}depe)$, containing one chelating depe ligand on each of the vanadium plus an additional depe ligand bridging the two metals. Three chlorides complete the octahedral coordination around each vanadium atom.

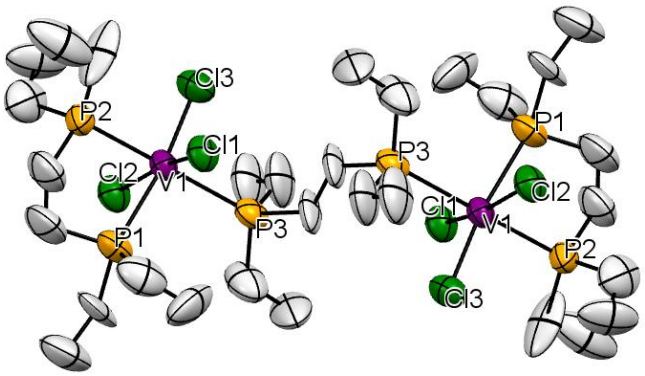

Figure 17 *ORTEP drawing of* ***2b****.*
Thermal ellipsoids are drawn at the 30% probability level. Hydrogen atoms are omitted for clarity.

The ability of bidentate phosphine ligands to form dimeric complexes for **2a** and **2b**, even in the presence of a low excess of the ligand (1.3 equiv. to V), resembles the results found by Lorber *et al.* on the aryl imido–vanadium(IV) complex containing dmpe ligand.[18] Indeed, they found that the addition of 1.5 equiv of dmpe to the imido complex $V(NAr)Cl_2$ (Ar = 2,6-*i*$Pr_2C_6H_3$) led to the formation of a dimer of formula $[V(NAr)Cl_2(dmpe)]_2$(μ-P,P′-dmpe), therefore confirming our results.

Numerous attempts to isolate single crystal of **2c**, suitable for structural determination, were unsuccessful. This complex has bulky phenyl groups on the phosphorous atoms (with respect to the alkyl groups of **2a** and **2b**) that increase steric interactions. Most probably, the significant steric hindrance around the vanadium for **2c** inhibits the formation of a dinuclear complex similar to those found for **2a** and **2b**, featuring a chelating and a bridging phosphine ligand. In this respect, the analytical data for **2c** are fully consistent with the formation of a mononuclear structure of stoichiometry $(Ph_2P(CH_2)_2PPh_2)VCl_3$ in which the diphosphine acts as a bidentate η^2–dppe ligand (Fig. 15). This result is also in agreement with previous works concerning the behavior of diphosphine ligands: it was reported that for transition metal complexes having diphosphine ligands of the type $R_2P(CH_2)PR_2$, the more stable form is the monomeric one for R = Ph, while it is the dimeric one for R = Me.[53]

5.4.2 Catalytic behavior

Polymerization of ethylene

Complexes **2a**–**2c** were first screened for the polymerization of ethylene under the same set of conditions of 1 atm of ethylene, at 20 °C, in toluene, with Et_2AlCl as cocatalyst (500 equiv. to V) and in the presence and absence of ETA (50 equiv. to V). The results are summarized in Table 8. A comparison with $VCl_3(THF)_3$ and $VCl_3(PMePh_2)_2$ (**1b**), having a cone angle close to that of **2a**–**2c**, is also reported.

Table 8 *Polymerization of ethylene catalyzed by bidentate phosphine V(III) complexes in combination with Et_2AlCl and in the presence or absence of ETA.*[a]

entry	catalytic system	β_n (θ)[b] (°)	T (°C)	time (min)	yield (mg)	act[c]	M_w[d] (kg mol^{-1})	M_w/M_n[d]
1	**2a**/Et_2AlCl	80 (107)	22	2	40	240	387.6	2.9
2	**2a** /Et_2AlCl/ETA	80 (107)	22	2	118	710	166.8	3.2
3	**2b** /Et_2AlCl/ETA	79 (115)	22	2	212	1270	75.8	5.1
4	**2c**/Et_2AlCl/ETA	85 (125)	22	2	247	1480	45.9	4.4
5	**1b**/Et_2AlCl/ETA	(136)	22	2	280	1690	44.6	3.9
6	$VCl_3(THF)_3$/Et_2AlCl		22	2	157	940	220.2	3.4
7	$VCl_3(THF)_3$/Et_2AlCl/ETA		22	2	361	2170	3.7	4.9
8	**2b** /Et_2AlCl/ETA	79 (115)	22	5	480	1150	52.3	3.1
9	**2b** /Et_2AlCl/ETA	79 (115)	22	10	709	850	49.9	2.8
10	**2b** /Et_2AlCl/ETA	79 (115)	22	18	900	600	50.2	2.8
11	**2b** /Et_2AlCl/ETA	79 (115)	50	5	375	900	24.2	2.7
12	**2b** /Et_2AlCl/ETA	79 (115)	70	5	274	660	20.9	2.3
13	**2b** /Et_2AlCl/ETA	79 (115)	0	5	395	950	352.3	3.2

[a] polymerization conditions: ethylene pressure, 1.01 bar; total volume, 25 mL (toluene); V-complex, 5 μmol; Al/V = 500; ETA/V = 50; [b] β_n is the phosphine bite angle as reported by van Leeuwen,[55-57] and θ is the ligand cone angle, as reported by Tolman;[32] [c] activity in $kg_{pol}\ mol_V^{-1}\ h^{-1}$; [d] determined by SEC.

Moderate activities were registered in the absence of ETA (Table 8, entries 1 *vs* 2), while good activities (from 710 to 1480 $kg_{pol}\ mol_V^{-1}\ h^{-1}$) were obtained in the presence of reoxidant (Table 8, entries 2 and 4, respectively). This suggests that even the use of bidentate phosphine ligands requires the presence of ETA to restore the active site and give enhanced activity.[54] The resulting PEs are linear, semicrystalline polymers with a melting temperature close to 135 °C and a crystallinity of about 85% (ΔH_m = 249 J/g).

A general trend emerges from the data collected in Table 8. Specifically, the activity increased in the order **2a** (dmpe, $7.10\times10^5\ g_{pol}\ mol_V^{-1}\ h^{-1}$) < **2b** (depe, 1.27×10^6) < **2c** (dppe, 1.48×10^6), while the molecular weight of PEs increased in the reverse order, that is **2c** (dppe, M_w = 45900 g mol^{-1}) < **2b** (depe, M_w = 75800) < **2a** (dmpe, M_w = 166800). This suggests that the substituents on the phosphorous atoms play a key role and have a great impact on the activity and on the molecular weight of the polymers.

In particular, it seems that the more electron-withdrawing phenyl groups on the ligand skeleton reduce electron density at the vanadium center, resulting in higher rates of chain transfer, but significantly increasing the overall productivity. This could be explained assuming that the chain transfer is the rate-determining step. It is likely that steric effects also play a role. Indeed, among the diphosphine ligands used in this work, the electron donor ability increases in the order dppe (**2c**) < depe (**2b**) ≤ dmpe (**2a**),[58] while the steric crowding increases in the reverse order, that is

dmpe < depe < dppe.[32] Therefore, the observed results may be due to concomitant effects of steric and electronic perturbations, and they can be explained in a twofold manner. First, considering the σ–donor character of the ligands, a more strongly electron-donating diphosphine should stabilize the catalytically active species (Fig. 18), making the coordination of the incoming ethylene more difficult. This may explain why **2a** (dmpe has a stronger σ–donor character) was less active than **2c** (dppe has a weaker σ–donor character). Likewise, an electron-donating ligand may stabilize the electron-deficient agostic complex (intermediate **I2** in Fig. 18) and reduce the rate of β–H elimination, formation of **I3** and subsquent chain transfer (Fig. 18).[49,59] This may explain why **2a** gave a polymer with a molecular weight higher than that obtained from **2c**.

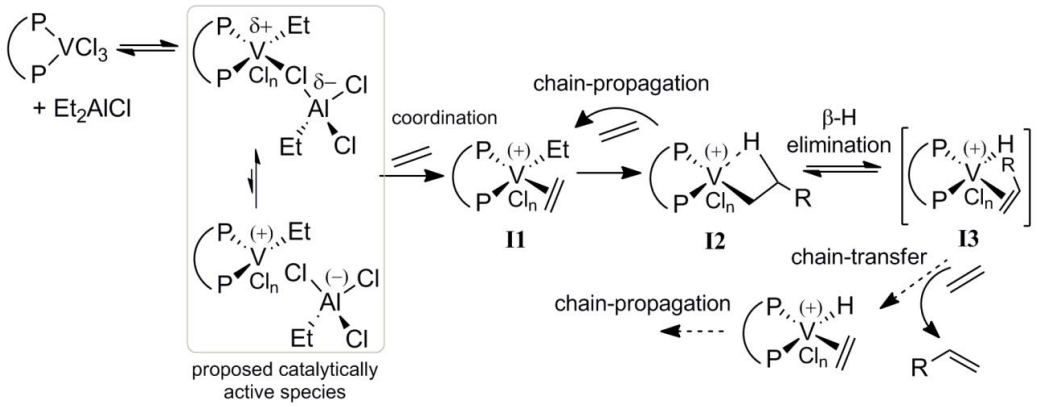

Figure 18 *Simplified representation for possible β–H elimination and subsequent chain transfer pathway (R = alkyl group or growing polymer chain). The chloro-bridged species was thought to be a key intermediate in vanadium-based olefinolymerization systems, although the exact nature of the catalytically active species still remains unknown.*

In contrast, considering steric effects, a diphosphine ligand with a larger bite angle and bulky substituents on the phosphorous atoms is expected to be weakly coordinated to the metal.[60] This might contribute to create coordinatively "open" and hence easily accessibile active sites for the incoming monomer and it can explain why **2c** (dppe, β_n = 85° and θ = 125°) was more active than **2a** (dmpe, β_n = 80° and θ = 107°). Besides, the fact that **2c** has the largest bite angle, close to 90°, may even more contribute to stabilize a square planar geometry of the vanadium based **I2** intermediate (which is the most favourable one for chain transfer, Fig. 18)[55,56] thus facilitating β–H elimination and the formation of low molecular weight polymers. Accordingly, the overall productivity of **2c** was increased compared to **2a** and **2b** likely because the β–H elimination was the rate-determining step.

Table 8 reports also the results for the polymerization of ethylene using $VCl_3(PMePh_2)_2$ (entry 5) and $VCl_3(THF)_3$ (entry 7) employed in this study for comparison. Generally, vanadium diphosphine complexes showed lower activity than $VCl_3(THF)_3$, as already observed in the case of monodentate phosphine complexes.[47] Likewise, **2a**–**2c** showed lower activity than $VCl_3(PMePh_2)_2$: the poorly coordinating $PMePh_2$ ligand creates more easily accessible and even more electron-

deficient coordination sites with respect to chelating diphosphines, and hence the facile activation,leads to higher activity.[47,55] Conversely, the molecular weight of PEs generated from **2a**–**2c** were higher than those of the polymers from $VCl_3(PMePh_2)_2$ and $VCl_3(THF)_3$. This may be related to the lower tendency of **2a**–**2c** to give β–H elimination, and, probably, a consequence of the ability of chelating diphosphines to stabilize the electron-deficient agostic intermediate, thus reducing the rate of chain transfer, at least more than $PMePh_2$ and THF ligands.

Complex **2b** was further selected to explore the effect of the polymerization time and temperature on the catalytic behavior. First, ethylene polymerization lifetime study in the range from 2 to 18 min was evaluated (Table 8, entries 3 and 8–10). The polymer yield increased with the increasing of the polymerization time, with product obtained in the order of grams. However, as is the case of most vanadium based catalysts,[8,13] there was a considerable drop-off in activity, indicating a limited stability of **2b** over time . The activity at 18 min was 600 $kg_{pol}\ mol_V^{-1}\ h^{-1}$, about 47% of that in the first 2 min. The catalyst deactivation is not the only factor determining the lower activity: it may be also due to the occurrence of mass transport limitations since large amounts of polymers were obtained during the polymerization, causing an increase of the viscosity medium.[10] A plot of yield and activity *vs* polymerization time is shown in Figure 19. A general first-order dependence of the polymer yield over time is only apparent because the trend deviates at longer polymerization time due to filling of the reactor with the polymer, thus lowering the overall productivity.

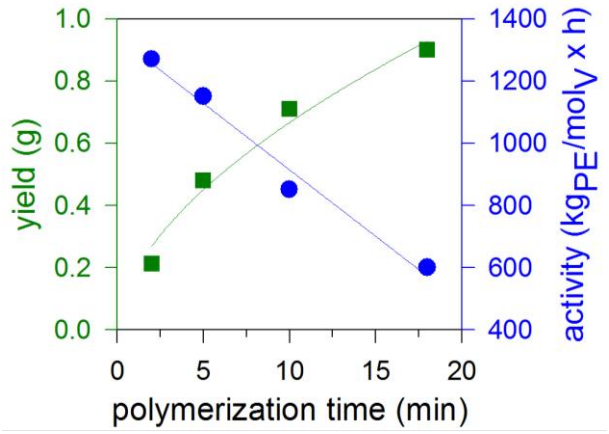

Figure 19 *Plots of the polymer yield and the catalytic activity of* ***2b*** *vs the polymerization time. The lines are guides to the eye and illustrate the overall trend.*

In order to evaluate the thermal stability of complex **2b**, a series of polymerizations were carried out at different temperatures, from 0 to 70 °C (Table 8, entries 8 and 11–13). By increasing the polymerization temperature from 0 to 22 °C, the activity increased, while on further temperature increasing the activity dropped off, suggesting a thermal deactivation likely associated with a faster reduction of the active V(III) species to low-valent less active or inactive

V(II) species. The instability over temperature correlates with the dominant chain transfer. Indeed, the molecular weight of the resultant polymers decreased with increasing the polymerization temperature, indicating that a higher temperature accelerates chain transfer. However, the molecular weight distribution remained quite narrow and unimodal, indicating that the polymerization took place with uniform catalytically active species even at 70 °C. A polymer with a molecular weight as high as 3523000 g mol^{-1} was obtained at low temperature (Table 8, entry 13).

Copolymerization of ethylene with norbornene

As already highlighted for monodentate phosphine V(III) complexes, also none of the bidentate phosphine complexes was active in the homopolymerization of NB under the conditions employed. However, the complexes exhibited from low to excellent activities in the E/NB copolymerization Table 9 summarizes the results obtained using complexes **2a**–**2c**, in the presence of Et_2AlCl (500 equiv. to V), ETA (50 equiv. to V) and for a NB/E feed ratio of 4. The copolymerizations were performed at short polymerization time (10 sec) to ensure the uniformity of the catalytic copolymerization process and thus to obtain copolymers with uniform composition. Indeed, as we also reported for $VCl_3(PMePh_2)_2$,[47] we found that the copolymerization rate at the initial stage for **2a**–**2c** was so high that immediately the conversion of NB reaches about 50%. Then, copolymers with a non-homogenous composition distribution (*i.e.*, copolymer chains are NB–rich at the beginning and E–rich at the end of polymerization, Fig. 8) were formed by performing the copolymerization for longer times. Thus, we set up a copolymerization time in the order of seconds to limit the undesired compositional drift.

As observed in the case of monodentate phosphine complexes, all the vanadium diphosphine complexes exhibited high activities in the copolymerization of ethylene with NB, higher than those found in the homopolymerization of ethylene. The general trend in activity is the same found for the polymerization of ethylene (Table 8). The activity strongly increased in the order **2a** (dmpe, 3670 $kg_{pol}\ mol_V^{-1}\ h^{-1}$) < **2b** (depe, 9460) < **2c** (dppe, 16800). The NB incorporation was also affected by the substituents on the phosphorus atoms: it increased in the same order found for the activity, namely **2a** (NB = 36.5 mol%) < **2b** (NB = 37.4) < **2c** (NB = 39.2).

In contrast, no significant ligand effect on the copolymers molecular weight was observed under these conditions, despite a strong impact of the type of ligand on the activity. A possible explanation is that the higher the content of comonomer, the lower the frequency of β–H elimination. Indeed, it is well know that the coordination of NB mitigates chain-transfer reactions for stereoelectronic reasons since the β–H elimination requires the coplanarity of the V–C(α) bond and the β–H atom, and this disposition is impossible when NB is the last inserted unit.[59]

Table 9 reports also the results for the E/NB copolymerization using $VCl_3(PMePh_2)_2$ and $VCl_3(THF)_3$ employed in this study for comparison. As observed for the homopolymerization of ethylene, **2a**–**2c** showed lower activity than $VCl_3(THF)_3$ and $VCl_3(PMePh_2)_2$, and no significant

differences were observed between **2c**, with phenyl groups at the phosphorus atoms, and $VCl_3(PMePh_2)_2$. Note that even for the copolymerization, **2a**–**2c** gave copolymers with higher molecular weight than those obtained from $VCl_3(PMePh_2)_2$ and $VCl_3(THF)_3$. As above suggested, this may be related to the lower tendency of vanadium diphosphine complexes to give β–H elimination at the last enchained ethylene unit.

Table 9 *Copolymerization of ethylene with NB catalyzed by bidentate phosphine V(III) complexes in combination with Et2AlCl and in the presence of ETA.a*

entry	complex	β_n (θ)[b] (°)	yield (mg)	act[c]	NB[d] (mol%)	M_w[e] (kg mol^{-1})	M_w/M_n[e]	T_g[f] (°C)
14	**2a**	80 (107)	52	3670	36.5	82.7	2.9	83
15	**2b**	79 (115)	134	9460	37.4	83.3	2.8	85
16	**2c**	85 (125)	238	16800	39.2	81.9	4.7	89
17	$VCl_3(PMePh_2)_2$	(136)	240	17350	37.8	61.4	3.8	90
18	$VCl_3(THF)_3$		395	28440	41.2	43.6	4.4	73

[a] polymerization conditions: ethylene pressure, 1.01 bar; total volume, 25 mL (toluene); V-complex, 5 μmol; Al/V = 500; ETA/V = 50; temperature, 22 °C; time, 10 sec; [NB]/[E] feed ratio, 4 mol/mol; NB feedstock concentration, 0.57 mol L^{-1}; [b] β_n is the phosphine bite angle as reported by van Leeuwen,[55-57] and θ is the ligand cone angle, as reported by Tolman;[32] [c] activity in $kg_{pol}\ mol_V^{-1}\ h^{-1}$; [d] determined by ^{13}C NMR; [e] determined by SEC; [f] determined by DSC.

Analysis of thermal properties by DSC revealed that all the copolymers did not exhibit melting events, but only a T_g. This suggests the formation of amorphous copolymers with possibly homogeneous composition. As expected for random copolymers,[61] T_gs increased with increasing the NB incorporation in the copolymers generated with **2a**–**2c**.

The NMR spectra of the copolymers obtained with bidentate V(III) complexes resulted very similar to those of the copolymers from monodentate phosphines (Fig. 9). The signals revealed an alternating random copolymer with isolated NB units and only tiny traces of diads. C2/C3 NB signals showed alternating isotactic and syndiotactic NB–E–NB–E–NB sequences, with ratios of isotactic and syndiotactic units ranging from 31:31 (Table 9, entry 16, NB content = 39.2 %mol) to 29:31 (Table 9, entry 15, NB content = 37.4 %mol). This result means that also the bidentate phosphine ligands do not affect the copolymers microstructure. Unexpectedly, no resonances were detected in the regions that would clearly identify longer comonomer blocks (53.7–49.3, 44.7–40.7 and 27.3–25.7 ppm) despite the high consumption of NB. This means that after two consecutive insertion of NB, a further insertion of ethylene is the only one possible.

5.5 Enhancing catalyst stability: imido–phosphine ligands

Since in our first investigations we demonstrated that the dissociation of the labile phosphine ligand could be likely the first and possibly the rate-determining step, we were interested in studying a class of phosphine vanadium complexes bearing an additional organic moiety. In this

respect, we synthesized a series of phosphine adducts of (imido)vanadium(IV) complexes in collaboration with dr. Christian Lorber (Laboratoire de Chimie de Coordination (LCC) – CNRS – Toulose).

The imido–bridged aryl cannot dissociate during activation, and this may ensure the presence of a shielding counterpart, making the transition state more stable during polymerization. This can then bring to (co)polymers with higher molecular weights and lower compositional drift, contributing to improve also the thermal properties of the obtained materials.

5.5.1 Synthesis and characterization of (imido)V(IV) phosphine complexes

Transiton metal imido complexes attracted particular interest for their potential for "metallocene-like" reactivity. From an electronic point of view, there is an isolobal analogy between transition metal imido complexes and the monoanionic Cp (Cp = Cyclopentadienyl) moiety, since they can bind to a metal using a combination of 1σ and 2π orbital interactions.[62] Moreover, as a π-donor ligand, the imido group is able to promote high oxidation state coordination chemistry.[63] In addition, the facile modification of steric and electronic properties of the ligand, by virtue of the number of alternative substituents, increases the potential of this type of ligand.

Extensive studies have been carried out with first row metals (especially Ti, V, and Cr).[63] In particular, the imido function has proven to stabilize alkyl groups in both V(IV) and V(V) complexes.[64] The use of imido ligands in V(V) chemistry is well documented,[8] and many different anionic ancillary donor ligands have been employed (for a more detailed digest on this topic see ref. 8).

Compared to V(V), terminal (imido)V(IV) complexes are still rare. A possible explanation is connected with the difficulties associated with the isolation of single crystals useful for X-ray structural characterization, which proves to be of fundamental importance dealing with the paramagnetism of d^1 vanadium(IV).

In this context, we synthesized three (imido)vanadium(IV) complexes (*i.e.*, **3a**, **3b**, **3c**) (Fig. 20) as catalyst pre-cursors for the homo- and co-polymerization of ethylene with NB. The three (imido)vanadium(IV) complexes were obtained as depicted in Figure 21. The synthesis consists of a three step procedure from $V(NMe_2)_4$ via the initial formation of imido-bridged dimers $[V(\mu\text{-}NR)(NMe_2)_2]_2$ that are further converted into the oligomeric $[V(NR)Cl_2]_n$. Upon treatment with monophosphines, the oligomeric $[V(NR)Cl_2]_n$ gives the bisphosphine imido adduct as already reported for the synthesis of the known $V(=N\text{-}2,6\text{-}i\text{Pr}_2\text{-}C_6H_3)Cl_2(PMe_2Ph)_2$ (**3b**)[18] and its analogous PMe_3 adduct $V(=N\text{-}2,6\text{-}i\text{Pr}_2\text{-}C_6H_3)\text{-}Cl_2(PMe_3)_2$.[16] Overall, **3a**–**3c** were obtained in moderate yields after recrystallization. All the complexes were characterized through elemental analysis, ^1H and ^{51}V NMR, and EPR spectroscopy.

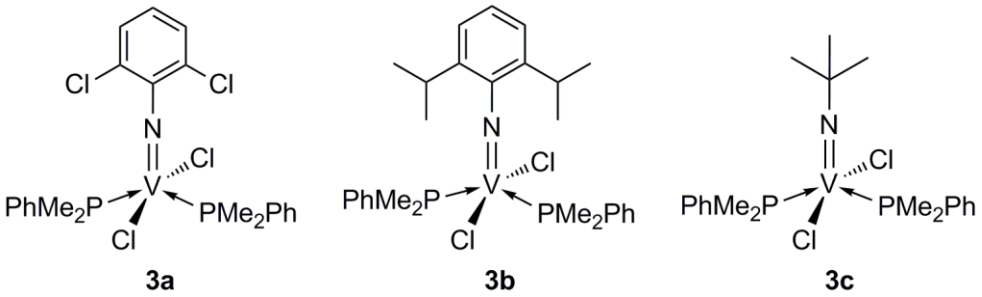

Figure 20 *Aryl (Imido)vanadium(IV) complexes synthesized in this work.*

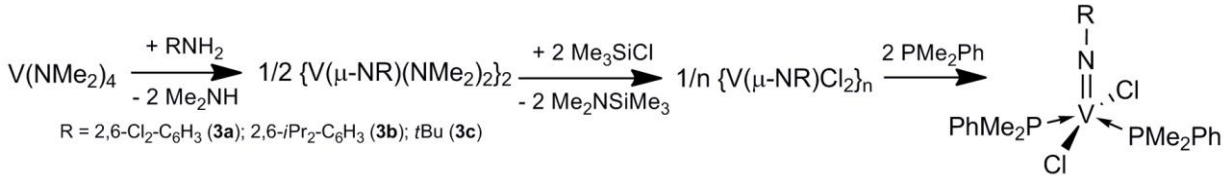

Figure 21 *Generic synthesis leading to $V(=NR)Cl_2(PMe_2Ph)_2$.*

Single crystal structure determination was used to compare the steric and electronic properties of the imido ligand in $V(=NR)Cl_2(PMe_2Ph)_2$ complexes. Crystals of **3a** suitable for crystal structure determination were obtained. Although suitable crystals of **3c** were not obtained, it was possible to solve the structure of its parent PMe_3–adduct $V(=NtBu)Cl_2(PMe_3)_2$ (**3c′**)**.** ORTEP drawings of the molecules of **3a** and **3c′** are shown in Figure 22 and 24, respectively. Both molecular structures allow a direct comparison with the know structure of **3b** (Fig. 23).[18]

The three compounds **3a**, **3b** and **3c′** exhibit similar features: a geometry around the metal center in between a distorted trigonal-bipyramid (with equatorial aryl-imido and chlorine atoms) and a square pyramid (τ parameter = 0.54–0.62) [τ is the angular parameter commonly used to describe the geometry around the metal center in penta-coordinate complexes, and defined as $\tau = (\alpha-\beta)/60$ (α and β are the two largest L–M–L bond angles, with $\alpha \geq \beta$)],[65] a short V–N distance with almost linear V–N–C imido linkage typical of such imido complexes, two mutually *cis* chlorine atoms (with Cl–V–Cl angle of *ca.* 130° and mean V–Cl bonds of *ca.* 2.31Å, and two mutually *trans* axial phosphine ligands [P–V–P = 164–169°] with V–P distances of *ca.* 2.50 Å. The phenyl substituent of PMe_2Ph phosphines is oriented differently in **3a** and **3b**; this doesn't seem to be due to steric effects, but most probably results from crystal packing.

Before getting to the catalytic behavior of **3a**–**3c**, it may be useful to make a rough classification based on the electronic and steric properties of the investigated complexes. Whereas the electron donor ability should increase in the order **3a** < **3b** < **3c** (as anticipated from the electron-donating or withdrawing nature of the substituents on the imido moiety), a tentative to rationalize the steric properties remains difficult at this stage. On the basis of structural data, **3a** and **3b** have almost a planar hindrance, while the *tert*-butyl-imido group in **3c** is a bulky group in all the three dimensions (see the structure of **3c′** in Figure 24).

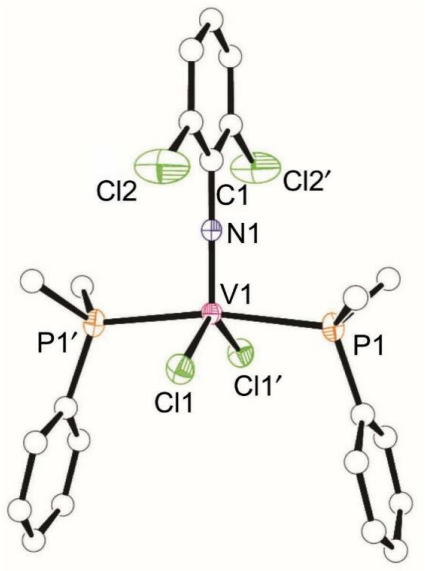

Figure 22 *ORTEP drawing of* ***3a****. Thermal ellipsoids are drawn at the 50% probability level. Hydrogen atoms are omitted for clarity and carbon atoms are drawn as spheres.*

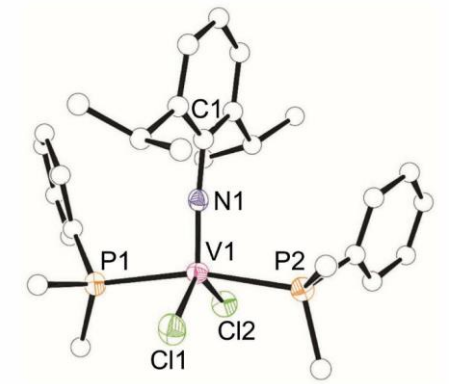

Figure 23 *ORTEP drawing of* ***3b****. Thermal ellipsoids are drawn at the 50% probability level. Hydrogen atoms are omitted for clarity and carbon atoms are drawn as spheres.*

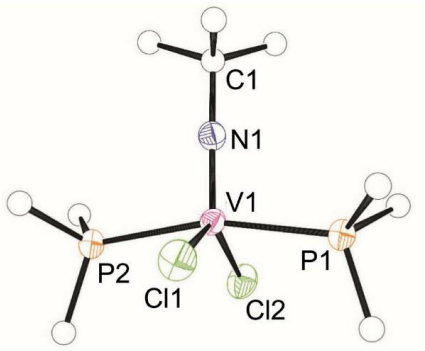

Figure 24 *ORTEP drawing of* ***3c′****. Thermal ellipsoids are drawn at the 50% probability level. Hydrogen atoms are omitted for clarity and carbon atoms are drawn as spheres.*

Topographic steric maps of imido ligands in **3a–3c′** for a qualitative analysis were generated using the open-source SambVca 2 Web,[66] and are reported in the Appendix at the end of this thesis. They showed that the *iso*-propyl *ortho* substituents in **3b** promote a higher steric protection to the vanadium compared to the chlorine substituents in **3a** and the *tert*-butyl imido moiety in **3c**.

5.5.2 Catalytic behavior

Polymerization of ethylene

Preliminary studies intended to establish the most suitable reaction conditions were performed with **3b**, and two different activators, namely MAO and Et_2AlCl. While the catalytic system **3b**/MAO produced PE in very low yield, **3b**/Et_2AlCl gave activities that are at least one order of magnitude higher. This result is consistent with those obtained with V(III) mono- and bidentate phosphine complexes, and it could be attributed to the formation of different catalytically active species (isolated or associated cation) from the combination of vanadium complexes and Al activator, depending on the nature of this last.[67] Hence, Et_2AlCl was chosen as activator for the following experiments. Table 10 summarizes relevant data for the polymerization of ethylene using **3a–3c**.

Table 10 *(Co)polymerization of ethylene with NB catalysed by (imido)vanadium(IV) complexes in combination with Et_2AlCl and in the presence of ETA.*[a]

entry	V-cat	NB (mol L^{-1})	NB/E	t (min)	yield (mg)	activity[b]	NB[c] (mol%)	M_w[d] (kg mol^{-1})	M_w/M_n[d]	T_g (T_m)[e] (°C)
1	**3a**			2	172	2072		140	2.4	(139)
2	**3b**			2	180	2168		163	2.2	(138)
3	**3c**			2	163	1956		198	2.4	(136)
4	**3c**			5	317	1522		109	2.2	*nd*
5[f]	**3c**			20	1280	1536		206	3.0	*nd*
6	**3b**	0.57	4	30''	94	4513	35.4	*nd*		81
7	**3b**	0.57	4	2	250	3012	35.7	147	2.1	82
8	**3b**	0.57	4	15	980	1568	35.8	107	2.5	83
9	**3a**	0.57	4	2	380	4578	36.4	137	2.0	85
10	**3c**	0.57	4	2	360	4320	36.8	155	2.1	85
11	**3c**	0.08	0.5	2	285	3420	13.0	110	1.9	–4 (50)
12	**3c**	0.29	2	2	458	5496	30.4	108	1.8	56
13	**3c**	1.16	8	2	109	1308	39.3	178	2.1	101

[a] polymerization conditions: ethylene pressure, 1.01 bar; total volume, 25 mL (toluene); V-cat, 2.5 μmol; Al/V = 500; ETA/V = 10; temperature, 20 °C; [b] activity in kg_{pol} mol_V^{-1} h^{-1}; [c] determined by ^{13}C NMR; [d] determined by SEC; [e] determined by DSC. [f] total volume, 50 mL.

All the complexes were instantaneously activated and good activities were obtained. Changes in the imido ligand substitution brought about little effect on the activity for the homopolymerization of ethylene under the conditions employed. In contrast, the type of imido ligand has a pronounced

influence on the PE molecular weight that increased in the order **3a** (M_w = 140000 g mol^{-1}, entry 1) < **3b** (M_w = 163000, entry 2) < **3c** (M_w = 198000, entry 3). The observed trend may be correlated to concomitant effects of steric and electronic ligand perturbations. Considering only the electronic properties of **3a**–**3c**, the fact that **3c** formed a PE with the highest molecular weight may be because the electron-donating *tert*-butyl group on the imido moiety strengthens the V–N bond, thus improving the stability of the electron-deficient catalytic intermediate and reducing the chain transfer. In the same way, however, we cannot rule out that the steric bulk of the *tert*-butyl imido group may also contribute to inhibit the associative chain transfer.[10]

The obtained PEs are linear polymers, with T_m in the range 136–139 °C, crystallinity of about 75% (ΔH_m *ca*. 216 J mol^{-1}), and reasonably narrow, unimodal molecular weight distributions (M_w/M_n *ca.* 2), suggesting the presence of well-defined active species.

Another interesting aspect that worthed studying is the stability over time of the investigated complexes. Indeed, generally, a drop-off in activity has been observed with vanadium based catalysts;[8,13] as previously reported in the case of mono- and bidentate V(III) complexes (Table 8). Hence, the catalytic system **3c**/Et_2AlCl/ETA was further examined for longer polymerization time (Table 10, entries 4 and 5). The polymer yield increased with increasing the polymerization time, but a decrease in activity was observed. The activity at 5 min was 1522 kg_{pol} mol_V^{-1} h^{-1}, about 78% of that in the first 2 min likely due to the catalyst deactivation and mass transport limitations caused by filling of the reactor with the swollen polymer. Indeed, the polymerization occurred so fast that the solution viscosity increased after a few minutes. Likewise, the molecular weight of the polymer obtained prolonging the reaction time was lower than that obtained at 2 min (Table 10, entries 3 *vs* 4). This may be due to the embedment of the active vanadium species that limits monomer diffusion and chain propagation, probably for the demand of a more diluted solution. In order to overcome this issue and keep the viscosity of the medium reasonable, a polymerization test in a more diluted solution was carried out (Table 10, entry 5, total volume = 50 mL, time = 20 min). Under these conditions, the overall productivity strongly increased with product obtained in the order of grams, and the polymer molecular weight remained reasonably high (Table 10, entry 5, M_w = 206000 g mol^{-1}). Also of note, the activity at 20 min was close to that at 5 min (1522 *vs* 1536 kg_{pol} mol_V^{-1} h^{-1}, entries 4 and 5, respectively). This result suggests that **3b** is fairly stable over the investigated polymerization time and that the use of a more dilute solution is beneficial.

Copolymerization of ethylene with norbornene

The results for the E/NB copolymerization by **3a**–**3c** in the presence of Et_2AlCl (500 equiv. to V) and ETA (10 equiv. to V) at NB/E feed ratio of 4 are summarized in Table 10.

Copolymerization lifetime study in the range from 30 s to 15 min was first evaluated with **3b** to explore the effect of the reaction time on the activity and comonomer incorporation (Table 10,

entries 6–8). The overall productivity increased with the increase of the polymerization time, and grams of product were recovered in 15 min (entry 8). There was, however, a drop-off in activity over time. The activity at 15 min was 1568 kg_{pol} mol_V^{-1} h^{-1}, about 52% of that in the first 2 min. Catalyst deactivation, even in the presence of reoxidant, is not the only factor determining the lower activity. It may also be due to the occurrence of mass transport limitations since a large amount of polymer was obtained during the copolymerization.

Successively, all the complexes were investigated under the same set of conditions for E/NB copolymerization. Differently from the case of V(III) complexes, thanks also to an improved catalyst stability over time as explained above, a reaction time of 2 min was chosen intentionally because such time with high and appropriate NB conversion allowed for a better differentiation and comparison of catalyst activities. The (imido)V(IV) complexes gave high molecular weight copolymers with narrow, unimodal molecular weight distribution, suggesting that the copolymerization took place with a single catalytically active species. The observed activities were higher than those found in the homopolymerization of ethylene. Once again, it was observed that the coordination of NB speeds up the propagation rate.

Complex **3b** having isopropyl substituents on the N–aryl ring exhibited lower activity compared to **3a** and **3c** under the same set of conditions (Table 10, entries 7, 9, and 10, respectively). This result is, so far, ambiguous regarding clear trends in the effect of electronic or steric ligand properties. The catalytic performance for the E/NB copolymerization deviates from an expected trend moving from the more electron-deficient **3a** to the more electron-rich **3c** (more *t*Bu-N → V donation). It is likely that steric effects could have a key role and some hypothesis can be extracted. Indeed, this result can be tentatively ascribed to the fact that the steric shielding by the bulkier isopropyl-aryl substituents in **3b**, which can arrange in the axial position of the vanadium center, leads to an enhanced discrimination between the two (co)monomers. The increased steric interaction between bulky NB and bulky isopropyl-aryl substituents would offer a significant impediment to the coordination and insertion of bulkier comonomer, thus depressing both chain propagation rate and NB incorporation. Consistent with this hypothesis, straight calculation of the topographic steric maps for **3a**, **3b**, and **3c′** (generated using the SambVca 2 Web[66] and reported in the Appendix at the end of this thesis) over just the stable conformation of the complexes in the crystals, showed that isopropyl-aryl substituents in **3b** promote higher steric protection to the metal.

Similarly to the results found for the homopolymerization of ethylene, **3c** formed the copolymer with the highest molecular weight, followed by **3b** and **3a**, respectively. The more electron-rich compound **3c** is less prone to chain transfer; it can be inferred that the presence of the alkyl imido moiety has an advantage in preparing polymers with high molecular weight.

Analysis of thermal properties of all the copolymers by DSC revealed the absence of any melting event, but only a T_g, consistent with the NB incorporation. This suggests the formation of amorphous copolymers with homogeneous composition,[68] and the limitation of the compositional drift, even for a prolonged reaction time and an extremely high NB conversion in the first seconds of the copolymerization (Table 10, entry 8).

Further investigations on the influence of the (co)monomers feed composition on the comonomer content incorporated in the copolymer, and on the effect of the ETA/V ratio and polymerization temperature were carried out.

E/NB copolymerization at different (co)monomers feedstock composition

A series of experiments were carried out with **3c**/Et_2AlCl with NB/E molar ratio from 0.5 to 8 (Table 10, entries 3 and 11–13). After an initial beneficial effect on activity going from NB/E = 0.5 to 2, a further increase in the comonomer concentration results in a decrement in activity, likely due to a favored NB coordination to the active sites,[68,69] and a preference for the copolymerization rather than the homopolymerization of each of the two monomers. Increasing the charged amount of NB, its content in the copolymer increased as well, although it did not exceed 39.3 mol% (entry 13). However, it is worth note that considerable NB content were reached already at NB/E ratio as low as 2 (entry 12, NB = 30.4 mol%).

The higher the NB feedstock concentration, the higher the copolymers molecular weight, meaning that the coordination of NB slows down the chain termination reactions. The coordination of NB mitigates chain transfer for stereoelectronic reasons, since the β–H elimination requires the coplanarity of the V–C(α) bond and the β–H atom, and this disposition is impossible when NB is the last inserted unit.[59] Narrow and unimodal molecular weight distributions were found at all the NB/E feed ratio investigated (M_w/M_n = 1.8–2.1).

Finally, except for entry 11, which has a low NB content (13.0 mol%) and hence exhibited also a T_m, all the other copolymers exhibited only a T_g; a linear correlation between the NB content and the T_g can be identified, revealing that the differences in thermal properties mainly arise from the different amount of incorporated NB.

E/NB copolymerization at different ETA/V ratio

The effect of ETA dosage was systematically examined at NB feedstock concentration of 0.57 mol L^{-1} (NB/E = 4) by using **3a** and **3c**. The copolymerizations were performed over the range of ETA/V mole ratio from 5 to 300. Relevant data are summarized in Table 11. Complexes **3a** and **3c** were chosen because these two complexes appear to be electronically and sterically rather different.

The plot of activity versus the ETA/V ratio, displayed in Figure 25a, shows that the amount of ETA strongly affects the activity. The trend in activity is strongly dependent on the complex

employed. It would be interesting to note that the activity of **3a** increased upon addition of ETA moving from 10 to 150 equivalents to V, but then the productivity drops off rapidly (Figure 25a). Conversely, **3c** gave a slight increase in activity going from 5 to 10 equivalents of ETA to V and then a rapid decrease in the activity was observed. The different behavior exhibited by **3a** and **3c** by varying the charged amount of ETA may be explained by considering the rough classification of the two imido ligands as rather electron-donating (N–*t*Bu, **3c**) and electron-withdrawing (N–^{Cl}Ar, **3a**). This because **3a**, bearing a 2,6-Cl-substitution on the aryl moiety, could have a pronounced preference to accept electron density by ETA through the chelation of the carbonyl oxygen to the metal active species as anticipated by Gibson.[70] This possible chelation of the carbonyl oxygen may contribute to stabilize the vanadium active intermediate and may explain the enhanced reactivity of **3a**.

Table 11 *Copolymerization of ethylene with NB catalyzed by (imido)vanadium(IV) complexes in combination with Et_2AlCl and in the presence of ETA at different ETA/V ratio[a].*

entry	V-cat	ETA/V	T (°C)	yield (mg)	act[b]	NB[c] (mol%)	M_w[d] (kg mol^{-1})	M_w/M_n[d]
9[f]	**3a**	10	20	380	4578	36.4	137	2.0
14	**3a**	50	20	483	5819	37.5	87	1.9
15	**3a**	150	20	598	7205	39.1	42	1.8
16	**3a**	300	20	353	4236	34.9	39	2.1
17	**3c**	5	20	292	3518	35.7	164	2.6
10[f]	**3c**	10	20	360	4320	36.8	155	2.1
18	**3c**	50	20	228	2684	34.8	143	1.7
19	**3c**	150	20	135	1627	33.6	103	1.7
20	**3a**	10	50	259	3108	35.1	44	1.8
21	**3a**	10	70	30	360	*n.d.*	*n.d.*	*n.d.*
22	**3b**	10	0	168	2016	34.1	516	1.8
7[f]	**3b**	10	20	250	3012	35.7	147	2.1
23	**3b**	10	50	210	2520	35.0	55	2.1
24	**3b**	10	70	60	720	*n.d.*	18	1.9
25	**3c**	10	50	312	3759	37.2	39	1.8
26	**3c**	10	70	165	1988	37.6	23	1.7

[a] polymerization conditions: ethylene pressure, 1.01 bar; total volume, 25 mL (toluene); V-cat, 2.5 μmol; Al/V = 500; temperature, 20°C; time, 2 min; [NB]/[E] feed ratio, 4 mol/mol; NB feedstock concentration, 0.57 mol L^{-1}; [b] activity in kg_{pol} mol_V^{-1} h^{-1}; [c] determined by ^{13}C NMR; [d] determined by SEC; [e] determined by DSC; [f] first reported in Table 10.

In contrast, in the case of the more electron-rich complex **3c**, 50:1 equivalents of ETA to V seem to be sufficient to poison the active sites and rapidly lower the productivity. In this case, it seems that the excess of ETA potentially competes with the (co)monomers coordination/insertion and suppresses the polymerization. This may account for inferior performance of **3c**.

The molecular weight of the resulting polymers was also strongly affected by the charged amount of ETA (Figure 25b): the higher the ETA/V ratio, the lower the molecular weight. As previously observed with some V(III) complexes, also in this case ETA behaves as a chain-transfer agent.[47,71]

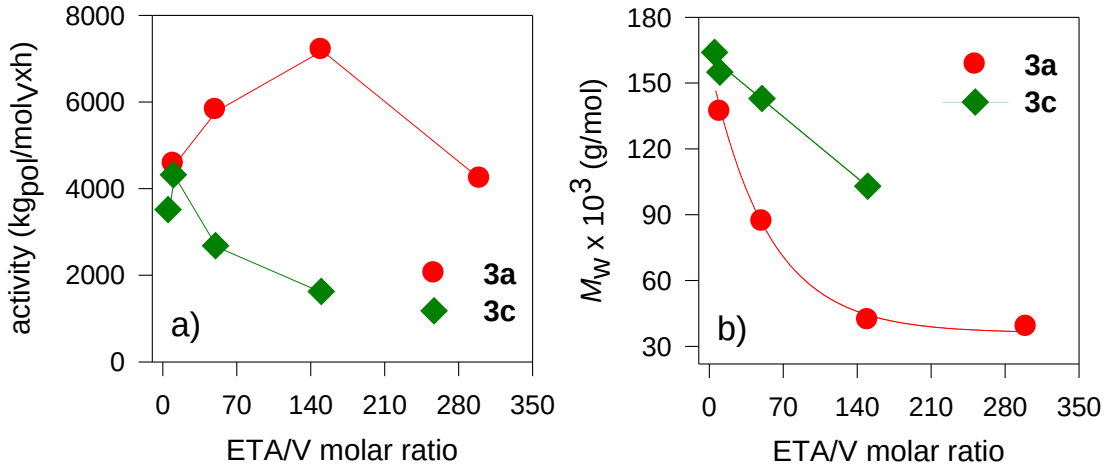

Figure 25 *Plot of activity (a) and copolymer molecular weight (b) versus the ETA/V molar ratio.*

Moreover, interestingly, the dependence of molecular weight on ETA/V ratio shown in Figure 25b proves once more a different ETA response exhibited by the two complexes. At ETA/V = 150, **3c** gave a copolymer with a molecular weight more than two times greater than the copolymer from **3a**. Although the structure of the catalytically active species (as well as the vanadium oxidation state and the specific interaction of ETA with the active sites) is still unclear at the moment, some clear trends have been identified experimentally by changing the amount of ETA and using the two electronically and sterically different complexes **3a** and **3c**. In light of these data, it is possible to speculate that the active intermediate is an intimate combination of the three reagents (the V–precursor, the Al–co-catalyst and ETA) and it shows single-site behavior.

E/NB copolymerization at different temperature

With the feed of 10 equivalents of ETA, a series of copolymerizations were carried out at different temperatures from 0 to 70 °C to evaluate the thermal stability of **3a**–**3c**. The results are summarized in Table 11. Despite a general decrease in activity with increasing the reaction temperature, as commonly observed for other vanadium catalysts,[72] changes in the ligand pattern had a strong influence on the catalyst stability over temperature (Fig. 26). A more pronounced reduction in activity was observed for **3a** and **3b** bearing a ligand with an aryl moiety, the highest one being for the most electron-poor *ortho*-Cl-substituted complex **3a**. It is likely that steric effects may also play a role. Indeed, the fact that **3a** decomposes faster at elevated temperature may be due to the lower steric hindrance around the vanadium active species provided by the N–2,6-Cl_2–C_6H_3 ligand (Fig. 22). On the contrary, **3c** gave a rather high productivity and an activity as high as 1988 $kg_{pol}\ mol_V^{-1}\ h^{-1}$ even at 70 °C.

The instability over temperature correlates with the dominant chain transfer. Indeed, the higher the temperature, the lower the molecular weight of the resulting polymers, suggesting that higher temperature accelerates chain transfer. The molecular weight distributions remained quite narrow and unimodal, indicating that the polymerization took place with uniform catalytically active species even at 70 °C. In addition, a copolymer with a molecular weight as high as 516000 g mol^{-1} and a NB content of 34.1 mol% was obtained at subambient temperature (Table 11, entry 22).

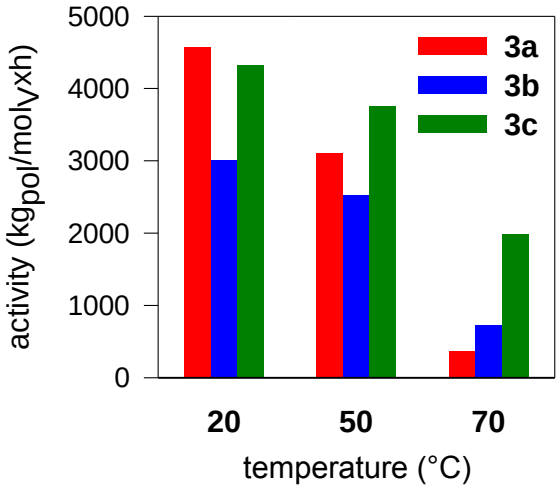

Figure 26 *Plot of activity versus copolymerization temperature.*

Copolymers microstructure

The microstructure of E/NB copolymers was investigated by ^{13}C NMR. The spectra show the typical pattern of an alternating copolymer from an addition–type NB copolymerization with *cis exo-exo* enchainment; the dominant signals are those of alternating and isolated NB units, with traces of NB diads. In addition, the comparable intensities of the peaks assigned to C2/C3 of NB in the alternating isotactic and syndiotactic NB–E–NB–E–NB sequences, respectively, revealed that the copolymers have a random tacticity.

No significant differences in the microstructure of the copolymers obtained by **3a–3c** were observed, nor differences with the copolymers obtained from V(III) complexes.

5.5.3 Copolymerization of ethylene with norbornene derivatives

In order to amplify the field of application of these complexes, the ability of **3a–3c** to incorporate NB derivatives was investigated. Some nice advantages can come out from the employment of these "functional" comonomers, since the availability of a reactive functionality (double bond) on the final copolymer allows for further modification, as will be discussed afterwards.

Keeping this in mind, we selected three different cyclic olefins, namely dicyclopentadiene (DCPD), 5-ethylidene-2-norbornene (ENB), and 5-vinyl-2-norbornene (VyNB) (Fig. 27). The results obtained are summarized in Table 12.

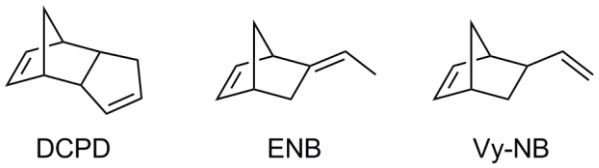

Figure 27 *Norbornene derivatives employed for the synthesis of COCs.*

Table 12 *Copolymerization of ethylene with dicylopentadiene, 5-ethylidene-2-norbornene and 5-vinyl-2-norbornene catalysed (imido)vanadium(IV) complexes in combination with Et_2AlCl and in the presence of ETA.*[a]

entry	V-cat	comonomer (Y)	yield (mg)	act[b]	Y[c] (mol%)	M_w[d] (kg mol^{-1})	M_w/M_n[d]	T_g[e] (°C)
27	**1**	DCPD	252	3036	20.9	51	2.0	62
28	**2**	DCPD	141	1692	19.1	64	2.3	54
29	**3**	DCPD	62	747	22.1	67	2.2	57
30	**1**	ENB	292	3518	33.7	166	3.2	76
31	**2**	ENB	279	3361	35.2	230	2.0	78
32	**3**	ENB	162	1952	31.4	239	1.7	74
33	**2**	VyNB	inactive					

[a] polymerization conditions: ethylene pressure, 1.01 bar; total volume, 25 mL (toluene); V-cat, 2.5 μmol; Al/V = 500; ETA/V = 10; temperature, 20°C; time, 2 min; [Y]/[E] feed ratio, 4 mol/mol; comonomer feedstock concentration, 0.57 mol L^{-1}; [b] activity in kg_{pol} mol_V^{-1} h^{-1}; [c] determined by ^1H NMR; [d] determined by SEC; [e] determined by DSC. DCPD = dicyclopentadiene; ENB = 5-ethylidene-2-norbornene; VyNB = 5-vinyl-2-norbornene.

All the complexes proved to be highly active in the copolymerization of ethylene with DCPD and ENB, while they seem to be poisoned by the extra vinyl double bond of VyNB (entry 33). At the moment we do not have an exhaustive explanation but it can be due to the vinylic C–H bond activation for VyNB, which determines facile β–H elimination and subsequent chain transfer. Both the two DCPD and ENB cyclic dienes insert into the macromolecular chain via the enchainment of the double bond of the NB ring, probably as a consequence of major ring strain, while the second C=C bond is retained without crosslinking. Steric influences emerge clearly in the copolymerization of ethylene with DCPD and ENB. The activities for the copolymerization of ethylene with DCPD and ENB were lower than those obtained for the copolymerization of ethylene with NB (Table 10). This can be due to the increased steric interaction with bulky DCPD and ENB but also, and in particular for DCPD, to a possible coordination of the extra C=C donor double bond (the one that is not involved in the copolymerization reaction) to the metal centre, thus inhibiting the propagation rate, as already observed by Li *et al.* in the case of some V(V) and zirconium based catalysts.[73] Nonetheless, for the rather unconstrained **3a**, with the less electron-donating imido ligand, a

rather high activity was observed (Table 12, entries 27 and 29). It is likely that electronic ligand effects may also play a role. Indeed, in analogous manner for both DCPD and ENB comonomers, but differently from what has been observed in the case of NB (Table 10), the activity increased as the electron-withdrawing character of the complexes increased, thus moving from **3c** to **3a**. The presence of chlorine atoms on the 2,6-position of the aryl-imido moiety (**3a**) has a positive effect on the activity,[74] and this beneficial effect was more evident in the case of DCPD. This may likely be due to the greater "accessibility" of the extra C=C double bond of DCPD compared with that of ENB (Table 12, entries 27 *vs* 28, and 30 *vs* 31) that increases the chance of the more electron-deficient **3a** to be active, at least more than **3b** and **3c**. Conversely, in the case of the more electron-rich **3c**, the interaction between the metal centre and the cyclopentene ring of DCPD may account for the inferior performance of **3c**.

On the other hand, electronic ligand influences on the comonomer incorporation are ambiguous, while the influence of the steric bulk is more explicit. Indeed, steric effects strongly limit incorporation of the more bulky DCPD, as concluded from the lower content of DCPD in the copolymers compared to ENB (Table 12, entries 27 *vs* 30, 28 *vs* 31 and 29 *vs* 32).

Similarly to the results found for the homopolymerization of ethylene and copolymerization of ethylene with NB, **3c** formed copolymers with the highest molecular weight, followed by **3b** and **3a**. This confirms that **3c** with the more electron-donating =N–*t*Bu imido ligand is less prone to chain transfer than **3a**–**b**. Remarkably, the copolymerization with ENB formed copolymers with the highest molecular weights, followed by those obtained with NB and DCPD, respectively. This indicates that the coordination of ENB slows down the chain termination reactions although, so far, the exact mechanism remains unclear. Experimentally, this behavior cannot be fully explained by taking into account the electronic and steric features of the vanadium complexes alone: additional factors such the different steric properties of the investigated cyclic olefins and the different deactivation (or stability) paths of the investigated complexes should also be considered.

The copolymers microstructure was established by ^{13}C NMR,[75] and a more detailed peaks assignment was reported in paragraph 3.6.2. In the case of E/DCPD copolymers, the peaks at 130.6 and 128.8 ppm in ^{13}C NMR spectrum (Fig. 28) as well as those at about 5.5 and 5.4 ppm in the ^{1}H NMR spectra were assigned to sp^2 C and H atoms, respectively, revealing that the copolymers contain unreacted cyclopentene units.[76] This suggests that the reaction took place selectively at the NB unit, and that no crosslinking occurred. Very small signals due to traces of diads and longer DCPD blocks were also detected, their large number being dependent on the different comonomer stereosequences and length.[77]

In the copolymerization with ENB, the side double bond of the cyclic monomer did not participate in the copolymerization, and each link of ENB in the copolymer contains an ethylidene group. The ^{1}H NMR spectrum shows signals at 5.1 and 5.3 ppm that were assigned to the

ethylidene groups; the absence of signals at about 6.0 ppm indicates that the polymerization occurs only *via* the intracyclic NB double bond. The ^{13}C NMR spectrum of entry 31 is shown in Figure 29. From the spectrum it can be seen that both the *E* and *Z* configurational ENB isomers reacted (signed with the subscript *e* and *z*, respectively, in Fig. 29), the ratio between them being 3:1, close to that in the neat monomer. Similar to the DCPD copolymers, the microstructure of ENB copolymers mainly consists of isolated and alternated ENB units, while no longer ENB sequences were detected even for sample 31 with a content of ENB of 35.3 mol%.

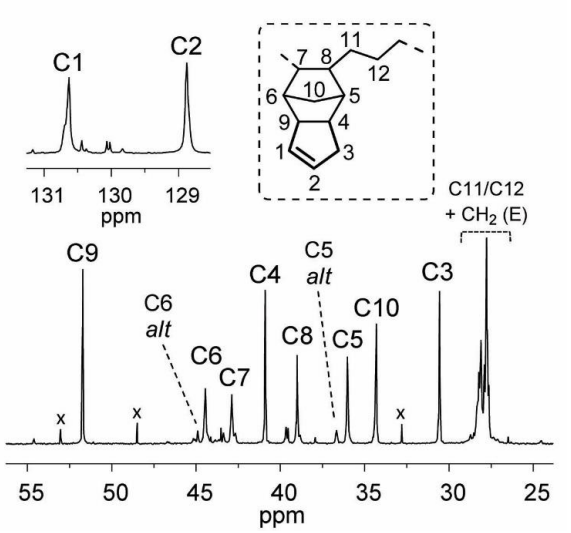

Figure 28 *^{13}C NMR spectrum of DCPD copolymer obtained with **3b**/Et_2AlCl/ETA (Table 5, entry 28, DCPD = 19.1 mol%). DCPD diad and blocks longer than dyads are marked with a cross.*

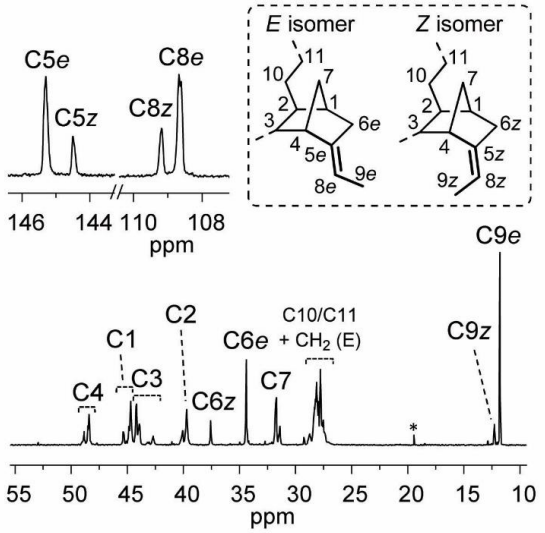

Figure 29 *^{13}C NMR spectrum of the E/ENB copolymer obtained with **3b**/Et_2AlCl/ETA (Table 5, entry 31, ENB = 35.3 mol%).*

5.6 Functionalization of COCs

The ability to insert functionalities into polyolefins is one of the long sought after capabilities in polyolefin chemistry, as already described in paragraph 1.6. The use of precursor monomers possessing reactive groups, which are inert in the copolymerization and can be modified afterwards, may be one of the plausible methods to synthesize functional polyolefins.[78]

Non-catalytic hydrogenation and epoxidation were performed on the copolymers of ethylene with DCPD and ENB obtained from (imido)vanadium(IV)/Et_2AlCl catalytic system. The same reactions were already tested and reported for DCPD homopolymers[76] (see paragraph 4.2.4), following the general procedures reported in Chapter 3 – Materials & Methods (paragraph 3.3). Hence analogous considerations can be proposed.

While the hydrogenation reaction is generally useful in terms of increasing the polymer stability (indeed the conversion of the ethylidene group to completely saturated ethyl group limits the crosslinking reactions), the insertion of the reactive functionalities such as epoxide groups is more interesting from a synthetic point of view. Indeed, the reactive group could then be converted into desirable polar groups by successive chemical reactions.[79]

Epoxidation

Epoxidation is generally performed with organic peroxides, either added directly,[80] or generated *in situ*.[81] In this thesis, epoxidation was performed with *m*-chloroperbenzoic acid (*m*-CPBA) (2 equiv. of the insaturations) in toluene at 50 °C for 4 h (Fig. 30).

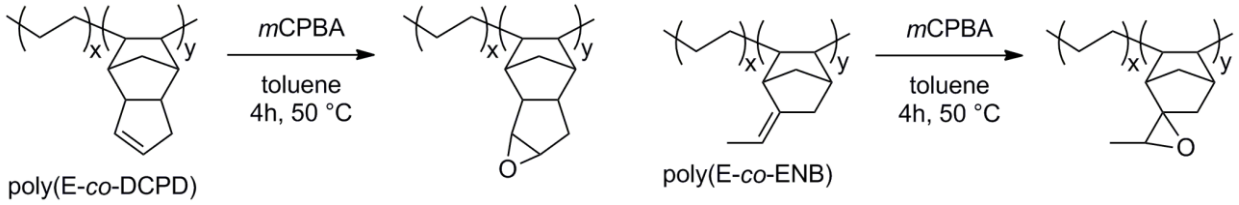

Figure 30 *Schematic representation of the epoxidation reaction of the copolymers.*

The epoxidation of E/DCPD and E/ENB copolymers was accomplished with complete conversion of the double bonds to the corresponding oxirane groups, as demonstrated by the disappearance of the peaks corresponding to =CH in cyclopentene (5.4–5.8 ppm) or ethylidene (4.8–5.3 ppm) groups and the appearance of the peaks of –CH in epoxy groups at 3.4 and 3 ppm respectively in the ^{1}H NMR spectra (Fig. 31).[78,82]

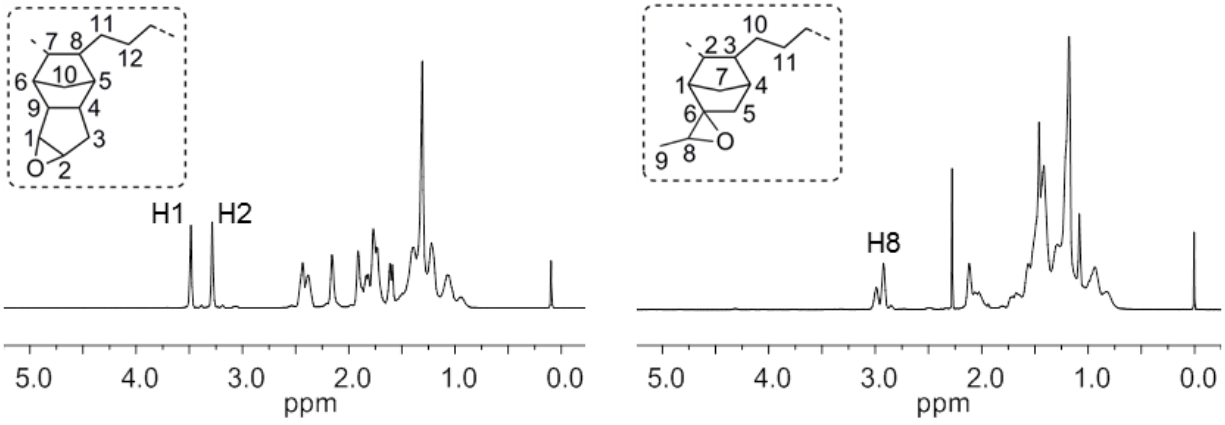

Figure 31 *^{1}H NMR spectra of the epoxidized E/DCPD (left) and E/ENB (right) copolymers.*

5.7 Beyond COCs: vanadium for the polymerization of 1,3-butadiene

Over and above the great success of vanadium for the synthesis of COCs, this transition metal should be mentioned also for its ability to polymerize 1,3-dienes, known since the dawn of Ziegler–Natta coordination–insertion polymerization. In particular, vanadium based catalysts are mainly known for their ability to give highly *trans*-1,4 poly(1,3-butadiene) (PB).[83] A crystalline, highly stereoregular *trans*-1,4 PB (*trans*-1,4 ≥ 99%) with high molecular weight and T_m of about 130 °C was synthesized with the heterogeneous systems obtained by combining a vanadium chloride (*e.g.*,

VCl_3, VCl_4) with an aluminum alkyl (e.g., $AlEt_3$, Et_2AlCl).[84] Many other catalytic systems were found to be active in the polymerization of this monomer, giving PB with different regio- and stereoselectivity, from highly *trans*-1,4,[85] to predominantly *cis*-1,4,[86] and even syndiotactic 1,2 PB.[87]

In recent years, several studies on the use of various transition metal phosphine complexes for the polymerization of 1,3-dienes have been reported,[88] but only few examples of vanadium(III) phosphine complexes were reported in the literature, and only some of them have been used for the polymerization of 1,3-butadiene.[89]

In this context, we became interested in the application of the synthesized vanadium(III) monodentate phosphine complexes of the type $VCl_3(PR_nPh_{3-n})_2$ (R = Me, Et, *n*Pr, *i*Pr, *t*Bu, Cy, Cyp; n = 0–3) (**1a**–**1n**) to the polymerization of 1,3-butadiene; some of these complexes were already employed for the synthesis of E/NB copolymers.

5.7.1 Catalytic behavior

Polymerization of 1,3-butadiene

The polymerization of 1,3-butadiene with all the vanadium(III) phosphine complexes synthesized, in the presence of white solid MAO [dMAO, prepared by removing toluene and $AlMe_3$ from commercially available MAO (sMAO)] or sMAO as co-catalyst, was examined (Fig. 32). The polymerization runs were carried out in toluene at room temperature. The most significant results are summarized in Table 13.

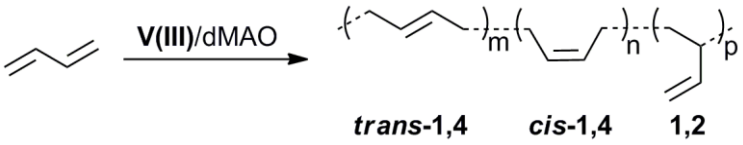

Figure 32 *Polymerization of 1,3-butadiene and the possible poly(1,3-butadiene) microstructures.*

All the vanadium complexes, in combination with dMAO, were active in the polymerization of 1,3-butadiene, giving from low to good polymer yields, ranging from 13 to 57% (Table 13, entries 17 and 1, respectively), within the first 2 h of polymerization. By extending the polymerization runs up to 24 h, it was possible to reach complete monomer consumption (Table 13, entry 2), meaning that the catalysts are not deactivated over time, as it occurs in the polymerization of ethylene where high concentration of reoxidant is required to keep the catalyst active.[47,71,90] This can be ascribed to the higher nucleophilicity of 1,3-butadiene with respect to a simple olefin, but mainly to the higher stability of the vanadium–π–allyl bond compared to the vanadium–alkyl bond of the intermediate species involved in the polymerization of 1,3-butadiene and ethylene, respectively.[91]

The results in Table 13 are presented as a function of the phosphine donor ability (measured with the Tolman electronic parameter, ν_{CO}) and steric properties (measured by cone angle, θ) as

defined by Tolman,[32] to highlight the influence of the ligand (*i.e.*, the type of substituents on the phosphorous atoms) on the catalytic activity and selectivity.

Table 13 *Polymerization of 1,3-butadiene with monomdentate phosphine V(III) complexes.*[a]

entry	catalyst	phosphine			yield	N^d	*cis*:*trans*:1,2[e]	M_w[f]	M_w/M_n[f]
		(type)	υ_{CO}[b] (cm^{-1})	θ[c] (°)	(%)	(h^{-1})	(mol%)	(kg mol^{-1})	
1	**1c**/dMAO	PPh_3	2068.9	145	57	739	33:31:36	275	1.9
2[g]	**1c**/dMAO	PPh_3	2068.9	145	93	115	30:34:36	290	1.6
3[g]	**1c**/sMAO	PPh_3	2068.9	145	51	63	65:19:16	175	4.2
4	**1b**/dMAO	$PMePh_2$	2067.0	136	46	593	29:37:34	270	2.1
5	**1b**/sMAO	$PMePh_2$	2067.0	136	7	93	69:17:14	164	1.9
6	**1f**/dMAO	$PEtPh_2$	2066.7	140	42	360	30:38:32	83	2.1
7	**1g**/dMAO	P*i*$PrPh_2$	2065.7	150	50	648	28:33:39	112	3.5
8	**1g**/sMAO	P*i*$PrPh_2$	2065.7	150	17	222	66:18:16	102	2.6
9	**1h**/dMAO	$PCyPh_2$	2064.8	153	46	593	37:28:35	116	3.0
10[g]	**1h**/sMAO	$PCyPh_2$	2064.8	153	43	46	67:15:18	100	2.9
11	**1a**/dMAO	PMe_2Ph	2065.3	122	43	556	41:20:39	75	3.8
12	**1i**/dMAO	PEt_2Ph	2063.7	136	37	480	36:24:38	97	2.7
13	**1l**/dMAO	PCy_2Ph	2060.6	159	25	324	14:73:13	274	2.8
14	**1m**/dMAO	$PCyp_3$			36	472	46:33:21	183	3.5
15	**1d**/dMAO	PCy_3	2056.4	170	21	269	34:46:20	45	2.6
16	**1n**/dMAO	P*n*Pr_3	2059.1	132	26	333	36:21:43	296	1.8
17	**1e**/dMAO	P*t*Bu_3	2056.1	182	13	167	45:34:21	233	5.9

[a] polymerization conditions: 1,3-butadiene, 2 mL (1.4 g); solvent, toluene (16 mL); V(III)-complex, 10 μmol; Al/V, 1000; time, 2h; [b] measure of the electron-donating properties of phosphine ligands, as reported by Tolman;[32] [c] phosphine cone angle, as reported by Tolman;[32] [d] N = moles of 1,3-butadiene polymerized per mol of vanadium per hour; [e] determined by ^1H and ^{13}C NMR; [f] determined by SEC; [g] time, 24h.

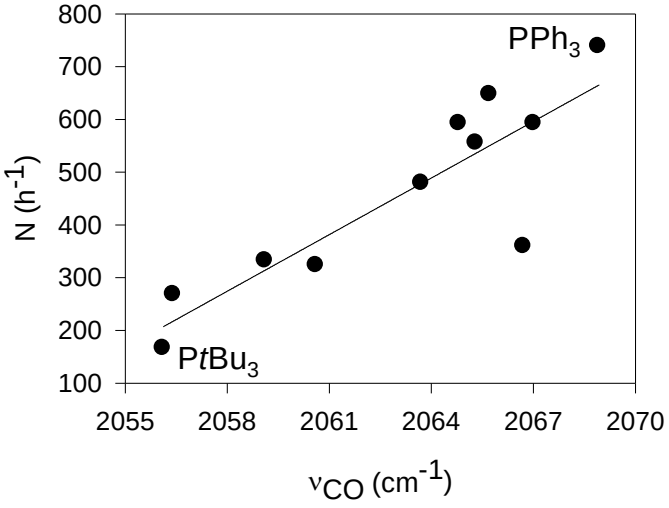

Figure 33 *Plot of N (moles of 1,3-butadiene polymerized per mol of vanadium per hour) vs the phosphine donor ability (as measured by the electronic parameter* ν_{CO}*).*

A general increasing of the activity by decreasing the σ–donor character (increasing π–acceptor character) of the phosphine ligand was observed, irrespective of the ligand steric hindrance. Electron-withdrawing groups on the ligand framework seem to enhance catalytic performance. Complexes with aryl phosphine exhibited higher activity than those bearing alkyl phosphines, as shown in Figure 33 (catalyst using $PCyp_3$ makes an exception to this trend). The P*t*Bu_3 (the strongest σ-donor) yields the least active system, confirming the strong influence of the phosphine basicity on the catalytic activity.

The type of phosphine ligand was also found to have some effect, though not very pronounced, on the polymerization selectivity, as suggested by the microstructure of the resulting PBs determined by ^1H and ^{13}C NMR (Table 13). Generally, all the vanadium complexes, in combination with dMAO, gave polymers with a mixed *cis*-1,4/*trans*-1,4/1,2 structure, the 1,4 and 1,2 units being randomly distributed along the polymer chain, as indicated by the fact that fractionation of the polymers with boiling solvents always gives polymeric fractions having practically the same structure of the pristine polymers; however, the 1,4 content seems to be higher for PBs obtained with catalysts based on vanadium complexes bearing more hindered phosphine ligands ($\theta \geq 150°$).

The influence of the type of alkylating agent (dMAO *vs* sMAO) on the catalytic activity and selectivity was also investigated: under the same polymerization conditions, catalysts using sMAO as co-catalyst resulted to be less active, giving polymers with higher 1,4 content, the *cis*-1,4 units being predominant (Table 13, entries 4 *vs* 5, 2 *vs* 3, 7 *vs* 8, and 9 *vs* 10).

A spread of the weight-average molecular weights, depending on the complex used, ranging from rather low (M_w = 75000 g mol^{-1}, entry 11) to significantly higher (M_w = 296000 g mol^{-1}, entry 16), was observed. The molecular weight distributions were fairly narrow, although tending to a certain broadening in some cases.

In comparison with other catalytic systems suitable for the polymerization of 1,3-butadiene based on transition metal phosphine complexes (*e.g.* Cr, Co, Fe and Ti),[88] vanadium systems are considerably less active and generally less stereospecific.

5.8 Experimental section

5.8.1 Synthesis of vanadium(III) complexes

Vanadium(III) chloride tetrahydrofuran complex (1:3) [$VCl_3(THF)_3$]

A 500 mL, single-neck, round-bottom flask equipped with a reflux condenser and magnetic stirring bar was charged with 250 mL of anhydrous THF and 12.5 g (79 mmol) of VCl_3. The solution was refluxed for 22 hours, then chilled to –80 °C with an ice bath and filtered through a medium fritted funnel. The pink crystals were washed with 70 mL of pentane and dried in vacuo under reduced pressure to give 26 g of a red/pink $VCl_3(THF)_3$ solid. FTIR (cm^{-1}): 3270 (w), 2957 (w),

2902 (w), 1619 (w), 1456 (w), 1340 (w), 1040 (w), 1005 (m), 844 (vs), 682 (mw). *Anal. Calcd*. for $C_{l2}H_{24}Cl_3O$,V: C, 38.57; H, 6.42. *Found*: C, 38.72; H, 6.43.

$VCl_3(PMe_2Ph)_2$ (1a)

PMe_2Ph (1.06 g, 7.7 mmol) was added to a suspension of $VCl_3(THF)_3$ (0.72 g, 1.92 mmol, P/V = 4:1) in toluene (15 mL) at room temperature. The solution turned brown rapidly and was kept under stirring overnight, then concentrated to half of its volume. Pentane (50 mL) was added dropwise, and a light brown precipitate was rapidly formed. The suspension was filtered and the solid on the filter washed with pentane (3×20 mL), then dried under vacuum to give $VCl_3(PMe_2Ph)_2$ as pale pink powder (Yield, 87%). Attempts to obtain crystals useful to determine the structure of the complex failed. FTIR (cm^{-1}): 3053 (w), 1435 (mw), 1140 (mw), 997 (mw), 951 (m), 840 (mw), 745 (vs), 693 (vs), 485 (m). *Anal. Calcd*. for $C_{16}H_{22}Cl_3P_2V$: C, 44.32; H, 5.11. *Found*: C, 42.7; H, 6.11.

$VCl_3(PMePh_2)_2$ (1b)

The complex was prepared according to the procedure described by Caulton.[30] $PMePh_2$ (2.19 g, 11 mmol) was added to a suspension of $VCl_3(THF)_3$ (1.02 g, 2.73 mmol, P/V = 4:1) in toluene (15 mL) at room temperature. A red-purple suspension was rapidly formed. The mixture was kept under stirring overnight, then filtered and concentrated to half of its volume. Pentane (50 mL) was added dropwise and a red-purple precipitate was rapidly formed. The suspension was filtered and the solid on the filter washed with pentane (3×20 mL), then dried under vacuum to give $VCl_3(PMePh_2)_2$ as a red-purple powder (Yield, 90%). FTIR (cm^{-1}): 3053 (w), 1588 (w), 1483 (mw), 1435 (m), 1296 (w), 1130 (s), 1096 (m), 1026 (w), 994 (m), 885 (s), 780 (mw) 741 (vs), 690 (vs), 505 (s), 477 (m). *Anal. Calcd*. for $C_{26}H_{26}Cl_3P_2$,V: C, 55.99; H, 4.70. *Found*: C, 56.01; H, 4.72.

$VCl_3(PPh_3)_2$ (1c)

1c was synthesized in the same way as described above for **1b** using PPh_3 (2.08 g, 10.6 mmol) and $VCl_3(THF)_3$ (1.0 g, 2.66 mmol), and it was obtained as lilac powder (Yield, 83%). Attempts to obtain crystals useful to determine the structure of the complex failed. FTIR (cm^{-1}): 3054 (vw), 1589 (w), 1482 (w), 1436 (m), 1158 (m), 1119 (m), 1093 (m), 991 (m), 748 (mw), 723 (s), 692 (s), 533 (s), 496 (mw). *Anal. Calcd.* for $C_{36}H_{30}Cl_3P_2V$: C, 63.41; H, 4.43; Cl, 15.60; P, 9.08; V, 7.47. *Found*: C, 63.30; H, 4.50; Cl, 15.50; P, 9.0; V, 7.60.

$VCl_3(PCy_3)_2$ (1d)

1d was synthesized in the same way as described above for **1b** using PCy_3 (2.47 g, 8.82 mmol) and $VCl_3(THF)_3$ (0.83 g, 2.20 mmol), and it was obtained as a light grey powder (Yield, 55%). Attempts to obtain crystals useful to determine the structure of the complex failed. FTIR (cm^{-1}): 3277 (vw), 2927 (vs), 2851 (vs), 1446 (s), 1262 (w), 1107 (m), 1006 (vs), 900 (m), 851 (m), 802 (m), 519 (mw), 467 (mw). *Anal. Calcd*. for $C_{36}H_{66}Cl_3P_2V$: C, 60.21; H, 9.26. *Found*: C, 60.24; H, 4.57.

$VCl_3(PtBu_3)_2$ (1e)

P*t*Bu_3 (1.74 g, 8.64 mmol) was added dropwise to a suspension of $VCl_3(THF)_3$ (0.46 g, 2.16 mmol) P/V = 2.6:1) in THF (25 mL) at room temperature. The solution was kept under stirring overnight, then concentrated to half of its volume. Pentane (50 mL) was added dropwise and a brown oily product formed. The mixture was kept under stirring overnight. The solvent was discarded, leaving the oily product behind, washed with pentane (3×40 mL) and finally dried in vacuo. A successive addition of a large excess of pentane, leaving at –30°C for 3h, produced a gray/brown powder of **1e** (Yield, 31%). Attempts to obtain crystals useful to determine the structure of the complex failed. FTIR (cm^{-1}): 3029 (vw), 2971 (w), 1592(w), 1472 (m), 1402 (w), 1379 (w), 1261 (w), 1175 (m), 1097 (w), 998 (s), 934 (w), 871 (m), 807 (m), 732 (w), 672 (m), 618 (w), 554 (m), 493 (m), 474 (m). *Anal. Calcd.* for $C_{24}H_{54}Cl_3P_2V$: C, 51.30; H, 9.69; Cl, 18.93; P, 11.02; V, 9.07. *Found*: C, 51.50; H, 9.50; Cl, 19.10; P, 11.20; V, 9.30.

$VCl_3(PEtPh_2)_2$, (1f)

1f was synthesized in the same way as described for **1a** using $PEtPh_2$ (2.9 g, 13.7 mmol) and $VCl_3(THF)_3$ (1.28 g, 3.42 mmol), and it was obtained as lilac powder (Yield, 91%). The solid was then extracted continuously with boiling pentane. Crystals of **1f** were formed directly on the bottom of the Schlenk tube during the extraction, and further crops of crystals were obtained by cooling the supernatant pentane solution at –30 °C. FTIR (cm^{-1}): 3054 (vw), 2927 (vs), 1587 (vw), 1484 (w), 1436 (m), 1144 (m), 1120 (m), 1098 (m), 1028 (w), 997 (m), 908 (w), 734(s), 691 (vs), 539 (m), 506 (m), 481 (m). *Anal. Calcd*. for $C_{28}H_{30}Cl_3P_2V$: C, 57.41; H, 5.16. *Found*: C, 57.53; H, 5.18.

$VCl_3(Pi PrPh_2)_2$ (1g)

1g was synthesized in the same way as described above for **1a** using P*i*$PrPh_2$ (2.0 g, 8.76 mmol) and $VCl_3(THF)_3$ (0.82 g, 2.19 mmol), and it was obtained as pink powder (Yield, 91%). FTIR (cm^{-1}): 3054 (vw), 2963 (w), 1587 (w), 1482 (w), 1460 (w), 1437 (m), 1153 (m), 1120 (m), 1100 (m), 1026 (m), 992 (m), 879 (w), 740 (s), 691 (vs), 538 (m), 521 (s), 509 (s), 490 (m), 460 (m). *Anal. Calcd*. for $C_{30}H_{34}Cl_3P_2V$: C, 58.70; H, 5.58. *Found*: C, 58.64; H, 5.54.

$VCl_3(PCyPh_2)_2$ (1h)

1h was synthesized in the same way as described above for **1a** using $PCyPh_2$ (2.4 g, 9.0 mmol) and $VCl_3(THF)_3$ (0.86 g, 2.3 mmol), and it was obtained as light blue powder (Yield, 56%). Attempts to obtain crystals useful to determine the structure of the complex failed. FTIR (cm^{-1}): 3055 (vw), 2930 (m), 2875 (w), 1589 (w), 1483 (w), 1437 (m), 1152 (m), 1118 (s), 1097 (m), 1028 (w), 999 (s), 917 (w), 888 (w), 851 (w), 822 (w), 741 (s), 724 (s), 690 (vs), 554 (s), 529 (vs), 499 (m), 486 (m), 463 (w). *Anal. Calcd*. for $C_{36}H_{42}Cl_3P_2V$: C, 62.31; H, 6.10; Cl, 15.33; P, 8.93; V, 7.34. *Found*: C, 62.40; H, 6.30; Cl, 15.50; P, 9.0; V, 7.20.

$VCl_3(PEt_2Ph)_2$ (1i)

1i was synthesized in the same way as described above for **1e** using PEt_2Ph (1.0 g, 6.1 mmol) and $VCl_3(THF)_3$ (0.85 g, 2.26 mmol, P/V = 2.6:1), and it was obtained as green chunks (Yield, 85%). Crystals of **1i** were formed directly on the bottom of the Schlenk tube during the extraction, and further crops of crystals were obtained by cooling the supernatant pentane solution at –30 °C. FTIR (cm^{-1}): 3054 (vw), 2938 (w), 1589 (w), 1485 (w), 1455 (m), 1438 (s), 1398 (m), 1268 (w), 1248 (w), 1130 (vs), 1107 (vs), 1072 (s), 1049 (s), 1020 (s), 1001 (vs), 934 (w), 898 (w), 762 (s), 746 (s), 725 (s), 678 (s), 515 (s), 477 (m). *Anal. Calcd*. for $C_{20}H_{30}Cl_3P_2V$: C, 49.05; H, 6.17. *Found*: C, 50.17; H, 6.23.

$VCl_3(PCy_2Ph)_2$ (1l)

1l was synthesized in the same way as described above for **1e** using PCy_2Ph (1.0 g, 3.65 mmol) and $VCl_3(THF)_3$ (0.55 g, 1.48 mmol), and it was obtained as light green powder (Yield, 76%). Attempts to obtain crystals useful to determine the structure of the complex failed. FTIR (cm^{-1}): 3054 (w), 2924 (vs), 2851 (s), 1588 (w), 1439 (s), 1328 (w), 1299 (w), 1271 (w), 1177 (w), 1125 (m), 1069 (w), 1003 (s), 905 (m), 850 (m), 747 (s), 696 (s), 530 (m), 493 (m). *Anal. Calcd*. for $C_{36}H_{54}Cl_3P_2V$: C, 61.24; H, 7.71. *Found*: C, 61.19; H, 7.68.

$VCl_3(PCyp_3)_2$ (1m)

1f was synthesized in the same way as described above for **1a** using $PCyp_3$ (2.9 g, 13.7 mmol) and $VCl_3(THF)_3$ (0.92 g, 2.44 mmol), and it was obtained as pink powder (Yield, 65%). The solid was then extracted continuously with boiling pentane. Crystals of **1m** were formed directly on the bottom of the Schlenk tube during the extraction, and further crops of crystals were obtained by cooling the supernatant pentane solution at –30 °C. FTIR (cm^{-1}): 2949 (vs), 2866 (vs), 1448 (m), 1299 (mw), 1261 (mw), 1231 (mw), 1126 (m), 1053 (m), 1028 (m), 994 (vs), 907 (mw), 806 (s), 508 (m), 487 (m). *Anal. Calcd*. for $C_{30}H_{54}Cl_3P_2V$: C, 56.83; H, 8.59. *Found:* C, 56.95; H, 8.64.

$VCl_3(P_nPr_3)_2$ (1n)

1n was synthesized in the same way as described above for **1e** using the ligand $PnPr_3$ (1.08 g, 6.72 mmol) and $VCl_3(THF)_3$ (1.0 g, 2.7 mmol), and it was obtained as a beige powder (Yield, 35%). Attempts to obtain crystals useful to determine the structure of the complex failed. FTIR (cm_{-1}): 2093 (mw), 2933 (mw), 2874 (mw), 2903 (mw), 1461 (m), 1403 (m), 1380 (mw), 1243 (vw), 1071 (m), 997 (m), 916 (m), 733 (mw). *Anal. Calcd*. for $C_{18}H_{42}Cl_3P_2V$: C, 45.25; H, 8.86. *Found*: C, 45.10; H, 8.78.

$(\mu\text{-}Me_2P(CH_2)_2PMe_2)V_2Cl_6(Me_2P(CH_2)_2PMe_2)$ (2a)

2a was synthesized in the same way as described above for **1b** using dmpe ligand (1.0 g, 6.6 mmol) and $VCl_3(THF)_3$ (1.81 g, 4.83 mmol, P/V = 1.4:1), and it was obtained as a green powder

(Yield, 80%). The solid obtained was then extracted continuously with boiling pentane, and then with diethyl ether. Crystals of (μ-$Me_2P(CH_2)_2PMe_2$)V_2Cl_6($Me_2P(CH_2)_2PMe_2$) were formed directly on the bottom of the Schlenk tube during the extraction with diethyl ether, and further crops of crystals were obtained by cooling the supernatant solution at –30 °C. FTIR: 2973 (w), 2906 (mw), 1633 (w), 1416 (m), 1281 (mw), 1260 (w), 1189 (w), 1137 (w), 1119 (w), 1091 (w), 935 (vs), 895 (m), 869 (w), 833 (w), 803 (w), 743 (m), 709 (m), 651 (w). *Anal. Calcd*. For $C_{18}H_{48}Cl_6P_6V_2$: C, 28.26; H, 6.32. *Found*: C, 27.58; H, 6.28.

(*μ*-$Et_2P(CH_2)_2PEt_2$)V_2Cl_6($Et_2P(CH_2)_2PEt_2$) (2b)

2b was synthesized in the same way as described above for **1b** using depe ligand (1.0 g, 4.85 mmol) and $VCl_3(THF)_3$ (1.51 g, 4.05 mmol, P/V = 1.2:1), and it was obtained as a mustard-colored powder (Yield, 83%). The solid obtained was then extracted continuously with boiling pentane and then with diethyl ether. Crystals of **2b** were formed directly on the bottom of the Schlenk tube during the extraction with diethyl ether, and further crops of crystals were obtained by cooling the supernatant solution at –30 °C. FTIR: 2973 (mw), 2878 (mw), 2908 (mw), 1455 (m), 1416 (m), 1252 (w), 1109 (w), 1044 (s), 997 (m), 935 (w), 869 (m), 823 (w), 722 (vs), 759 (vs), 676 (w). *Anal. Calcd*. for $C_{30}H_{72}Cl_6P_6V_2$: C, 38.61; H, 7,78. *Found*: C, 35.21; H, 7.34.

VCl_3($Ph_2P(CH_2)_2PPh_2$) (2c)

2c was synthesized in the same way as described above for the synthesis of **1b** using dppe ligand (1.5 g, 3.82 mmol) and $VCl_3(THF)_3$ (1.16 g, 3.17 mmol, P/V = 1.2:1), and it was obtained as a beige powder (Yield, 85%). Attempts to obtain crystals useful to determine the structure of the complex failed. FTIR: 3055 (vw), 1587 (vw), 1485 (mw), 1435 (m), 1099 (mw), 998 (w), 867 (vw), 739 (s), 689 (vs), 515 (m), 493 (m), 484 (m). *Anal. Calcd*. for $C_{26}H_{24}Cl_3P_2V$: C, 56.20; H. *Found*: C, 55.81; H, 4.78.

5.8.2 Synthesis of (imido)vanadium(IV) complexes

Synthesis of (imido)vanadium precursor for 3a and 3b

A toluene solution (2 g) of 250 mg of $V(NMe_2)_4$ (1.10 mmol) and 1 equiv of aniline $ArNH_2$ (Ar = 2,6-*i*Pr_2-C_6H_3 (**3a**), 2,6-Cl_2-C_6H_3 (**3b**)) (1.10 mmol) was heated at 100 °C for 1 day giving a dark-red solution. After removal of the volatiles, toluene (2 g) and excess Me_3SiCl (1.20 g) were added and the solution was stirred for 2 days at 100 °C. Removal of the volatiles under vacuum and washing with pentane afforded dark red-purple solids (240-300 mg).

[V(=N-2,6-Cl_2-C_6H_3)Cl_2(PMe_2Ph)$_2$] (3a)

To a dichloromethane solution (5 mL) of 150 mg of the precursor [V(=N-2,6-Cl_2-C_6H_3)Cl_2] (0.532 mM) was added 300 mg of PMe_2Ph (2.172 mM) at room temperature. After 2 days of

stirring at room temperature, the resulting solution was evaporated to dryness under vacuum. The solid was extracted with toluene, and the solution was filtered on Celite before being evaporated to dryness. The solid was washed with 2 × 5 mL of pentane and then recrystallized by diffusion of pentane into a 1 mL toluene solution, affording red crystals of **3a** (yield after drying under vacuum 105 mg, 35%). EPR (CH_2Cl_2, 20 °C) g = 1.976, $A_{iso}(^{51}V)$ = 81 G, $A_{iso}(^{31}P)$ = 30 G. μ_{eff} (C_6D_6, Evans) = 1.7 μ_B (300 K). *Anal. Calcd.* for $C_{22}H_{25}Cl_4NP_2V$: C, 47.34; H, 4.51; N, 2.51. *Found*: C, 47.28; H, 4.45; N, 2.62.

[V(=N-2,6-*i*Pr$_2$-C$_6$H$_3$)Cl$_2$(PMe$_2$Ph)$_2$] (3b)

To a dichloromethane solution (2 mL) of 150 mg of the precursor [V(=N-2,6-*i*Pr$_2$-C$_6$H$_3$)Cl$_2$] (0.5048 mM) was added 209 mg of PMe_2Ph (1.515 mM) at room temperature. After 3 days, the resulting dark yellow solution was evaporated to dryness under vacuum giving red-orange crystals that were washed with pentane (2 x 2 mL) (yield: 250 mg, 86%). EPR (CH_2Cl_2, 20°C) g = 1.993, $A_{iso}(^{51}V)$ = 83 G, A_{iso} (^{31}P) = 30 G, A_{iso} (^{14}N) = 5 G. μ_{eff} = 1.77 μ_B (300K). *Anal. Calcd.* for $C_{28}H_{39}Cl_2NP_2V$: C, 58.65; H, 6.86; N, 2.44. *Found*: C, 58.37; H, 6.85; N, 2.53.

[V(=N-^{t}Bu)Cl$_2$(PMe$_2$Ph)$_2$] (3c)

Step 1. A toluene solution (5 mL) of 400 mg of $V(NMe_2)_4$ (1.760 mM) and 283.2 mg of $^tBuNH_2$ (3.872 mM) was heated overnight at 100°C giving a dark brown-red solution. Removal of the volatiles under vacuum gave a sticky solid that was triturated several times with 2 mL of pentane and dried under vacuum for a prolonged period of time to afford a red solid (composed of [V(μ-N-*t*Bu)$(NMe_2)_2]_2$ and a minor amount of [(*t*BuNH)(Me_2N)V(μ-N-*t*Bu)$_2$V$(NMe_2)_2$].

Step 2. To this solid was added toluene (2 mL) and excess Me_3SiCl (2.0 g) and the red-purple solution was stirred overnight at 100°C. Removal of the volatiles under vacuum, and washing with cold pentane afforded dark pink solid (150 mg) that is attributed to a complex of composition closed to $[V(\mu\text{-N-}tBu)Cl_2]_n$.

Step 3. To this pink solid (150 mg of $[V(\mu\text{-N-}tBu)Cl_2]_n$ was added 3 mL of toluene and then 322.2 mg of PMe_2Ph (2.332 mM). The brown-red solution was stirred at room temperature for 3 days. The volatiles were removed under for a prolonged period of time to get rid of excess PMe_2Ph (that render **3c** more soluble in pentane). The solid was extracted with toluene (3×1 mL), the solution was filtered through a bed of celite, and the filtrate was evaporated to dryness. The resulting brown-red solid was briefly washed with 2 mL of cold pentane, and dried under vacuum to afford 345 mg of **3c** (yield: 42% based on $V(NMe_2)_4$). EPR (pentane, 20°C) g = 1.978, $A_{iso}(^{51}V)$ = 85 G, $A_{iso}(^{31}P)$ = 29 G. μ_{eff} (Evans)= 1.8 μ_B (300K). *Anal. Calcd*. for $C_{20}H_{31}Cl_2NP_2V$: C, 51.19; H, 6.66; N, 2.98. *Found*: C, 50.88; H, 6.89; N, 3.02.

[V(=N-^{t}Bu)Cl_2(PMe_3)$_2$] (3c′)

3c′ was prepared by the method described above for **3c**. Crystals were obtained by cooling a pentane solution of **3c′** to –20°C. EPR (CH_2Cl_2, 20°C) g = 1.994, A_{iso}(^{51}V) = 85 G, A_{iso}(^{31}P) = 29 G. μ_{eff} (Evans)= 1.7 μ_B (300K). *Anal. Calcd*. for $C_{10}H_{27}Cl_2NP_2V$: C, 34.80; H, 7.89; N, 4.06. *Found*: C, 35.20; H, 7.88; N, 4.07.

References

[1] R.R. Langeslay, D.M. Kaphan, C.L. Marshall, P.C. Stair, A.P. Sattelberger, M. Delferro *Chem. Rev.* **2018**, DOI: 10.1021/acs.chemrev.8b00245

[2] (a) G. Natta, G. Dall'Asta, G. Mazzanti, I. Pasquon, A. Valvassori, A. Zambelli *Makromol. Chem.* **1962**, *54*, 95–101; (b) G. Natta, G. Dall'Asta, G. Mazzanti *Angew. Chem., Int. Ed.* **1964**, *3*, 723–729.

[3] G. Natta, P. Pino, P. Corradini, F. Gianrusso, E. Mantica, G. Mazzanti, G. Moraglio *J. Am. Chem. Soc.* **1955**, *77*, 1708-1710.

[4] W.L. Carrick *J. Am. Chem. Soc.* **1958**, *80*, 6455-6456.

[5] (a) E. Junghanns, O. Gumboldt, G. Bier *Makromol. Chem*. **1962**, *58*, 18; (b) G. Natta, G. Mazzanti, A. Valvassori, G. Sartori, D. Fiumani *J. Polym. Sci.* **1961**, *51*, 411-427.

[6] S.C. Davis, W. von Hellens, H. Zahalka *Polymer Material Encyclopedia* **1996**, *Vol. 3* Salamone, J.C. Ed.; CRC Press Inc., Boca Raton, FL.

[7] S. Gambarotta *Coord. Chem. Rev.* **2003**, *237*, 229-243.

[8] K. Nomura, S. Zhang *Chem. Rev.* **2011**, *111*, 2342–2362.

[9] (a) W. Wang, K. Nomura *Adv. Synth. Catal.* **2006**, *348*, 743-750; (b) W. Wang, K. Nomura *Macromolecules* **2005**, *38*, 5905-5913.

[10] J. B. Wang, L. P. Lu, J. Y. Liu, Y. S. Li *Dalton Trans.* **2014**, *43*, 12926-12934.

[11] J. Q. Wu, J. S. Mu, S. W. Zhang, Y.S. Li *J. Polym. Sci. A: Polym. Chem*. **2010**, *48*, 1122–1132.

[12] C. Lorber "*Vanadium Organometallics*" **2007**, Elsevier Ltd.

[13] J.Q. Wu, Y.S. Li *Coord. Chem. Rev.* **2011**, *255*, 2303–2314.

[14] G. Dall'Asta, G. Mazzanti, *Makromol. Chem.* **1963**, *61*, 178–197.

[15] A.K. Tomov, V.C. Gibson, D. Zaher, M.R.J. Elsegood, S.H. Dale *Chem. Commun.* **2004**, 1956–1957.

[16] A.Y. Khalimon, E. Peterson, C. Lorber, L.G. Kuzmina, J.A.K. Howard, A. van der Est, G.I. Nikonov *J. Inorg. Chem.* **2013**, *12*, 2205–2211.

[17] C. Lorber, R. Choukroun, L. Vendier *Inorg. Chem.* **2007**, *46*, 3192–3202.

[18] C. Lorber, R. Choukroun, B. Donnadieu *Inorg Chem.* **2003**, *42*, 673–675.

[19] C. Lorber, R. Choukroun, B. Donnadieu *Inorg. Chem.* **2002**, *41*, 4216–4226.

[20] C. Lorber, B. Donnadieu, R. Choukroun *Dalton Trans.* **2000**, 4497–4498.

[21] (a) N. Desmangles, S. Gambarotta, C. Bensimon, S. Davis, H.J. Zahalka *Organomet. Chem.* **1998**, *562*, 53-60; (b) C. Cuomo, A. Milione, A. Grassi *J. Polym. Sci., Part A: Polym. Chem.* **2006**, *44*, 3279-3289; (c) C. Lorber, B. Donnadieu, R. Choukroun *Organometallics* **2000**, *19*, 1963-1966.

[22] H. Hagen, J. Boersma, M. Lutz, A.L. Spek, G. van Koten *Eur. J. Inorg. Chem*. **2001**, 117-123.

[23] (a) M. Biazek, K. Czaja *J. Polym. Sci., Part A: Polym. Chem.* **2008**, *46*, 6940-6949; (b) M. Biazek, K. Czaja *Polimery* **2008**, *53*, 364-370.

[24] C. Lorber, F. Wolff, R. Choukroun, L. Vendier *Eur. J. Inorg. Chem.* **2005**, 2850–2859.

[25] L.M. Tang, J.Q. Wu, Y.Q. Duan, L. Pan, Y.G. Li, Y.S. Li *J. Polym. Sci., Part A: Polym. Chem*. **2007**, *19*, 2038–2048.

[26] J.Q. Wu, L. Pan, Y.G. Li, S.R. Liu, Y.S. Li *Organometallics* **2009**, *28*, 1817–1825.

[27] (a) J. Burt, W. Levason, G. Reid *Coord. Chem. Rev*. **2014**, *260*, 65-115; (b) C. Cheng, J.F. Hartwig *Science* **2014**, *343*, 853-857.

[28] (a) M.L. Scheuermann, E.J. Johnson, P.J. Chirik *Org. Lett*. **2015**, *17*, 2716-2719; (b) M. Murai, H. Takeshima, H. Morita, Y. Kuninobu, K. Takai *J. Org. Chem.* **2015**, *80*, 5407-5414; (c) K. Nomura, K. Suzuki, S. Katao, Y. Matsumoto *Organometallics* **2012**, *31,* 5114-5120; (d) J.R.V. Lang, C.E. Denner, H.G. Alt *J. Mol. Catal. A: Chem*. **2010**, *322*, 45-49: (e) Z.L. Niemeyer, A. Milo, D.P. Hickey, M.S. Sigman *Nature Chem*. 2016, 81, 610-617; (f) M. Carravetta, M. Concistre, W. Levason, G. Reide, W. Zhang *Inorg. Chem.* **2016**, *55*, 12890-12896; (g) E. Despagnet-Ayoub, M.K. Takase, J.A. Labinger, J.E. Bercaw *J. Am. Chem. Soc.* **2015**, *137*, 10500-10503; (h) Z. Xi, H.S. Bazzi, J.A. Galdysz *J. Am. Chem. Soc.* **2015**, *137*, 10930-10933; (j) J.A. Love, M.S. Sanford, M.W. Day, R.H. Grubbs *J. Am. Chem. Soc.* **2003**, *125*, 10103-10109.

[29] G. Leone, A. Boglia, A.C. Boccia, S. Taglialatela Scafati, F. Bertini, G. Ricci *Macromolecules* **2009**, *42*, 9231–9237.

[30] R.L. Bansemer, J.C. Huffman, K.G. Caulton *Inorg. Chem.* **1985**, *24*, 3003-3006.

[31] (a) D.G.L. Holt, L.F. Larkworthy, D.C. Povey, G.W. Smith, G.J. Leigh Inorg. Chim. Acta. 1993, 207, 11-19; (b) J. Bultitude, L.F. Larkworthy, D.C. Povey, G.W. Smith, J.R. Dilworth Dalton *Trans*. **1986**, 2253-2258; (c) J. Nieman, J.H. Teuben, J.C. Huffman, K.G. Caulton *J. Org. Chem*. **1983**, *255*, 193-204.

[32] A.C. Tolman *Chem. Rev*. **1977**, *77*, 313-348.

[33] P. Dierkes, P.W.N.M. van Leeuwen *Dalton Trans.* **1999**, 1519–1529.

[34] C.P. Casey, G.T. Whiteker *Isr. J. Chem.* **1990**, *30*, 299–304.

[35] K. Feghali, D.J. Harding, D. Reardon, S. Gambarotta, G. Yap, Q. Wang *Organometallics* **2002**, *21*, 968-976.

[36] E. Addison, A. Deffieux, M. Fontanille, K. Bujadoux *J. Polym. Sci. Part A: Pol. Chem.* **1994**, *32,* 1033-1047.

[37] Y. Yoshida, J.I. Mohri, S.I. Ishii, M. Mitani, J, Saito, S. Matsui, H. Makio, T. Nakano, H. Tanaka, M. Onda, Y. Yamamoto, A. Mizuno, T. Fujita *J. Am. Chem. Soc.* **2004**, *126*, 12023-12032.

[38] The phosphine dissociation in the activation process of phosphine-containing Grubbs-Hoveyda Ruthenium complexes is a well-accepted mechanism. For example, see: (a) F. Nuñez-Zarur, X. Solans-Monfort, L. Rodríguez-Santiago, M. Sodupe *Organometallics* **2012**, *31*, 4203-4215; (b) G. C. Vougioukalakis, R.H. Grubbs *Chem. Eur. J.* **2008**, *14*, 7545-7556; (c) M.S. Sanford, J.A. Love, R.H. Grubbs *J. Am. Chem. Soc*. **2001**, *123*, 6543-6554.

[39] Y. Ma, D. Reardon, S. Gambarotta, G. Yap, H. Zahalka, C. Lemay *Organometallics* **1999**, *18*, 2773-2781.

[40] T.R. Younkin, E.F. Connor, J.I. Henderson, S.K. Freidrich, R.H. Grubbs, D.A. Bansleben *Science* **2000**, *287*, 460-462.

[41] G.L. Liu, D.J. Beetstra, A. Meetsma, B. Hessen *Organometallics* **2004**, *23*, 3914-3920.

[42] H. Lasarov, K. Mönkkönen and T. Pakkanen *Macromol. Chem. Phys.* **1998**, *199*, 1939-1942.

[43] G.M. Benedikt, E. Elce, B.L. Goodall, H.A. Kalamarides, L.H. McIntosh, L.F. Rhodes, K.T. Selvy, C. Andes, K. Oyler, A. Sen *Macromolecules* **2002**, *35*, 8978–8988.

[44] M.P. Shaver, L.E.N. Allan, V.C. Gibson *Organometallics* **2007**, *26*, 2252-2257.

[45] B.C. Xu, T. Ju, J.Q. Wu, N.H. Hu, Y.S. Li *Dalton Trans.* **2009,** 8854-8863.

[46] L.M. Tang, J.Q. Wu, Y.Q. Duan, L. Pan, Y.G. Li, Y.S. Li *J. Polym. Sci. Part A: Pol. Chem.* **2008**, *46*, 2038-2048.

[47] G. Leone, I. Pierro, G. Zanchin, A. Forni, F. Bertini, A. Rapallo, G. Ricci *J. Mol. Catal. A: Chem.* **2016**, *424,* 220-231.

[48] J.A. Love, M.S. Sanford, M.W. Day, R.H. Grubbs *J. Am. Chem. Soc.* **2003**, *125*, 10103-10109.

[49] C.S. Popeney, Z. Guan *Macromolecules* **2010**, *43*, 4091-4097.

[50] C. De Rosa, A. Buono, F. Auriemma, A. Grassi *Macromolecules* **2004**, *37*, 9489-9502.

[51] (a) J. Kiesewetter, B. Arikan, W. Kaminsky *Polymer* **2006**, *47*, 3302–3314; (b) A. Ravasio, C. Zampa, L. Boggioni, I. Tritto, J. Hitzbleck, J. Okuda *Macromolecules* **2008**, *41*, 9565–9569.

[52] (a) P.W.N.M. van Leeuwen, P.C.J. Kamer, J.N.H. Reek *Pure Appl. Chem.* **1991**, *71*, 1443–1452; (b) A.L. Balch "*Binuclear, Phosphine-Bridged Complexes: Progress and Prospects*" **1983** (p.167) in Pignolet L.H. (eds) Homogeneous Catalysis with Metal Phosphine Complexes. Modern Inorganic Chemistry. Springer, Boston, MA.

[53] R.J. Puddephatt *Chem. Soc. Rev.* **1983**, *12*, 99–127.

[54] E. Addison, A. Deffieux, M. Fontanille, K. Bujadoux *J. Polym. Sci. Part A: Pol. Chem.* **1994**, *32*, 1033-1047.

[55] P.W.N.M. van Leeuwen, P.C.J. Kamer, J.N.H. Reek, P. Dierkes *Chem. Rev.* **2000**, *100*, 27412769.

[56] Z. Freixa, P.W.N.M. van Leeuwen *Dalton Trans*. **2003**, 1890–1901.

[57] M.N. Birkholz, Z. Freixa, P.W.N.M. van Leeuwen *Chem. Soc. Rev*. **2009**, *38*, 1099-1118.

[58] J.R. Sowa, R. J. Angelici *Inorg. Chem*. **1991**, *30*, 3534-3537.

[59] D. Ruchatz, G. Fink *Macromolecules* **1998**, *31*, 4684-4686.

[60] B.C. Hamann, J.F. Hartwig J. *Am. Chem. Soc*. **1998**, *120*, 3694-3703.

[61] G.M. Benedikt, E. Elce, B.L. Goodall, H.A. Kalamarides, L.H. McIntosh, L.F. Rhodes, K.T. Selvy, *Macromolecules* **2002**, *35*, 8978-8988.

[62] (a) T.R.J. Cundari *J. Am. Chem. Soc.* **1992**, *114*, 7879−7888; (b) M.P. Coles, V.C. Gibson *Polym. Bull.* **1994**, *33*, 529-533; (c) M.P. Coles, C. Dalby, V.C. Gibson, I.R. Little, E.L. Marshall, M.H. Ribeiro da Costa, S. Mastroianni *J. Organomet. Chem*. **1999**, *591*, 78-87.

[63] P.D. Bolton, P. Mountford *Adv. Synth. Catal*. **2005**, *347*, 355−366.

[64] C. Lorber, *Chemistry, Molecular Sciences and Chemical Engineering* (Major Reference Works) **2015** (pp 1−78) Reedijk, J., Ed.; Elsevier: Waltham, MA.

[65] A.W. Addison, T.N. Rao, J. Reedijk, J.V.J. van Rijn *Dalton Trans*. **1984**, 1349–1356.

[66] (a) L. Falivene, R. Credendino, A. Poater, A. Petta, L. Serra, R. Oliva, V. Scarano, L. Cavallo *Organometallics* **2016**, *35*, 2286–2293;
(b) https://www.molnac.unisa.it/OMtools/sambvca2.0/.

[67] A. Macchioni *Chem. Rev*. **2005**, *105*, 2039–2074.

[68] A. Ravasio, L. Boggioni, I. Tritto *Macromolecules* **2011**, *44*, 4180-4186.

[69] (a) W. Wang, T. Tanaka, M. Tsubota, M. Fujiki, S. Yamanaka, K. Nomura *Adv. Synth. Catal*. **2005**, *347*, 433-446; (b) K. Nomura, A. Sagara, Y. Imanishi *Macromolecules* **2002**, *35*, 1583-1590.

[70] M.P. Shaver, L.E.N. Allan, V.C. Gibson *Organometallics* **2007**, *26*, 2252-2257.

[71] G. Zanchin, I. Pierro, E. Parisini, J. Martí-Rujas, G. Ricci, G. Leone *J. Organomet. Chem*. **2018**, *861*, 142-150.

[72] X. Hao, C. Zhang, L. Li, H. Zhang, Y. Hu, D. Hao, X. Zhang *Polymers* **2017**, *9*, 325-336.

[73] (a) K. Wang, J. Wang, Y. Li, L. Pan, Y.S. Li *Polymers* **2017**, *9*, 353-364; (b) Y. Li, J. Yang, B. Wang, Y.S. Li *RSC Adv.* **2016**, *6*, 59590-59599.

[74] N. Diteepeng, X. Tang, X. Hou, Y.S. Li, K. Phomphrai, K. Nomura *Dalton Trans*. **2015**, *44*, 12273- 12281.

[75] (a) X. Li, Z. Hou *Macromolecules* **2005**, *38*, 6767-6769; (b) T. Hasan, T. Ikeda, T. Shiono *J. Polym. Sci., Part A: Polym. Chem*. **2007**, *45*, 4581-4587.

[76] G. Zanchin, G. Leone, I. Pierro, A. Rapallo, W. Porzio, F. Bertini, G. Ricci *Macromol. Chem. Phys*. **2017**, *218*, 1600602.

[77] G. Leone, M. Mauri, S. Losio, F. Bertini, G. Ricci, L. Porri *Polym. Chem*. **2014**, *5*, 3412-3423.

[78] B.C. Peoples, V.N. Dougnac, G.B. Galland, F.M. Rabagliati, R. Quijada *Polym. Bull.* **2012**, *70*, 117-129.

[79] (a) X. Ren, F. Guo, H. Fu, Y. Song, Y. Li, Z. Hou *Polym. Chem*. **2018**, *9*, 1223-1233; (b) M. Hong, L. Pan, W.P. Ye, D.P. Song, Y.S. Li *J. Polym. Sci., Part A: Polym. Chem.* **2010**, *48*, 1764-1772; (c) F. Song, D. Pappalardo, A.F. Johnson, B. Rieger, M. Bochmann *J. Polym. Sci., Part A: Polym. Chem*. **2002**, *40*, 1484-1497.

[80] J. Suzuki, Y. Kino, T. Uozomi, T. Sano, T. Teranishi, J. Jin, K. Saga, T. Shiono *J. Appl. Polym. Sci*. **1999**, *72*, 103-108.

[81] (a) X. Wang, H. Zhang, Z. Wang, B. Jiang *Polymer* **1997**, *38*, 5407-5410; (b) B.C. Peoples, V.N. Dougnac, G.B. Galland, F.M. Rabagliati, R. Quijada *Polym. Bull*. **2013**, *70*, 117-129.

[82] H. Li, J. Li, Y. Zhang, Y. Mu *Polymer* **2008**, *49*, 2839-2844.

[83] L. Porri, A. Giarrusso "*Part II*" **1989** (pp. 53-108) in *Conjugated Diene Polymerization in Comprehensive Polymer Science*; Pergamon: Oxford, UK.

[84] G. Natta, L. Porri, P. Corradini, D. Morero *Chim. Ind*. *(Milan)* **1958**, *40*, 362-371.

[85] (a) G. Natta, L. Porri, A. Carbonaro *Atti Accad. Naz. Lincei Cl. Sci. Fis. Mat. Nat. Rend.* **1961**, *31*, 189. *Chem. Abstr*. 1962, *57*, 4848; (b) L. Porri, A. Carbonaro, F. Ciampelli *Makromol. Chem*. **1963**, *61*, 90-103; (c) G. Ricci, S. Italia, C. Comitani, L. Porri *Polym. Commun*. **1991**, *32*, 514–517; (d) G. Ricci, L. Zetta, E. Alberti, T. Motta, F. Canetti, F. Bertini *J. Polym. Sci., Part A: Polym. Chem*. **2007**, *45*, 4635-4646.

[86] (a) L. Porri, A. Giarrusso, G. Ricci, J. Scheirs, W. Kaminsky **2000** (p.115) Eds.; John Wiley & Sons Ltd., London, UK. (b) G. Ricci, A. Panagia, L. Porri *Polymer* **1996**, *37*, 363-365; (c) S. Bradley, K.D. Camm, S.J. Furtado, A.L. Gott, P.C. McGowan, T.J. Podesta, M. Thornton-Pett *Organometallics* **2002**, *21*, 3443-3453.

[87] (a) G. Natta, L. Porri, G. Zanini, L. Fiore *Chim. Ind. (Milan)* **1959**, *41*, 526–532; *Chem. Abstr.* **1960**, *54*, 1258.

[88] G. Ricci, A. Sommazzi, F. Masi, M. Ricci, A. Boglia, G. Leone *Coord. Chem. Rev*. **2010**, *254*, 661-676.

[89] G. Ricci, G. Leone, A. Sommazzi, A. Forni, F. Masi U.S. Patent Application **2017**, 20, 170, 275, 312.

[90] G. Zanchin, L. Vendier, I. Pierro, F. Bertini, G. Ricci, C. Lorber, G. Leone *Organometallics* **2018**, *37*, 3181-3195.

[91] P.J.T. Tait, N.D. Watkins "*Comprehensive Polymer Science*" **1989** (p.27) G.C. Eastmond, A. Ledwith, S. Russo, P. Sigwalt, Eds.; Pergamon Press Ltd.: Oxford, UK.

Chapter 6
Chromium

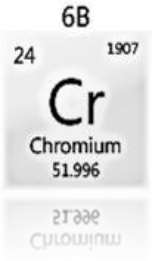

Chapter highlights

- → Iminopyridines were used as ligands with Cr(II) and Cr(III)
- → The non-innocent nature of iminopyridines requires discriminating between *formal* and *physical* oxidation states of Cr complexes
- → Chromium–to–ligand transfer was observed
- → Non–innocent ligands and metal–to–ligand electron transfer make the difference in ethylene polymerization, but not in the polymerization of cyclic olefins and 1,3-butadiene
- → Chromium–porphyrinato complexes are active catalysts for the copolymerization of epoxides and anhydrides

Parts of this chapter have been published and are reproduced here from:

G. Leone, E. Groppo, **G. Zanchin**, G.A. Martino, A. Piovano, F. Bertini, J. Martí-Rujas, E. Parisini, G. Ricci *Organometallics* **2018**, *37*, 4827–4840.

Chromium is the element of the periodic table with atomic number 24 belonging to the Group 6 of the transition series; it exhibits a wide range of oxidation states, with (III) being the most stable.

The main applications are in stainless steel and chrome plating, which together comprise 85% of the commercial use.

In the world of catalysis for olefin polymerization, chromium recovers a leading role, together with titanium. Indeed, as will be discussed more in detail further, chromium oxides are employed in the Phillips catalysts, used in the production of about half of the world's PE.

6.1 Chromium: the state-of-the-art

6.1.1 The Phillips catalyst

Chromium ions grafted on a porous support material, traditionally amorphous silica, play a central role in the worldwide production of PE. This catalytic system, able to polymerize ethylene, was accidentally discovered more than half a century ago at Phillips Petroleum Company.[1] The same catalyst system, modified and evolved, is used even today by dozens of companies throughout the world, and it accounts for ~40–50% of the world's High-Density PE (HDPE) supply, and some Low-Density PE grades (LDPE and LLDPE). The catalyst is now more active and has been tailored in numerous ways for many specialized modern applications.

As heterogeneous catalyst, it has not proved amenable to be studied, and even to these days an ongoing debate about the nature of the reduced active Cr sites (in terms of molecular structure, oxidation state, local geometry) is still open.[2-4]

The development of homogeneous molecular chromium catalysts is therefore an important objective, since these systems offer the potential for understanding the *modus operandi* of supported chromium catalysts and may provide new opportunities for tuning activity and selectivity.

6.1.2 Homogeneous chromium catalysts

With the aim of preparing homogeneous single–site chromium catalysts, a great number of reports have appeared in the recent literature. Various molecular chromium complexes have been developed and used for the selective oligomerization[5] and polymerization of ethylene.[6] Most of the recently reported chromium complexes are enveloped by non–cyclopentadienyl ligands,[5] namely multidentate ligands with phosphine, amine, ether, and thioether donors because of their easy tuning of steric and electronic properties.[7] Notable examples are chromium complexes ligated by tetradentate N_2P_2,[8] tridentate S^N^S,[9] P^N^P,[10] O^N^N,[11] N^N^N,[12] and bidentate N^N ligands.[13]

Bidentate iminopyridine ligands and their non–innocent nature

While tridentate pyridine-bis(imine) ligands have been deeply studied and applied to the synthesis of complexes for olefin polymerization,[14] bidentate analogous iminopyridines have been

less studied. However, from the first reports on their synthesis at the beginning of 2000s,[15] they have recently received attention as ancillary ligands in coordination chemistry by virtue of their low cost, easy preparation and the fine tunability of their steric and electronic properties.

Iminopyridines belong to the family of electronically non–innocent ligands, that is the family of ligands that are able participate in electron transfer with a metal, thus acting as reversible electron sink rather than existing as spectators.[16] The occurrence of this ligand–metal synergy brings to situations where the formal oxidation state, the one determined by a preset of rules, differ from the oxidation state that is determined by experiment.[17]

Single-electron transfer from the metal (Mt) involving non–innocently behaving redox–active ligands (L) leads to the monoanionic radical $(L^{\bullet})^{-}$, while two-electron transfer leads to the doubly reduced dianion $(L)^{2-}$ (Fig. 1).

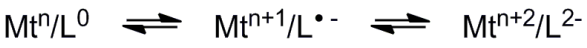

Figure 1 *Different redox states associated with electron transfer.*

To the best of our knowledge, among non–innocent ligands, iminopyridines complexes are less investigated than diimine or pyridine-bis(imine) analogues, and metal complexes ligated by $(L^{\bullet})^{-}$ and $(L)^{2-}$ iminopyridines are rare and not structurally characterized.

Structural, spectroscopic, and computational studies can be applied to examine the redox events and distinguish among the different oxidation states. For example, analysis of the C–C and C–N bond distances can be used when the exact molecular structure is available from X-ray spectroscopy. Optical spectroscopies, such as FTIR and UV–vis, have also aided in the experimental identification between *formal* and *physical* oxidation states, in particular when X-ray data are unavailable, as in our case.

6.1.3 The versatility of chromium catalysts

In addition to its renewed relevance for ethylene oligomerization and polymerization, chromium catalysts have received special attention also for the polymerization of 1,3-butadiene.[18] Catalytic systems obtained by combining a soluble Cr compound (*e.g.*, $Cr(acac)_3$, $Cr(CO)_5py$, acac = acetylacetonate, py = pyridine) with $AlEt_3$ gave a 1,2-poly(butadiene) with an iso- or syndiotactic structure, depending on the Al/Cr mole ratio (syndiotactic for Al/Cr = 2–6 and isotactic for Al/Cr = 6–10).[19] Most recently, Cr(II) complexes with bidentate phosphines (*e.g.*, $CrCl_2(dmpe)_2$, $CrCl_2(depe)_2$, $CrCl_2(dmpm)_2$, dmpe = 1,2-bis(dimethylphosphino)ethane, depe = 1,2-bis(diethylphosphino)ethane, dmpm = 1,2-bis(dimethylphosphino)methane) in combination with methylaluminoxane (MAO), were extremely active, giving highly syndiotactic and predominantly isotactic 1,2-poly(butadiene)s, depending on the type of phosphine.[20] Cr(III) complexes bearing

bis(pyrazolyl)pyridine,[21] and bis(benzimidazolyl)amine exhibited high activities and high *trans*-1,4 selectivity.[22]

In contrast, the polymerization of cyclic olefins mediated by chromium catalysts has been rarely described.[23] In 2001, Heitz *et al.* reported the addition polymerization of norbornene (NB) with homogeneous Cr(III) complexes of the type $[Cp'CrMeCl]_2$ (Cp' = C_5H_5, C_5Me_5, indenyl, fluorenyl). They obtained partly crystalline poly(norbornene)s (PNBs), whose crystallinity degree strongly depends on the electron donating character of the Cp–ligand.[24] A divalent Cr(II) complex of the type $Cr[1,3\text{-}C_3H_3(SiMe_3)_2]_2$ was also found to exhibit high activity in the polymerization of NB, giving a crystalline PNB whose structure was not determined.[25] More recently, Cr(II) complexes with bidentate phosphines, in combination with MAO, were active in the polymerization of NB, giving a highly stereoregular PNB with an unusual 2,3-*exo*-diheterotactic structure.[26]

In this context, during my PhD research activity, a series of chromium complexes bearing three different iminopyridine ligands (Fig. 2) was synthesized; they were then intended as pre-catalyst for various (di)olefins polymerization. The aim was to get better insight into the questions correlated with chromium based catalysts, in particular concerning the oxidation state of intermediates and/or active site, and the influence of ligand substituents on the catalytic behavior of the obtained complexes.

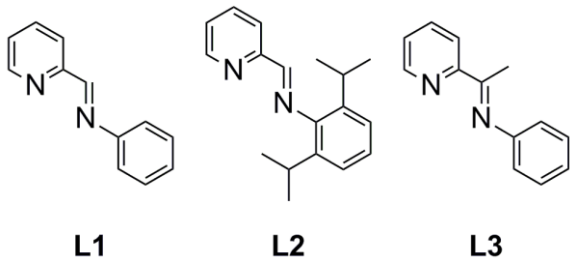

Figure 2 *Iminopyridine ligands surveyed in this thesis.*

The **main difficulties** tackled in this part of the research activity were connected to the great sensitivity of chromium species to air and moisture, due also to the high oxophilicity, and the tendency of Cr(II) to oxidize to the more stable Cr(III) state. Moreover, the coordinative unsaturation of these complexes made the isolation of single crystals, suitable for X-ray structure determination, rather difficult. In addition to these facts, the redox–active nature of iminopyridines imparts additional complexity to the electronic structure of the coordination complexes.

For all these reason, UV–vis–NIR spectroscopy has been applied to investigate the electronic properties of the complexes and to discriminate between the *formal* (*i.e.,* the *d*-electron configuration determined by a prescribed set of rules) and the *physical* (or *spectroscopic*) (*i.e.*, the *d*-electron configuration determined by experimental measures) oxidation state of chromium;

indeed UV–vis–NIR spectroscopy has been demonstrated to be a sensitive tool for discriminating between neutral and charged redox ligands,[27] the latter being characterized by extremely intense electronic transitions in the visible range.

The section concerning the UV–vis–NIR spectroscopy was developed in collaboration with prof. Elena Groppo (University of Turin – Department of Chemisty), while the molecular structure of complex **Cr4** determined by X-ray diffraction was obtained in collaboration with dr. Emilio Parisini (IIT Milan). The results on this subject were succesfully published in *Organometallics* while this thesis was under revision (*Organometallics* **2018** doi: 10.1021/acs.organomet.8b00812).

6.2 Iminopyridine chromium complexes

6.2.1 Synthesis and characterization of the complexes

The research on chromium started from the synthesis of the iminopyridine ligands, according to the procedure reported in the literature.[28] The ligands were later employed to prepare the chromium complexes starting from two different precursors: **Cr1**–**Cr3** from a Cr(II) source, while **Cr4** from a Cr(III) one. In details, **Cr1**–**Cr3** were synthesized by reaction of $CrCl_2$ with the stoichiometric amount of the corresponding **L1**–**L3** ligands in THF at room temperature. The complexes immediately formed, and rapidly precipitated from an initially clear solution. By this procedure, the solids were isolated in high yield, ranging from 70 to 94%. **Cr4** was prepared by reaction of $CrCl_3(THF)_3$ with the stoichiometric amount of **L1** in THF at room temperature. The complex was isolated as a green powder in good yield (77%). All the complexes were highly air- and moisture-sensitive, thus requiring characterization under strictly inert conditions. Each complex was characterized by elemental analysis, attenuated total reflection (ATR) FTIR and ^{1}H NMR spectroscopy, the elemental analysis being consistent with the formation of complexes of (L)$CrCl_n$(THF) composition (n = 2, **Cr1**–**Cr3**; n = 3, **Cr4**). In addition, the electronic properties of all the investigated complexes were determined by UV–vis–NIR spectroscopy.

As expected, isolation of single crystals of **Cr1**–**Cr4**, suitable for X–ray diffraction, proved problematic. The use of $CrCl_3(THF)_3$ was crucial to the successful isolation of a microcrystalline, characterizable product. Hence, single crystals, suitable for X–ray diffraction, were obtained only for **Cr4** from a concentrated dichloromethane solution, cooled down to –18 °C for days. The crystal structure of **Cr4** is provided in Figure 3, along with a selection of its main structural details (bond lengths (Å) and angles (°)).

The X-ray diffraction analysis shows that the Cr atom is six-coordinated and that a hydroxide anion completes the octahedral coordination sphere of the metal by binding to the chromium atom *trans* to the N1 atom of **L1** ligand (Cr1–O1 = 2.014(8)Å, Cr1–N1 = 2.07(1)Å, O1–Cr1–N1 = 172.9(4)°). Traces of adventitious water during the work-up for the single crystal growth are the likely source of the formation of the unexpected coordination of oxygen, whose binding to the

chromium atom likely occurs with the simultaneous dissociation of a coordinated THF molecule. Consistent with this hypothesis, the ATR–IR spectrum of pristine solid **Cr4** did not show any band associable to the presence of a hydroxide anion, while it shows bands due to THF (*vide infra* Fig. 4a′).

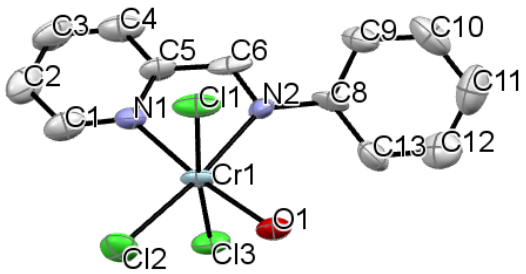

Figure 3 *ORTEP drawings of* ***Cr4***·*OH.*
Thermal ellipsoids are drawn at the 50% probability level. Hydrogen atoms are omitted for clarity.

Unfortunately, despite numerous attempts, single crystals of **Cr1**–**Cr3** suitable for X–ray diffraction analysis were not obtained, thus preventing their structural characterization. In addition, the paramagnetism of the complexes made uncertain any structural characterization via NMR. The difficulties encountered in obtaining single crystals for these divalent chromium complexes could be due to their unsaturated coordination and electronic structures. The solid state structure for **Cr1**–**Cr3** is more difficult to discern although on the basis of elemental analysis and by analogy with the synthetic procedure for **Cr4**, we speculate that **Cr1**–**Cr3** have a five-coordinate structure with a bidentate chelating ligand, one THF molecule and two chloride ions binding to the chromium atom. Nonetheless, the question regarding the chromium oxidation state remains open; it is well-established that Cr(II) complex may be reoxidized to Cr(III) by disproportionation.[29] This implies that the exact assignment of the chromium oxidation state is central, even more because the chromium complexes are intended as catalyst pre-cursors for conversion of ethylene and (di)olefins. Therefore, the assignment of the chromium oxidation state, also by virtue of the redox properties of iminopyridines, is highly desirable and useful. In an effort to access the ligand electronic structure and the associated chromium oxidation state, UV–vis–NIR absorption spectra were collected for **Cr1**–**Cr4** and **L1**–**L3** (Fig. 4a–4c).

The UV–vis–NIR spectra of all the chromium complexes are dominated by the π–π* transitions characteristic of the ligand above 24000–28000 cm^{-1}. In addition, very weak absorption bands (ε ~ $5{\cdot}10^2$ $M^{-1}cm^{-1}$) were observed at 22000 and 16500 cm^{-1} for **Cr4** (red in Figure 4a) and at about 15400 cm^{-1} for **Cr2** (red in Figure 4c). The position and the intensity of these bands are those expected for d–d transitions of highly coordinated Cr(III) and Cr(II) ions respectively,[30] consistent with the expected complex stoichiometry.

The ATR–IR spectra of **Cr4** and **Cr2** (red in Figure 4a' and 4c', respectively) closely resemble those of the corresponding ligands (**L1** and **L2**, respectively) except for the absorption bands

associated with the vibrations localized around the C=N iminic bond, which shift and/or split in multiple components due to the coordination of the chromium ion. For example, the ν(C=N) band observed at 1623 and 1632 cm^{-1} for pristine **L1** and **L2**, respectively, splits in two components at about 1655 and 1600 cm^{-1} in the spectrum of **Cr4**, and at about 1654 and 1620 cm^{-1} in the spectrum of **Cr2**. Moreover, in both cases, additional bands are observed around 1010 and 850 cm^{-1}, which are assigned to the asymmetric and symmetric ν(C–O–C) modes of coordinated THF, in agreement with the expected composition.

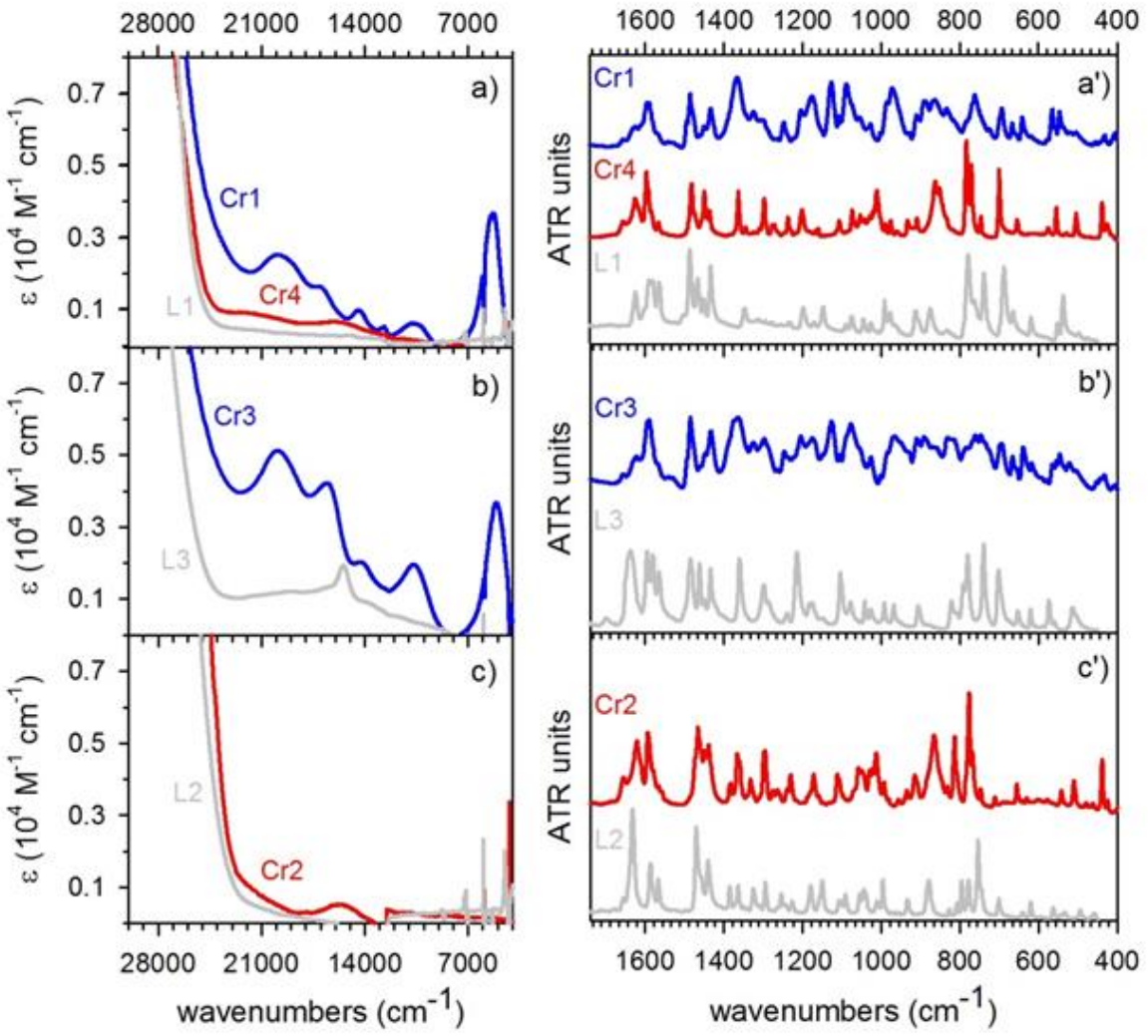

Figure 4 *UV-vis-NIR absorption spectra and ATR-IR spectra of* ***Cr1*** *and* ***Cr4*** *(blue and red in part a and a'),* ***Cr3*** *(blue in part b and b') and* ***Cr2*** *(red in part c and c'), compared to those of the corresponding ligands (dotted grey). All the UV-vis-NIR spectra have been measured in chloroform, and reported after subtraction of the spectrum of the solvent. The ATR-IR spectra have been collected on the samples in the powder form.*

In contrast, the UV–vis–NIR spectra of **Cr1** (blue in Fig. 4a) and **Cr3** (blue in Fig. 4b) are characterized by much more intense absorption bands in the 21000–4000 cm^{-1} region (maxima observed at about 20000, 16500, 14000, 10500 and 5050 cm^{-1}), which are too intense (ε ~ 10^3–10^4 $M^{-1}cm^{-1}$) to be classified as *d–d* transitions associated with the Cr(II) ions. The first four bands are

very similar to those observed in the spectra of π–radical monoanionic ligands of the type $(bpy^{\bullet})^{-}$ or $(tpy^{\bullet})^{-}$ (bpy = bipyridine, tpy = terpyridine).[31,32] For example, intense (~10^4 M^{-1} cm^{-1}) bands have been reported at 22220, 16130, 14200 and 10640 cm^{-1}, and assigned to intra–ligand π–π* transitions for $(tpy^{\bullet})^{-}$.[33] The presence of these bands in the spectra of **Cr1** and **Cr3** clearly indicates that **L1** and **L3** are redox non–innocent ligands,[34] and that **Cr1** and **Cr3** should be formulated as $[(L1^{\bullet})Cr^{III}Cl_2(THF)]^{-}$ and $[(L3^{\bullet})Cr^{III}Cl_2(THF)]^{-}$ species, rather than $(L1)Cr^{II}Cl_2(THF)$ and $(L3)Cr^{II}Cl_2(THF)$. In other words, **Cr1** and **Cr3** are only *formally* divalent chromium complexes, while the metal is described better as adopting the trivalent oxidation state (Fig. 5).

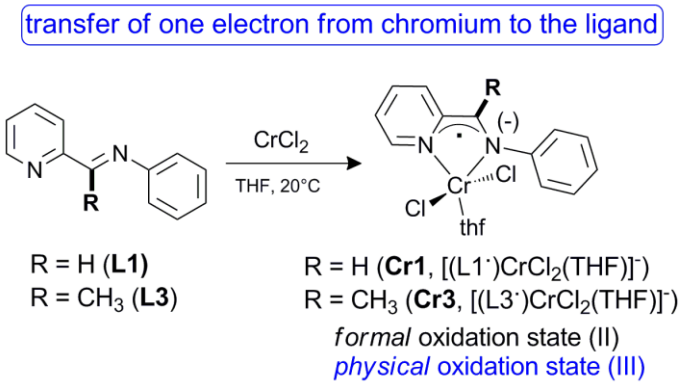

Figure 5 *Synthesis of **Cr1** and **Cr3** and formalism in the chromium oxidation state as determined by UV-vis-NIR spectroscopy.*

This is a quite common phenomenon for chromium complexes of N–, S– and O–donor ligands, due to the low covalence of their bonding and the high stability of the high–spin Cr(III) ion. Indeed, it has been reported that several formally low–spin Cr(II) complexes actually contain Cr(III) antiferromagnetic coupled to a π–radical anion, and that their redox chemistry is entirely ligand–centred.[31] This picture is confirmed by the ATR–IR spectra of **Cr1** and **Cr3** (blue in Fig. 4a' and 4b'), which are sensibly different from those of the corresponding **L1** and **L3** ligands, respectively. In particular, most of the absorption bands in the 1400–800 cm^{-1} region are enhanced in intensity and broadened, a fact that is well documented for radical anions of conjugated molecules.[35]

The origin of the intense band centered at 5050 cm^{-1} that can be observed both in the UV–vis–NIR spectra and in the ATR–IR spectra of **Cr1** and **Cr3** is less straightforward. An electronic absorption band in the near–infrared region has been often reported for ligand mixed–valent species, and assigned as a ligand–to–ligand intervalence charge transfer (LLIVCT) band, diagnostic of the co-presence of two equal ligands in a different redox state.[31,32] However, this assignment is not compatible with our situation, because it implies a Cr:L = 1:2 ratio, that does not match with the expected stoichiometry and the elemental analysis. On the other hand, a few examples can be found in the literature about bpy complexes of the type $[Mt^{n}(bpy)]^{0}$, where the transition of an electron from the metal to the ligand to give $[Mt^{n+1}(bpy^{\bullet})]^{-}$ originates a band in the

NIR region.[80] Hence, in our case, we can tentatively ascribe the band at 5050 cm^{-1} to the specular electronic transition from the $[(L1^{\bullet})Cr^{III}Cl_2(THF)]^-$ and $[(L3^{\bullet})Cr^{III}Cl_2(THF)]^-$ ground states to the respective $(L1)Cr^{II}Cl_2(THF)$ and $(L3)Cr^{II}Cl_2(THF)$ excited states.

Summarizing, the UV–vis–NIR and ATR–IR spectra shown in Figure 4 clearly reveal that **Cr1** and **Cr3** differ from **Cr4** and **Cr2**, in that the former have a marked tendency to undergo an electron transfer from the metal to the ligand (either **L1** or **L3**), while such electron transfer does not take place in **Cr4** either in **Cr2**. The reason for the inhibition of chromium–to–**L1** electron transfer in **Cr4** may be likely due to the fact that the oxidation of a Cr(III) ion to Cr(IV) is thermodynamically unfavorable, but also to a lower chance of a close approach between the metal and the ligand as a consequence of the metal ion size decrease in the case of a Cr(III)/Cr(IV) oxidation. Similarly, the reticence of **Cr2** to undergo chromium–to–**L2** electron transfer is proposed to be a consequence of the steric demand of the *ortho-iso*-propyl substituents, which weakens the chromium–ligand interaction, and prevents an efficient electronic delocalization. As a whole, **Cr4** and **Cr2** can be formulated as $[(L1)Cr^{III}Cl_3(THF)]^0$ and $[(L2)Cr^{II}Cl_2(THF)]^0$ species, respectively, with the ligand in the neutral state (Fig. 6).

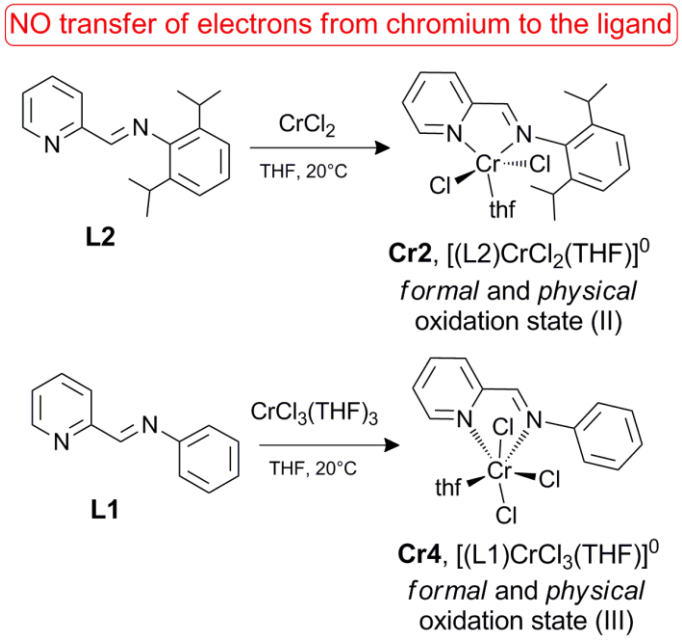

Figure 6 *Synthesis of **Cr2** and **Cr4** and formalism in the chromium oxidation state as determined by UV-vis-NIR spectroscopy.*

The interpretation emerged from the UV–vis–NIR absorption spectrum of **Cr4** is in good agreement with the X–ray diffraction (Fig. 3). In the ligand N–C–C–N backbone for **Cr4** the C–C, C–N_{imine} and C–$N_{pyridine}$ bond lengths are 1.42(3), 1.28(2) and 1.34(2) Å, respectively. These metric parameters are consistent with those expected for the ligand in the neutral state. The bond lengths fall in a close range of those formerly reported for related compounds coordinated by a neutral iminopyridine ligand.[36] With respect to the ligand electronic structures and oxidation state

formalism, both the UV–vis–NIR and X-ray diffraction study corroborate our hypothesis that **Cr4** should be formulated as $[(L1)Cr^{III}Cl_3(THF)]^0$ with trivalent chromium ligated by the iminopyridine ligand in the neutral state. As described below, all these electronic features have significant consequences on the course of the ethylene polymerization.

6.2.2 Catalytic behavior

The catalytic behavior and the consequences of the chromium–ligand synergy on the catalytic performances have been tested in the polymerization of ethylene, cyclic olefins and 1,3-butadiene, to prove the wide applicability of these systems. In polymerization tests, the complexes were activated using MAO, while during the spectroscopic investigations both MAO and triethylaluminium (TEA) were employed as activators; the use of TEA resembles the free trimethylaluminum alkyl in the commercial MAO solution.

Before discussing in detail the performance of the iminopyridine chromium complexes, it is worth mention that the catalytic behaviour of the precursors $CrCl_2$ and $CrCl_3(THF)_3$ was tested as well. Under the same polymerization conditions considered for the synthesized complexes **Cr1**–**Cr4**, at Al/Cr = 250 a small amount of PE was obtained only with $CrCl_3(THF)_3$/MAO (0.17 g, 0.51 × 10^5 g_{PE} mol_{Cr}^{-1} h^{-1}), while increasing the Al/Cr up to 1000, only traces of polymer were recovered. In comparison with these results, in the following paragraphs it will be discussed how the **L1** ligand strongly increases the overall PE productivity.

Polymerization of ethylene

Rationalizing the important parameters for Cr–iminopyridines to polymerize ethylene

Table 1 summarizes relevant data for the polymerization of ethylene using **Cr1**–**Cr4**.

Table 1 *Polymerization of ethylene catalyzed by* ***Cr1–Cr4****.*[a]

entry	Cr	Al/Cr	aging time [b] (min)	PE yield (g)	act [c] (×10^5)	M_w [d] (kg mol^{-1})	M_w/M_n [d]	T_m [e] (°C)
1	**Cr1**	250	–	1.86	5.58	131.6	35.6	103/113/127
2	**Cr2**	250	–	none				
3	**Cr3**	250	–	none				
4	**Cr4**	250	–	none				
5	**Cr1**	250	1	0.45	1.35	26.7	18.4	89/103/123
6	**Cr1**	250	3	0.40	1.21	18.6	11.3	105/124
7	**Cr4**	1000	–	0.10	0.30	68.4	3.8	130

[a] polymerization conditions: ethylene pressure, 1.01 bar; total volume, 20 mL (toluene); Cr, 10 μmol; MAO as cocatalyst; time, 20 min; temperature, 20°C; [b] pre-contact between **Cr1** and MAO (Al/Cr = 200); this treatment acts in two ways: it helps to solubilize the poorly soluble complex and, second, it preforms the active species; [c] activity in g_{PE} mol_{Cr}^{-1} h^{-1}; [d] determined by SEC; [e] by DSC (second heating).

Most active ethylene polymerization catalysts contain multidentate ligands,[37,38] while a large range of N,N bidentate ligands, in combination with various chromium sources, have been reported to be active for ethylene trimerization and tetramerization.[6] Compared to the well-known tridentate N^N^N ligands,[12] iminopyridines were expected to provide a less efficient shielding to stabilize the chromium active species and suppress chain transfer in the polymerization of olefins. Nonetheless, and quite surprisingly, **Cr1**, in combination with MAO (250 equiv. to Cr), afforded a highly active catalyst for the polymerization of ethylene under mild conditions. A solid PE, in the order of grams, was obtained (Table 1, entry 1, activity = 5.58×10^5 g_{PE} mol_{Cr}^{-1} h^{-1}). In contrast, **Cr2**–**Cr4** did not exhibit any polymerization activity under the same conditions, neither waxy products were recovered (Table 1, entries 2-4). The lack of polymerization activity by **Cr2**–**Cr4** coordinated by a neutral (L^0) ligand may be due to the quick ethylene displacement or to faster termination paths involving either β–H elimination or transfer to monomer and subsequent chain transfer than chain propagation. The latter reductive elimination paths are commonly observed for insertion ethylene (or growing chain) intermediates, their relative stability determining the selectivity toward oligomerization or polymerization products. It is worth noting that the formation of liquid oligomers is intentionally not factored in Table 1.

Given the structural similarity between **Cr1** and **Cr4**, which are both ligated by **L1**, the activity exhibited by **Cr1** is ascribed to the pristine radical anion $(L1^{\bullet})^-$ ligand state, while in the case of **Cr4** the same ligand is neutral and essentially unperturbed. The chromium ion in **Cr1**, less rich in electrons, has a pronounced preference to accept electron density by the ethylene monomer. Therefore, it can be inferred that the presence of an intermediate akin to $[(L^{\bullet})Cr^{III}]^-$ is the *necessary condition* for iminopyridine chromium complexes to exhibit ethylene polymerization activity.

As far as **Cr2** is concerned, besides the absence of the necessary $[(L^{\bullet})Cr^{III}]^-$ intermediate, we must also consider that the sterically demanding *iso*-propyl substituents at the *ortho* positions of the aniline, perpendicular to the coordination plane, might hinder olefin binding and insertion at the metal, accelerating chain transfer over the chain propagation.[38,40,41] Related arguments have been invoked by Sun *et al.* to rationalize the unique behavior of chromium complexes where sterically demanding alkyl substituents at the ligand weaken the interaction between the metal and the π–electrons of ethylene, increasing the nucleophilicity of the metal and simultaneously decreasing the rate of monomer insertion.[37]

However, the presence of an intermediate of the type $[(L^{\bullet})Cr^{III}]^-$ is *not sufficient*, as demonstrated by the lack of activity of **Cr3**, which is also of the type $[(L^{\bullet})Cr^{III}]^-$ as **Cr1** (Fig. 5). The different catalytic behavior exhibited by **Cr1** and **Cr3** indicates that the *physical* oxidation state of chromium and the redox state of the ligand in the precursor are not the *only* factors influencing their reactivity, which probably depends also on further transformations undergone in the presence of MAO, including further metal reduction or different deactivation paths. A possibility is

the rearrangement of ketimine **L3** ligand, where the lability of hydrogen atoms of methyl groups attached to the imine moiety is well established.[42]

To provide insight into the unusual features of **Cr1** and **Cr3**, UV–vis–NIR absorption spectra were acquired upon the addition of the Al–activator (Fig. 7a–7d). To keep the conditions as close as possible to those employed for the polymerization tests, both TEA, and MAO were evaluated. Due to the available experimental set-up, the first spectra have been collected after a few minutes since the addition of the activator and in the absence of the monomer; hence they are representative of the phenomena occurring during the aging of the chromium complexes in the presence of the activator rather than of the activation process itself. The spectra of the two complexes greatly change after the addition of TEA and MAO. In all the cases, the absorption bands characteristic of the initial complexes, diagnostic for the presence of π–radical monoanionic $(L^{\bullet})^{-}$ ligands, disappear. This evidence univocally indicates that, at the end of the aging process, **L1** and **L3** are no more π–radicals. Moreover, the following comments can be made:

(*i*) The transformation is very fast for **Cr3** (Figure 7c–7d), for which the first spectra collected after the pre-contact with TEA or MAO do not contain anymore the fingerprints of the π–radical $(L3^{\bullet})^{-}$. In contrast, the spectra evolution is much slower for **Cr1** (Figure 7a–7b), suggesting a slower rearrangement of this complex in the presence of both the Al–activators;

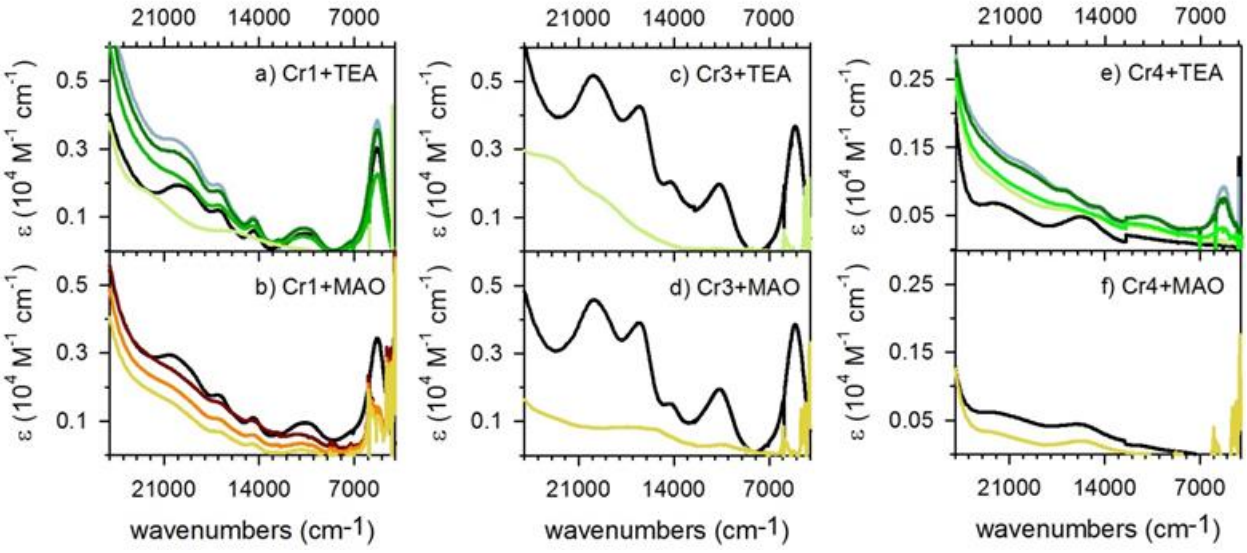

Figure 7 *Part a): UV-vis-NIR absorption spectra of* ***Cr1*** *in chloroform before (black)and after addition of TEA (from blue to green).Part b): UV-vis-NIR absorption spectra of the* ***Cr1*** *complex in chloroform before (black) and after addition of MAO (from orange to dark yellow). The spectrum of chloroform has been subtracted to all the spectra. Parts c) and d): the same for* ***Cr3****. Parts e) and f): the same for* ***Cr4****.*

(*ii*) The spectra collected at the end of the aging process are different for the four complex–activator combinations. This indicates that the final oxidation state/coordination geometry of the two chromium complexes is different. However, more detailed information would require to disentangle the effect of the symmetry from that of the oxidation state, which is far behind the scope of this work.

Once that **Cr1** in the presence of MAO is transformed into a *formal* and *physical* Cr(II) complex with neutral **L1**, the polymerization of ethylene is strongly inhibited. This is evident by looking at entries 5 and 6 in Table 1. In these two experiments, **Cr1** was previously dissolved and pre-activated with MAO at different time. We observed that the activities were more than four times lower with respect to the same run without the pre-contact between **Cr1** and MAO. Altogether, the spectroscopic data discussed in Figure 7a–d and the experimental studies indicate that the active species (or intermediates) involved in the polymerization of ethylene, of the type $[(L^{\bullet})Cr^{III}]^{-}$, are not very robust in the presence of MAO and even less robust in the absence of the monomer. These species are rapidly transformed into new species with neutral ligands, no more active in the ethylene conversion to high–molecular weight PEs. Whether the catalyst deactivation involves instability of the Cr–alkyl moiety or further chromium reduction with or without ligand involvement cannot be established at this moment.

Furthermore, it is interesting to note that traces of solid PE were recovered with **Cr4** by increasing the amount of MAO up to Al/Cr = 1000 (Table 1, entry 7). This intriguing behavior was investigated following the evolution of the UV–vis–NIR spectra of **Cr4** in the presence of TEA and MAO (Fig. 7e–7f). The addition of an excess of TEA (Fig. 7e) causes the appearance of the absorption bands characteristic of the $(L1^{\bullet})^{-}$ radical anion. This suggests that TEA has the capability to reduce **Cr4**, being the reduction ligand centered. However, the reduced complex has only a transient character, and the successive evolution of the spectra is the same as for **Cr1** (Fig. 7a–7b). The same phenomenon was not observed in the presence of MAO, likely due to the low Al/Cr ratio used for the spectroscopic experiments and to the fact that MAO is a mild reducing and alkylating agent compared to TEA. Nonetheless, the close similarity of the UV–vis–NIR spectra of pristine **Cr1** with that of **Cr4** upon the addition of the Al–activator substantiates our hypothesis that the polymerization of ethylene might be mediated by $[(L^{\bullet})Cr^{III}]^{-}$ species or, in any case, takes place through this intermediate.

On the whole, the tendency of chromium to undergo one electron transfer to the iminopyridine ligands is claimed to be fundamental in the catalytic transformation of ethylene to high–molecular weight PE (Fig. 8). Both **Cr1** and **Cr4** in the formal oxidation state (II) and (III), respectively, contain the ligand in the $(L^{\bullet})^{-}$ form as a result of a formal one electron oxidation of the chromium ion along with ligand reduction to the radical anionic state. However, for the *formal* and *physical* trivalent **Cr4** this transformation occurs only once the Al–activator is added. Given the inclination of trivalent chromium complexes toward reduction upon the addition of the Al–activator,[43] we hypothesize that the reduction initially takes place at the chromium, forming divalent chromium, followed by a further rapid transfer of one electron from the metal to the ligand, forming the ligand radical anion. For the *physical* trivalent **Cr1** and **Cr3**, which contain the ligand in the radical anion

state from the beginning, the important parameter that discriminates their catalytic behavior in the polymerization of ethylene is the stability of the complex in the presence of the Al–activator.

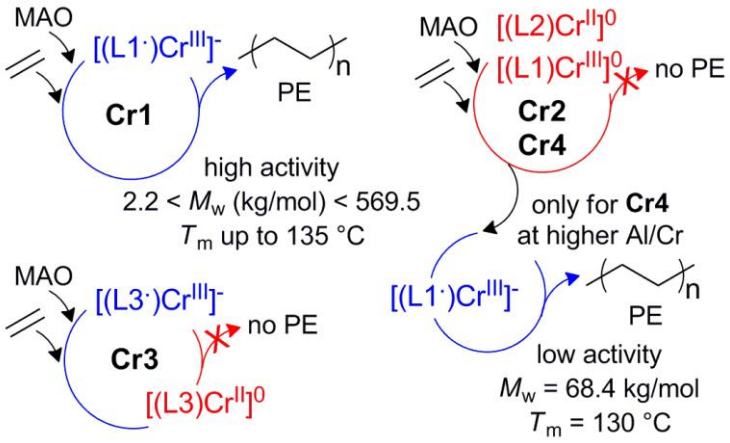

Figure 8 *Simplified scheme summarizing the results from the polymerization of ethylene catalyzed by* ***Cr1–Cr4****/MAO.*

The effects of polymerization conditions on the catalytic behavior of Cr1/MAO and PE's properties

The effects of some different polymerization conditions (*i.e.*, Al/Cr ratio, temperature and solvent) were explored in details for **Cr1**. The results are summarized in Table 2.

Table 2 *Polymerization of ethylene catalyzed by* ***Cr1****/MAO.*[a]

entry	T (°C)	Al/Cr	PE yield (g)	act[b] (×10^5)	M_w[c] (kg mol^{-1})	M_w/M_n[c]	$^{HF}M_p$[d] (kg mol^{-1})	$^{LF}M_p$[d] (kg mol^{-1})	T_m[e] (°C)
1[f]	20	250	1.86	5.58	131.6	35.6	broad tail	2.4	103/113/127
8	20	1000	1.41	4.23	2.2	1.5			93/103/119
9	20	50	1.20	3.60	569.5	18.7	648.1	44.7	134
10	0	250	0.39	1.16	275.3	20.7	57.8[g]	3.5	135
11	40	250	0.86	2.57	3.6	1.8			105/113/123
12[h]	20	1000	1.77	5.36	59.3	10.1	66.2	4.7	130

[a] polymerization conditions: ethylene pressure, 1.01 bar; total volume, 20 mL (toluene); Cr, 10 μmol; MAO as cocatalyst; time, 20 min; [b] activity in g_{PE} mol_{Cr}^{-1} h^{-1}; [c] determined by SEC; [d] $^{HF}M_p$ and $^{LF}M_p$, the peak molecular weight of the high–M_w and low–M_w fraction, respectively; [e] by DSC (second heating); [f] first reported in Table 1; [g] the $^{HF}M_p$ peak broadened to its high molecular weight side (see Figure 4b); [h] solvent: CH_2Cl_2.

Generally, all the PEs generated by **Cr1** are fully saturated semicrystalline polymers with a very low amount of branching

The formation of saturated PEs can be accounted by a termination path involving chain transfer to the aluminium. Their general properties resemble those of PEs by heterogeneous chromium catalysts,[4] and some pyridinebis(imino),[44] and (bis(pyridylmethyl)amine) chromium complexes.[37] **Cr1**/MAO produces PEs with molecular weight ranging from 569500 to 2000 g mol^{-1}, and broad multi-component molecular weight distributions in the range 1.5–35.6 with the shape depending

on the polymerization conditions. This clearly indicates the presence of several active species under certain polymerization conditions. Multicomponent molecular weight distributions cannot be meaningfully described by the average molecular weight value only; most of the SEC curves are dominated by two components, namely a low molecular weight fraction and a high molecular weight fraction. The peak molecular weight for each of these two fractions (*i.e.*, ${}^{LF}M_p$ and ${}^{HF}M_p$, respectively) is also reported in Table 2.

A series of polymerizations with **Cr1**/MAO were performed over the range of Al/Cr from 50 to 1000. A relatively low excess of MAO (Al/Cr = 50) was sufficient for exhibiting activity as high as 3.60×10^5 g_{PE} mol_{Cr}^{-1} h^{-1} (Table 2, entry 9), whereas the maximum value of 5.58×10^5 g_{PE} mol_{Cr}^{-1} h^{-1} was reached at Al/Cr = 250 (Table 2, entry 1). The Al/Cr ratio significantly affects both the polymers molecular weight and the molecular weight distribution. First, as the Al/Cr increases, the molecular weight of the resulting PEs drops from 569500 to 2200 g mol^{-1}, likely due to the chain transfer of the growing polymer chain to the free $AlMe_3$ present in MAO. Second, the relative amount of the low–molecular weight (${}^{LF}M_p$) and the high–molecular weight (${}^{HF}M_p$) fractions significantly changes. The SEC traces in Figure 9a clearly show a dramatic increase of the high–molecular weight PE fraction as the Al/Cr ratio decreases. This result is a reminiscence of the well-known behavior of Fe(II) based catalysts,[44,45] and Cr(II) and Cr(III) complexes bearing tridentate pyridine ligands.[44]

With the feed of 250 equivalents of MAO, a series of polymerizations were carried out at different temperature from 0 to 40 °C (Table 2, entries 1, 10 and 11). By increasing the polymerization temperature from 0 to 20 °C, the activity strongly increased from 1.16 to 5.58×10^5 g_{PE} mol_{Cr}^{-1} h^{-1} (Table 2, entries 10 and 1, respectively). A further increase to 40 °C leads to a decreased activity while maintaining a high level of productivity (Table 2, entry 11). This may be due to the increased instability of the Cr–alkyl bond and the lower solubility of ethylene in the reaction medium at higher temperatures. This strong reduction in activity upon increasing the temperature correlates with the dominant chain transfer.[37] The molecular weight of the resulting PEs decreases from 275300 to 3600 g mol^{-1} with increasing the polymerization temperature (Table 2, entries 10 and 11, respectively), an effect that is common to most metallocene and post–metallocene catalysts as well.[46] This effect may be likely due to the higher tendency to give β–H elimination at a last enchained ethylene unit followed by chain transfer, and it is explained by a lower activation energy of β–H elimination over chain propagation with increasing the reaction temperature. Moreover, the relative amount of the low–molecular weight and the high–molecular weight fraction significantly changes. The SEC traces in Figure 9b clearly show a dramatic increase of the high–molecular weight PE fraction as the polymerization temperature decreases.

We have also attempted to utilize dichloromethane as solvent, since toluene is known to occasionally have a poisoning effect (Table 2, entry 12).[29,47] The choice of medium solvent does not

dramatically impact on activity. Conversely, as shown in Table 2 and Figure 9c, using dichloromethane as solvent has a strong impact on the polymer molecular weight and molecular weight distribution. The SEC trace of the polymer generated in dichloromethane clearly shows a bimodal character, with the low–molecular weight and the high–molecular weight component centred at 4670 and 66210 g mol^{-1}, respectively. In contrast, for the polymer generated in toluene under the same conditions, a large fraction of the molecular weight distribution can be described by a single component with a low molecular weight (M_w = 2200 g mol^{-1}, M_p = 1700 g mol^{-1} and M_w/M_n = 1.5) with the peak only slightly broadened at its low molecular weight side (Figure 9c).

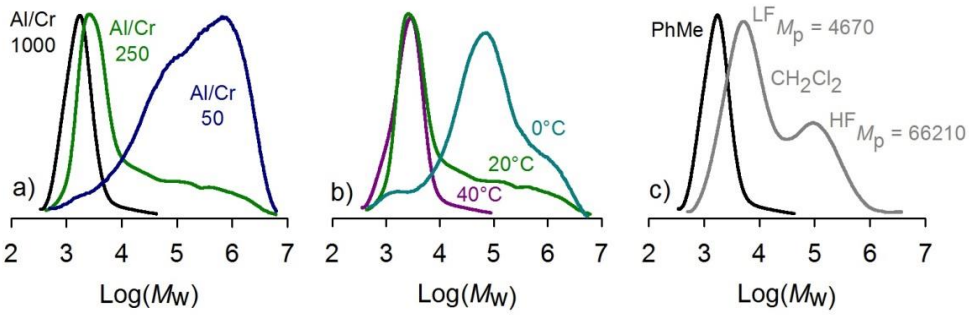

Figure 9 *SEC traces (refractive index plots) for the PEs obtained by* ***Cr1****/MAO at different Al/Cr ratio (a), polymerization temperature (b), and with different solvents (c).*

The heterogeneous composition of the obtained polymers is reflected in their thermal properties.

The DSC heating curves of the PE crystallized from the melt at 20 °C/min are reported in Figure 10. The PEs with higher molecular weight, regardless of their molecular weight distribution, show a single melting event with a maximum at about 135 °C (Table 2, entries 9 and 10). In contrast, the PEs with a low molecular weight, and even more those with a broad molecular weight distribution, exhibit multiple endotherms upon heating (Table 2, entries 1, 5, 6, 8 and 11). The enthalpy of fusion, which ranges from 210 to 230 J g^{-1}, means bulk crystallinity higher than 70%, in agreement with crystallinity determined by XRD.

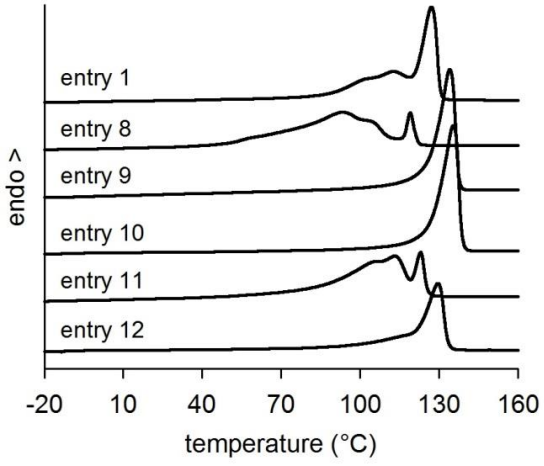

Figure 10 *DSC profile of poly(ethylene)s obtained with* ***Cr1****/MAO.*

FTIR and NMR spectroscopic characterization further confirms the results discussed above. FTIR spectra show three sets of peaks characteristic of PE: strong absorbances due to the C–H stretching (very strong peaks at 2919 and 2851 cm^{-1}), C–H bending (two strong peaks at 1472 and 1462 cm^{-1}) and C–H rocking (two medium-strong peaks at 730 and 720 cm^{-1}).[48] These two last bands are representative of the ethylene crystallinity and correspond to long ethylene sequences.[49] Nevertheless, in basically all the spectra recorded a weak signal at 1380 cm^{-1} can be detected; this peak is attributed to the C–H bending of a CH_3 group, revealing the presence of branches in the polymer. This is also confirmed by the ^{13}C NMR spectra, in which resonances attributed to the C1–C4 carbon atoms in a longer branches can be identified (12.02 ppm ($1B_n$), 20.70 ppm ($2B_n$), 27.30 ppm ($3B_n$), 29.95 ppm ($4B_n$)). However, the amount of branches in these samples is relatively low: calculations from the ^1H NMR spectrum revealed a number of CH_3 groups per 1000 carbon atoms which is around 10. As a consequence, the melting temperatures of these polyethylenes are above 130 °C, with the exception of the PEs obtained with the aged catalyst (Table 1, entries 5 and 6) that show a broader melting event and generally lower melting temperatures, significant of the formation of many catalytically active species during the "ageing" time.

Polymerization of cyclic olefins: norbornene and dicyclopentadiene

Secondly, it was investigated the ability of all the chromium–iminopyridine complexes to polymerize NB and dicyclopentadiene (DCPD) cyclic olefins (Fig. 11). Unlike ethylene, cyclic olefin insertion prevents β–H elimination for stereoelectronic reasons, avoiding the alignment in a *syn* coplanar arrangement of the metal–C_α and C_β–H bonds, according to Bredt's rule. The results are summarized in Table 3.

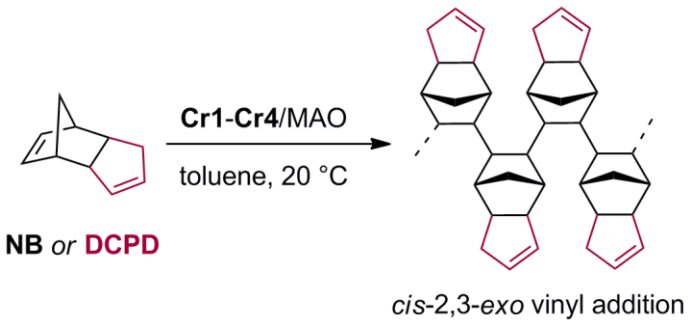

Figure 11 *Vinyl-type addition polymerization of norbornene and dicyclopentadiene.*

All the complexes when activated with MAO proved to be active in the polymerization of NB and DCPD, affording solid oligomers with molecular weight from 970 to 6590 g mol^{-1}. In particular, **Cr1** and **Cr4**, both ligated by the aldimine **L1** ligand, were highly and almost equally active. On the contrary, the ketimine **L3** ligand shuts down the activity of **Cr3**, particularly for DCPD. Likewise, a detrimental effect on the activity was observed for **Cr2** ligated by the aldimine **L2** ligand having

bulky substituents at the aniline. Steric effects play a fundamental role because of enhanced repulsion between the increased bulkiness of the *ortho* substituents and the monomer, particularly for bulkier DCPD, reducing the propagation rate.[41,44]

Table 3 *Polymerization of NB and DCPD catalyzed by* ***Cr1–Cr4****.*[a]

entry	Cr	monomer	yield		M_w [b]	M_w/M_n [b]
			(g)	(%)	(g mol^{-1})	
13	**Cr1**	NB	1.14	84	970	1.2
14		DCPD	1.10	46	1600	1.1
15	**Cr2**	NB	0.45	33	6590	3.9
16		DCPD	0.10	10		
17	**Cr3**	NB	0.58	42	1270	1.5
18		DCPD	*traces*			
19	**Cr4**	NB	1.10	81	1410	1.1
20		DCPD	0.99	43	1400	1.1

[a] polymerization conditions: NB, 1.35 g; DCPD, 2.36 g; total volume, 18 mL (toluene); Cr, 10 μmol; MAO as co-catalyst; Al/Cr =1000; time, 24 h; [b] determined by SEC.

Overall, regardless of the ligand electronic structure and the chromium oxidation state all the complexes are active for the polymerization of the investigated cyclic olefins, albeit to a different extent, while **Cr2–Cr4** were not in the polymerization of ethylene (Table 1). This nicely corroborates the hypothesis about the poor stability of the catalytic active intermediate on ethylene insertion for the latter compounds. As also illustrated in Figure 7c–d, in the case of **Cr3** this may be the consequence of the rapid transformation (or ligand rearrangement) of $[(L3^{\bullet})CrCl_2(THF)]^-$ species when the complex reacts with MAO, that seems to favor faster chain termination than chain propagation. Otherwise, in the case of **Cr2** and **Cr4** the "lack of communication" between the chromium and the ligand may disadvantage the polymer chain growth and facilitate ethylene displacement or faster termination paths involving β–H elimination, which is prohibited in the case of the polymerization of the cyclic olefins.

All the obtained products were characterized by FTIR spectroscopy: the spectra of the oligomers of both NB and DCPD show the characteristic absorption bands of a 2,3–vinyl type addition polymerization of monomers, involving only the bicycloheptene double bonds, rather than ROMP (Fig. 11).[50]

The obtained products were characterized by thermal analysis. DSC scans carried out from –40 to 200 °C did not show any thermal event. TGA performed under inert atmosphere evidenced that NB and DCPD oligomers are thermally stable up to about 220 °C, in analogy with the results found also in the case of $TiCl_4$–promoted polymerization of DCPD (Chapter 4 – Titanium).

Polymerization of 1,3-butadiene

Finally, the catalytic activity toward the polymerization of 1,3-butadiene was tested. The results are summarized in Table 4.

Table 4 *Polymerization of 1,3-butadiene catalyzed by* ***Cr1–Cr4****.*[a]

entry	Cr	yield		M_w[b]	M_w/M_n[b]	microstructure (%)[c]	T_g[d]
		(g)	(%)	(kg mol^{-1})		*cis*-1,4/*trans*-1,4/1,2	(°C)
22	**Cr1**	1.37	~100	428.9	2.0	52/12/36	–85
23	**Cr2**	1.40	~100	323.0	1.5	2/66/32	–64
24[e]	**Cr3**	0.13	10	248.7	2.0	16/17/67	–56
25[f]	**Cr4**	1.20	90	503.8	1.9	54/13/33	–85

[a] polymerization conditions: 1,3-butadiene, 1.4 g; total volume, 18 mL (toluene); Cr, 10 μmol; MAO as cocatalyst; Al/Cr =1000; time, 2 h; [b] by SEC; [c] by ^{13}C NMR and ATR–IR in the case of entry 24; [d] by DSC; [e] polymerization time, 4.5 h; [f] polymerization time, 1 h.

Despite the different ligand redox state and structure, **Cr1**, **Cr2** and **Cr4** with the aldimine counterparts, gave an almost quantitative conversion in less than 2 h, affording high molecular weight poly(1,3-butadiene)s with a mixed 1,4/1,2 structure. It can be inferred that such a different behavior between the polymerization of ethylene and 1,3-butadiene for **Cr1** (the only one active in the polymerization of ethylene), **Cr2** and **Cr4** is reasonably ascribed to the enhanced stability of chromium–monomer (or growing chain) interaction, which is of the allylic type in the case of the more electron rich 1,3-butadiene, while of the σ–type in the case of ethylene.

Cr1 and **Cr4**, bearing the same **L1** ligand, produced polymers with almost the same microstructure, the ratio of 1,4/1,2 being in the range from 64/36 to 67/33 (Table 4, entries 21 and 25, respectively). This suggests that the different ligand redox state found for these two complexes did not affect significantly the chemoselectivity, *i.e.*, the formation of 1,4 or 1,2 units. Interestingly, moving to the aniline–substituted **Cr2**, a strong inversion in *cis*-1,4/*trans*-1,4 selectivity was observed, the *trans*-1,4 content increasing with respect to the substituent–free **Cr1** and **Cr4**. This intriguing behavior could be attributed to a preferred *trans*-η^2 coordination of 1,3-butadiene in the presence of the bulky **L2**, with the consequent formation of a *syn* allylic unit, giving rise to a *trans*-1,4 or 1,2 unit, depending on the insertion of the monomer at C1 or C3 of the allylic unit, respectively (Fig. 12).[18] A faster *anti–syn* isomerization of the last polymerized unit, with respect to the insertion of the new incoming monomer on the allylic group, could be also responsible for the preferred formation of *trans*-1,4 units. Generally, the *anti–syn* isomerization occurs with a significant decrease of the polymerization rate, as reported, for instance, for the polymerization of isoprene by V(acac)$_3$/MAO.[51] In our case we did not observe such a reduction, and that is why we tend to favour the first hypothesis.

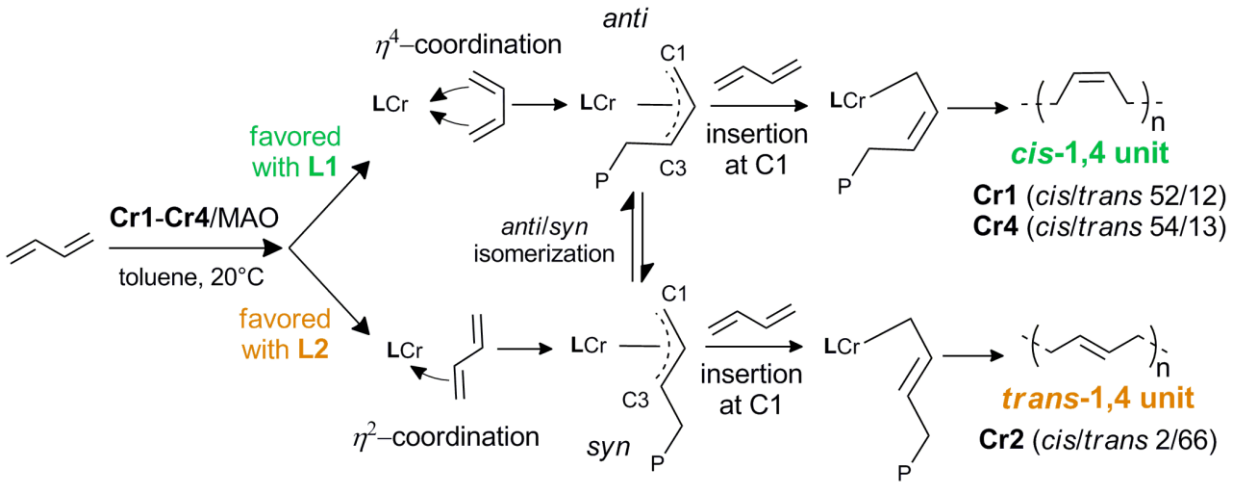

Figure 12 *Simplified scheme for the formation of a cis- or trans-1,4 monomeric units (P = polymer chain).*

Conversely, in the case of **Cr3**, ligated by the substituent–free methyl–ketimine **L3**, the reactivity strongly decreased with respect to the analogue aldimine compounds (Table 4, entries 24). The substitution of hydrogen by a methyl group at the imine moiety shuts down the activity. This different behavior exhibited by aldimine and ketimine compounds in the polymerization of 1,3-butadiene was not surprising; Bai and Hu have previously attributed this poisoning effect of ketimine ligands to a different ligand reorganization in the presence of the Al–activator.[52] Moreover, it is tempting to attribute this result to the evolution product of **Cr3** in the presence of MAO, as shown by UV–vis–NIR spectroscopy (Figure 6c–d).

Glass transition temperatures (T_gs) of the obtained polymers varied from –85 to –56 °C, depending on their microstructure. Sample 22 and 25 with the highest content of *cis*-1,4 units show the lowest T_g, while sample 24, the polymer richest in 1,2 units, the highest one.

6.3 Porphyrin chromium complexes

Recently the interest toward chromium complexes has been magnified for their potential application in the synthesis of aliphatic polyesters and polycarbonates.[53] These classes of polymers have received attention as appealing, potentially sustainable alternatives to petroleum-based polymers because of their numerous renewable sources, facile hydrolytic degradation to typically benign products, and high biocompatibility.[54] In this respect, the increasing environmental concern about the negative impact of non-degradable polyolefins is providing a potent stimulus to find bio-degradable polymers of comparable physical properties, boosting the research on these topics.

In this context, we were interested in the ring–opening alternating copolymerization (ROCOP) of epoxides and cyclic anhydrides to give the corresponding polyester. To these days, a diverse array of metal complexes has been used to catalyze this reaction (including Zn, Mg, Cr, Co, Mn, Fe, Al, Ni), and many of them showed high catalytic activity when applied in combination with a nucleophilic cocatalyst [including bis(triphenylphosphine)-iminium salts ([PPN]X, X = Cl^-, N_3^-), 4-

(*N*,N-dimethylamino)-pyridine (DMAP), phosphines, and ammonium salts]. Exhaustive and elegant reviews have been recently published on this topic.[55,56]

Metalloporphyrins

Among all the possible organometallic complexes available, we focused our attention on chromium porphyrin complexes, because we were interested in expanding the applicable class of N–ligands useful with chromium. The choice of porphyrin allows the substituents to influence electronic factors without having any significant steric influence at the metal center. In contrast to Schiff bases, to which iminopyridines belong, the porphyrin restricts the other ligands to the *trans* geometry, the metal can move in and out of the plane of the porphyrin, and the dissociation of the ligand is unfeasible.

6.3.1 Synthesis of porphyrin chromium complexes

Our research on this topic started from the synthesis of two chromium complexes ligated by tetraphenylporphyrin (TPP) and tetrakis(*p*-chlorophenyl)porphyrin (TCP) (Fig. 13). The complexes were synthesized following the procedures reported in the literature.[57]

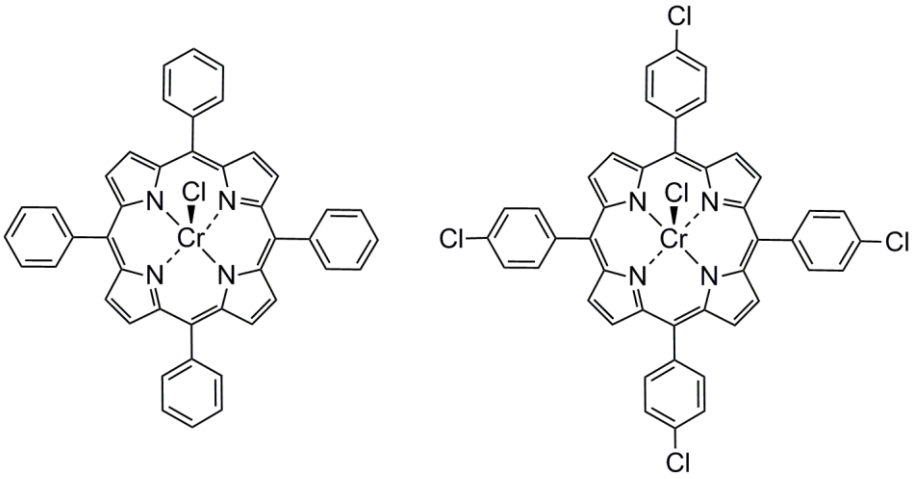

Figure 13 *Cr-porphyrin complexes investigated in this thesis.*

The synthetic procedure consists simply of allowing the porphyrin and the divalent metal salt to react in refluxing dimethylformamide; the crude products were later purified by column chromatography to give the final products in good yields (65% and 50% respectively).

6.3.2 Copolymerization of cyclohexene oxide and succinic anhydride

To test the catalytic activities of complexes **Cr(TPP)Cl** and **Cr(TCP)Cl**, and to study the influence of the *para*-Cl substituents, the copolymerization of cyclohexene oxide (CHO) with succinic anhydride (SA) to give the corresponding polyester was selected as model reaction (Fig.

14). These two chromium complexes are known to catalyze the copolymerization of CO_2 with oxiranes or oxetanes.[58]

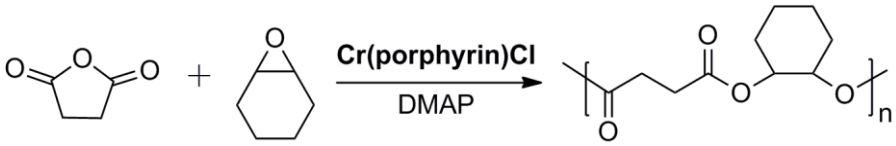

Figure 14 *Copolymerization of CHO and SA to give the corresponding polyester.*

It has been reported that most porphyrinato complexes used for this kind of copolymerization gave far higher activities and better selectivity in the presence of the nucleophilic cocatalyst. We therefore explored the use of one of the most common cocatalyst, DMAP.[59] The copolymerizations were performed at 100 °C in bulk (*viz*. without the use of solvents) with an oxirane : anhydride : catalyst : cocatalyst ratio of 250 : 250 : 1 : 1.

A problem connected with these polymerization experiments was the recovery of the final product, due to the great viscosity of the reaction mixture: indeed, the precipitation of the polyesters in acidic methanol or pentane resulted in the formation of pitchy products that made the recovery of the polymer difficult. Generally, in the present literature, this problem is overcome by analysing the crude samples.

In combination with DMAP, the chromium complexes synthesized proved to be effective catalysts for the CHO–SA copolymerization (Table 5), affording either polyesters or poly(ester-*co*-ethers). Indeed, in all the cases presented here, the formation of a variable despite low percentage of polyether was detected. This known undesired side product is formed during the reaction when the insertion of two successive oxirane units takes place. Generally, this can be attributed to a higher reactivity of the oxirane in comparison with that of anhydrides, as a consequence of the higher ring strain.

Table 5 *Polymerization of 1,3-butadiene catalyzed by* ***Cr(TPP)Cl*** *and* ***Cr(TCP)Cl****.*[a]

entry	cat	precontact (h)	time (h)	conv. (%)	PEt[b] (mol %)	E[b] (mol %)	A[b] (mol %)	M_n[c] (g mol^{-1})	M_w[c] (g mol^{-1})	M_w/M_n[c]	X_n[d]
1	**TPP**	–	5	89	10	–	1	*n.a.*	*n.a.*	*n.a.*	–
2	**TPP**	–	2	69	6	–	11	*n.a.*	*n.a.*	*n.a.*	–
3	**TPP**	2	3	98	8	–	2	990	1622	1.6	10
4	**TCP**	2	3	87	8	–	–	1124	1660	1.6	11

[a] polymerization conditions: [SA]:[CHO]:[cat]:[DMAP] = 250:250:1:1, T = 100 °C; [b] PEt = polyether, E = unreacted epoxide, A = unreacted anhydride, determined by ^{1}H NMR; [c] determined by SEC; [d] the number-average degree of polymerization is based on the average weight of both comonomers.

The reaction promoted by **Cr(TPP)Cl** was initially run for 5 h (entry 1), but a great amount of polyether (10%) was detected. Hence, a shorter reaction time of 2 h was selected (entry 2); despite

an increased amount of residual SA (from 1.1 to 11%), the polyether formed is diminished from 10 to 6% of the overall product formed. An intermediate reaction time of 3 h was chosen.

Aiming at improving the catalytic performances, a pre-contact between the catalyst and the cocatalyst was applied, by dissolving the two components in dry dichloromethane and allowing them stirring for 2 h. After the removal of the solvent in vacuum, the two comonomers were added, and the reaction proceeded as usual. This preliminary reaction between **Cr(TPP)Cl** and DMAP allows the pre-formation of the active site, and enhances the nucleophilic character of the metal. This has a beneficial effect on the copolymerization (entry 3): compared to a slight increase in the amount of polyester formed, we obtain a quantitative conversion of the monomers, as shown also by the small amount of residual anhydride.

With these optimized polymerization conditions, the chlorinated analogue **Cr(TCP)Cl** was surveyed (entry 4). The presence of the *para*-Cl atoms on the porphyrin has a beneficial effect, decreasing the polyether formation, while maintaining a complete comonomers conversion.

The observed molecular weights are not very high (990–1100 g mol^{-1}), but comparable to analogous catalytic systems.[59] This is most probably caused by intramolecular transesterification leading to the formation of cyclics or by chain-transfer reactions.

The polyesters were characterized by FTIR and ^{1}H NMR spectroscopy, and the signals were assigned according to the literature.[60,61] By way of example, Figure 15 reports the FTIR and ^{1}H NMR spectra of entry 3.

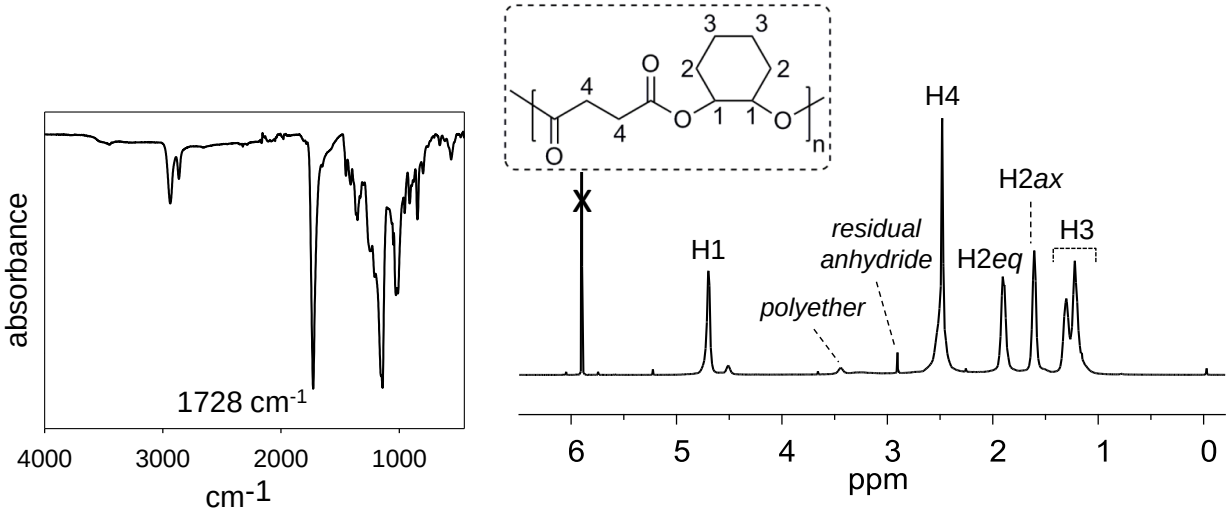

Figure 15 *FTIR (left) and ^{1}H NMR (right) spectra of poly(CHO-co-SA) (entry 3).*

The FTIR spectrum shows the appearance of the band at 1728 cm^{-1} attributable to the carbonyl bond in the polyester and disappearance of the epoxide band (802 cm^{-1}), and no traces of the residual comonomers were detected (C=O of succinic anhydride can be found at 1786 cm^{-1}). The ^{1}H NMR spectrum instead is more instructive: the signals of the hydrogen atoms of the poly(CHO-*co*-SA) can be clearly identified at 4.7 ppm (H1, 2*H*), 2.48 ppm (H4, 4*H*), 1.91 ppm (H2*eq*, 2*H*), 1.61

ppm (H2*ax*, 2*H*), 1.30-1.22 ppm (H3, 4*H*). The spectrum shows only a small amount of consecutive epoxide sequences (3.4 ppm), and an even smaller amount of residual anhydride (2.9 ppm).

These preliminary results served as initial investigation on the copolymerization of epoxides and anhydride. Although further research in this area is necessary, the know-how acquired on polyester synthesis can possibly be transferred to the copolymerization of CO_2 and epoxides to give polycarbonates.

6.4 Experimental section

6.4.1 Synthesis of chromium iminopyridine complexes

All the chromium complexes were synthesized following the method reported in the literature for analogous compounds.[62] The general procedure is reported for **Cr1**.

Dichloro N-(pyridin-2-ylmethylene)aniline chromium·THF (Cr1)

To a stirred suspension of $CrCl_2$ (0.24 g, 2.0 mmol) in 25 mL of THF at room temperature **L1** ligand (0.44 g, 2.4 mmol) was added. The suspension was kept under stirring for 24 h and then filtered. The residue on the filter was thoroughly washed with pentane (3×25 mL), dried under vacuum, and stored under nitrogen in a Schlenk tube. The dark brown solid **Cr1** was dried overnight *in vacuo*. Yield (based on $CrCl_2$): 92%. FTIR ν (cm^{-1}) 1592 (w), 1485 (m), 1433 (w), 1366 (s), 1246 (w), 1174 (m), 1126 (s), 1087 (s), 971 (s), 887 (s), 864 (s), 761 (s), 692 (m), 666 (m), 640 (m), 564 (s), 545 (s). Anal. Calcd. for $C_{16}H_{18}Cl_2CrN_2O$: C, 50.94; H, 4.81; N, 7.43. Found: C, 49.68; H, 4.17; N, 7.25. The difference between C, H found and C, H calculated values are likely due to the volatile THF and the incomplete combustion that can cause inaccurate results. Such deviation from the calculated values has been reported for many other chromium complexes.[44,62]

Dichloro 2,6-diisopropyl-N-(pyridin-2ylmethylene)aniline chromium·THF (Cr2)

Dark green solid, yield 70%. FTIR ν (cm^{-1}) 1592 (m), 1465 (m), 1365 (m), 1294 (m), 1230 (w), 1171 (w), 1110 (w), 1057 (m), 1012 (m), 913 (m), 865 (s), 813 (s), 777 (vs), 767 (m), 654 (w), 541 (w), 509 (m). Anal. Calcd. for $C_{22}H_{30}Cl_2CrN_2O$: C, 57.27; H, 6.55; N, 6.07. Found: C, 57.0; H, 6.20; N, 6.35.

Dichloro N-(1-(pyridin-2ylethylidene)aniline chromium·THF (Cr3)

Dark grey solid, yield 94%. FTIR ν (cm^{-1}) 1592 (m), 1486 (m), 1437 (m), 1387 (m), 1377 (m), 1351 (w), 1290 (m), 1213 (s), 1140 (s), 1075 (s), 932 (s), 909 (vs), 814 (vs), 789 (s), 732 (s), 700 (s), 666 (m), 636 (s), 616 (m), 551 (m), 522 (m). Anal. Calcd. for $C_{17}H_{20}Cl_2CrN_2O$: C, 52.19; H, 5.15; N, 7.16. Found: C, 52.26; H, 5.15; N, 7.15.

Trichloro N-(pyridin-2-ylmethylene)aniline chromium·THF (Cr4)

The same complexation procedure as for Cr1 was employed for Cr4 but using $CrCl_3(THF)_3$ source. After drying, a light green solid was isolated. Yield (based on $CrCl_3(THF)_3$): 77%. FTIR ν (cm^{-1}) 1595 (m), 1481 (m), 1448 (m9; 1361 (m), 1296 (w), 1272 (w), 1235 (w), 1200 (m), 1105

(w), 1072 (w), 1010 (m), 931 (w), 908 (w), 861 (s), 782 (vs), 770 (s), 745 (w), 699 (s), 653 (w), 574 (w), 554 (m), 503 (m). Anal. Calcd. for $C_{16}H_{18}Cl_3CrN_2O$: C, 46.57; H, 4.40; N, 6.79. Found: C, 46.25; H, 4.35; N, 6.90. ^{1}H NMR ($C_2D_2Cl_4$) broad peaks δ (ppm) 5.211 (1H), 3.142 (2H), 1.299 (2H).

6.4.2 Synthesis of chromium porphyrin complexes

The synthesis were performed according to the literature.[57]

Synthesis of tetraphenylporphyrin-chromium chloride [Cr(TPP)Cl]

(TPP)H_2 (130 mg, 0.211 mmol) was added to 15 mL of dry dimethylformamide (DMF). The mixture was stirred at 150 °C, until complete dissolution of the compound. After cooling to room temperature, $CrCl_2$ (38 mg, 0.317 mmol) was dissolved in 5 mL DMF and added to the reaction mixture. The reaction was left stirring at 150 °C. After 4 h, an aliquot was taken from the mixture for UV–vis. The TLC of the sample (stationary phase: alumina; mobile phase: $CHCl_3$) showed free (TPP)H_2 still remained in solution. A further addition of $CrCl_2$ (14 mg, 2 mL DMF solution) was added to the solution, refluxing for another 5 h. No free (TPP)H_2 was found. The reaction mixture was allowed to cool to room temperature and poured into 30 mL of ice-cold 0,1%*w* HCl aqueous solution, and a green precipitate is formed. After the solid was filtered out and washed three times with acid water, it was dried under vacuum at room temperature. The crude product was purified by column chromatography over alumina column with $CHCl_3$ as the eluent, and increasing the polarity of the eluent with methanol to recover the purified product, that was later dried over vacuum. UV–vis spectroscopy was used to confirm the formation of Cr(TPP)Cl. Yield: 96 mg, 65% conversion.

Synthesis of tetrakis(*p*-chlorophenyl)porphyrin chromium chloride [Cr(TCP)Cl]

The procedure for the synthesis of **Cr(TCP)Cl** is analogous to the one reported above for **Cr(TPP)Cl**. Yield: 56 mg, 50% conversion.

6.4.3 General epoxide – anhydride copolymerization procedure

Polymerizations were carried out in a 5 mL Schlenk tube equipped with a stirring bar. Prior to starting polymerization, the reactor was heated to 110°C under vacuum for 1 h and backfilled with nitrogen. Chromium complex, DMAP, SA and CHO were added in the order, and the vial was posed in a pre-heated oil bath at 100 °C. After the allotted reaction time, the vial was removed from the oil bath, cooled to room temperature and the viscous reaction mixture was dissolved in a minimum amount of dichloromethane and transferred into a vial. The polymer was collected and dried over vacuum at 60 °C to constant weight. When a precontact time was required, the addition order changed slightly. Chromium complex and DMAP were dissolved in 2 mL of dry dichloromethane in

the vial, and stirred for 2 h. Then the solvent was removed in vacuum, and the comonomers were added.

References

[1] E.W. Fawcett, R.O. Gibson, M.W. Perrin, J.G. Patton, E.G. Williams, British Patent **1937**, 472,590, to Imperial Chemical Industries.

[2] E. Groppo, G.A. Martino, A. Piovano, C. Barzan *ACS Catal*. **2018**, DOI: 10.1021/acscatal.8b02521.

[3] M.P. McDaniel *Adv. Catal*. **2010**, *53*, 123-606.

[4] E. Groppo, C. Lamberti, S. Bordiga, G. Spoto, A. Zecchina *Chem. Rev*. **2005**, *105*, 115-183.

[5] V.C. Gibson, S.K. Spitzmesser *Chem. Rev*. **2003**, *103*, 283-315.

[6] D.S. McGuinness *Chem. Rev*. **2011**, *111*, 2321-2341.

[7] T. Agapie, J.A. Labinger, J. Bercaw *J. Am. Chem. Soc*. **2007**, *129*, 14281-14295.

[8] S.S. Rozenel, W.A. Chomitz, J. Arnold *Organometallics* **2009**, *28*, 6243-6253.

[9] (a) D.S. McGuinness, P. Wasserscheid, W. Keim, D. Morgan, J.T. Dixon, A. Bollmann, H. Maumela, F. Hess, U. Englert *J. Am. Chem. Soc*. **2003**, *125*, 5272-5273; (b) T. Agapie, S.J. Schofer, J.A. Labinger, J.E. Bercaw *J. Am. Chem. Soc.* **2004**, *126*, 1304-1305.

[10] D.S. McGuinness, P. Wasserscheid, D.H. Morgan, J.T. Dixon *Organometallics* **2005**, *24*, 552-556.

[11] D.J. Jones, V.C. Gibson, S.M. Green, P.J. Maddox *Chem. Commun*. **2002**, 1038-1039.

[12] (a) Z. Hao, B. Xu, W. Gao, Y. Han, G. Zeng, J. Zhang, G. Liand, Y. Mu *Organometallics* **2015**, *34*, 2783-2790; (b) R.D. Köhn, M. Haufe, G. Kociok-Köhn, S. Grimm, P. Wasserscheid, W. Keim *Angew. Chem. Int. Ed.* **2000**, *39*, 4337-4339; (c) T. Rüther, K.J. Cavell, N.C. Braussaud, B.W. Skelton, A.H. White *Dalton Trans*. **2002**, 4684-4693; (d) P. Wasserscheid, S. Grimm, R.D. Köhn, M. Haufe *Adv. Synth. Catal*. **2001**, *343*, 814-818; (e) D.J. Jones, V.C. Gibson, S.M. Green, P.J. Maddox *Chem. Commun*. **2002**, 1038-1039.

[13] (a) L.J. Ackerman, X. Bei, T.R. Boussie, G.M. Diamond, K.A. Hall, A.M. Lapointe, J.M. Longmire, V.J. Murphy, P. Sun, D. Verdugo, S. Schofer, E. Dias, D.H. McConville, R.T. Li, J. Walzer, F. Rix, M. Kuchta, M. WO 2006/096881 (Exxon-Mobil), **2006**; (b) L.A. MacAdams, G.P. Buffone, C.D. Incarvito, A.L. Rheingold, K.H. Theopold *J. Am. Chem. Soc.* **2005**, *127*, 1082-1083; (c) V.C. Gibson, C. Newton, C. Redshaw, G.A. Solan, A.J.P. White, D.J. Williams, P.J. Maddox *Chem. Commun*. **1998**, 1651-1652; (d) K. Albahily, D. Al-Baldawi, S. Gambarotta, R. Duchateau, E. Koç, T.J. Burchell *Organometallics* **2008**, *27*, 5708-5711.

[14] B.L. Small *Acc. Chem. Res*. **2015**, *48*, 2599-2611.

[15] (a) T. Takahashi, F.Y. Tsai, Y. Li, H. Wang, Y. Kondo, M. Yamanaka, K. Nakajima, M. Kotora *J. Am. Chem. Soc.* **2002**, *124*, 5059-5067; (b) A. Köppl, H.G. Alt *J. Mol. Catal. A: Chem.* **2000**, *154*, 45-53.

[16] W. Kaim *Inorg. Chem*. **2011**, *50*, 9752-9765.

[17] (a) C.K. Jørgensen Coord. *Chem. Rev*. **1966**, *1*, 164-178; (b) P.J. Chirik *Inorg. Chem*. **2011**, *50*, 9737-9740.

[18] G. Ricci, A. Sommazzi, F. Masi, M. Ricci, A. Boglia, G. Leone *Coord. Chem. Rev*. **2010**, *254*, 661-676.

[19] G. Natta, L. Porri, P. Corradini, D. Morero *Chim. Ind. (Milan)* **1959**, *41*, 1163-1167.

[20] (a) G. Ricci, M. Battistella, L. Porri *Macromolecules* **2001**, *34*, 5766-5769; (b) G. Ricci, A. Forni, A. Boglia, M. Sonzogni *Organometallics* **2004**, *23*, 3727-3732; (c) G. Ricci, A. Boglia, T. Motta *J. Mol. Catal. A: Chem*. **2007**, *267*, 102-107.

[21] Y. Nakayama, K. Sogo, Z. Cai, H. Yasuda, T. Shiono *Polym. Int*. **2011**, *60*, 692-697.

[22] R. Cariou, J. Chirinos, V.C. Gibson, G. Jacobsen, A.K. Tomov, M.R.J. Elsegood *Macromolecules* **2009**, *42*, 1443-144.

[23] F. Blank, C. Janiak *Coord. Chem. Rev*. **2009**, *253*, 827-861.

[24] A.S. Abu-Surrah, K. Lappalainen, M. Kettunen, T. Repo, M. Leskelä, H.A. Hodali, B. Rieger *Macromol. Chem. Phys*. **2001**, *202*, 599-603.

[25] T.J. Woodman, Y. Sarazin, S. Garrat, G. Fink, M. Bochmann *J. Mol. Cat A: Chemical* **2005**, *235*, 88-97.

[26] G. Ricci, A. Boglia, A.C. Boccia, L. Zetta, A. Famulari, S.V. Meille *Macromolecules* **2008**, *41*, 3109-3113.

[27] (a) M.D. Ward, J.A. McCleverty *Dalton Trans*. **2002**, *3*, 275-288; (b) K. Ray, T. Petrenko, K. Wieghardt, F. Neese *Dalton Trans*. **2007**, *16*, 1552–1566.

[28] T. Takahashi, F.Y. Tsai, Y. Li, H. Wang, Y. Kondo, M. Yamanaka, K. Nakajima, M. Kotora *J. Am. Chem. Soc*. **2002**, *124*, 5059-5067.

[29] A. Jabri, C.B. Mson, Y. Sim, S. Gambarotta, T.J. Burchell, R. Duchateau *Angew. Chem. Int. Ed.* **2008**, *47*, 9717-9721.

[30] (a) J. Fackler, D. Holah Inorg. Chem. **1965**, 4, 954-958; (b) B.N. Figgis "*Introduction to ligand fields*" **1966** John Wiley & Sons, New York, USA.

[31] C.C. Scarborough, K.M. Lancaster, S. DeBeer, T. Weyhermüller, S. Sproules, K. Wieghardt *Inorg. Chem.* **2012**, *51*, 3718-3732.

[32] (a) M. Wang, J. England, T. Weyhermüller, S.L. Kokatam, C.J. Pollock, S. DeBeer, J. Shen, G.P.G. Yap, K.H. Theopold, K. Wieghardt *Inorg. Chem*. **2013**, *52*, 4472–4487; (b) C.C. Scarborough, S. Sproules, C.J. Doonan, K.S. Hagen, T. Weyhermüller, K. Wieghardt *Inorg. Chem*. **2012**, *51*, 6969-6982.

[33] P.S. Braterman, J.L. Song, R.D. Peacock *Inorg. Chem*. **1992**, *31*, 555-559.

[34] (a) W. Kaim *Inorg. Chem*. **2011**, *50*, 9752-9765; (b) W. Kaim *Coord. Chem. Rev*. **2011**, *55*, 2503-2513.

[35] (a) S.H.R. Brienne, P.D.W. Boyd, P. Schwerdtfeger, G.A. Bowmaker, R.P. Cooney *J. Chem. Soc. Faraday Trans.* **1993**, *89*, 3015-3020; (b) M. Zamadar, S. Asaoka, D.C. Grills, J.R. Miller *Nature Commun.* **2013**, *4*, 2818.

[36] C.C. Lu, E. Bill, T. Weyhermüller, E. Bothe, K. Wieghardt *J. Am. Chem. Soc*. **2008**, *130*, 3181-3197.

[37] W. Zhang, W.H. Sun, S. Zhang, J. Hou, K. Wedeking, S. Schultz, R. Fröhlich, H. Song *Organometallics* **2006**, *25*, 1961-1969.

[38] M.A. Esteruelas, A.M. López, L. Méndez, M. Oliván, E. Oñate *Organometallics* **2003**, *22*, 395-406.

[39] M.J. Carney, N.J. Robertson, J.A. Halfen, L.N. Zakharov, A.L. Rheongold *Organometallics* **2004**, *23*, 6184-6190.

[40] C. Bianchini, G. Giambastiani, G. Mantovani, A. Meli, D. Mimeau *J. Organomet. Chem.* **2004**, *689*, 1356-1361.

[41] D. Wang, S. Liu, Y. Zeng, W.S. Sun, C. Redshaw *Organometallics* **2011**, *30*, 3001-3009.

[42] H. Sugiyama, G. Aharonian, S. Gambarotta, G.P.A. Yap, P.H.M. Budzelaar *J. Am. Chem. Soc.* **2002**, *124*, 12268-12274.

[43] T. Gunasekara, J. Kim, A. Preston, D.K. Steelman, G.A. Medvedev, W.N. Delgass, O.L. Sydora, J.M. Caruthers, M.M. Abu-Omar *ACS Catal*. **2018**, *8*, 6810-6819.

[44] B.L. Small, M.J. Carney, D.M. Holman, C.E. O'Rourke, J.A. Halfen *Macromolecules* **2004**, *37*, 4375-4386.

[45] Y. Zhang, H. Suo, F. Huang, T. Liang, X. Hu, W.H. Sun *J. Polym. Sci., Part A: Polym. Chem*. **2017**, *55*, 830-842.

[46] (a) E.P. Talsi, D.E. Babushkin, N.V. Semikolenova, V.N. Zudin, V.N. Panchenko, V.A. Zakharov *Macromol. Chem. Phys*. **2001**, *202*, 2046-2051; (b) G. Leone, I. Pierro, G. Zanchin, A. Forni, F. Bertini, A. Rapallo, G. Ricci *J. Mol. Catal. A: Chem*. **2016**, *424*, 220-231.

[47] W.H. Sun, X. Tang, T. Gao, B. Wu, W. Zhang, H. Ma *Organometallics* **2004**, *23*, 5037-5047.

[48] S. Jie, R. Pattacini, G. Rogez, C. Loose, J. Kortus, P. Braunstein *Dalton Trans*. **2009**, 97-105.

[49] D. Daoust, S. Bebelman, N. Chaupart, R. Legras, J. Deveaux, J. Costa *J. Appl. Pol. Sci*., **2000**, *75*, 96-106.

[50] (a) G. Ricci, G. Leone, A. Rapallo, P. Biagini, G. Guglielmetti, L. Porri *Polymer* **2011**, *52*, 5708-5715; (b) A. Rapallo, G. Ricci, W. Porzio, G. Arrighetti, G. Leone *Cryst. Growth. Des*. **2014**, *14*, 5767-5772; (c) G. Zanchin, G. Leone, I. Pierro, A. Rapallo, W. Porzio, F. Bertini, G. Ricci *Macromol. Chem. Phys*. **2017**, *218*, 1600602.

[51] G. Ricci, S. Italia, L. Porri *Macromol. Chem. Phys.* **1994**, *195*, 1389-1397.

[52] Q. Dai, X. Jia, F. Yang, C. Bai, Y. Hu, X. Zhang *Polymers* **2016**, *8*, 12-27.

[53] (a) X. Zhang, M. Fevre, G.O. Jones, R.M. Waymouth *Chem. Rev*. **2018**, *118*, 839-885; (b) Y.W. Wang, D.J. Darensbourg *Coord. Chem. Rev*. **2018**, *372*, 85-100.

[54] Y. Zhu, C. Romain, C.K. Williams *Nature* **2016**, *540*, 354-362.

[55] S. Paul, Y. Zhu, C. Romain, R. Brooks, P.K. Saini, C.K. Williams *Chem. Commun*. **2015**, *51*, 6459-6479.

[56] J.M. Longo, M.J. Sanford, G.W. Coates *Chem. Rev*. **2016**, *116*, 15167-15197.

[57] (a) A.D. Adler, F.R. Longo, F. Kampas, J. Kim *J. Inorg. Nucl. Chem*. **1970**, *32*, 2443-2445; (b) D.J. Liston, B.O. West *Inorg. Chem*. **1985**, *24*, 1568-1576.

[58] (a) W.J. Kruper, D.V. Dellar *J. Org. Chem.* **1995**, *60*, 725-727; (b) S. Mang, A.I. Cooper, M.E. Colclough, N. Chauhan, A.B. Holmes *Macromolecules* **2000**, *33*, 303-308.

[59] S. Huijser, E. Hosseini-Nejad, R. Sablong, C. de Jong, C.E. Koning, R. Duchateau *Macromolecules* **2011**, *44*, 1132-1139.

[60] R.C. Jeske, A.M. Di Ciccio, G.W. Coates *J. Am. Chem. Soc.* **2007**, *129*, 11330-11331.

[61] C. Chatterjee, M.H. Chisholm *Inorg. Chem*. **2012**, *51*, 12041-12052.

[62] K.A. Kreisel, G.P.A. Yap, K.H. Theopold *Inorg. Chem*. **2008**, *47*, 5293-5303.xR.F.J. Fischer *Polym. Sci*. **1960**, *44*, 155-172.

Chapter 7
Conclusions

During this three-year PhD research activity, the synthesis of a series of first row transition metal (*i.e.*, Ti, V, Cr) complexes and their use as catalyst precursors in the (co)polymerization of olefins were explored. The main results achieved can be summarized as follows:

- Light has been shed on some aspects concerning the $TiCl_4$–promoted polymerization of DCPD. The results prove that the presence of the double bond in the cyclopentene ring, the peculiar spatial disposition of the cyclopentene in the *endo*-DCPD and the polymerization conditions play a key role in the formation of a unique crystalline polymer.
- A library of V(III) and V(IV) complexes was synthesized, allowing the comprehension of the influence of the steric and electronic properties of the employed ligand on the catalytic behavior and polymerization mechanism. The copolymerization of ethylene with various cyclic olefins brought to mainly alternating copolymers. In addition, the study on vanadium complexes allowed us to get more insight into some drawbacks correlated with vanadium catalysis, such as the facile reduction to V(II), and the compositional drift that takes place during the copolymerization experiments.
- A study on Cr–iminopyridine complexes (including their synthesis and characterization through UV–Vis–NIR spectroscopy), focusing in particular on the metal–ligand synergy, has been accomplished. This investigation demonstrated that in some cases an electron transfer from Cr to the ligand is possible, thus making fundamental the exact determination of the "true" Cr oxidation state. This Cr–to–ligand synergy has repercussions on the complexes reactivity, particularly for the polymerization of ethylene. In contrast, the formalism in the metal oxidation state does not affect the reactivity toward the cyclic olefins and 1,3-butadiene, while ligand steric effects emerge clearly.
- The post–polymerization modification of DCPD and ENB homo- and copolymers through epoxidation and hydrogenation has been developed, bringing to functionalized polymers with improved properties such as solubility and thermal stability, and useful reactive functionalities.

In addition to the scientific results, this PhD course has also led to other "soft" results that, even though they cannot be published in scientific journals, are equally important. Among them I would like to cite the awareness of the importance of reproducibility of the data and the improved communication skills. I learned how to critically deal with problems and solutions, and that rejections can become opportunities. Finally, I have experienced how much research is a matter of team working and of creation of connections between research groups.

Chapter 8
Other projects

In parallel to the PhD project on Ti, V, and Cr based catalysts, I was also involved in the other research projects that involve the laboratory of ISMAC with which I collaborated, namely:

- **Ni(II)–catalyzed polymerization of α–olefins**

Late–transition metal catalysts have shown great potential in their ability to afford branched polyolefins. A milestone in this field was the discovery of α–diimine Ni(II) and Pd(II) complexes by Brookhart in the 1990s. The peculiarity of these complexes is the ability of the active site to "walk" on the growing polymer chain during the propagation step (chain-walking) so that the new incoming olefin monomer is assembled onto the polymer backbone rather than at the end, thus giving branched PE–like materials. In this context, we studied the polymerization of α–olefins, focusing on C_8–C_{18} monomers, catalyzed by differently substituted α–diimine Ni(II) complexes. These systems prove great prospect thanks to the low cost and accessibility of starting reagents and monomer feedstocks, the high turnovers/h together with the reusability of the resulting polymers that retain excellent mechanical properties even after being melted and reprocessed several times.

My contribution was mainly focused on the synthesis of the α–diimine ligands and the Ni(II) complexes. The results have been published on *Macromolecules* **2018**, *51*, 801, and *European Polymer Journal* **2017**, *93*, 200.

- **Hydrogenation of stereoregular poly(1,3)dienes**

Transition metal and lanthanide based catalysts are able to promote the polymerization of 1,3-dienes to highly stereoregular polymers. Beyond the synthesis, we were interested in the hydrogenation of these poly(1,3-diene)s, performed via a non-catalytic route with the aid of *p*-toluenesulfonyl hydrazide. Indeed, this procedure allows to obtain a whole series of olefin homo- and perfectly alternating copolymers with novel molecular architectures which, in some cases, were not obtainable through stereospecific polymerization of the corresponding monomers. These highly stereoregular polymers proved to be polymeric models extremely useful for the structural, morphological and mechanical characterization of homo- and olefin copolymers obtained through various polymerization routes.

My contribution was mainly focused on the polymerization of 1,3-dienes and the subsequent hydrogenation. The results have been published on *Macromolecules* **2018,** *51*, 488, *Macromolecules* **2017**, *50*, 541, *Macromolecules* **2017**, *50*, 754, and *Molecules* **2017**, *22*, 755.

Chapter 9
What's next?

«*Oh great, you almost got your PhD degree! And now…* ***what's next?***»

While I'm writing this PhD thesis, the times I've been asked this question are almost countless; and I'm not complaining, it is completely reasonable. Hence, to find a good answer, I asked this question to research and world's trends, and to myself.

What's next for research? And for the world trends?

No reaction of the same academic and technological magnitude as Ziegler–Natta catalysis has withstood the passage of time so well: despite more than 60 years have passed since the pioneer works, and despite all the multitudinous number of discoveries made, «*polymer science is only beginning to understand polymers*».[1]

In the first two chapters of this thesis I have already pointed out the relevance of polyolefins in research and industry; I do not think it is necessary to explain how the polyolefins are now an indissoluble part of everyday life (this same thesis dissertation could not exist without "plastic").

Despite this, and perhaps due in large part to its success, until just a few years ago there had been a growing sentiment that polyolefin research was a "mature" field, and that any further innovation would be only incremental as the result of additional small refinements being made, rather than radical in nature as the result of an infusion of a new fundamental paradigms. This feeling caused a decreasing interest also from governmental institutions and national or trans-national science foundations, that do not list olefin polymerization in their strategic objectives anymore.[2]

However, this opinion can be considered somewhat unfounded, since many researchers involved in the field have opposite point of views.[2-5] Indeed, «*innovations in the field of polyolefins are not only possible, but rather desirable, and are driven by improvements in the catalyst process as well as in the polyolefins applications*».[3]

Hence, there's still room for research on this topic. But, in which direction? Where is this domain evolving?

Concerning homogeneous catalysis, and the topic more related to this thesis, some hints can be found in the recent literature to answer the question:

- "old" (co)monomers and (co)polymers for new applications, through the synthesis and organization of new, detailed, tailored polymer molecules, enabling the creation of materials with exciting properties, starting from the well-known (and economically sustainable) common synthetic monomers;[1]

- a deep understanding of structure–property relationships could allow to assure the successful and competitive development of polymeric materials;[4]
- the design of strategies for the polymerization of precision and functional olefins, considering also all those aspects concerning the translation of the high-level academic knowledge into cost-effective, scalable and processable polymer products, and reducing the complexity for the development of market-ready products;[4]
- bridging the gap between the realm of coordination polymerization and the realm of free-radical polymerizations;[6]
- the development of environmentally-benign and sustainable methods for polymer synthesis.[7]

It is worth spending a few more words on this last target. Since, by far, the largest volume of chemicals produced are polymers, it is essential to develop new catalysts and processes considering also the reduction of the energy and chemicals needed to produce a given amount of polymer. This attitude can be applied rendering sustainability (in terms of reduced energy-, environmental-, and health-related impact) a key-parameter attractive not only for funding agencies, but a major task of academic and industrial research. This coincides with an ever-increasing need for new classes of sustainable polymers, either as biodegradable polymers, or made up of monomers from renewable sources or bioderived feedstocks in a cost-effective way (*e.g.* the use of CO_2 for polycarbonate synthesis)[8] to meet the dwindling of petroleum reserves.

Another interesting aspect of sustainability is the possibility of recycling polymeric materials, especially those from single-use disposables that used once, last forever. The vast majority of polyolefins are fabricated for performance, not for durability and recyclability; this has resulted in the tremendous growth of polymer wastes over the past few decades. However, current paradigms for the generation and disposal of plastic are unsustainable. Therefore, creating an effective after-use plastics economy is fundamental. For example, applying circular economy principles to global plastic packaging flows is at the cornerstone of the "New Plastic Economy" and it could transform the plastics economy and drastically reduce negative externalities such as leakage into oceans.[9]

Many private and public funding agencies, the governments and also the European Commission itself with the Horizon2020 program aim to promote this second polymer revolution, both from an academic and an industrial point of view, with a particular emphasis on aspects concerning the environmental sustainability. So we can happily hope that there's room but also fundings for research on this topic, and for developing these new themes.

What's next for me?

While I was still a freshman at the beginning of my academic career in Chemistry, the PhD degree seemed to me the end of a long academic journey. As years went on, I graduated, and later I got enrolled in this doctoral course. Now that I'm very close to the end, I realize that getting the

PhD degree is not an end-point, but rather a stake from which to go on this journey into the world of research. Then, like all journeys that deserve the name, now is the time for a next step… but where? In which direction?

Looking back to this three-year journey, I can realize how the PhD allowed me to go deeper into the fascinating world of research, a nice blend of concreteness and planning held together by creativity and enthusiasm, with all the correlated ups and downs.

In addition, working in research permits to observe and tackle questions and problems from a different point of view. As an example, I would mention the environmental question that is pretty close to my heart (and awakens those lessons I received during the Bachelor degree in Environmental Chemistry). I reported in the previous paragraph some possible solutions to face the problem of plastic pollution. However, this cannot be considered as the sole solution, since the mere replacement of the polymers currently in use with others biodegradable or from renewable sources would only be a shift the problem. At these days, there is also the necessity to develop greater awareness on environmental issues. In this sense, being a researcher in the field of polymers allows to have the appropriate tools, and a favorable point of view and of expression to pursue the objectives, through both basic research and also dissemination activities.

It is in this direction that I hope my future as chemist will go, continuing this journey from this privileged point of view, always widening my horizons, working in a stimulating environment like the one in which I had the good fortune to conduct this doctorate, making the talents profit, remaining faithful to the nobility in conquering and handling matter invoked by Primo Levi, and keeping wearing a lab coat as long as possible.

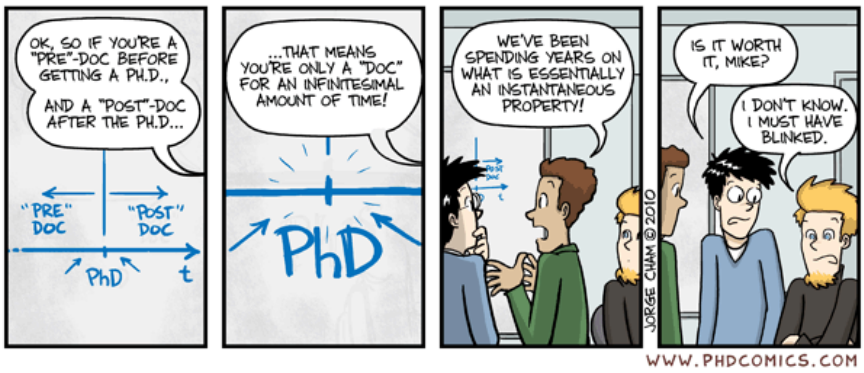

References

[1] W. Kaminsky *Macromol. Chem. Phys.* **2008**, *209*, 459-466.

[2] V. Busico *Dalton Trans.* **2009**, 8794-8802.

[3] E. Groppo, G.A. Martino, A. Piovano, C. Barzan *ACS Catalysis* **2018**, *8*, 10846-10863.

[4] B. Voit *Angew. Chem. Int. Ed.* **2017**, *56*, 2810-2812.

[5] K. Matyjaszewski *Chemistry International*, **2017**, *39*, 7-11.

[6] J.P. Claverie, F. Schaper *MRS Bulletin*, **2013**, *38*, 213-218.

[7] G.W. Coates *Dalton Trans*. **2002**, 467-475.

[8] X. Zhang, M. Fevre, G.O. Jones, R.M. Waymouth, *Chem. Rev*. **2018**, *118*, 839-885.

[9] *The new plastic economy: Rethinking the future of plastics*, Ellen MacArthur Foundation, **2016** (https://www.ellenmacarthurfoundation.org/publications/the-new-plastics-economy-rethinking-thefuture-of-plastics).

Appendix

In the following, the topographic steric maps of imido ligands in **3a–3c'** for a qualitative analysis, generated using the open-source SambVca 2 Web (see ref. 66 chapter 5 – Vanadium), are reported.

Complex [V(=N-2,6-Cl_2-C_6H_3)Cl_2(PMe_2Ph)$_2$] (3a)

SambVca–Result

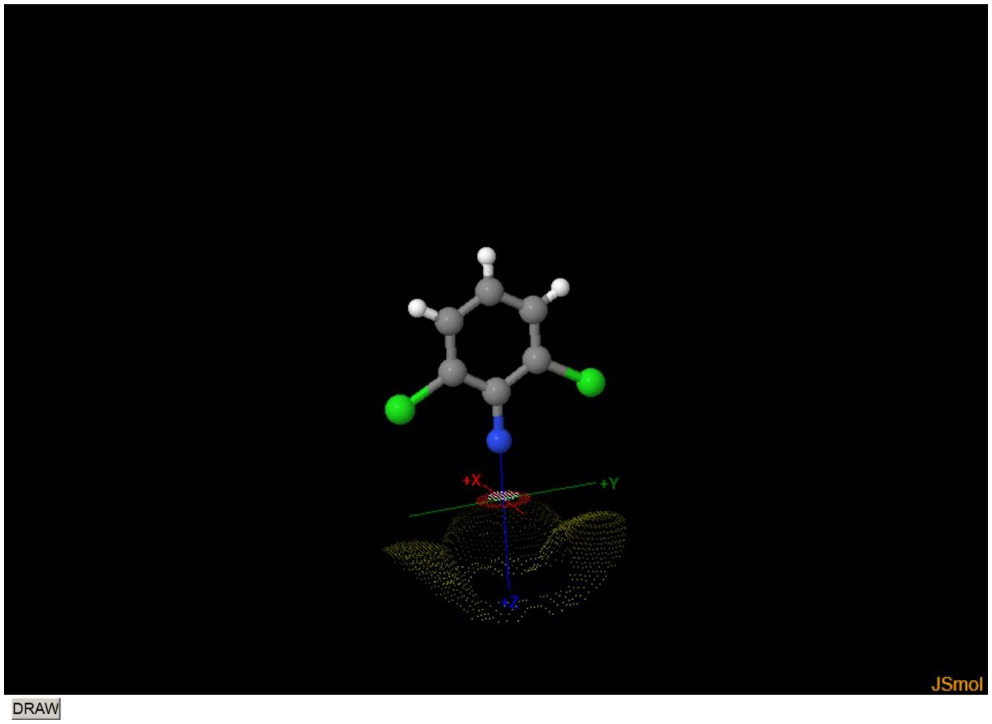

DRAW

V Free	V Buried	V Total	V Exact
138.8	40.7	179.5	179.6

%V_Free	**%V_Bur**	% Tot/Ex
77.3	**22.7**	100.0

Quadrant	V_f	V_b	V_t	%V_f	**%V_b**
SW	35.1	9.8	44.9	78.2	**21.8**
NW	34.3	10.6	44.9	76.5	**23.5**
NE	35.1	9.8	44.8	78.2	**21.8**
SE	34.3	10.6	44.9	76.5	**23.5**

Steric Map

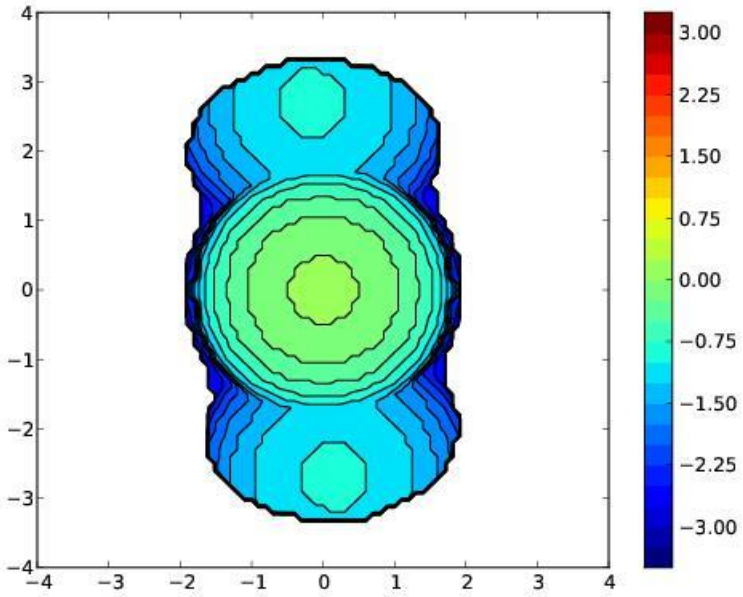

Complex [V(=N-2,6-*i*Pr$_2$-C$_6$H$_3$)Cl$_2$(PMe$_2$Ph)$_2$] (3b)

SambVca–Result

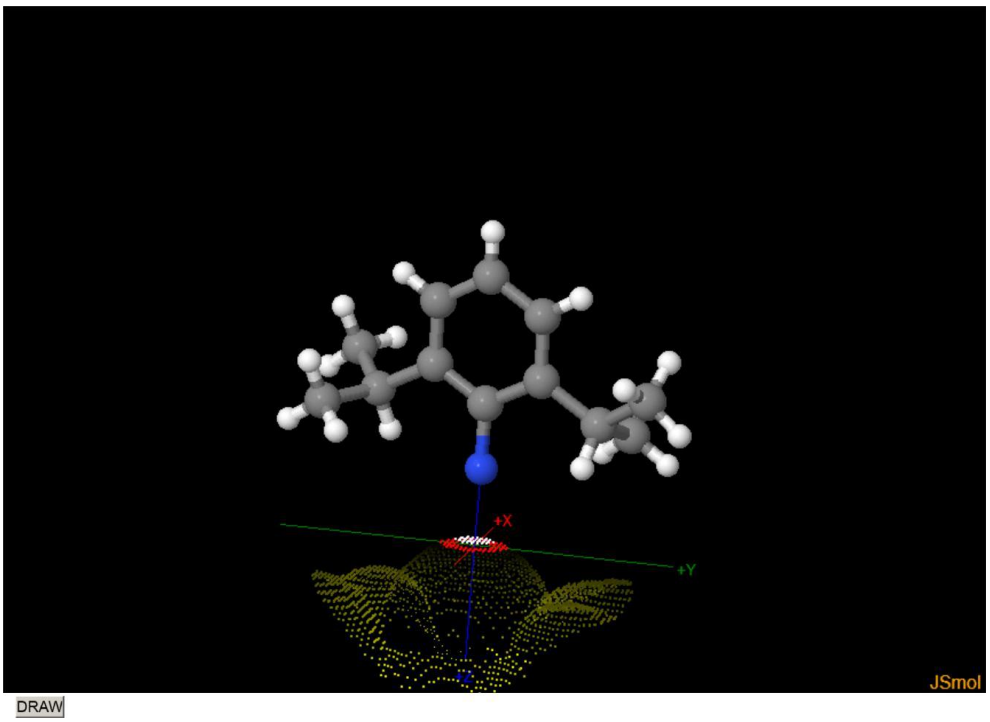

DRAW

V Free	V Buried		V Total		V Exact
134.5	45.1		179.5		179.6
%V_Free		**%V_Bur**		% Tot/Ex	
74.9		**25.1**		100.0	

Quadrant	V_f	V_b	V_t	%V_f	**%V_b**
SW	34.7	10.1	44.9	77.4	**22.6**
NW	33.0	11.9	44.9	73.6	**26.4**
NE	33.0	11.8	44.8	73.6	**26.4**
SE	33.7	11.2	44.9	75.1	**24.9**

Steric Map

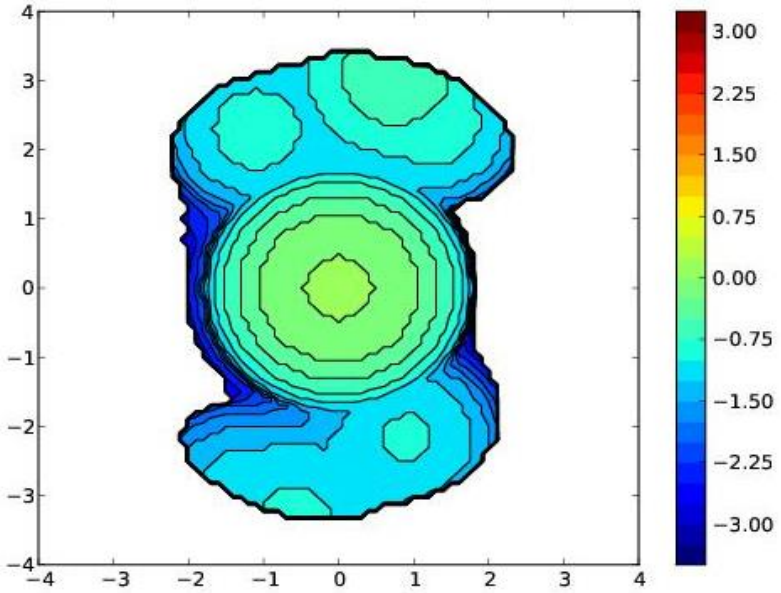

Complex $[V(=N\text{-}^{t}Bu)Cl_2(PMe_3)_2]$ (3c′)

SambVca–Result

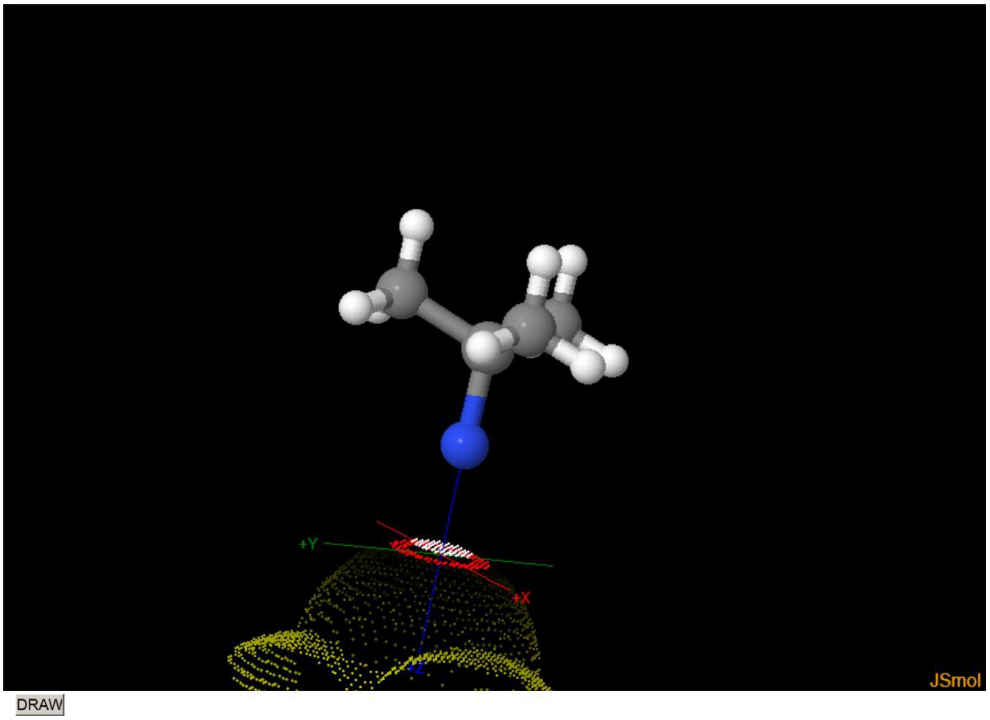

DRAW

V Free	V Buried		V Total		V Exact
143.7	35.8		179.5		179.6
%V_Free		**%V_Bur**		% Tot/Ex	
80.1		**20.0**		100.0	

Quadrant	V_f	V_b	V_t	%V_f	**%V_b**
SW	35.6	9.2	44.9	79.4	**20.6**
NW	35.6	9.2	44.9	79.4	**20.6**
NE	36.3	8.6	44.8	80.9	**19.1**
SE	36.2	8.7	44.9	80.6	**19.4**

Steric Map

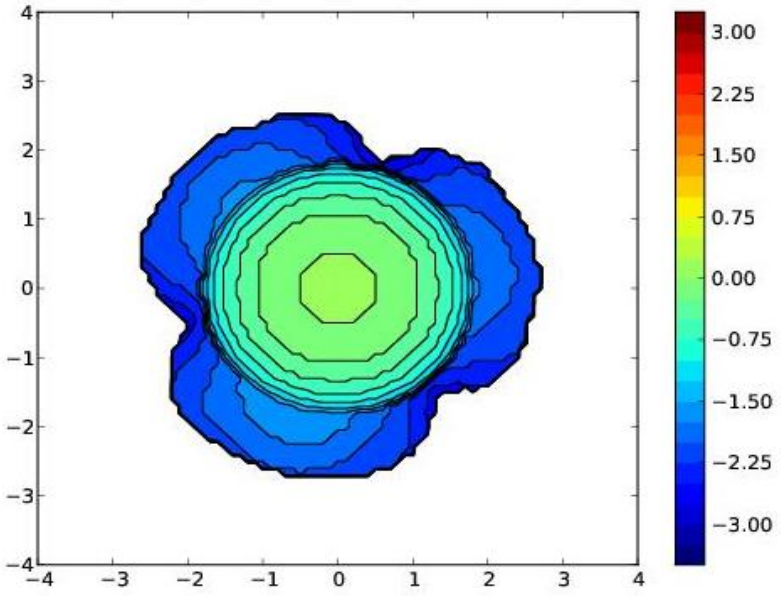

Acknowledgments

(*ovvero, se bastasse un semplice grazie*)*

19/12/2018

Milano, Lab CHI3

Caro Giulio,

manca oramai soltanto un mese alla discussione di dottorato, e la tesi è qua vicino a me pronta… chi l'avrebbe mai detto che sarebbe arrivato questo momento. Io da sola, contando solo sulle mie forze, di certo no; probabilmente sarei ancora lì seduta su una panchina come in quei primi giorni del giugno 2015 a pensare se iniziare quest'avventura o meno. Ma per fortuna nella ricerca, così come nella vita, è il noi che vince e che salva, e quindi eccomi qua alla fine di questi tre anni.

Ti confesso che mi piacerebbe poter conferire un dottorato *honoris causa* in Chimica a tutte quelle persone che mi hanno aiutato e supportato in questi anni, e permesso di essere qua ora, per poter condividere con loro questo titolo che non è soltanto mio. Mi piacerebbe presentarteli perché questa tesi è anche merito loro, e, nel farlo, vorrei che a loro arrivasse il mio semplice ma sincero grazie.

Sai, sono tante queste persone, ma ci terrei a fartele conoscere tutte, iniziando da quelle che ci hanno fatto incontrare, quando a malapena sapevo che cosa fosse un polimero. Il primo di loro è Giuseppe, non soltanto capo e (co)tutor di questo dottorato, ma una persona sempre presente, soprattutto in lab, su cui sapevo poter contare per un consiglio o supporto, e che in questi anni col suo esempio e la passione per la ricerca mi ha insegnato molto, davvero tanto; tra tutti gli insegnamenti, uno che vorrei sempre portare con me è la capacità di saper guardare avanti e oltre. E poi c'è Giovanni, il grande capo, una persona davvero di cuore, con grandi passioni per la ricerca, la montagna e il buon cibo, non lo si può negare; il suo arrivo al mattino viene sempre anticipato da una canzone fischiettata che ti mette di buon umore, e non c'è genere musicale che non sia nelle sue corde, dall'ultima novità passata in radio alla musica classica. Giuseppe e Giovanni sono stati i primi a credere in questo dottorato, e lo hanno reso possibile giorno dopo giorno, dall'inizio alla fine, con la passione e dedizione verso questo meraviglioso lavoro; gliene sarò sempre grata, perché devo molto a loro.

Un altro tassello fondamentale di questi anni è stata Ivana: compagna di avventure e sventure tra l'ufficio e il lab, nei congressi in giro per l'Italia, passando per le macchinette del caffè. Insieme abbiamo costruito un gruppo di auto-mutuo aiuto, un vero, prezioso e fondamentale supporto in tutto; in questi anni abbiamo imparato a conoscerci, ci siamo confrontate, e insieme cresciute

molto. La ringrazio perché mi ha sempre saputo accogliere negli sfoghi, nelle lacrime, e nelle grasse risate. Credo che sarebbe stato tutto meno divertente e più difficile senza di lei!

Con Giuseppe e Ivana in laboratorio (e nelle immancabili merende), tra una distillazione del norbornene e una pulizia della vetreria incrostata di polimeri, oltre a tanti esperimenti abbiamo fatto anche grandi e belle chiacchierate, arricchenti, che mi hanno permesso di conoscerli e così coltivare e far crescere la relazione con loro, che spero possa continuare a crescere da qui in poi. Se guardo indietro a questi quasi quattro anni insieme, mi rendo conto di quante cose siano accadute, e quanto ognuna di essa sia stata un tassello importante e necessario.

Ti dicevo prima che in questi anni ho capito come il lavoro di squadra sia fondamentale; e qua all'ISMAC siamo una squadra davvero grande! Ognuno ha avuto il suo ruolo anche nel mio dottorato, piccolo o grande che sia stato non è importante, perché importante è stata la presenza. Servirebbe un'altra tesi per presentarteli nel dettaglio uno ad uno, però mi piacerebbe citare almeno alcuni nomi: Alessia, la tesista più tosta che abbia mai conosciuto, con cui ho imparato a conoscere il vanadio e le schiscette "sane" (per non dire misere); Sara, che col suo tempo donato al nostro laboratorio è stata un aiuto prezioso in un tempo di iperattività; Arnaldo, con i suoi appunti e i conti sul diclopentadiene, e l'eterno tunnel del norbornadiene; tutti i ricercatori e tecnologi che hanno contribuito a portare avanti e a termine i nostri lavori (e tra loro vorrei ricordare Fabio, William, Fulvia, Daniele, Alberto); Pilade, Elena, Francesco, l'amministrazione più divertente del mondo; tutti i ragazzi con cui ho condiviso la pausa pranzo, una breve parentesi leggera anche nelle giornate più impegnative; e anche tutte le persone di questo istituto che lo rendono una grande famiglia.

Ci sono anche altre persone, alcune a pochi passi da questi laboratori, altre qualche km più in là, che sono state importanti in questi anni: tra di loro la professoressa Emma Gallo (il suo appoggio e la sua disponibiltà a collaborare sono stati molto importanti sin dall'inizio), il mitico CroMiTo team con la bella, fruttuosa e speriamo lunga collaborazione, e gli altri ricercatori che hanno collaborato con noi.

Ti vorrei parlare poi di tutte quelle persone che con me hanno provato a capirci qualcosa in più di legami chimici e "polimerali", mentre da loro imparavo l'importanza di legami ben più forti. Sono innanzitutto la mia famiglia: i miei genitori che mi hanno accompagnata in questa scelta, anche da sotto un altro tetto, i miei fratelli Matteo e Dario, Daniela e Jessica, e la piccola Agata. E poi c'è la famiglia di amici, la rete di relazioni donate che ho imparato a costruire e custodire con loro, che tiene uniti un nodo con l'altro e gli impedisce di disperdersi; una rete come quella dei pescatori che sa raccoglierti nel mare, ma anche come quella degli acrobati che è sempre pronta a proteggerti in caso di cadute. Non sai quanto sono cresciuta con loro, a iniziare dalla condivisione delle giornate in quel di via Cavallotti, fino ad arrivare a Santiago de Compostela la scorsa estate, attraverso avventure e momenti memorabili, cene, confronti, pianti, e grandi risate, ma anche momenti di

straordinaria ordinarietà, triangolando la Lombardia e non solo. Ogni minuto è stato prezioso, e ne è valsa la pena di tutti i treni presi (e persi). Anche qua per presentarteli tutti ci vorrebbe davvero un'eternità, ma ti assicuro che sono stati tutti dei preziosi compagni di avventura, motivatori quando il morale scendeva un po' di tono, accoglienti nelle giornate più impegnative, e sempre sempre presenti anche solo con un abbraccio silenzioso.

Non so se anche tu hai fatto questa esperienza nella tua brillante carriera, ma, tra le tante cose che ho imparato, c'è anche il fatto che alcune persone possono contribuire ad un percorso come questo in modo molto inconsapevole. Personalmente, ne ho fatto esperienza con quelle persone a cui ho dedicato un po' di tempo la sera, in una casa accogliente, o per le vie del centro qua a Milano: anche se arrivavo da una giornata difficile o impegnativa, in cui era andato tutto storto, c'erano i loro sorrisi e i loro grazie per le quattro chiacchiere scambiate, la partita a scala quaranta o il caffè preso insieme, a confermarmi che comunque ne era valsa la pena alzarsi dal letto la mattina. E allora tutto tornava a girare per il verso giusto.

Come avrai potuto capire meglio da queste ultime righe, non è sempre stato tutto rose e fiori: i catalizzatori che speravamo fossero dei fulmini, erano delle vere lumache, oppure dei fulmini sì, ma un po' storti; il vanadio si riduceva senza neanche chiedere il permesso, mentre il cromo si ossidava come gli pareva, e non stava fermo e stabile per una "foto" neanche a pregarlo in cinese; il diciclopentadiene si metteva in fila e in ordine in modo speciale ma tutto suo, uscendo un po' dalle righe; gli articoli a volte rimbalzavano indietro come se fossero stati lanciati contro un muro di gomma; quando identificavamo un trend, ecco lì che arrivava la prova che sconvolgeva tutto e allora rivedi tutti i piani. Ma questo, lo sai anche tu, fa parte del gioco, ed ora ho imparato ad apprezzarlo, e capire che può essere un'opportunità: senza tutto ciò, questo dottorato non sarebbe stato altrettanto formativo, accrescente, umano, e alla fine anche divertente!!

Chissà cosa sarebbe di questa tesi se quell'11 marzo di alcuni anni fa tu non ti fossi svegliato con tutta la passione per la chimica che la ricerca richiede e non avessi "*fatto il polipropilene*" … forse non sarei qui a scriverti ora. E invece, per dono sono qui oggi, e con queste parole vorrei ringraziare tutte quelle persone che ci tenevo a farti conoscere, che insieme a me hanno raggiunto questo traguardo.

Traguardo che diventa ora un nuovo punto di partenza.

Con stima,

Giorgia

*P.S. for the non-italian speaking readers: sorry for the Italian! To sum up, a huge thank from the bottom of my heart to all the people who collaborated with me along the years, both chemically and non-chemically. I wouldn't be here all by myself!!!